On the Degradation Behavior of Magnesium, Magnesium Hydroxide Derived Coatings and Magnesium Containing Layered Double Hydroxides with Regard to Medical Applications

Von der Naturwissenschaftlichen Fakultät der
Gottfried Wilhelm Leibniz Universität Hannover
zur Erlangung des Grades

Doktor der Naturwissenschaften
Dr. rer. nat.

genehmigte Dissertation von

Dipl.-Chem. Marc Dong Kil Kieke

geboren am 16. November 1985 in Daegu City (Südkorea)

2014

Referent: Prof. Dr. Peter Behrens

Korreferent: Prof. Dr. Peter Paul Müller

Tag der Promotion: 19. Dezember 2014

Abstract

As an element which occurs in the body in comparatively high concentrations, magnesium attracts considerable interest as a component in biomaterials. This is true for the pure metal, some of its alloys as well as for magnesium-containing compounds. This thesis addresses the degradation behavior of pure magnesium and its ZEK100 alloy as well as the properties of magnesium hydroxide and magnesium-containing layered double hydroxides (LDHs). For these investigations, the magnesium hydroxide compounds were processed to powder pellets and coatings. Processing and degradation behavior are discussed in context of *in vitro* and *in vivo* studies with regard to medical applications. In particular, osteoinductive properties are of interest for orthopedic applications and implant-directed drug delivery is of interest for otolaryngology. The results part of the thesis consists of three parts wherein the results are presented as publications or manuscripts for publications.

The examination of the corrosion behavior of magnesium and its ZEK100 alloy is in the focus of the first part. For the estimation of magnesium corrosion rates and products, discs made of pure magnesium were exposed to three different aqueous fluids under physiological conditions. For the examination of the influence of proteins, further corrosion experiments were performed in their presence. X-ray diffraction examination of the corrosion layer revealed the presence of nesquehonite, $Mg(HCO_3)(OH)\cdot 2H_2O$, as the dominant corrosion product formed in all test series, whereas magnesium hydroxide was found to have formed only under lowly buffered conditions. The corrosion behavior of ZEK100 plates was examined by using a test setup featuring the possibility of applying the medium in flow mode. In this study, magnesium hydroxide was found as the prevalent corrosion product. The results of the studies emphasize that the formation of different magnesium compounds strongly depends on the conditions, and hence has to be considered for further studies in order to increase the predictive power of *in vitro* corrosion studies.

Studies in the second part aimed at the evaluation of magnesium-containing LDHs as a class of variable magnesium compounds with regard to their potential use as coating materials for bone implant. The release of Mg^{2+} from $Mg(OH)_2$ coatings and from LDH coatings with different Mg^{2+}:Al^{3+} cation ratios was examined by exposing the samples to aqueous conditions and determining the Mg^{2+} concentration. Varying stabilities of the coatings were also tracked by SEM and XRD investigations. Pellets made of $Mg(OH)_2$, Mg-Al-LDH and Mg-Fe-LDH powders were also examined *in vitro* and *in vivo*. Very good cytocompatibility was assessed for NIH3T3 and MG63 cells. The *in vivo* study comprised implantation into femur condyles of rabbits and subsequent µCT and histology examination and showed a favourable host response. The Mg-Al-LDH system was thus found to be a promising material for orthopedic implant coatings.

In the third part, Mg-Al-LDHs are assessed with regard to their applicability as key components in drug delivery systems, especially in view of applications in the middle ear. The *in vivo* stability and biocompatibility of pristine Mg-Al-LDH coatings in this unique site were tested in the rabbit middle ear using coated middle ear prostheses. Suspensions of LDH nanoparticles were synthesized and spray-coating techniques were established in order to coat the middle ear prostheses for this study. Degradation was evaluated indirectly by *ex vivo* EDX

measurements of explanted specimens. The absence of harmful effects on the animals and a distinctive stability of the LDH coatings were found. For drug delivery studies, LDH nanosuspensions were mixed with ciprofloxacin and applied as coatings on middle ear prostheses in rabbits. These implants successfully curbed bacterial infections triggered during and subsequent to the implantation. Additionally, prolongation of the *in vitro* drug release and efficacy against bacteria were shown for titanium alloy discs coated with ciprofloxacin/LDH coatings. Excellent cell compatibility was observed for NIH3T3 cells. Furthermore, these coatings were also shown to feature antibacterial effects for extended periods of time when subcutaneously implanted into white mice. In these studies, intercalation of the antibiotic into the interlayers of the LDH materials appeared to be not necessary in order to combat bacteria. Biocompatibility and processability make LDHs a promising class of biomaterials for future drug delivery systems based on simple drug/LDH mixtures.

Keywords: magnesium, layered double hydroxides, corrosion, degradation, implants

Kurzzusammenfassung

Als ein Element, welches in vergleichsweise hohen Konzentrationen im Körper vorkommt, zieht Magnesium großes Interesse als Komponente in Biomaterialien auf sich. Dies gilt für das reine Metall ebenso wie für einige seiner Legierungen als auch für Magnesium-haltige Verbindungen. Diese Dissertation behandelt das Degradationsverhalten von reinem Magnesium und seiner Legierung ZEK100 und die Eigenschaften von Magnesiumhydroxid und Magnesium-haltigen Doppelhydroxiden mit Schichtstruktur (LDHs). Für diese Untersuchungen wurden die Magnesiumhydroxid-Verbindungen zu Pulverpresslingen und Beschichtungen verarbeitet. Verarbeitung und Abbauverhalten werden im Kontext von *in vitro*- und *in vivo*-Studien mit Hinsicht auf medizinische Anwendungen diskutiert. Insbesondere sind osteoinduktive Eigenschaften von Interesse für orthopädische Anwendungen, und die implantat-basierte Wirkstofffreisetzung für die Otolaryngologie. Der Ergebnisteil der Dissertation besteht aus drei Teilen, in denen die Ergebnisse in Form von Publikationen oder Manuskripten für Publikationen präsentiert werden.

Die Untersuchung des Korrosionsverhaltens von Magnesium und seiner Legierung ZEK100 steht im Fokus des ersten Teils. Zur Bestimmung der Korrosionsraten und–produkte von Magnesium wurden Scheiben aus reinem Magnesium unter physiologischen Bedingungen drei unterschiedlichen wässrigen Medien ausgesetzt. Zur Untersuchung des Einflusses von Proteinen wurden weitere Experimente in deren Gegenwart durchgeführt. Röntgenbeugungsuntersuchungen an den Korrosionsschichten zeigten Nesquehonit, $Mg(HCO_3)(OH)\cdot 2H_2O$, als das in allen Versuchsreihen dominierende Korrosionsprodukt an, während die Bildung von Magnesiumhydroxid nur unter schwach gepufferten Bedingungen festgestellt wurde. Das Korrosionsverhalten von Platten aus ZEK100 wurde mittels eines Versuchsstandes untersucht, welcher die Möglichkeit bietet das Medium im Durchfluss anzuwenden. In dieser Studie wurde Magnesiumhydroxid als das vorherrschende Korrosionsprodukt gefunden. Die Ergebnisse der Studien zeigen, dass die Bildung unterschiedlicher Magnesiumverbindungen stark von den Bedingungen abhängen, und demnach für weitere Studien berücksichtigt werden müssen, um die Vorhersagekraft von *in vitro*-Korrosionsstudien zu vergrößern.

Die Studien im zweiten Teil zielten auf die Evaluierung von magnesiumhaltigen LDHs als eine variierbare Klasse von Magnesium-Verbindungen mit Hinblick auf ihre potentielle Verwendung als Beschichtungsmaterial für Knochenimplantate. Die Freisetzung von Mg^{2+} aus $Mg(OH)_2$-Beschichtungen und aus LDH-Beschichtungen mit unterschiedlichen Mg^{2+}:Al^{3+}-Kationenverhältnissen wurde untersucht, indem die Proben wässrigen Bedingungen ausgesetzt und die Mg^{2+}-Konzentrationen bestimmt wurden. Variierende Stabilitäten der Beschichtungen wurden durch REM- und XRD-Untersuchungen erfasst. Presslinge aus $Mg(OH)_2$-, Mg-Al-LDH- und Mg-Fe-LDH-Pulvern wurden des weiteren *in vitro* und *in vivo* untersucht. Die Cytokompatibilität mit NIH3T3- und MG63-Zellen wurde als sehr gut bewertet. Die *in vivo*-Studie umfasste die Implantation in Femurkondylen von Kaninchen und die anschließende µCT- und histologische Untersuchung und zeigte eine günstige Wirtantwort. Das Mg-Al-

LDH-System wurde dementsprechend als vielversprechendes Material für orthopädische Implantatbeschichtungen befunden.

Im dritten Teil werden Mg-Al-LDHs im Hinblick auf ihre Anwendbarkeit als Schlüsselkomponenten in Wirkstofffreisetzungs-Systemen bewertet, insbesondere für Anwendungen im Mittelohr. Die *in vivo*-Stabilität und -Biokompatibilität von reinen Mg-Al-LDH-Beschichtungen in der besonderen Umgebung des Kaninchen-Mittelohrs wurden unter Verwendung von entsprechend beschichteten Mittelohrprothesen getestet. LDH-Nanosuspensionen wurden synthetisiert und Sprühbeschichtungsverfahren wurden etabliert, um die Mittelohrprothesen für diese Studie zu beschichten. Die Degradation wurde indirekt durch *ex vivo*-EDX-Messungen an explantierten Proben bewertet. Dabei wurde gefunden, dass es zu keinerlei schädlichen Wirkungen auf die Tiere kam und dass die LDH-Beschichtungen eine ausgeprägte Stabilität zeigten. Für Wirkstofffreisetzungs-Studien wurden LDH-Nanosuspensionen mit Ciprofloxacin gemischt und als Beschichtungen auf Mittelohrprothesen in Kaninchen eingesetzt. Diese Implantate konnten erfolgreich bakterielle Infektionen hemmen, die während oder nach der Implantation ausgelöst wurden. Zusätzlich wurde eine Verlängerung der *in vitro*-Wirkstofffreisetzung und der Wirksamkeit gegenüber Bakterien für mit Ciprofloxacin/LDH beschichtete Scheiben aus einer Titanlegierung gezeigt. Gegenüber NIH3T3-Zellen zeigten diese Proben eine ausgezeichnete Zellkompatibilität. Weiterhin wurde durch subkutane Implantation in Mäuse gezeigt, dass sich diese Beschichtungen durch eine länger anhaltende antibakterielle Wirkung auszeichneten. Gemäß dieser Studien scheint es nicht notwendig zu sein, das Antibiotikum in die Zwischenschichten der LDH-Materialien zu intercalieren, um Bakterien zu bekämpfen. Ihre gute Biokompatibilität und Verarbeitbarkeit machen LDHs zu einer vielversprechenden Klasse von Biomaterialien für zukünftige Wirkstofffreisetzung-Systeme, die auf einfachen Wirkstoff/LDH-Mischungen basieren.

Schlüsselwörter: Magnesium, Doppelhydroxide mit Schichtstruktur, Korrosion, Degradation, Implantate

Danksagung

Es ist mir eine Freude an dieser Stelle Danke sagen zu dürfen, denn die Arbeiten zu der vorliegenden Dissertation wären ohne die fachliche und menschliche Unterstützung, die mir zu Teil wurde, in dieser Form nicht möglich gewesen.

Zuerst möchte ich mich bei Herrn Prof. Dr. Peter Behrens bedanken, der mich in seinen Arbeitskreis aufgenommen hat und mir das Vertrauen schenkte auf diesem abwechslungsreichen und spannenden Gebiet meine Dissertation anfertigen zu dürfen. Seine Betreuung war mir stets eine große Hilfe und Wegweiser.

Herrn Prof. Dr. Peter Paul Müller möchte ich für die Übernahme des Korreferats und für Jahre der fruchtbaren Zusammenarbeit im Sonderforschungsbereich 599 (des SFB 599, finanziert durch die Deutsche Forschungsgemeinschaft, DFG) danken.

Herrn Prof. Dr. Michael Fröba danke ich für die Begutachtung der Dissertation.

Herrn Prof. Dr. Franz Renz danke ich für die Übernahme des Prüfungsvorsitzes.

Einen großen Dank möchte ich für viele Messungen und viel Unterstützung bei den dazugehörigen Auswertungen aussprechen, jeweils in alphabetischer Reihenfolge (i.a.R.): Britta Hering, Fabian Kempf, Florian Waltz, Gesa Zahn, Hendrik Fullriede, Imke Bremer, Janosch Cravillon, Katharina Nolte, Maria Schweinefuß und Philip Zerner für REM/EDX-Messungen; Benjamin Geppert, Hans-Christoph Schwarz und Susanne E. Thürer für Konfokalmikroskopie-Aufnahmen; Chrstian Schröder, Katharina Nolte und Sergej Springer für TG-Messungen; Claudia Schulze für CS-Messungen; Jann Lippke, Georg Platz und Natalja Wendt für Sorptionsmessungen.

Den aktuellen und ehemaligen Mitgliedern des Arbeitskreis Behrens möchte ich für das schöne Miteinander in den Laboren, in Seminar- und Kaffeeräumen, auf dem Wasser und als unaufhaltbare Lokomotive auf dem Rasen Danke sagen (irgendwann gewinnen wir ein Spiel gegen die Organiker!). Insbesondere Sebastian Lilienthal und Fabian Kempf sind mir wertvolle Freunde geworden, ob es um die Uni ging oder nicht. Meine ehemaligen Laborkollegen Christian Schröder und Georg Platz werde ich ebenfalls nicht vergessen und denke gerne an die Zeit mit ihnen und an all das, was sie mir beibrachten.

Doch auch ohne die beiden war das Labor selten leer. Wertvolle Unterstützung, für die ich sehr dankbar bin, fand ich durch (i.a.R.) Alexander Mohmeyer (HiWi, Bachelorarbeit), Alexandra Satalov (Bachelorarbeit), Bastian Hoppe (HiWi), Benjamin Geppert (Forschungspraktikum), Dennes Nettelroth (HiWi, Bachelorarbeit), Dominik Hinrichs (HiWi-Kollege), Michael Wolling (HiWi), Sebastian Stelljes (HiWi-Kollege), Tim-Joshua Pinkvos (Bachelorarbeit). Ein weiterer Dank gilt an dieser Stelle Susanne E. Thürer (Masterarbeit), die mir während meiner Diplomarbeit und bei der Betreuung einiger Bachelorarbeiten hilfreich zur Seite stand.

Die interdisziplinäre Forschung wurde möglich durch das Zusammenwirken verschiedener Institutionen, und wichtiger, durch die ineinandergreifende Zusammenarbeit der Leute, die diese Institutionen sind. Namentlich möchte ich folgenden Personen, stellvertretend für viele weitere, danken (i.a.R. der Erstgenannten): Andreas Weizbauer und Henning Windhagen (MHH, Orthopädie), Frank Feyerabend und Regine Willumeit (HZG), Franziska Duda und Nils Prenzler (MHH, HNO), Imran Rahim, Muhammad Badar und Peter Müller (HZI), Philip Dellinger und Kai Möhwald (IW-Fortis), Susanne E. Thürer und Sabine Behrens (IW-Garbsen).

Auch neben der Uni erfuhr ich viel Unterstützung durch viele liebe Leute, die mein Leben zu dem machen, was es ist. Mein Dank geht an (i.a.R. der Erstgenannten): Maren und Alexander Möller, Björn und Susanne und Lenia Isabelle Licht, Christian Knieper, Dennis Schmelzer, Dennis Schreier, Fabian Homeyer, Florian Grube, Florian Herrmann, Gerrit Jürjens, Maren und Johannes Melcher, Michael Krüger, Michael Merwart, Vanessa und Philipp Brose, Susanne Herrmann, Sven Benkelberg, Sven Wiebeck, sowie an Ulf und Anke Mowschek. Ein großer Dank für die großartige Zeit geht an dieser Stelle an meine Mannschaftskameraden von den Hannover Spartans.

Ein lieber Dank für Alles geht an Sabine Thürer, die mir liebevoll und mit viel Verständnis zur Seite steht und mich in meinem Leben begleitet.

Das Studium und die Dissertation waren weiterhin nur mit der finanziellen und moralischen Unterstützung meiner Familie machbar. Allen voran hat mir meine Mutter Ingetraut Kieke das Studium ermöglicht, wofür ich ihr aus tiefstem Herzen dankbar bin und immer sein werde.

Table of Contents

1 Introduction

Magnesium and its alloys have a long standing history in the fields of various applications. Over the years, numerous magnesium alloys were processed into magnesium based workpieces for various applications, in particular in automotive and biomedical applications [1,2]. The first mentioned field in particular exploits the low density of magnesium alloys, whereas the latter field benefits from moderate mechanical stabilities. The pronounced susceptibility to corrosion is a major challenge as well as an opportunity for further application of magnesium and its alloys. Mostly deceleration of the corrosion is desired, hence a set of anticorrosion strategies such as the targeted supplementation with alloying elements and the shielding of the substrates surfaces by coating were developed [3,4]. On the other hand, controlled degradation can be beneficial in the field of biodegradable biomaterials.

With regard to both fields of applications, the choice of examination setups is crucial for the course of corrosion and its tracking. Of course, the setups should be adjustable with regard to the conditions of exposure of the respective applications. By the employment of sophisticated and combinatory analyses the predictive power of the test setups might be increased. To this end, choice and variation of flow rate of the corrosion medium has been frequently in the focus of *in vitro* corrosion analyses. Depending on the parameters of the corrosion setups, different magnesium compounds were reported to form in course of magnesium corrosion [5,6]. In turn, identification of these is crucial for the deciphering of magnesium corrosion pathways.

Whereas the corrosion frequently occurs as a problem in the fields of technical applications, the biodegradability of magnesium offers various opportunities in medical fields. Implants made of magnesium are, ideally, expected to fulfill their designation as long as intended and to be decomposed afterwards, neglecting the necessities, risks and costs of retrieving surgeries [1,7,8]. Hence, a thorough understanding of the corrosion is desired in order to either prevent or to exploit the corrosion.

Implants made of magnesium and some of its alloys were frequently reported to enhance bone growth adjacent to the implant [9,10]. This is of interest, since the need for orthopedic implants, in particular hip prostheses, has increased over the last years as did the number and percentage of revision surgeries, and both are expected to increase further as a consequence of the ageing population [11,12]. Hence, biocompatible materials are needed that promote implant incorporation. However, the application of load-bearing prostheses as hip prostheses made entirely from metal magnesium is not promising, due to the expected functional loss in the course of decomposition.

Besides for metallic magnesium and its alloys, osteoinductive properties were also reported for magnesium hydroxide (which may form on metallic magnesium surfaces in the course of corrosion). Hence, a magnesium hydroxide coating on a permanent implant could also be expected to promote implant integration. The osteoinductive effect of magnesium or magnesium hydroxide has not been explained entirely yet. In different proposals, it was attributed to increased Mg^{2+} concentrations or to mildly alkaline effect adjacent to the implant [13].

As a single compound, magnesium hydroxide is fixed in its composition and most of its properties, significantly also the solubility and the dissolution rate. By replacing a certain amount of bivalent Mg^{2+} ions with trivalent metal cations in the layered structure of magnesium hydroxide and balancing the additional positive charges with anions, which are placed (together with water molecules) in the galleries between the layers, magnesium-containing layered double hydroxides (LDHs) can be derived from magnesium hydroxide. The compositions of the respective LDHs can be varied within wide ranges while maintaining the basic LDH structure. Variations of the composition includes the choice of trivalent cations, in particular Al^{3+} and Fe^{3+}, the metal cation ratio M^{II}:M^{III} and the choice of anion [14]. Over the years, a wide selection of LDHs with varied relative stabilities was reported. With regard to various applications, in particular medical ones, variability in the composition and properties of magnesium-containing compounds are of high interest.

Various conventional and sophisticated approaches were developed and employed for the synthesis of LDH materials. In particular, the inherent capability for anion exchange reactions [15] and a structural memory effect allowing recrystallization of LDHs amorphized by thermal treatment [16], highlight the promise of LDH materials to be vastly adaptable. Tuning of LDH materials furthermore includes variation of particle morphologies. Especially, the synthesis of suspensions of LDH nanoparticles [17,18] allows the application of post-synthesis fabrication protocols, for example coating techniques for different substrates.

An established application of LDHs is the supplementation of LDHs as fillers to polymers which endows the composite materials with high heat resistance [19,20]. Also the catalytic activity of some LDH systems towards organic reactions is employed [21]. An established medical use relies on the mildly basic properties of LDHs, namely their use as antacids [22]. The incorporation of a variety of functional anions into the LDH materials widens the spectrum of potential applications. In particular, a vast variety of biologically active anions can be combined with LDHs and was examined in the course of various *in vitro*

and *in vivo* studies. The LDH host material proves valuable in stabilizing the interlayer anions and in promoting cellular uptake [23,24]. Whereas most of the studies employed drug-LDH intercalation compounds, drug/LDH mixtures are also in the focus of recent research. The application of mixtures appears to be promising, since intercalation is a labor-intensive process, whereas mixtures are more simply prepared, while the tunability of LDH materials can still be exploited.

According to the respective medical situations, LDHs could be of interest as adaptable magnesium hydroxide derivates and as key components in drug delivery systems for the coating of medical implants. The application of Mg-LDHs as magnesium-containing coating materials could contribute to the development of osteoinductive coatings that promote implant incorporation. Drug-loaded coatings on middle ear implants could combat infections triggered during or subsequent to surgery. With regard to both fields, orthopedics and otolaryngology, biocompatible and variably degradable implant coatings could enhance success rates of the respective medical implants. For the development of these, knowledge on the degradation behavior appears to be crucial.

The scientific background of the topics mentioned above is discussed in more detail in chapter 2, concluded by the bibliography (section 2.3). The results are summarized in seven articles, which are presented in chapters 3 to 5. Chapter 3 addresses the examination of the corrosion behavior of pure magnesium and magnesium alloy ZEK100 under physiological conditions by employing comprehensive testing setups. In the course of the *in vitro* examinations, physiological media were used and the crystalline corrosion products formed were identified. The scientific background for chapter 3 is for the most part given in section 2.1. With regard to their resemblance to magnesium hydroxide, the evaluation of Mg-LDHs as biocompatible, versatile implant coating materials for orthopedics is given in chapter 4. The evaluation focuses on the *in vitro* stability of Mg-Al-LDHs and the *in vitro* and *in vivo* examination of Mg-Al- and Mg-Fe-LDHs. Both studies were performed in comparison with magnesium hydroxide. In chapter 5, the efficacy and biocompatibility of Mg-Al-LDHs as key components in drug delivery systems, based on mixtures of an antibiotic drug and an LDH, are evaluated. The studies comprised *in vitro* and *in vivo* assays and were performed with regard to the application in the middle ear. The scientific background for chapters 4 and 5 is for the most part given in section 2.2.

For four of the seven articles, the author of this thesis is the first author (including three shared first authorships) and for a further three articles he is a co-author. The work presented in this thesis was for the most part performed within the collaborative research centre SFB 599 “Sustainable bioresorbable

and permanent implants of metal and ceramic materials", funded by the Deutsche Forschungsgemeinschaft (DFG). Cooperating institutions come from the Hannover Medical School (MHH), specifically the Departments for Orthopedics and for Otorhinolaryngology, the Helmholtz Centre for Infection Research (HZI) in Braunschweig, several institutes from the Leibniz University Hannover (LUH), and the University of Veterinary Medicine in Hannover (TiHo). Further cooperation was maintained with the Institute for Materials Research of the Helmholtz-Zentrum Geesthacht (HZG). To a minor part, this work also profited from cooperation within the Cluster of Excellence "Hearing4all".

2 General Principles

This chapter contains a brief overview on the scientific background for the publications presented in chapters three to five. In section 2.1 techniques for the examination of magnesium corrosion and the importance of a thorough understanding of magnesium corrosion are discussed. Section 2.2 comprises the topics of versatility and applicability of layered double hydroxides (LDHs).

2.1 Corrosion of magnesium and its alloys

In the following subsections the corrosion properties of magnesium and its alloys are discussed with regard to technical and biomedical applications. Also, an overview on different techniques for the examination of the degradation process is given. Furthermore, formation and identification of degradation products found in the course of magnesium degradation are addressed.

2.1.1 Properties and application of magnesium and its alloys

Magnesium features various advantages such as light weight, moderate mechanical stability and the capacity to fuse into various alloys. However, their high susceptibility to corrosion limits the number of further technical applications. In order to overcome this limitation, effort concentrated on the development of anticorrosion strategies. Whereas corrosion of metallic magnesium is a key problem in the fields of technological applications, it is an opportunity in the fields of biomedical applications. Magnesium and its alloys were applied in degradable implants and showed osteoconductive properties.

Technical aspects and alloying

Magnesium has been widely available since it was identified 1808 by Sir Humphry Davy, whose assistant, Michael Faraday, obtained it in 1833 by electrolysis [1]. Nowadays, most metallic magnesium is obtained in China via the Pidgeon process (700 000 tons in 2006 and 550 000 tons in 2007). As magnesium sources various minerals are being used, e.g. dolomite and magnesite [25,26].

Magnesium is, amongst other properties, characterized by a moderate Young's modulus (45 GPa) and a low density (1.75 $g \cdot cm^{-3}$) [27]. The first mentioned property makes implants made of magnesium interesting for the application in orthopedics and trauma surgery. Implants with elastic moduli similar to the one of human bone are expected to provide mechanical stability without stress-

shielding [28]. In addition, the biodegradability of magnesium and its alloys allows for the application as temporary implants [29]. Due to the low density, magnesium is of interest for applications in which weight reduction are crucial. Hence, magnesium is a favorable metal in automobile manufacturing [2,30]. However, magnesium's applicability is limited by its vast susceptibility to corrosion.

With regard to both types of application, magnesium was fused into various alloys. Alloying elements were shown to influence the corrosion resistance of the respective alloys depending on the choice, percentage and combination of the elements fused into the respective magnesium alloy [31,32]. Furthermore, mechanical properties could be enhanced by alloying [33]. In order to further improve the mechanical properties, e.g. by grain refinement, a set of thermo-mechanical techniques, e.g. extrusion techniques, was established over the years that work for pure magnesium and its alloys [34]. With regard to medical applications, biocompatibility and potential toxicity of the elements employed have to be considered. In general, elemental components were found to be non-toxic; however, risks and compatibility problems with some elements, e.g. nickel and vanadium, have also been reported [29].

Amongst other elements, aluminium, zirconium, zinc and rare earth metals are of central interest for the casting of magnesium alloys. In particular, aluminium and its alloys themselves are used in automobile manufacturing [30] and in airplane construction [35]. Commonly, the alloys designations allow for a quick overview on the elements contained. Supplemented metals are abbreviated (e.g. Al: A, K: Zr, Z: Zn, RE/E: rare earth elements) and the approximate percentage contributions to the alloy are stated with a single-digit in the same order [31]. Exemplarily, a ZEK100 alloy contains about 1% Zn and each <1% rare earth metals and Zr, respectively. However, this designation system is not obligatory; hence, variation in nomenclature and the use of trade names are frequently met. Samples made of pure magnesium were in the focus of corrosion examinations as described in section 3.2, whereas magnesium alloy ZEK100 samples were examined as described in section 3.3.

Magnesium is an available and extensively studied metal that allows for large scale production and modification by alloying and processing. Due to their light weight, magnesium and its alloys have proven their potential for technical, in particular automotive, application. Their moderate mechanical stability was shown to be of promise for application in biomedical fields. The strong susceptibility of magnesium and its alloys to corrosion was shown to be a challenge with regard to technical application and a chance with regard to biomedical application.

Corrosion as a challenge for technical use

The susceptibility of magnesium to corrosion is a key problem in the fields of technical applications and efforts have been made to delay and to decelerate the corrosion. A key challenge in order to answer this issue is the avoidance of impurities which might act as cathodes and cause galvanic corrosion [3]. However, supplementation with aluminium in magnesium-aluminium alloys was shown to enhance the corrosion resistance by the formation of protective aluminium oxide films on the surface [4]. Furthermore, the addition of a certain amount of manganese to a magnesium-iron alloy improved its corrosion resistance by manganese atoms surrounding the iron atoms and acting as local cathodes [33].

Another principle to hinder corrosion is to shield the substrate surfaces from the environment by coating. Many different coating techniques have been developed and addressed in literature, e.g. anodizing, electrochemical plating and conversion coatings [36]. As an example for conversion coatings, phosphate conversion coatings have been successfully established for magnesium and other metals. By using plasma electrolytic oxidation (PEO) specimen made of WE43 (containing magnesium, $\approx 4\%$ Y, $\approx 3\%$ rare earths and $< 0.5\%$ Zr) and AZ91D (containing magnesium, $\approx 9\%$ Al, $< 1\%$ Zn and each $< 0.5\%$ Si, Fe, Cu, Ni) were phosphate conversion coated electrochemically in water [37]. Phosphate conversion coating was also achieved by heat treatment (300 °C) of an ionic liquid (tetraoctylammonium di(2-ethylhexyl)phosphate) applied to the surface of an AZ31B (containing magnesium, $\approx 3\%$ Al, $< 1\%$ Zn and $< 0.5\%$ Mn) specimen [38].

Furthermore, coating of magnesium with oxidized magnesium compounds could succeed in protecting the material. Plasma spray coating of magnesium with magnesium fluoride (MgF_2) nanoparticles was reported [39]. Exploiting the above mentioned protective properties of aluminium oxides, cold spray coating with pure aluminium and Al_2O_3 particles, respectively, was reported to enhance the surface properties of an AZ91E (containing magnesium, $\approx 9\%$ Al, $< 1\%$ Zn and each $< 0.5\%$ Si, Fe, Cu, Ni, with slightly altered contributions of the latter four elements) magnesium alloy [40].

Another noteworthy class of materials that has been employed for corrosion protection of metallic magnesium is that of layered double hydroxides (LDHs). As explicated in subsection 2.2.2, magnesium-containing LDHs are widely tunable in terms of their compositions and by this in their properties, while the close relation to $Mg(OH)_2$ is maintained. In brief, LDH films comprising from the Mg^{2+}-Fe^{3+} system or the Mg^{2+}-Al^{3+} system, respectively, were synthesized directly on the magnesium surface and increased the substrates corrosion

resistance [41,42]. In another case, an LDH containing Mg^{2+}, Al^{3+} and WO_4^{2-}, was supplemented to a resin-based coating which also showed anticorrosive properties. The anticorrosive properties were attributed to the exchange of WO_4^{2-} with corrosive Cl^- from the corrosion medium [43].

Due to magnesium's distinct susceptibility to corrosion, anticorrosion techniques and anticorrosive substances are of particular interest with regard to technical applications of magnesium. In particular, the differentiated avoidance or employment of impurities and alloying elements, respectively, plays a key role to this manner. In addition, oxidized species, such as phosphates, fluorides and layered double hydroxides, were applied as coatings on magnesium surfaces in order to prevent corrosion. A thorough understanding of magnesium and its corrosion might promote development and enhancement of anticorrosion strategies.

Degradability as an opportunity for biomedical applications

Magnesium and its alloys have a long standing history in the field of biomedical application and have recently gained an increasing interest for the application as biodegradable, temporary implant materials, avoiding secondary surgery for removal [1,8]. In the following, an overview on selected applications and on the osteoconductive properties of magnesium and its alloys with regard to medical applications is given.

In 1878 Edward C. Huse successfully treated bleeding vessels with a magnesium wire ligature [1]. At present, magnesium wires are of relevance for orthopedic fixation and their corrosion resistance is in the focus of recent research [44]. Another promising application of magnesium wires is based on the supplementation of magnesium alloy wires to calcium phosphate cements that are used for the treatment of bone defects. Wires made of ZEK 100 were shown to reinforce the cement towards a potential use for load-bearing purposes [45].

Magnesium and its alloys have also attracted interest in the field of cardiovascular diseases. Coronary stents made of magnesium alloys were considered of high interest due to their biodegradable nature and mechanical properties (Fig. 1) [46] and were tested in the course of clinical trials for the treatment of coronary artery disease patients [47]. Furthermore, absorbable magnesium stents are promising for the treatment of coronary diseases in pediatrics, considering the vessel growth and remodeling in the course of ageing and growth of the patient [48].

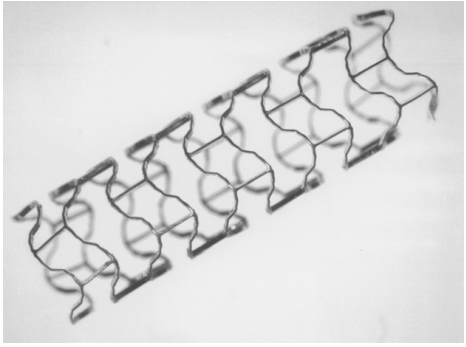

Fig. 1: Absorbable magnesium stent (from ref. [46]).

Degradable magnesium stents are also of interest for the treatment of chronic rhinosinusitis in order to maintain ventilation of the paranasal sinuses and to avoid the formation of scar tissue [49].

Exploiting the favorable properties for stent applications, magnesium alloy scaffolds are expected to stabilize lesioned ventricular myocardium in combination with biological graft material. The design of the magnesium scaffolds is intended to provide proper mechanical stability until the biological material has reached sufficient strength [50].

Various magnesium and magnesium alloy based implants have been in the focus of recent developments and examinations in orthopedics and trauma surgery [1,27]. A selection of degradable implants for orthopedic application is shown in Fig. 2. For this purpose, mechanical and corrosion properties of magnesium alloys are in the focus of recent examinations [51]. In particular, magnesium plates (Fig. 2, middle) have been employed to stabilize fractured bones in comparison to frequently used surgical steel [1,27] and are also in the focus of the results described in section 3.3.

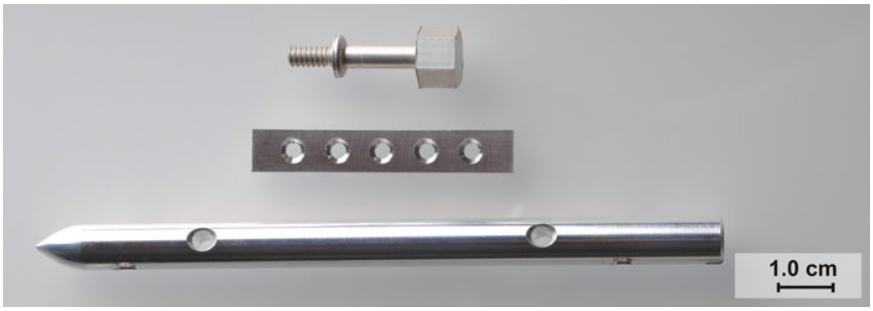

Fig. 2: Orthopedic implants. From top to bottom: A MgCa0.8 screw, a ZEK100 plate and an intramedullary LAE442 nail (modified from ref. [27]).

Biodegradable screws for application in orthopedics were manufactured from MgYREZr alloy and inserted into the marrow cavity of rabbit femora (Fig. 3). Good biocompatibility and osteoconductivity were found and no toxic effects were observed [52]. Recently, the absorbable bone compression screw MAGNEZIX® CS 3.2, produced by the medical technology company Syntellix AG, has reached marketability. However, due to the fading of the implants, the applicability of magnesium for load-bearing, large-scale prostheses is limited.

Fig. 3: A biodegradable orthopedic MgYREZr screw, length is 6 mm (from ref. [52]).

Biocompatility is a major precondition for biomedical applicability and has been reported for magnesium and many of its alloys [9,10,31]. Biocompatibility problems are reported scarcely. Exemplarily, local pathological effects were reported in a long-term study (12 months) of ZEK100 tibia implants in rabbits, although general negative effects on the animals were not found [53].

In summary, application of magnesium and its alloys as biodegradable implant materials have been reported since the 19th century and have recently attained high interest again. The promise of magnesium-based implants with regard to cardiovascular disease treatment was shown within clinical trials. Furthermore, magnesium-based implants are of high interest for orthopedic application, e.g. in osteosynthesis systems, amongst other advantages due to their mechanical properties.

Osteoinductive properties of magnesium and magnesium hydroxide

In various studies, including different compositions, magnesium and some of its alloys were shown to have osteoinductive properties [9,10]. Implants made from these materials induced bone growth adjacent to the fading implant, promoting bone healing. The mechanism of the osteoinductive effects of

magnesium have not been explained yet, however, many different theories exist and many factors have to be considered. Electrical stimulation of osteoblast (bone synthesizing cells) in the course of magnesium/alloy corrosion was presumed to be crucial for the osteoinduction [13,54]. Furthermore, the presence of alloying elements or elements released from implant coatings has been suspected to be responsible for enhanced bone growth [7,13]. In addition, implant surface properties such as roughness and shape were found to be decisive for bone-implant interactions [13,55].

In 2010, a prominent corrosion product of magnesium came into focus of this topic. Janning et al. implanted cylinders made of pure $Mg(OH)_2$ into the femur condyles of rabbits (Fig. 4). In the following weeks an increased bone growth was observed adjacent to the $Mg(OH)_2$ cylinders lacking metal characteristics, in particular their electrochemical properties, and alloying elements.

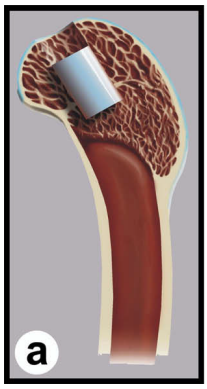

Fig. 4: Schematic depiction of implantation site of the magnesium hydroxide cylinder in the femur condyle of a rabbit (modified from ref. [13]).

Enhanced bone growth around the $Mg(OH)_2$ cylinders was attributed to an increased osteoblast activity due to the Mg^{2+} rich environment [13]. This is in accordance with the observation that osteoblast numbers were shown to be reduced in a magnesium deficiency diet, which in turn led to a decrease in bone density [56]. Furthermore, enhanced osteoblast activity was observed in alkaline environments as well [57], which are to be expected adjacent to a degrading metal hydroxide. Hence, magnesium hydroxide and related compounds are interesting as a coating material for sustainable implants (see sections 4.2 and 4.3).

Amongst other advantages, osteoinductive properties of magnesium, a variety of its alloys and magnesium hydroxide contribute to the potential of magnesium based implant materials. Magnesium hydroxide might be of interest for osteoinductive coatings, but is fixed in its properties, whereas application fields

differ in their respective demand. This emphasizes the need for magnesium-containing and –releasing compounds which can be adapted to the desired application. The properties of a group of such compounds, magnesium-containing layered double hydroxides, are described in section 2.2.

2.1.2 Corrosion examination

The general applicability of magnesium and alloys for automotive and biomedical applications was shown. By a thorough understanding of the corrosion process, the spectrum of further applications could be widened. Corrosion of magnesium is a complex process, the exact mechanisms of which have not been fully understood yet. Different efforts have been made to track the course of corrosion and to examine the effects of the medium on the corrosion. Furthermore, identification of the compounds formed under different conditions is of interest in order to increase the predictive power of *in vitro* studies.

Tracking of the corrosion

Over the years, various methods and testing setups have been established in order to track the course of magnesium corrosion and to examine the influence of the different parameters. In the following, a selection of methods applied, focusing on the tracking of the respective corrosion rates, is discussed.

The examination of the magnesium specimens themselves gives a first insight into the corrosion mechanisms in their *ex vivo* state or in an *in vivo* assay. With regard to load-bearing applications, appropriate mechanical integrity throughout the corrosion process is desired [58]. Hence, methods for the estimation of mechanical properties were applied as described in section 3.3.

A simple method for tracking the course of degradation is to estimate the mass loss of magnesium samples over time. In typical setups, samples were exposed to chromium acid, dissolving the corrosion products while leaving the magnesium sample intact [59,60].

Since magnesium corrosion is accompanied by the chemical formation of various compounds, monitoring the amount and concentration of these is also a possibility to track the course of corrosion. Ultimately, Mg^0 dissolves under the formation of Mg^{II}, which can be bound in a corrosion layer in form of various amorphous and crystalline compounds, e.g. in form of magnesium hydroxides or magnesium carbonate derivates. The corrosion layers and the Mg^{2+} compounds

present therein have been investigated by physicochemical analysis methods such as spectroscopic methods, microscopy or X-ray diffraction [6,61].

In the course of corrosion, Mg^{2+} ions also occur in the solution and are hence principally detectable in the environment. Mg^{2+} determination in the medium of *in vitro* setups can be performed by collecting the medium and performing elemental analysis, e.g. ICP-OES [5]. The *in vivo* determination of ions such as Mg^{2+} or Ca^{2+} directly in the tissue surrounding the implants is a major challenge of *in vivo* studies. A possibility to determine ion concentrations semi-online is given by microdialysis. Adjacent to the implants, ion conductive probes are inserted into the tissue. Dialysates taken were analyzed with means suitable for the determination of ion concentrations, e.g. ICP-OES, AAS [62].

With regard to biological environments as in cell culture assays or *in vivo* studies, osmotic pressure variations of the solutions caused by Mg^{2+} and other species are of interest. Hence, estimation of osmolarity was part of the examination in some studies [5,63].

Another species the formation of which is commonly expected to occur in the course of magnesium degradation are hydroxide ions. By monitoring the evolution of pH values, Mg^{2+} concentrations can principally be estimated by the concentration of the hydroxide ions derived from the pH value. However, local pH values, close to the magnesium specimen, commonly differ from the pH values in solution [64], amongst others depending on turbulence in the setup [65]. Furthermore has the corrosion medium, such as simulated body fluids (SBFs), has influence on the pH; hence the reliability of pH monitoring in order to track the course of corrosion is limited [66].

The formation of hydrogen in the course of magnesium degradation is expected and has been observed in several studies. In principle, formed hydrogen gas can be collected, and the degradation rate can be calculated according to the captured gas volume [59,66]. However, depending on the experimental setup and methodology, the “negative difference effect” (NDE) has to be considered, which leads to a non-compliance between hydrogen evolution and electrochemically estimated corrosion rates [3,67]. Hydrogen evolution was also reported in context of *in vivo* studies. Degradation of magnesium implants at high rates led to the formation of subcutaneous gas bubbles [9]. However, these bubbles were shown to contain other gases than hydrogen as well [9,68], as hydrogen was shown to be highly diffusive [68].

With regard to established and potential applications, a thorough understanding of corrosion properties, such as corrosion rates, is of high interest in order to either prevent or exploit the corrosion. A variety of testing methods with focus on the magnesium specimen and on the substances formed was developed and

various studies reported. Taking into account a selection of the approaches explicated, i.e. estimation of weight loss, change of osmolality and pH, the corrosion behavior of magnesium samples was examined as described in section 3.2.

Corrosion media

Magnesium and most of its alloys are prone to corrosion under conditions that can be met with regard to outdoor conditions, technical applications and biomedical purposes. Whereas corrosion occurs only slowly in air contact [3,69], magnesium is vastly susceptible to corrosion when stored under aqueous conditions [3,65]. For a better understanding of the corrosion, test setups are needed that allow for the examination of the influence of liquid phases with which magnesium is in contact. For this, different aqueous media were examined with regard to their applicability in these setups.

The application of deionized water as the medium allows for a simplified tracking and analysis of the specimen in *in vitro* setups. Unfortunately, complex technical conditions, not to mention *in vivo* environments, are not reproduced well. As a first approach, ion loadings of complex systems can often be matched by the use of sodium chloride solutions, e.g. 0.9% (0.154 $mol \cdot L^{-1}$) for the imitation of physiological conditions. Sodium chloride solution with varying concentrations, e.g. 0.2 – 1 $mol \cdot L^{-1}$, have been used in salt spray corrosion tests [70].

For approximation of the respective setups to *in vivo* conditions, different aqueous media proved to be interesting for the examination of magnesium under physiological *in vitro* conditions. Hank's balanced salt solution (HBSS) is a comparably simple saline solution which contains a selection of inorganic salts and is characterized by a low buffering capacity [5,6]. Simulated body fluids (SBFs) also comprise a solution of inorganic salts and reflect the inorganic part of human blood plasma [6,71]. Dulbecco's modified eagle medium (DMEM) is a more complex solution, which also features organic substances, e.g. amino acids, vitamins or glucose and is characterized by a comparably high buffering capacity [6,72]. These media were employed in the course of the examinations discussed in section 3.2 and their respective compositions are listed in this section. Degradation setups however are not limited to aqeous solutions, also liquid fuels are relevant media for corrosion examination. Exemplarily, magnesium was shown to degrade faster than aluminium in palm biodiesel; however, no crystalline corrosion products were detectable after 60 days at room temperature [73].

Not only the choice of the medium influences the corrosion behavior, but also turbulence and exchange of the medium are relevant parameters. Local alkalization adjacent to corroding metal surfaces was shown to decrease corrosion rates [3,74]. The change from a static medium to a stirred medium was shown to balance the local pH and by this to increase degradation rates [3,65]. Depending on the application, the medium can also be exchanged continuously by applying a constant flow rate as described in section 3.3.

Further important parameters for degradation setups are composition and pressure of the gas phase in contact with the medium. By introduction of further species, chemical equilibria are shifted and additional reaction pathways might lead to the formation of alternative compounds. Exemplary, different amounts of CO_2 and SO_2 led to the formation of magnesium carbonates and sulfates, respectively [6,65,69].

Despite the number of studies and the employment of sophisticated methods, results gained from *in vitro* studies often differ considerably from responding *in vivo* studies [7,75]. *In vivo* environments, such as blood plasma and intercellular fluid, contain proteins, which might decrease corrosion rates presumably due to adsorption on the metal surfaces. However, amino acids and organic chelating compounds might complex metal ions and by this increase corrosion rates [64]. In order to examine the effect of proteins on degradation, the medium in the respective *in vitro* setup can be supplemented with proteins and protein mixtures, such as fetal bovine serum (FBS) [6]. Hence, applicability of corrosive media lacking these bio-organic compounds, such as SBF, has to be examined critically [76].

Corrosion behavior of magnesium and its alloys was shown to depend on the conditions of the respective corrosion environments, in particular complex *in vivo* conditions. In order to reproduce these conditions to some extent, *in vitro* corrosion test setups frequently include differently composed and differently buffered media, e.g. HBSS, SBF and DMEM. These media were part of the examinations described in section 3.2, also considering the influence of further parameters such as CO_2 gassing and protein supplementation. Furthermore, amount and turbulence of the media can be varied in order to examine the corrosion behavior (see section 3.3). Results collected from *in vitro* corrosion studies often differ from results gained from *in vivo* studies. Nonetheless, sophisticated test setups and differentiated analysis of the data gained might increase the predictive power of *in vitro* studies.

Corrosion layer compounds

In order to better understand the corrosion and to increase the predictive power of *in vitro* studies, it is crucial to identify the corrosion products that form along the reaction pathway. In the following, an overview of species found and reported in some studies is given.

A magnesium oxide layer is the natural corrosion product that forms on magnesium surfaces. In contrast to aluminium oxide layers on aluminium, the MgO layers are not dense. The reason can be found in the fact that the molar volume of MgO is considerably lower than that of magnesium [77].

In presence of water, commonly conversion to a magnesium hydroxide occurs [32]. The overall passivating effect of magnesium hydroxide layers, however, is considered as low [3]. Furthermore, solubility of the magnesium hydroxide layer was shown to be enhanced in the presence of certain concentrations of chlorides, which can be met under physiological [78] and *in vivo* conditions [7]. Dissolution of the protective hydroxide layer and by this release of ions opens additional pathways for following reactions.

The formation of phosphate containing layers at the surface of magnesium is well known and even desired if conversion coating is performed [36–38]. Phosphorous and oxygen could be found by EDX in some degradation studies [5,64,78]. Since widely used physiological media contain phosphate sources such as Na_2HPO_4 (HBSS and SBF) and NaH_2PO_4 (DMEM), magnesium phosphates are likely to occur in course of degradation studies. Exemplarily, amorphous, $(Mg,Ca)_x(PO_4)_y(CO_3)_z(OH)_i$, was reported on the surface of a magnesium rare-earth alloy in an *in vitro* study employing SBF as the medium [79]. Structure and composition of calcium phosphates were shown to be dependent on the HCO_3^- content in SBF [80]. Formation of crystalline phosphate compounds was reported in only few cases. Exemplarily, the formation of struvite, $MgNH_4PO_4{\cdot}6H_2O$, on a magnesium-sputtered titanium substrate was reported, after the sample had been exposed to an ammonium phosphate solution. In the presence of Ca^{2+} ions, struvite was expected to be dissolved for the formation of calcium phosphates [81]. In an *in vivo* (rats) assay, magnesium-containing calcium phosphates, $Mg_xCa_y(PO_4)_z$, were found on a Mg-Mn-Zn alloy. The fast deposition of biological calcium phosphate was attributed to the presence of a corrosion layer, however, its crystallinity was not discussed [54].

In the presence of dissolved CO_2 from the gas phase or supplementation of the medium with soluble CO_3^{2-}/HCO_3^- salts, respectively, corrosion layers were shown to contain CO_3^{2-}/HCO_3^- ions [82]. Hence, a variety of magnesium carbonate and hydrogen carbonate compounds were found as corrosion products in some degradation studies. Nesquehonite, $Mg(HCO_3)(OH){\cdot}2H_2O$, was

found as a corrosion product on magnesium that was immersed in HBSS and DMEM, respectively, under cell culture conditions [5]. It was also found on AZ91D alloys samples exposed to atmospheric conditions after preliminary treatment with NaCl. Furthermore, it was stated that nesquehonite could be formed either by hydration of magnesite, $MgCO_3$, or by transformation of hydromagnesite, $Mg_5(CO_3)_4(OH)_2{\cdot}4H_2O$, depending on the CO_2 pressure [83]. Nesquehonite was also found in course of the examinations described in section 3.2.

Interestingly, nesquehonite found in mines (Sounion, Lavrion mining district, Greece) was reported to be associated amongst others with hydromagnesite and hydrotalcite [84]. The latter can be described as the prototype compound of Mg-Al-CO_3-LDHs (subsection 2.2.1).

Whereas the respective formulae of magnesium carbonates and hydrogen carbonates are often similar or even the same ($Mg_5(CO_3)_4(OH)_2{\cdot}5H_2O$ for both dypingite and giorgiosite), their crystalline structures can differ fundamentally. Hence, elemental analysis methods, e.g. EDX, are often not suited to distinguish between different magnesium carbonates. X-ray diffraction is a method capable to distinguish between different crystalline products and the structures of various magnesium carbonates, which are well investigated. Fig. 5 gives an overview of a selection of XRD patterns (reflection positions) of magnesium carbonates, hydrates, hydroxides and hydrogen carbonates, respectively.

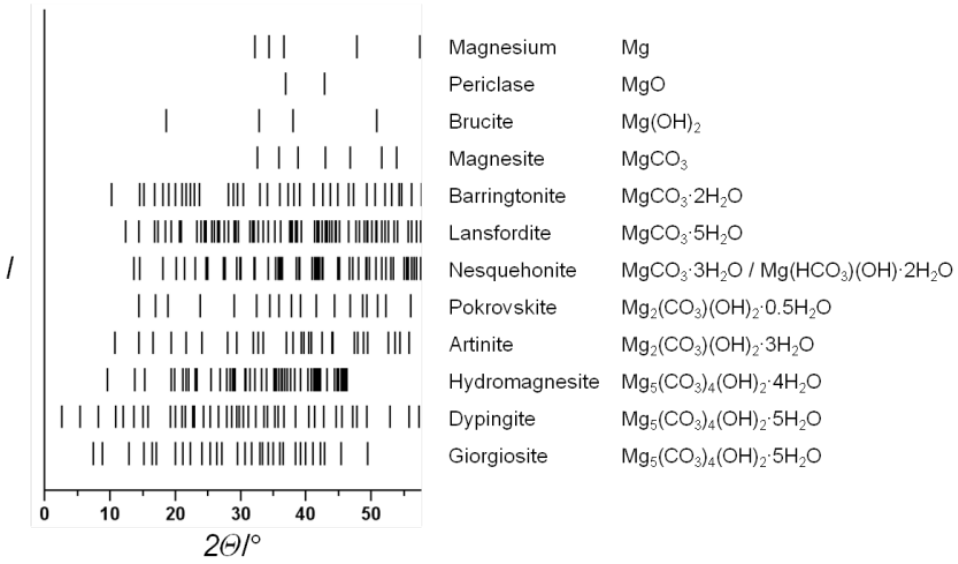

Fig. 5: Overview of XRD patterns (reflection patterns) of a selection of magnesium carbonates (WinXPow database, Stoe).

Formation of magnesium sulfates and sulfites such as $MgSO_4 \cdot 6H_2O$ and $MgSO_3 \cdot 6H_2O$ were attributed to increased SO_2 contents in the atmosphere of industrial environments [65,69].

Various magnesium compounds were found in corrosion layers on magnesium specimen. Furthermore, conversion of certain magnesium carbonate compounds was reported also. Inherent to the different compounds are different reactivities and solubilities, respectively, also depending on the medium. Identification of the species can be performed by various methods, e.g. X-ray diffraction for the identification of crystalline compounds. Knowledge on the corrosion products formed is crucial in order to get a better picture of the corrosion processes.

2.2 Layered double hydroxides as a versatile class of biomaterials

In the following subsections layered double hydroxides are introduced as a promising class of material with special regard to their applicability as novel biomaterials. Versatility of these materials is emphasized by a discussion of the numerous possibilities to vary the composition and the synthetic methods by which LDHs can be obtained and their properties be tuned. Furthermore, processing of LDH materials towards their application in technical and medical fields is discussed.

2.2.1 Structural aspects

Layered double hydroxides (LDHs) with the formula $[M^{II}_{1-x}M^{III}_{x}(OH)_2^{x+}][A^{n-}]_{x/n}\cdot yH_2O$ LDHs are also known as anionic clays or hydrotalcite-like compounds. Hydrotalcite, $[Mg_6Al_2(OH)_{16}][CO_3]\cdot 4H_2O$, which can be considered as the prototype compound for this class of clay-type materials, was discovered in 1842 by Carl Hochstetter. Over the years, various LDHs have been obtained synthetically. Besides their potential for various applications, also structural features were in the focus of the examination of LDHs.

The respective LDHs can be derived from their according M^{II} hydroxides (e.g. $Mg(OH)_2$, CdI_2 type) by substituting a certain amount of the bivalent cations M^{II} with trivalent cations M^{III} (e.g. Al^{3+}), which generates surplus positive charges in the M^{II}/M^{III}-hydroxide layers. Commonly these positively charged metal hydroxide layers are referred to as main layers. These main layers are built from compressed, edge-sharing metal hydroxide octahedra with hydroxide ions occupying positions of densely packed layers and oriented perpendicular to the plane of the layers. The surplus positive charges in the main layers are balanced by anions A^{n-}, which are placed together with water molecules in the interlayer regions or galleries. Whereas ionic bonding is prevalent within the main layers, the layer stacking is stabilized by hydrogen bonding and dispersion forces [14]. A schematic depiction of the structures of magnesium hydroxide and magnesium-containing layered double hydroxides is shown in Fig. 6. The presence of anions in the interlayers of the LDH increases the distance between the main layers compared to magnesium hydroxide layers, as it is implied in Fig. 6. Basal spacings depend on size, arrangement and orientation of the anions (explicated in subsection 2.2.2).

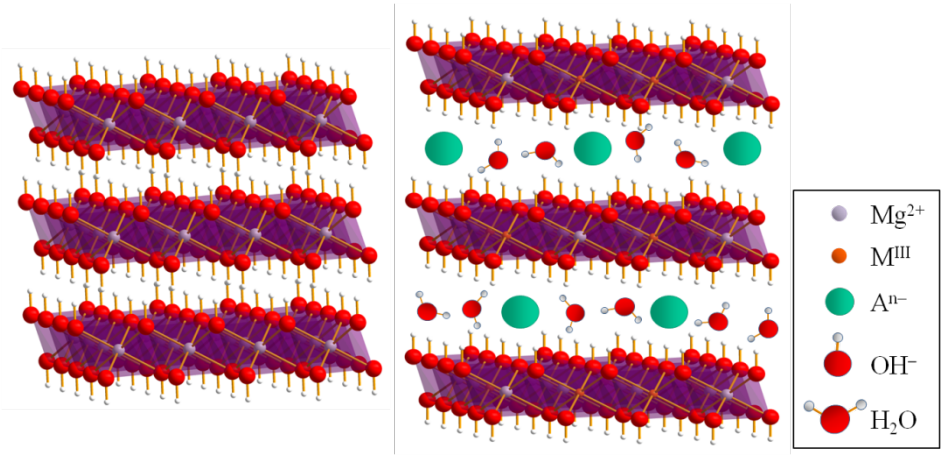

Fig. 6: Schematic depiction of the structures of magnesium hydroxide (left) and magnesium-containing layered double hydroxides (right).

The brucite-like layers in LDHs may be stacked in manifold ways, resulting in different polytypes. In principle, when hydroxyl groups of one sheet are located vertically above the hydroxyl groups of the adjacent sheet (AA stacking), this results in the formation of trigonal-prismatic sites between them; an offset arrangement of the hydroxyl groups (AB) of adjacent sheets creates octahedralsites. The polytypes may comprise a variety of stacking sequences (like ABAB or ABCABC), but disorder is also common; especially early X-ray diffraction analyses did not always take into account signs of stacking disorder (broadened reflections, higher background diffraction) and therefore, the often complicated stacking sequences derived in early X-ray diffraction work on LDHs have to be viewed with care. The different stacking sequences or polytypes are denoted according to the number of the sheets stacked along the *c* axis and according to the symmetry resulting from the stacking. A hexagonal symmetry is denoted by "H" and a rhombohedral symmetry is denoted by "R". Hence, brucite, $Mg(OH)_2$, is denoted by "1H". Stacking sequences for multi-layer polytypes and according denotations were systematically derived by Bookin and Drits. It was shown that there are three two-layer polytypes with hexagonal stacking ($2H_1$ to $2H_3$), whilst there are nine possible three-layer polytypes including two with rhombohedral symmetry ($3R_1$ and $3R_2$) and seven with hexagonal symmetry ($3H_1$ to $3H_7$) [14].

X-ray diffraction (XRD) is routinely employed to gain information on the LDH crystal structure. A typical XRD pattern of LDHs is shown in Fig. 7 (from ref. [85]).

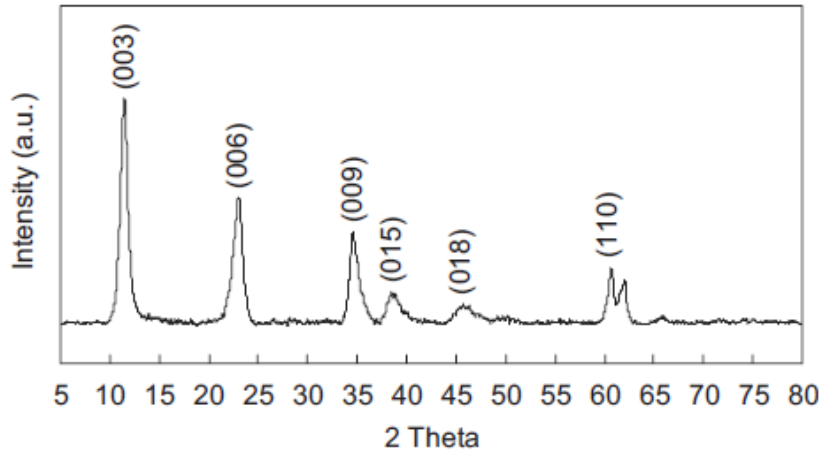

Fig. 7: Typical XRD pattern of LDHs (from ref. [85]).

In principle, there are three groups of reflections in XRD patterns of LDHs. (A) At low diffraction angles a series of (00*l*) reflections is characteristic, by which basal spacings along the *c* axis can be calculated. Basal spacings are of particular interest for the characterization of LDHs with different anions in the interlayers. A selection of XRD patterns of Mg-Al-LDHs with different anions is given in Fig. 8 (from ref. [86]). (B) At higher angles the (110) reflection (and possibly other *hk*0 reflections) can be detected, which allow the determination of the lattice constant *a* within the main layers and thus of the cation-cation distances. (C) Information on the stacking patterns of the layers can be gained from (*hkl*) reflections, e.g. from the (10*l)* reflections at intermediate diffraction angles.

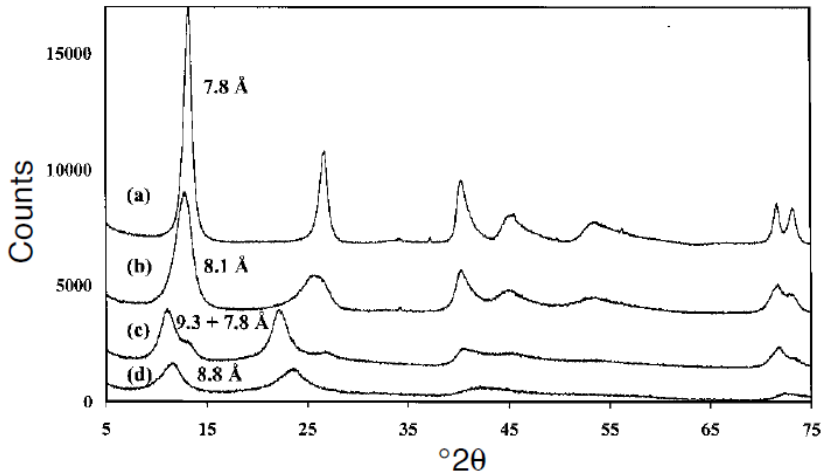

Fig. 8: XRD patterns of Mg-Al-LDHs with (a) $CO_3 2^-$, (b) NO_3^-, (c) ClO_4^- and (d) SO_4^{2-} in the LDH interlayers. XRD pattern (c) shows a second phase with a (003) reflection similar to that of the carbonate-bearing material (from ref. [86]). Broadening of reflections can clearly be recognized around 55° 2Θ.

However, deduction of information may be affected by certain structural features of LDHs, which lead to shifts and increased broadening of XRD reflections. Two frequently found features are interstratification and turbostratic disorder. Interstratification occurs in LDHs that comprise interlayers with varying interlayer anions and/or varying water content, and mainly affects the relationship between (00*l*) reflections of different order. In case of turbostratic disorder, LDH main layers are shifted as well as twisted against each other, leading to a broadening of (*hkl*) reflections [14].

2.2.2 Tunable composition

In accordance with the general formula, various combinations of bivalent M^{II}, trivalent M^{III} cations and anions A^{n-} have been reported to form LDHs. Also, LDHs with varying M^{II}/M^{III} ratios were found. In the following, the LDHs are named according to M^{II}-M^{III}-A-LDH; e.g. a LDH containing Mg^{2+}, Al^{3+} and CO_3^{2-} ions is named Mg-Al-CO_3-LDH.

As explicated above (subsection 2.1.1), magnesium hydroxide is one of the dominant corrosion products of metallic magnesium and its alloys under various aqueous conditions. It shows promising properties like osteoinductivity, but due to its single-compound nature its composition is fixed and its properties, like the solubility and dissolution rate, can only be varied in a narrow window, for example by changing the size of (small) particles. Magnesium-containing layered double hydroxides can be derived from magnesium hydroxide as explained above, and are tunable in their composition and by this, properties. With regard to the close relation to $Mg(OH)_2$ and the publications (in particular chapters 4 and 5) in this thesis, Mg-LDHs are in the focus of the discussion.

Cation combinations and cation ratios

Various LDH systems which comprise a wide repertoire of bivalent and trivalent cations were found, making this class of material favorable for many purposes. Depending on the demands of the respective application, different elements can be incorporated in the material whilst avoiding the creation of a multiphase system. With regard to the publications in chapters 4 and 5, a selection of elements that have been reported to form Mg-LDHs, Al-LDHs and Fe-LDHs, respectively, is listed in Table 1 [87].

Table 1: Selection of cation combinations that form Mg-LDHs, Al-LDHs and Fe-LDHs (according to information from ref. [87]).

M^{II}	M^{III}
Mg	Al, Cr, Fe, V
Ca, Cd, Co, Cu, Li, Mg, Mn, Ni, Zn	**Al**
Mg, Ni	**Fe**

Stability of LDHs was shown to depend on the choice of cations. For LDHs with $M^{III} = Al^{3+}$ or Fe^{3+} an increasing stability sequence was reported depending on the choice of M^{II}: $Mg^{2+} < Mn^{2+} < Co^{2+} \approx Ni^{2+} < Zn^{2+}$ [88], which was confirmed for $M^{III} = Cr^{3+}$ [89]. Furthermore, Al-LDHs were found to be more stable than Fe^{III}-LDHs [88].

LDHs with more than two sorts of cations were reported also. Partial substitution of Mg^{2+} ions with noble metal ions led to the formation of Mg-Pd^{II}-Al-LDH and Mg-Pt^{II}-Al-LDH [90]. Mg-LDHs with two sorts of trivalent cations such as Mg-Al-Fe-LDH [91] and also with noble metal cations as in Mg-Al-M^{III}-LDH (with $M^{III} = Rh^{3+}$, Ir^{3+} and Ru^{3+}) were found [90]. Furthermore, LDHs with four cations: Cu-Co-Zn-Al-LDH [92] and five cations Cu-Zn-Mn-Fe-Al-LDH were described. The latter was active towards hydrogen peroxide oxidation of phenol [21].

Not only could the choice of the cations be altered, also the cation ratios were varied for some LDH systems, allowing for a further tuning of the properties of the materials [93]. In the case of the Mg-Al-LDHs, M^{II}:M^{III} ratios between 2:1 and 4:1 were reported [94]. In this LDH system, attempts for higher ratios led to the formation of $Mg(OH)_2$, whereas higher contributions of Al^{3+} led to the formation of $Al(OH)_3$. Similar results were observed for Ni-Al-LDHs [95]. Variation of the cation ratio can be detected by elemental analysis and indirectly by X-ray diffraction. In case of Mg-Al- and Mg-Fe-LDHs, the respective (003) reflections were as expected reported to shift to smaller reflection angles when the amount of larger cations was increased [94,96].

In the context of the adsorption of norfloxacin (a broad-spectrum antibiotic) a Mg-Al-LDH system with varying Mg:Al ratios and supplementations with Sn^{4+} ions was investigated. It was found that the increase of Al^{3+} ion contribution led to enhanced sorption properties, whereas incorporation of Sn^{4+} led to an attenuation [97].

Besides the mentioned M^{II}-M^{III} systems, also Li-Al-LDHs can form according to the more general LDH formula $[M^{z+}_{1-x}M^{III}_x(OH)_2]^{\zeta+}[A^{n-}]_{\zeta/n}{\cdot}yH_2O$ with z=1 and

$\zeta = 2x-1$ (adapted from [87]). This formula also describes the M^{II}-M^{III}-LDHs for which z=2 and $\zeta = x$. In accordance with their M^{II}-M^{III} counterparts, inorganic and organic anions were intercalated into Li-Al-LDHs. Exemplarily, fenbufen was intercalated into Li-Al- as well as into Mg-Al-, Zn-Al- and Fe-Al-LDHs [98]. Whereas Mg-LDHs can be derived from brucite ($Mg(OH)_2$), Li-Al-LDHs can be derived from $Al(OH)_3$. Exemplarily, a Li-Al-Cl-LDH was obtained by the intercalation of LiCl in $Al(OH)_3$ (gibbsite), with Li^+ ions filling vacant octahedral voids in the hexagonal $Al(OH)_3$ lattice [99]. Intriguingly, a Li-Al-Cl-LDH with a rhombohedral stacking sequence was synthesized by intercalation of LiCl in bayerite. This LDH system showed anion exchange capability towards dicarboxylate anions, e.g. malonate and fumarate [100]. However, a variation of the cation ratio could not be found in literature, hence the formulae reported comprised $[Li_{0.33}Al_{0.66}(OH)_2]$ and $[LiAl_2(OH)_6]$, respectively [87].

Various cations and cation combinations were reported to form LDHs. In contrast to single compounds, such as the corresponding M^{II}- or M^{III} hydroxides, properties of the LDHs can be altered by the variation of the ion species, cation ratios and by incorporation of further elements. Mg-LDHs with different trivalent cations and Mg-Al-LDHs with different cation ratios were employed in course of the examinations described in sections 5.2 and 5.3.

Inorganic anions

Besides the variation of cations, the targeted intercalation of inorganic anions into the interlayers is another possibility to tune the composition and by this properties of the respective LDH system. Furthermore, the uptake of potentially hazardous anions by LDH materials is of interest with regard to safety applications.

As in hydrotalcite, simple anions such as Cl^-, HPO_4^{2-}, I^-, NO_3^-, OH^- and SO_4^{2-} were found in the interlayers of different LDHs [87]. In general, the following schematic stability sequence of monovalent mineral acid anions was found: $OH^- > F^- > Cl^- > Br^- > NO_3^- > I^-$, whereas for bivalent anions $CO_3^{2-} > SO_4^{2-}$ was reported [15]. This sequence was complemented with further species and the comparison between monovalent and bivalent anions, leading to: $SO_4^{2-} > F^- > HPO_4^{2-} > Cl^- > B(OH)_4^- > NO_3^-$ [101]. These sequences imply the particular challenge of the exclusion of carbon dioxide and carbonate ions in the syntheses of LDHs of other anions, which are less stable. Exemplarily, the extensive affinity of carbonate ions in the Mg-Al-LDH system and, by this, the decrease in anion adsorption and exchange properties (for 2,4,6-trinitrophenol and dodecylbenzylsulfonate, respectively) of the CO_3-LDH in comparison to a Cl-LDH were shown [102].

The capability to incorporate various inorganic anions opens the possibility to use LDHs for the uptake of anions that have to be removed from the respective environments. For example, the uptake of boron species [103] and oxyanions such as arsenate or chromate [85] in the context of water purification were evaluated. Oxyanions of heavy metals such as $V_{10}O_{28}^{6-}$ and $Mo_7O_{24}^{6-}$ [104] and Keggin ions ($H_2W_{12}O_{40}^{6-}$) [105] were intercalated into Mg-Al-LDHs, whereas the stability sequence SeO_4^{2-} > CrO_4^{2-} > MoO_4^{2-} was found for a Ca-Al-SO_4-LDH system [106]. Furthermore, Ni-Al-LDHs with intercalated coordination compounds such as hexacyanoferrate(II) [107] and hexacyanoferrate(III) [108] were synthesized.

Various inorganic anions, including simple anions derived from mineral acids as well as more complex polyoxometalates were incorporated into LDH interlayers. Stability sequences depending on the intercalant were found, allowing for targeted variation of LDHs and LDHs based materials.

Organic anions

Besides the inorganic anions mentioned, a variety of organic anions were reported to be suitable intercalants for different LDH systems allowing for further variation of this class of materials. Intercalation of functional and bioactive anions, respectively, gives possibilities for potential bio applications. Also, the potential for a controlled release from LDH based materials was in the focus of many studies. In the following, a brief overview on organic intercalants and potential application fields is given.

Comparison of inorganic LDHs with organically modified LDHs emphasizes the influence of the interlayer anion. Particle charge, surface polarity, exchange and adsorption properties were shown to be affected strongly by the interlayer anion, as it was exemplarily assessed for a Mg-Al-Cl-LDH and a dodecylsulfate-LDH [109].

Intercalation and combination, respectively, with functional organic anions might widen the spectrum of applications of LDH-based materials. In some cases, enhanced acid resistance [110] and thermal stability [111] were reported for intercalated organic molecules. LDHs with thermally stabilized dyes were considered for the potential application in paints [112] and for the use in solid-state dye lasers and chemical sensors [113]. Labeling of LDH particles with fluorescent dyes for particle tracking in biological environments was evaluated [114], and the uptake of non-biodegradables and dyes is also of interest for wastewater cleaning [115].

Combination with bioactive agents opens pathways for various applications in the field of biomaterials and biomedicine. Hence, this topic has found consideration in numerous journal articles and reviews and merely an overview and comparably few examples can be considered for this discussion. With regard to medical application (subsections 2.2.4 and 2.2.5) different substance classes were reported to be suitable for intercalation and release systems: e.g. antibiotics, anticancer agents, vitamins, amino acids and peptides, anticardiovascular agents, agents for diabetes or osteoporosis treatment, antifibrinolytic agents, antihypertensives, liposomes, antimycotic, anticoagulants, antioxidants immunosuppressant corticosteroids and nucleosides [24]. Numerous non-steroidal antiinflammatory drugs (NSAIDs) were found to be suitable for the intercalation in LDH interlayers [23]. In some cases, multiple organic modifications were performed with LDHs, exemplarily, the enzyme penicillin G acylase was immobilized on a glutamate-Mg-Al-LDH [110].

With regard to the use for pharmaceutical and nutraceutical applications, Zn-Al-LDHs with vitamins (vitamin A: retinoic acid, vitamin C: ascorbic acid and vitamin E: tocopherol) as intercalants were synthesized and examined [116].

A LDH system that can be found remarkable frequently is the Mg-Al-LDH system. Many examples of organically modified Mg-Al-LDH were reported, comprising substances from the classes mentioned above [24]. Amongst various others, vitamin derivates (thiamine pyrophosphate) [117], NSAIDs (diclofenac and ibuprofen) [118,119], antibiotics (chloramphenicol) [120,121], amino acid anions (derived from L-proline, aspartic acid and glutamic acid) [122,123] and nucleoside monophosphates (CMP, AMP and GMP) were intercalated. Even the intercalation of DNA was reported [124,125], but doubts remain with regard to the actual nature of the material, i.e. whether it is a true intercalation compound. A selection of intercalants is shown in Fig. 9.

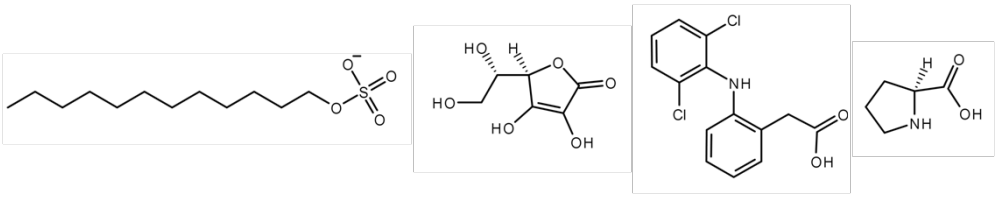

Fig. 9: From left to right: dodecylsulfate (anionic surfactant), ascorbic acid (vitamer, vitamin C), diclofenac (NSAID) and L-proline (amino acid).

Numerous intercalation compounds comprising different organic anions with various LDHs were reported, indicating a vast tunability of LDHs. In particular

the organic modification with bioactive compounds might vastly widen the spectrum of possible application. Also, enhanced stability of intercalated species in comparison to pristine substances was reported in some cases. However, stability and exchange properties of the intercalants under *in vivo* or complex *in vitro* conditions have been barely in the focus of investigations.

Orientation of anions

Not only can the choice of the respective anions, but also their orientation within the interlayers influence the properties of the respective LDH. Furthermore, stability and properties of the anions were also affected by intercalation as reported in some cases. Variations of the orientation and the alignment of the interlayer anions result in a shift of interlayer distances, which can be easily detected by X-ray diffraction [126].

Orientation and alignment of the respective anions was shown to depend on the choice of intercalant. Exemplarily, ascorbate and citrate anions were found as a monolayer stacking in Zn-Al-LDHs, whereas retinoate and indole acetate were found as a bilayer stacking in similarly prepared Zn-Al-LDHs (Fig. 10) [116].

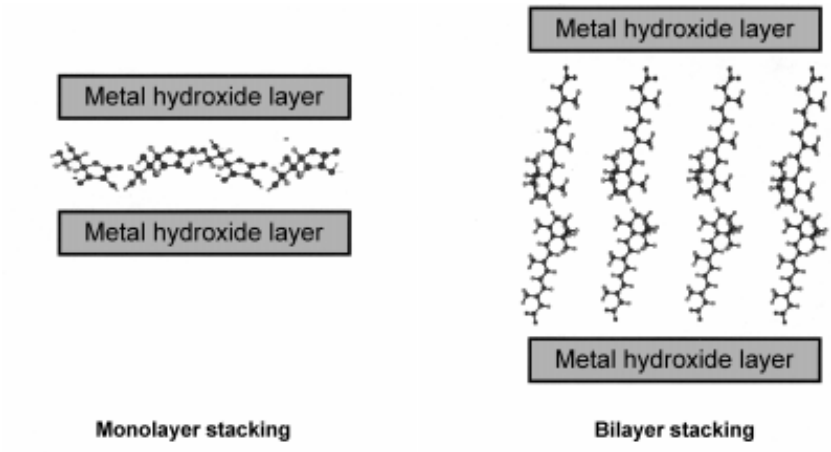

Fig. 10: Anion stacking in the interlayers of LDHs (modified from ref. [116]).

The orientation and in particular the alignment of methyl orange intercalated in Mg-Al-LDH were considered to be responsible for the photostability of the dye molecules. The rigid LDH layers stabilized certain configurations and by this hindered photoisomerization [113]. Tilt angle (74°), arrangement and enhanced stability of the methyl orange ions were confirmed by molecular simulation [127].

Also, orientation can be influenced by the synthesis conditions. Sterically demanding dodecyl sulfate ions were reported to be intercalated via different methods. Depending on the synthesis protocols, varying degrees of interlacing of the dodecyl chains were found, leading to LDHs with different basal spacings: ≈ 26 Å, ≈ 36 Å and ≈ 47 Å (Mg-Al- and Ni-Al-LDH systems). Two different cases of interlacing are schematically shown in Fig. 11 (according to information from ref. [128]). However, basal spacings in these systems were reported to be independent of the amount of dodecyl sulfate in the interlayers [128]. Besides orientation, swelling behavior of Mg-Al-, Ni-Al- and Co-Al-LDHs intercalated with 2-hydroxyethanesulfonate was examined. Basal spacing were found to be increased, depending on relative humidity [129].

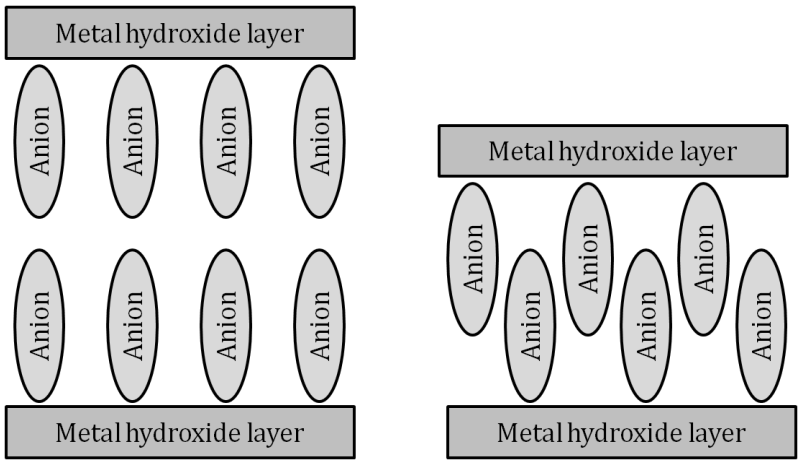

Fig. 11: Two different forms of anion interlacing in LDH interlayers (according to information from ref. [128]).

Orientation and alignment of the interlayer anion were shown to influence the properties of both the intercalated species and the resulting LDH. In particular the interlayer distance is affected by orientation and alignment, and hence was in the focus of material characterization. Thus, besides composition, orientation and alignment are variable attributes that have to be considered in the course of LDH material evaluation.

Morphology

Variation of particle morphology offers further possibilites for the modification of LDHs. Commonly, LDH particles found were reported as hexagonal plates [130]. SEM images of hexagonally shaped Mg-Al-CO_3-LDH nanoparticles are shown in Fig. 12. The SEM images were collected in the course of the diploma thesis of the author of this thesis: “Doppelhydroxide mit Schichtstruktur: ihr

Auflöseverhalten und ihre Eignung als Implantatbeschichtung" ("Layered double hydroxides: their degradation behavior and their applicability as implant coatings", 2010, Leibniz Universität Hannover).

Employing sophisticated synthesis protocols that included the addition of, e.g., organic solvents and surfactants, and various types of heat treatment, respectively, a variety of morphologies were generated. However, novel morphologies predominantly resulted from stacking and intergrowth of the hexagonal particles mentioned.

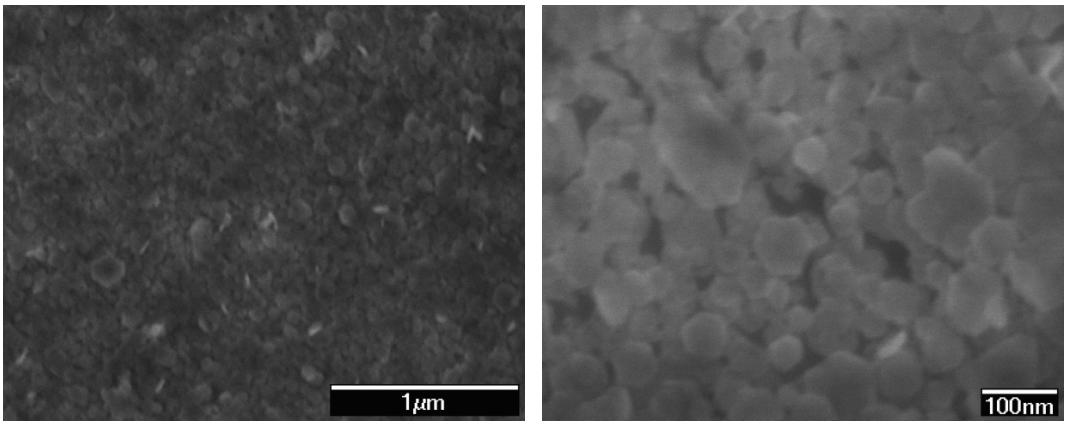

Fig. 12: SEM images of hexagonally shaped Mg-Al-CO_3-LDH nanoparticles as a coating on a TiAl6V4 substrate.

Assembly of sheet-shaped LDH particles led to the formation of flower-like and octahedron-shaped Co-Fe-LDH particles, respectively. Synthesis protocols comprised an ethylene glycol based reaction solution in the presence of lysine [131]. Rod-like LDH particles with stacked platelets were obtained from an isooctane based solution with dodecylsulfate, 1-butanol, and a nonionic triblock copolymer P1940 as surfactants [132]. Interestingly, the morphology changed to belt-like structures in which the LDH particles exhibited an oriented growth, corresponding to a varied aspect ratio, when P1940 was added during an earlier step in the synthesis [132]. Another approach that resulted in LDH particles with varied aspect ratio employed high concentrations of H_2O_2. LDH sheets with reduced thickness were obtained via the separation of Zn-Al-LDH layers, presumably triggered by the decomposition of the H_2O_2 [133].

Also hollow particles at the low micrometer scale were obtained. Ni-Co-LDH nanocages were obtained by exposing a metal-organic framework precursor, in particular zeolithic imidazolate framework-67 (ZIF-67), to a solution of nickel nitrate in ethanol. After reflux, hollow LDH nanocages formed from thin LDH platelets (Fig. 13) [134].

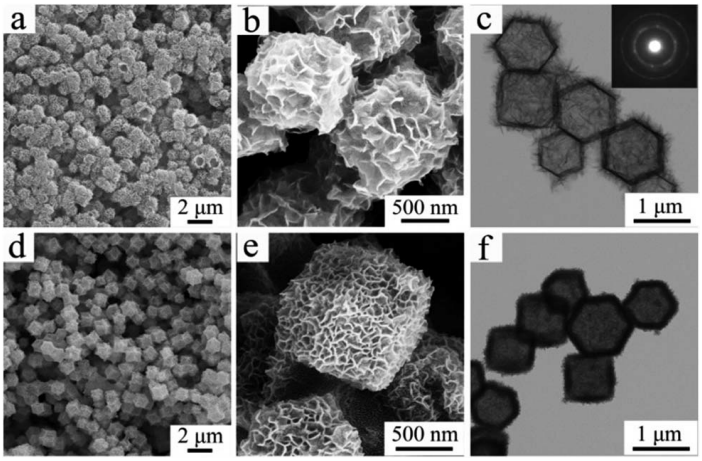

Fig. 13: SEM and TEM images of Co-LDH (a-c: Mg-Co-LDHs, d-f: Ni-Co-LDHs) cages. The selected selected area electron diffraction (SAED) pattern of a single Mg-Co-LDH cage is shown in the inset of c) (modified from ref. [134]).

Mg-Fe-LDH microspheres were synthesized by an autoclave treatment of a metal salt solution in ethylene glycol. The microspheres were also composed of LDH platelets [135]. Solid Mg-Al-LDH microspheres, also consisting of smaller flake-shaped LDH particles, were obtained by spray drying of an LDH aerosol dispersion [136].

A centimeter scale monolithic xerogel from a Mg-Al-LDH system was obtained by a LDH precursor which was synthesized by sol-gel reaction in water/ethanol with poly(ethylene oxide) and propylene oxide. Subsequently to calcination, the precursor was exposed to a sodium carbonate solution, and exhibited hierarchical channels and enhanced sorption affinity for pyranine [137]. Neglecting the exposure to an aqueous solution subsequent to calcination, the thermally caused decomposition of a Mg-Al-LDH was further employed for the targeted synthesis of a hierarchical, porous mixed Mg-Al oxide [138]. Both hierarchical materials, LDHs and mixed metal oxides, were considered interesting for applications in, e.g., catalysis and adsorption [137,138].

LDH particles at nanometer and micrometer scale with novel morphologies such as hollow and solid spheres, respectively, were obtained via different synthesis routes. Commonly, novel morphologies were deducible from smaller, platelet-like LDH particles. By employing sophisticated reaction protocols, also particles with varied aspect ratios and substances with enhanced surface properties were obtained.

2.2.3 Synthetic methods

An overview on various possibilities to obtain and modify LDHs is given in the following subsection. In accordance with the variability described above, composition and morphology and thus the properties of the products can be influenced at various steps of the synthesis protocols. Precipitation is commonly the method of choice in order to obtain LDHs. Depending on the affinity of the interlayer anion, anion exchange reactions can be employed to obtain novel materials such as organically modified LDHs. Calcined LDHs also feature a structure memory effect, which allows the LDHs to be reformed from the mixed metal oxides when exposed to aqueous conditions [16]. For many LDH systems, protocols for the synthesis of colloidal suspension were reported. Furthermore, novel and rare syntheses are discussed.

Precipitation

Coprecipitation is a common approach which was successfully applied in the synthesis of various LDHs. This method was also chosen for the synthesis of the LDH materials applied in our work as described in chapters 4 and 5. In principle, precursor solutions of metal salts and base are either combined in a reaction vessel or one solution is added to the other. Different anions can be added in form of soluble salts to the base solution, if the respective anion is stable under these alkaline conditions. Coprecipitation can be performed including pH control, where the range is determined by the solubility of the separated metal hydroxides. As expected, the pH required to form the desired LDH system is increased with increased solubility of the M^{II} hydroxide. For a sufficiently soluble M^{III} hydroxide (e.g. Cr^{3+}) the precipitation occurs in one step, whereas for lowly soluble M^{III} hydroxides (e.g. Al^{3+} and Fe^{3+}) the metal hydroxides were found as intermediates. Due to their role as reactants for the LDH formation, the pH is increased with decreased M^{III} hydroxide solubility. [88,89]. If applicable, amphoteric properties of the respective M^{III} hydroxides have to be considered in the course of precipitation and further treatment including strong bases in order to avoid dissolution of the products formed.

Coprecipitation can be performed with various simple anions; however, the exclusion of carbonate is a key challenge. Whereas according to many synthesis protocols NaOH is used as the base, ammonium hydroxide was used for the synthesis of nitrate LDHs (Mg-Al) which are of high interest for anion exchange reactions due to the facile exchange of nitrate ions. Despite the absence of an inert gas blanket, nitrate ions were intercalated preferentially, presumably due to a complexation of carbonate ions by ammonium ions [139].

Following an alternative pathway, the homogeneous precipitation is triggered at elevated temperatures by the decomposition of urea, which is added to the metal salt solution prior to heating. The homogeneous precipitation occurs due to the formation of ammonium carbonate in this one-pot approach. Following this method, aluminium-LDHs with Mg^{2+}, Ni^{2+} and Zn^{2+} as bivalent cations were successfully synthesized first [140]. A similar approach was used for the precipitation of hydrotalcite [141] which can be designated the prototype for Mg-Al-LDHs. However, this method is accompanied by the presence of large amounts of carbonate ions, which renders this method unpractical for the synthesis of reactive precursor LDHs such as nitrate LDHs.

Anion exchange

The inherent capability of LDHs to perform anion exchange reactions is based on different affinities of anions to the respective interlayers and entropical reasons. This method was used and investigated for various LDH, including inorganic LDHs [15,142] as well as organically modified LDHs [143]. Despite the large and increasing number of LDH compounds obtained via the anion exchange route, the exact mechanism has not been described yet.

Commonly, anion exchange reactions are performed by adding a solution containing the dissolved anion to a dispersion of the precursor-LDH. The mixture is subsequently stirred for a period of days at room temperature or slightly elevated temperatures.

Availability of a reactive precursor LDH with a weakly bonded anion is crucial for the anion exchange. Since anions such as nitrate or chloride anions can be relatively easily replaced by various other anions, NO_3-LDHs and Cl-LDHs are interesting precursors for the synthesis of various other LDHs. Exemplarily, ciprofloxacin (a broad-spectrum antibiotic) was intercalated into a Zn-Al-NO_3-LDH system [111], and diclofenac (an NSAID) was intercalated into a Mg-Al-Cl-LDH [119].

Intercalation of hydrophobic drugs into the LDH interlayers is of high interest for biomedical application; however, the hydrophobic nature presents the need for sophisticated reaction protocols, comprising auxiliary substances. Hydrophobic agents, i.e. gramicidin and amphotericin B, were successfully intercalated into a NO_3-LDH system using cholate and 6-*O*-(*N*-heptylcarbamoyl)-methyl-α-D-glucopyranoside (Hecameg), respectively, as detergents [144]. The structures of ciprofloxacin and amphotericin B are shown in Fig. 14.

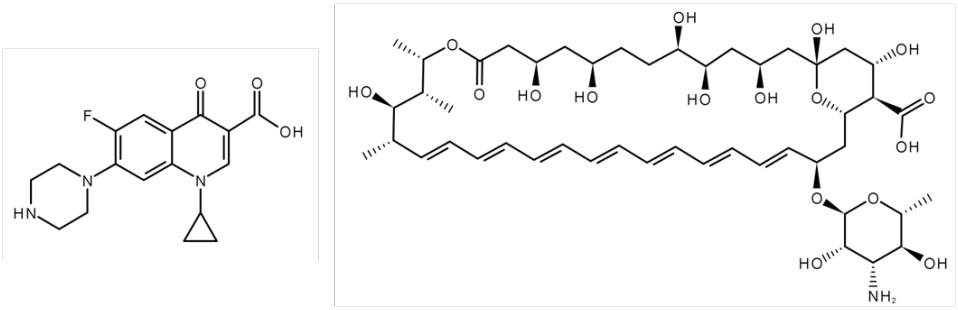

Fig. 14: Intercalated anions, left: ciprofloxacin (antibiotic) and right: amphotericin B (pharmaceutical fungicide).

Recrystallization

Another possibility for the variation of LDHs with regard to the anion in the interlayer exploits the structural memory effect of LDHs. After calcination at moderate temperatures (typically between 573 K and 773 K) the calcination products, mixed metal oxides, were shown to reform the layered structure when exposed to aqueous solutions. In the course of the recrystallization of the mixed metal oxides, anions from the respective solutions are incorporated in the structure of the re-formed LDH [16].

This method was shown to be suitable for the targeted intercalation of inorganic and organic anions such as polyoxometallates and dodecyl sulfates, respectively. For this, calcined Mg-Al-LDHs (723 K) were added to decarbonated, water-based solutions of the respective anions [145]. Over the years, various sophisticated LDHs were obtained following and adjusting this approach. Comparison of Mg-Al-Cl- with Mg-Al-CO_3-LDH indicated that reconstruction and anion adsorption properties of the calcined material depend on interlayer anion and crystallinity of the pre-calcined LDH [102].

Colloidal suspensions

Research on LDH particles with small size gained an increasing interest, and availability of long-term stable nanosuspensions is of high interest for many applications [146]. In the following, an overview on synthesis, particle size control and potential with regard to biomedical applications of LDH nanosuspensions is given.

The successful synthesis of Mg-Al-LDH nanosuspensions was reported for different anions and also for varying Mg:Al ratios. Fabrication of sols from bulk material comprised energy intake from ultrasonication or hydrothermal conditions. Average particle sizes were reported to be increased by hydrothermal treatment time. It is noted that both a too short and a too long

hydrothermal treatment resulted in unstable suspensions [17,18]. Particle size distribution curves of Mg-Al-Cl-LDHs in the course of hydrothermal treatment are shown in Fig. 15 (from ref. [17]).

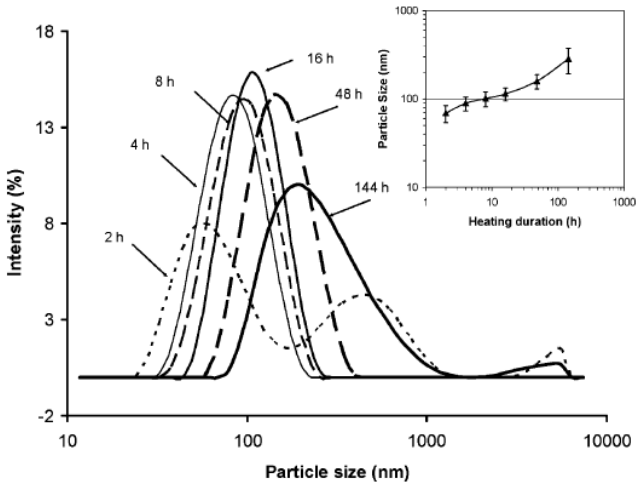

Fig. 15: Particle size distribution of Mg-Al-Cl-LDHs in the course of hydrothermal treatment at 100 °C. Distribution curves were obtained via photon correlation spectroscopy (from ref. [17]).

Employing an alternative source of energy intake, a colloidal Mg-Al-OH-LDH suspension was obtained by using laser ablation of magnesium and aluminium targets in water. Cation ratio and phase purity depended on the synthesis parameters, in particular ablation duration [147].

The particle size distribution was reported to be narrowed by separation of nucleation and aging steps in course of the precipitation. Thus, coprecipitation of a metal salt precursor solution and an alkaline solution in a colloid mill with a following aging phase resulted in a narrow size distribution for Mg-Al-LDHs [148]. Following a different approach, a narrow size distribution of Ca-Al-LDH nanoparticles was reported to be achieved by using the aqueous phase of reverse micelles (dodecylsulfate in isooctane and butan-1-ol) as nanoscale reactors for precipitation. Furthermore, particles size was varied by the water:dodecylsulfate ratio [149].

With regard to biomedical applications, LDH particles with small size are interesting as delivery vehicles with regard to protection of the intercalated drug and cellular uptake capacity. Exemplarily, Mg-Al-LDH nanoparticles were shown to be an interesting delivery system for intercalated Green Fluorescent Protein (GFP) [150] and intercalated, small interfering RNAs (siRNAs). In the latter study, intercalation and delivery were investigated depending on the

average size of the LDH nanoparticles, whereas smaller particles were found to be of more promise [151].

Synthesis of nanosuspensions and control of particle size were achieved by energy intake, i.e. ultrasonication and hydrothermal treatment, for different LDH systems. Organically modified LDH nanoparticles are also of interest for biomedical applications, due to their promise as delivery vehicles. Furthermore, LDH nanosuspensions are expected to feature a homogeneous distribution of the particles, which are orders of size smaller than the components of typical processing systems such as nozzles of spray-coating devices (see subsection 2.2.4 and sections 4.2 and 5.2).

Further approaches

The synthesis methods presented above each present their own advantages and disadvantages. Development of new synthesis routes or the transfer of synthesis routes known from other chemical systems might contribute to the versatility of layered double hydroxides. Some sophisticated, yet rarely used, synthesis protocols are discussed here.

As mentioned above, in the context of corrosion protection, the formation of Mg-LDHs on the surface of metallic magnesium was used as a synthesis route (subsection 2.1.1.). Pure magnesium was exposed to a moderately acidic, aqueous solution of Fe^{3+} and a hydrogen carbonate / carbonate system in order to generate Mg^{2+} ions. In principle, an increase of pH and temperature resulted in the growth of an oriented Mg-Fe-LDH film that increased the substrates corrosion resistance [41]. A similar approach utilizing a Mg-Al-Zn alloy led to the formation of a LDH film comprising Mg^{2+} and Al^{3+} [42]. In a different approach, a Mg-Al-LDH was synthesized by hydrolysis of metal hexanolate precursors, which in turn were obtained by reaction of the respective metals with the alcohol [152].

An approach in the solid state that excluded the employment of a solvent was carried out for the synthesis of a Li-Al-LDH by grinding precursors, i.e. $LiOH{\cdot}H_2O$ and polycrystalline $Al(OH)_3$, in a mortar, and subsequently exposing the mixture to water vapor [153]. Also a Mg-Al-LDH with hydrogen carbonate and carbonate as anions was obtained by grinding $Mg(OH)_2$, $Al(OH)_3$ and $NaHCO_3$ in a planetary mill. The product was obtained after washing with water and subsequent drying [154]. As mentioned above, successful exclusion of carbonate ions in the preparation of NO_3-LDHs is of interest for subsequent use of the LDHs as reactive precursors for organically modified LDHs. Employing the mechanochemical approach, grinding of NaOH pellets with magnesium nitrate

and aluminium nitrate led to the formation of a carbonate-free Mg-Al-NO_3-LDH. Further treatment and purification included washing with deionized water and drying under vacuum [155].

Another approach for the intercalation of organic substances into LDHs, avoiding the employment of water as solvent, comprised the thermal reaction of molten sebacic acid with Mg-Al-CO_3-NO_3-LDH. The substances were mixed thoroughly and heated to 150 °C. Intercalation occurred to a certain degree, however a polyphasic product was obtained [156]. A precursor approach was used for the intercalation of cobalt phthalocyanine into the layered antimony hydrogen phosphate ($HSb(PO_4)_2$). For this, cobalt exchanged (8%) phosphatoantimonic acid was refluxed with molten 1,2-dicyanobenzene, hence, the guest molecule was synthesized *in situ* [157].

2.2.4 Development of layered double hydroxides directed towards application

Layered double hydroxides are a versatile class of materials, providing a variety of possibilities in order to meet the demands of respective applications. In particular, the inherent possibility to vary the composition of the respective LDH system within wide ranges while maintaining the general formula is interesting for numerous potential applications. Over the years, LDHs were shown to be of interest as antacids and as components in various systems such as in catalysts and polymers. LDH particles were shown to enhance key properties when supplemented, and appear to be promising components in sophisticated drug delivery systems. For both technical and biomedical applications, various methods were developed and applied in order to coat substrates with LDHs. In the following, a selection of promising LDH based systems and their development for application are presented.

Antacids

An established application of the Mg-Al-CO_3-LDH system is its administration in case of acid indigestion. Hydrotalcite, $[Mg_6Al_2(OH)_{16}][CO_3]\cdot 4H_2O$, has emerged as a commercially available antacid (e.g. Talcid®, Bayer AG), which is promising with regard to potential clinical applications of Mg-Al-CO_3-LDHs derived from the studies presented in chapters 4 and 5. Synthesis protocols and antacid activity of the Mg-Al-CO_3-LDH system have also been in the focus of recent investigations [22].

The proton scavenging properties of LDHs are also of interest with regard to the supplementation of LDH particles to poly(vinyl chloride), PVC. Thermal

decomposition of PVC proceeds with the formation of hydrochloric acid, which entails certain danger potential and furthermore autocatalyses dehydrochlorination of PVC. Mg-Al-CO_3-LDH particles were shown to compensate the protons of the acid and stabilize the PVC by electrostatic attraction of the chloride ions [158].

Polyglycolic acid (PGA), polylactic acid (PLA) and their copolymers (PLGA), are known as established biomaterials. However, in the course of the biodegradation of these polyesters acidification, caused by acidic monomers, is expected. Supplementation with alkaline inorganic, filler materials was reported to successfully compensate this acidification [159]. Hence, the mildly alkaline properties of CO_3-LDHs could also contribute to combined materials comprising biodegradable polyesters and LDHs.

Catalysts

A traditional field of application is catalysis, exploiting the reactivity of certain LDH systems in organic reactions as reported in some studies. Exemplarily, a Cu-Zn-Mn-Fe-Al-LDH showed reactive behavior towards hydrogen peroxide oxidation of phenol [21] and Mg-Fe-LDH microspheres towards the electrooxidation of ethanol [135]. Hybridization of LDHs with semiconducting nanoparticles was found to be of promise for photocatalysis, due to lifetime increase of transient electrons and holes [19]. Exemplarily, ZnO nanoparticles deposited on a Mg-Al-LDH showed enhanced photocatalytic activity towards the decolorization of Acid red G in comparison to pristine ZnO particles [160].

Polymer fillers

Application of LDHs as components in nanocomposites and nanohybrids gained interest due to processability and variability of LDHs. The latter includes the possibility of LDHs to be organically modified [19,20]. For large- and small-scale applications, LDHs were supplemented to rubber composites, such as nitrile rubber composites, butadiene rubber composites and silicone rubber composites in order to improve optical, mechanical and thermal properties [126].

With regard to thermal resistance of the composite material, LDHs were also combined with carbon modifications. The joint heat protection effect of LDHs (Li-Al, Mg-Al and Co-Al) and carbon nanotubes (MWCNTs) in silicones demonstrated the applicability of LDHs as flame-retardants [161]. A Ni-Fe-LDH/graphene combination showed activity for reducing fire hazard in epoxy composites [162].

The enhancement of thermal resistance by the supplementation with LDH particles is attributed to the release of water vapor and a barrier effect, separating the substrate from the oxygen [126]. Depending on the polymer/LDH combination, the formation of an oxidative resistant char layer, potentially promoted by the LDH, contributes to the thermal resistance [126,162].

Drug delivery vehicles

LDHs as key components in sophisticated drug delivery systems have gained an increasing interest in the field of degradable biomaterials. Over the years, a vast selection of drug/LDH compounds and combinations, respectively, were synthesized and evaluated for their potential as release systems [23,24]. In the following, an overview on approaches in order to control release rates and methods for the examination of drug-LDH compounds is given. Furthermore, the necessity of the application of intercalation compounds in contrast to more simple systems is discussed.

A central issue of drug release systems is the control of the release rates. Since depending on the application, a burst release of the agent can be advantageous or detrimental [163], release systems have to be adjustable. A schematic release profile of with burst release characteristics in comparison with a release profile of a controlled release is shown in Fig. 16 (according to information from ref. [163]).

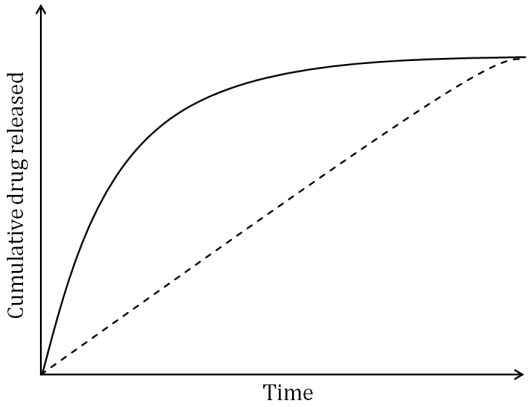

Fig. 16: Schematic comparison of release profiles with burst release profile (solid line) and with controlled release behavior (dashed line), according to information from ref. [163].

Release from LDHs was shown to be basically controlled by the pH of the environment and the properties intrinsic to the drug/LDH system. In particular,

cation binding strength and nature of the intercalant were shown to determine the dissolution kinetics. Dissolution was shown to be influenced by surface acid-base equilibria and detachment of metal cations from protonated LDH surface sites [164]. Hence, variation of the LDH system in a particular drug/LDH combination might be sufficient in order to influence the release properties [165].

As stated above, intercalation of drugs into LDH interlayers is not limited to hydrophilic agents. Intercalation of hydrophobic agents gramicidin and amphotericin B into Mg-Al-LDH was performed by the use of detergents [144]. Additionally, an LDH-based release system for neutral and lipophilic substances was obtained by intercalation of a phospholipid bilayer into Mg-Al-LDH. As a model for a release system for lipophilic drugs, release of 1,6-diphenyl-1,3,5-hexatriene was analyzed and found to be attenuated for a period of weeks [166].

The various studies on intercalation and release of various drugs performed [23,24] mainly focused on the physicochemical *in vitro* properties of the drug-LDH compounds. For some drug-LDH systems, subsequent and complementary cell culture studies comprising different approaches were reported. Exemplarily, a Mg-Al-heparin-LDH was obtained, and found to be a promising nanocarrier system due to its *in vitro* release behavior and the stability of the heparin in the interlayers [167]. Stability was confirmed by molecular dynamics simulations with regard to the use of heparin-LDH systems for cellular delivery [168]. In subsequent assays with smooth muscle cells, the potential of heparin-LDHs for anti-restenotic therapy was examined [169], focusing amongst others on the uptake of the drug by the cells and the influence of the LDH on cellular delivery [170].

Despite the vast number of drug-LDH systems investigated, few *in vivo* studies were performed. As for synthesis and *in vitro* studies, NSAID-LDHs were of central interest. Mice were fed with indomethacin-LDH and ketoprofen-LDH, respectively, and showed enhanced gastrointestinal compatibility for the drug-LDH system in comparison to the pure drugs [171,172]. Furthermore, a Zn-Al-diclofenac-LDH containing dispersion was administered as eye-drops to New Zealand rabbits. No eye irritation was found and LDH was considered as a promising ocular drug delivery system [173]. In another mice study, a Mg-Al-LDH was evaluated as a DNA vaccine delivery vector with regards to restrain tumor formation and melanoma growth [174]. When intercalated with podophyllotoxin, Mg-Al-LDH was found effective against tumor cells *in vitro* and *in vivo* (mice) [175].

Most studies concentrated on the intercalation of the drugs and on the properties of the drug-LDH intercalation compounds. However, intercalation of

drugs into LDH interlayers is a demanding process that has to be adjusted for every drug/LDH system. Drug delivery systems that comprise mixtures of the respective drugs with LDH can be obtained more simply. Exemplary, drug-loaded LDH films (e.g. with tetracycline or vancomycin) were in principle synthesized by solvent evaporation of a Mg-Al-CO_3-LDH suspension which was supplemented with the respective drug solutions [176]. Besides simplicity in production and processing of the mixtures, synthesis protocols seem to be more easily transferable. Drug delivery performances of ciprofloxacin/LDH mixtures as coatings are discussed in chapter 5.

Adsorption is a further method of interest to immobilize drugs on LDHs. Interactions between drugs and LDHs are expected to depend on the charge of the respective drugs [176]. The expectation would be that the positively charged LDH layers would preferable adsorb species with negative charges [177]. Nonetheless, ibuprofen could be adsorbed both as an anion as well as in form of a neutral copper complex on a Mg-Al-LDH. However, in comparison to a Mg-Al-ibuprofen-LDH intercalation compound, the amount of immobilized drug was decreased [178]. Furthermore, zwitterionic tetracycline and positively charged vancomycin were found to bind to Mg-Al-CO_3-LDHs [176]. As mentioned above, adsorption ability of the clay-type material was found to be tunable by the cation ratio M^{II}:M^{III} [97] (subsection 2.2.2). Also, adsorption properties depended on the choice of anion in the interlayers, e.g. Cl-LDHs showed enhanced performances in comparison to CO_3-LDHs [97,102].

An LDH based nanohybrid system that allows for an external control was obtained and examined for the magnetic field controlled release of diclofenac and ibuprofen. Drug release from the magnesium ferrite/Mg-Al-LDH core-shell nanoparticles depended on particle size, core content of the particles and strength of the external magnetic field. Intriguingly, the on-off operation of the magnetic field yielded in a pulsatile drug release profile. The nanohybrids were assessed suitable for the administration by injection and for drug targeting [179,180].

LDHs served as drug delivery vehicles and key components in drug delivery systems, respectively, applied in the course of *in vitro* and *in vivo* studies. Whereas most studies concentrated on intercalation compounds, studies on drug/LDH mixtures and adsorption compounds were reported, as well. The latter two would allow for a simplified preparation, still exploiting the variability of the LDH material class. Coating of implants with drug-loaded LDHs might allow for a local drug delivery, avoiding a systemic dosage with the respective drug. This is of high relevance for antibiotics, since bacterial infection

during and after surgery is a major concern, as is the formation of antibiotic resistances.

Feasibility of LDH coatings for technical and medical applications

Functional coatings on substrates can provide a wide spectrum of advantages besides aesthetic demands. Coatings made of LDHs and derived of LDHs, respectively, can be prepared by various approaches and are of interest for technical and biomedical applications [181].

LDH coatings can either be grown *in situ* on the surface of metal substrates or can be obtained by the processing of precursor suspensions. As mentioned above, magnesium and magnesium alloys were endowed with *in situ* grown LDH layers in order to enhance the corrosion resistance of the metal substrates [41,42]. An *in situ* grown Zn-Al-LDH on aluminium substrates was reported to feature intrinsic self-healing properties by dissolution/recrystallization processes in NaCl solution [182]. In order to coat substrates with LDHs storable and processable LDH suspensions are of importance. In general, LDH coating techniques comprise the targeted separation of LDH particles from a solvent/dispersion medium.

Employing LDH suspensions as precursors, layer-by-layer coating techniques were proven to be practicable for many LDH coatings. Based on the positive zeta potential of LDH particles [177], LDH coatings are expected to attract negatively charged species. By applying alternating sequences of LDH suspensions and solutions/suspensions of the second species, the coating is expected to form due to the electrostatic interaction. By this means, a Mg-Al-LDH based coating was fabricated on quartz substrates for antireflection and antifogging purposes [183] and a Ni-Al-LDH/bi-protein film on an ITO-coated glass substrate. The latter system exhibited electrocatalytic properties towards catechol [184]. Also exploiting the surface charge of LDHs, electrophoretic deposition was applied in order to create LDH coatings. By applying electric fields, Mg-Al-LDHs were successfully attached to aluminium and ITO substrates. In both cases, the LDH coatings exhibited a high degree of orientation [185,186]. Furthermore, a magnetic field assisted layer-by-layer deposition of a Co-Fe-LDH was reported [187].

Another approved method for the fabrication of LDH coatings is spin coating. In course of this method, the glass substrate is wetted with the LDH suspension and subsequently rotated in order to remove the liquid [181]. This method was successfully performed with LDH suspensions comprising different cation combinations (Mg-Al-, Zn-Al- and Co-Al-) and ratios. For the same group of LDH

systems investigated, thinner, yet more stable coatings were obtained following the layer-by-layer approach [188].

It has to be noted that some coating techniques, such doctor blading, are limited to simple substrate geometries and hence inappropriate for geometrically demanding substrates such as medical implants (see subsection 2.2.5). Hence, the shapes of prostheses have to be taken into account for development and employment of LDH coating techniques. Following a simple approach, coating could in principle performed by wetting a substrate with an LDH containing suspension and subsequently applying elevated temperatures. Removal of the solvent/dispersion phase should result in a crust of the formerly mobile particles. Temperature has to be chosen carefully with regard to thermal stability of substrates and coating materials. This approach has been followed in order to fabricate the substrates for the studies presented in sections 5.3 and 5.4. Implants employed in the examinations described in sections 4.2 and 5.2 were coated by spray coating. This technique comprises the application of a nebulized LDH suspension to a previously heated substrate surface. Also when following this approach, temperatures have to be chosen with regard to the substances applied.

Various approaches in order to coat substrates with LDHs were developed and reported. Whereas coating of metallic magnesium with Mg-LDHs was performed following a conversion coating protocol, coating of alternative substrates included application of LDH particles from precursor suspensions. Derived from the vast variety of LDHs synthesized, various precursor suspensions and nanosuspensions are available and LDH particles proved stable under various conditions that can be met in course of processing. Hence, LDHs are a tunable class of material, suitable for various coating techniques with regard to various applications.

2.2.5 Potential application of Mg-LDHs in orthopedics and otolaryngology

In order to increase the longevity of medical implants, functionalization with sustainable biomaterials is of high interest. In this context, the favourable general tunability and processability of LDHs and LDH-based materials have been described above. In particular, magnesium-containing LDHs were evaluated as a promising class of materials. In the following, the applicability of Mg-LDHs with regard to orthopedics and otolaryngology is briefly discussed, and a short overview on the respective medical situations of the application fields is given.

Hip joint replacement

Occurring with more than 800,000 annual cases, total hip arthroplasty (THA) is one of the most common surgeries worldwide [11,189]. THA comprises the restoration of damaged or degenerated structures, mainly caused by osteoarthritis, and furthermore by femoral neck fracture and tumours [190]. Various prostheses were developed to replace damaged areas of bone from the hip joint. A selection of hip prostheses made of titanium alloy and Co-Cr-Mo alloy is shown in Fig. 17 (from ref. [12]). In principle, the stems of the prostheses are designed to be placed into the thighbone, and the cups are designed to fit to the socket of the pelvis bone.

Fig. 17: Photographs of different hip prostheses made of titanium alloy (nr. 1, 3 and 4) and Co-Cr-Mo alloy (nr. 2). The prostheses are equipped with heads made of stainless steel (nr. 2 and 3) and of ceramic material (nr. 4) (from ref. [12]).

Limited longevity and early loosening of the prostheses are key challenges, in particular with regard to young patients and prosthesis revision. Longevity of artificial joint replacements is limited, amongst other causes, by aseptic loosening [190,191]. Therefore, improving the implant fixation by enhancement of the bone ongrowth to the implant is of high interest. A central approach is the development of bioactive coating systems for metal and metal alloy implants. A widely used substance class are calcium phosphates, e.g. hydroxyapatite, $Ca_{10}(PO_4)_6(OH)_2$ [192]. They can be viewed as a current industrial gold standard, and attempts to improve the osseointegration of hip implants have to take their performance as a benchmark. These coating systems are supposed to enhance the bioactivity of the implant surfaces towards the stimulation of bone growth and by this, to minimize the formation of gaps between the bones and the implants.

The promise of magnesium-containing implant coatings with regard to prospective osteoconductive and osteoinductive properties has been explicated in subsection 2.1.1. As described in subsection 2.2.2, magnesium-containing LDHs can be derived from magnesium hydroxide, resulting in a tunable class of magnesium compounds. Furthermore, the processability of LDHs allows for the coating of various substrates, as described in subsection 2.2.4. Hence, magnesium-containing LDH systems have come into focus of biomaterial research with regard to the coating of joint replacement prosthesis. The *in vitro* and *in vivo* evaluation of Mg-Al- and Mg-Fe-LDHs as orthopedic implant coating materials is discussed in chapter 4.

Middle ear ossicular chain replacement

Middle ear diseases, such as chronic otitis media or cholesteatoma, might lead to the loss of the malleus, incus and stapes. These bones are part of the mechanical sound transduction system, the loss of which results in sound conduction impairment. In the course of the medical treatment, these bones can be replaced by a total ossicular replacement prosthesis (TORP) in order to re-construct the sound transduction system from the outer to the inner ear [193]. A depiction of the healthy middle ear, implanted middle ear and prosthesis is shown in Fig. 18a to Fig. 18c (from ref. [193]).

Depending on the indications, functionalization with growth factors and equipment of the prostheses with collagen pads are of interest. The functionalization with growth factors is supposed to enhance implant fixation by improving the connection to the residual stapes at the intersection to the inner ear (Fig. 18b, from ref. [193]). For this, protein-based growth factors, such as the Bone Morphogenetic Protein (BMP2), were attached to a mesoporous silica film at the tip of the prosthesis (in direction to the inner ear). The collagen pad (Fig. 18b, from ref. [193]), commonly made of the patient's own collagen, is inserted in order to enable mechanical mediation of pressure variations and to protect the tympanic drum membrance from contact with sharp edges of the prosthesis. Sound transmission shall be improved by synthetic composite pads featuring adaptable viscoelastic properties [193].

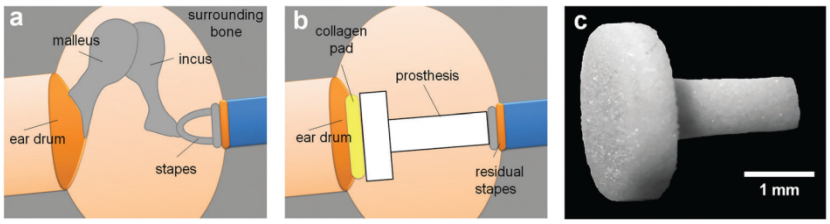

Fig. 18: From left to right: Schematic cross section views of a healthy middle ear (a) and of an implanted middle ear prosthesis (b), as well as a photography of a middle ear prosthesis made of Bioverit® II (from ref. [193]).

Besides sound transmission, also the combating of bacterial infections and formation of bacterial biofilms are major challenges for middle ear surgery. Infections can occur due to persistence or recidivism of the chronic infection, which initially had caused the destruction of the middle ear bones, but can also be introduced during the operation. Hence, antibiotic functionalization of the prostheses with drug delivery systems is of high interest [194,195].

In order to allow for the equipment of the implants with drug delivery systems, biocompatible materials that can be attached to implant surfaces are of interest. A promising class of novel biomaterials with regard to application in otolaryngology are magnesium-containing LDHs. Their processability to coatings and their applicability in drug delivery systems have been discussed in subsection 2.2.4. Furthermore, their tunability and hence adaptability makes them favorable for many application sites, as discussed in subsection 2.2.2. Examination of drug-loaded Mg-Al-LDH coatings on middle ear prostheses in rabbits as well as the *in vivo* degradation behavior and the biocompatibility of pristine Mg-Al-LDH coatings in this unique operation site are discussed in chapter 5. Furthermore, the *in vitro* activity and *in vitro* cell compatibility of ciprofloxacin/LDH mixtures are discussed.

2.3 Bibliography

1. Witte F. The history of biodegradable magnesium implants: a review. Acta Biomater. Acta Materialia Inc.; 2010;6:1680–92.

2. Kulekci M. Magnesium and its alloys applications in automotive industry. Int. J. Adv. Manuf. 2008;39:851–65.

3. Song G, Atrens A. Corrosion mechanisms of magnesium alloys. Adv. Eng. Mater. 1999;11–33.

4. Zeng R, Zhang J, Huang W. Review of studies on corrosion of magnesium alloys. Trans. Nonferrous Met. Soc. China (English Ed. 2006;16:763–71.

5. Feyerabend F, Drücker H, Laipple D, Vogt C, Stekker M, Hort N, et al. Ion release from magnesium materials in physiological solutions under different oxygen tensions. J. Mater. Sci. Mater. Med. 2012;23:9–24.

6. Tie D, Feyerabend F, Hort N, Willumeit R, Hoeche D. XPS Studies of Magnesium Surfaces after Exposure to Dulbecco's Modified Eagle Medium, Hank's Buffered Salt Solution, and Simulated Body Fluid. Adv. Eng. Mater. 2010;12:B699–B704.

7. Witte F, Hort N, Vogt C, Cohen S, Kainer KU, Willumeit R, et al. Degradable biomaterials based on magnesium corrosion. Curr. Opin. Solid State Mater. Sci. Elsevier Ltd; 2008;12:63–72.

8. Zeng R, Dietzel W, Witte F, Hort N, Blawert C. Progress and Challenge for Magnesium Alloys as Biomaterials. Adv. Eng. Mater. 2008;10:B3–B14.

9. Witte F, Kaese V, Haferkamp H, Switzer E, Meyer-Lindenberg A, Wirth CJ, et al. In vivo corrosion of four magnesium alloys and the associated bone response. Biomaterials. 2005;26:3557–63.

10. Staiger MP, Pietak AM, Huadmai J, Dias G. Magnesium and its alloys as orthopedic biomaterials: A review. Biomaterials. 2006. p. 1728–34.

11. Ingham E, Fisher J. The role of macrophages in osteolysis of total joint replacement. Biomaterials. 2005;26:1271–86.

12. Nielsen MS, Carl J, Nielsen J. A phantom study of dose compensation behind hip prosthesis using portal dosimetry and dynamic MLC. Radiother. Oncol. 2008;88:277–84.

13. Janning C, Willbold E, Vogt C, Nellesen J, Meyer-Lindenberg A, Windhagen H, et al. Magnesium hydroxide temporarily enhancing osteoblast activity and decreasing the osteoclast number in peri-implant bone remodelling. Acta Biomater. 2010;6:1861–8.

14. Evans D, Slade R. Structural Aspects of Layered Double Hydroxides. Layer. Double Hydroxides. 2006. p. 1–87.

15. Miyata S. Anion-Exchange Properties of Hydrotalcite-Like Compounds. Clays Clay Miner. 1983;31:305–11.

16. Erickson KL, Bostrom TE, Frost RL. A study of structural memory effects in synthetic hydrotalcites using environmental SEM. Mater. Lett. 2005;59:226–9.

17. Xu ZP, Stevenson GS, Lu C-Q, Lu GQM, Bartlett PF, Gray PP. Stable suspension of layered double hydroxide nanoparticles in aqueous solution. J. Am. Chem. Soc. 2006;128:36–7.

18. Xu ZP, Stevenson G, Lu C-Q, Lu GQM. Dispersion and size control of layered double hydroxide nanoparticles in aqueous solutions. J. Phys. Chem. B. 2006;110:16923–9.

19. Park DH, Hwang SJ, Oh JM, Yang JH, Choy JH. Polymer-inorganic supramolecular nanohybrids for red, white, green, and blue applications. Prog. Polym. Sci. 2013;38:1442–86.

20. Leuteritz a., Kutlu B, Meinl J, Wang D, Das A, Wagenknecht U, et al. Layered Double Hydroxides (LDH): A Multifunctional Versatile System for Nanocomposites. Mol. Cryst. Liq. Cryst. 2012;556:107–13.

21. Zhang L, Li F, Evans D, Duan X. Cu–Zn–(Mn)–(Fe)–Al Layered Double Hydroxides and Their Mixed Metal Oxides: Physicochemical and Catalytic Properties in Wet Hydrogen Peroxide Oxidation of Phenol. Ind. Eng. Chem. Res. 2010;49:5959–68.

22. Parashar P, Sharma V, Agarwal DD, Richhariya N. Rapid synthesis of hydrotalcite with high antacid activity. Mater. Lett. 2012;74:93–5.

23. Rives V, Del Arco M, Martín C. Layered double hydroxides as drug carriers and for controlled release of non-steroidal antiinflammatory drugs (NSAIDs): a review. J. Control. Release. 2013;169:28–39.

24. Rives V, Arco M del, Martín C. Intercalation of drugs in layered double hydroxides and their controlled release: A review. Appl. Clay Sci. 2014;88-89:239–69.

25. Cherubini F, Raugei M, Ulgiati S. LCA of magnesium production. Technological overview and worldwide estimation of environmental burdens. Resour. Conserv. Recycl. 2008;52:1093–100.

26. Du J, Han W, Peng Y. Life cycle greenhouse gases, energy and cost assessment of automobiles using magnesium from Chinese Pidgeon process. J. Clean. Prod. 2010;18:112–9.

27. Waizy H, Seitz J-M, Reifenrath J, Weizbauer A, Bach F-W, Meyer-Lindenberg A, et al. Biodegradable magnesium implants for orthopedic applications. J. Mater. Sci. 2012;48:39–50.

28. Niinomi M, Nakai M. Titanium-Based Biomaterials for Preventing Stress Shielding between Implant Devices and Bone. Int. J. Biomater. 2011;2011:836587.

29. Niinomi M, Nakai M, Hieda J. Development of new metallic alloys for biomedical applications. Acta Biomater. 2012;

30. Hirsch J, Al-Samman T. Superior light metals by texture engineering: Optimized aluminum and magnesium alloys for automotive applications. Acta Mater. 2013;61:818–43.

31. Ding Y, Wen C, Hodgson P, Li Y. Effects of alloying elements on the corrosion behavior and biocompatibility of biodegradable magnesium alloys: a review. J. Mater. Chem. B. 2014;2:1912.

32. Shaw BA. Corrosion Resistance of Magnesium Alloys. ASM Handbook, Vol. 13A Corros. Fundam. Test. Prot. 2003. p. 692–6.

33. Persaud-Sharma D, McGoron A. Biodegradable Magnesium Alloys: A Review of Material Development and Applications. J. Biomim. Biomater. Tissue Eng. 2012. p. 25–39.

34. Kubota K, Mabuchi M, Higashi K. Processing and mechanical properties of fine-grained magnesium alloys. J. Mater. Sci. 1999;34:2255–62.

35. Dursun T, Soutis C. Recent developments in advanced aircraft aluminium alloys. Mater. Des. 2014;56:862–71.

36. Gray JE, Luan B. Protective coatings on magnesium and its alloys — a critical review. J. Alloys Compd. 2002. p. 88–113.

37. Arrabal R, Matykina E, Viejo F, Skeldon P, Thompson GE. Corrosion resistance of WE43 and AZ91D magnesium alloys with phosphate PEO coatings. Corros. Sci. 2008;50:1744–52.

38. Elsentriecy HH, Luo H, Meyer HM, Grado LL, Qu J. Effects of pretreatment and process temperature of a conversion coating produced by an aprotic ammonium-phosphate ionic liquid on magnesium corrosion protection. Electrochim. Acta. 2014;123:58–65.

39. Waltz F, Swider M a., Hoyer P, Hassel T, Erne M, Möhwald K, et al. Synthesis of highly stable magnesium fluoride suspensions and their application in the corrosion protection of a Magnesium alloy. J. Mater. Sci. 2011;47:176–83.

40. Spencer K, Fabijanic DM, Zhang MX. The use of Al-Al2O3 cold spray coatings to improve the surface properties of magnesium alloys. Surf. Coatings Technol. 2009;204:336–44.

41. Lin J-K, Uan J-Y, Wu C-P, Huang H-H. Direct growth of oriented Mg–Fe layered double hydroxide (LDH) on pure Mg substrates and in vitro corrosion and cell adhesion testing of LDH-coated Mg samples. J. Mater. Chem. 2011;21:5011.

42. Uan J-Y, Lin J-K, Tung Y-S. Direct growth of oriented Mg–Al layered double hydroxide film on Mg alloy in aqueous HCO3−/CO32− solution. J. Mater. Chem. 2010;20:761.

43. Li D, Wang F, Yu X, Wang J, Liu Q, Yang P, et al. Anticorrosion organic coating with layered double hydroxide loaded with corrosion inhibitor of tungstate. Prog. Org. Coatings. 2011;71:302–9.

44. Chu CL, Han X, Xue F, Bai J, Chu PK. Effects of sealing treatment on corrosion resistance and degradation behavior of micro-arc oxidized magnesium alloy wires. Appl. Surf. Sci. 2013;271:271–5.

45. Krüger R, Seitz J-M, Ewald A, Bach F-W, Groll J. Strong and tough magnesium wire reinforced phosphate cement composites for load-bearing bone replacement. J. Mech. Behav. Biomed. Mater. 2013;20:36–44.

46. Erne P, Schier M, Resink TJ. The road to bioabsorbable stents: reaching clinical reality? Cardiovasc. Intervent. Radiol. 2006;29:11–6.

47. Waksman R, Erbel R, Di Mario C, Bartunek J, de Bruyne B, Eberli FR, et al. Early- and long-term intravascular ultrasound and angiographic findings after bioabsorbable magnesium stent implantation in human coronary arteries. JACC. Cardiovasc. Interv. American College of Cardiology Foundation; 2009;2:312–20.

48. Zartner P, Cesnjevar R, Singer H, Weyand M. First successful implantation of a biodegradable metal stent into the left pulmonary artery of a preterm baby. Catheter. Cardiovasc. Interv. 2005;66:590–4.

49. Schumacher S, Roth I, Stahl J, Bäumer W, Kietzmann M. Biodegradation of metallic magnesium elicits an inflammatory response in primary nasal epithelial cells. Acta Biomater. 2014;10:996–1004.

50. Bauer M, Schilling T, Weidling M, Hartung D, Biskup C, Wriggers P, et al. Geometric adaption of biodegradable magnesium alloy scaffolds to stabilise biological myocardial grafts. Part I. J. Mater. Sci. Mater. Med. 2013;

51. Kraus T, Fischerauer S, Hänzi A. Magnesium alloys for temporary implants in osteosynthesis: in vivo studies of their degradation and interaction with bone. Acta Biomater. 2012;8:1230–8.

52. Waizy H, Diekmann J, Weizbauer A, Reifenrath J, Bartsch I, Neubert V, et al. In vivo study of a biodegradable orthopedic screw (MgYREZr-alloy) in a rabbit model for up to 12 months. J. Biomater. Appl. 2014;28:667–75.

53. Dziuba D, Meyer-Lindenberg A, Seitz JM, Waizy H, Angrisani N, Reifenrath J. Long-term in vivo degradation behaviour and biocompatibility of the magnesium alloy ZEK100 for use as a biodegradable bone implant. Acta Biomater. Acta Materialia Inc.; 2013;9:8548–60.

54. Xu L, Yu G, Zhang E, Pan F, Yang K. In vivo corrosion behavior of Mg-Mn-Zn alloy for bone implant application. J. Biomed. Mater. Res. A. 2007;83:703–11.

55. Puleo DA, Nanci A. Understanding and controlling the bone-implant interface. Biomaterials. 1999;20:2311–21.

56. Rude RK, Gruber HE, Wei LY, Frausto A, Mills BG. Magnesium deficiency: effect on bone and mineral metabolism in the mouse. Calcif. Tissue Int. 2003;72:32–41.

57. Bushinsky DA. Metabolic alkalosis decreases bone calcium efflux by suppressing osteoclasts and stimulating osteoblasts. Am. J. Physiol. 1996;271:F216–F222.

58. Zheng YF, Gu XN, Witte F. Biodegradable metals. Mater. Sci. Eng. R Reports. 2014;77:1–34.

59. King AD, Birbilis N, Scully JR. Accurate electrochemical measurement of magnesium corrosion rates; A combined impedance, mass-loss and hydrogen collection study. Electrochim. Acta. 2014;121:394–406.

60. Yang L, Zhang E. Biocorrosion behavior of magnesium alloy in different simulated fluids for biomedical application. Mater. Sci. Eng. C. 2009;29:1691–6.

61. Willumeit R, Fischer J, Feyerabend F, Hort N, Bismayer U, Heidrich S, et al. Chemical surface alteration of biodegradable magnesium exposed to corrosion media. Acta Biomater. Acta Materialia Inc.; 2011;7:2704–15.

62. Schumacher S, Stahl J, Bäumer W, Seitz J-M, Bach F-W, Petersen LJ, et al. Ex vivo examination of the biocompatibility of biodegradable magnesium via microdialysis in the isolated perfused bovine udder model. Int. J. Artif. Organs. 2011;34:34–43.

63. Weizbauer A, Seitz J-M, Werle P, Hegermann J, Willbold E, Eifler R, et al. Novel magnesium alloy Mg-2La caused no cytotoxic effects on cells in physiological conditions. Mater. Sci. Eng. C. 2014;41:267–73.

64. Yamamoto A, Hiromoto S. Effect of inorganic salts, amino acids and proteins on the degradation of pure magnesium in vitro. Mater. Sci. Eng. C. Elsevier B.V.; 2009;29:1559–68.

65. Ghali E, Dietzel W, Kainer K-U. Testing of General and Localized Corrosion of Magnesium Alloys: A Critical Review. J. Mater. Eng. Perform. 2004;13:517–29.

66. Kirkland NT, Birbilis N, Staiger MP. Assessing the corrosion of biodegradable magnesium implants: A critical review of current methodologies and their limitations. Acta Biomater. 2012. p. 925–36.

67. Bender S, Goellner J, Heyn A, Schmigalla S. A new theory for the negative difference effect in magnesium corrosion. Mater. Corros. 2012;63:707–12.

68. Kuhlmann J, Bartsch I, Willbold E, Schuchardt S, Holz O, Hort N, et al. Fast escape of hydrogen from gas cavities around corroding magnesium implants. Acta Biomater. 2013;9:8714–21.

69. Ferrando W. Review of corrosion and corrosion control of magnesium alloys and composites. J. Mater. Eng. 1989;11:299–313.

70. Dhanapal A, Boopathy SR, Balasubramanian V. Developing an empirical relationship to predict the corrosion rate of friction stir welded AZ61A magnesium alloy under salt fog environment. Mater. Des. 2011;32:5066–72.

71. Kokubo T, Takadama H. How useful is SBF in predicting in vivo bone bioactivity? Biomaterials. 2006. p. 2907–15.

72. Carboneras M, Garcia-Alonso M, Escudero M. Biodegradation kinetics of modified magnesium-based materials in cell culture medium. Corros. Sci. 2011;53:1433–9.

73. Chew K V., Haseeb ASMA, Masjuki HH, Fazal MA, Gupta M. Corrosion of magnesium and aluminum in palm biodiesel: A comparative evaluation. Energy. 2013;57:478–83.

74. Song G, Atrens A. Understanding Magnesium Corrosion—A Framework for Improved Alloy Performance. Adv. Eng. Mater. 2003;5:837–58.

75. Mueller W-D, Lucia Nascimento M, Lorenzo de Mele MF. Critical discussion of the results from different corrosion studies of Mg and Mg alloys for biomaterial applications. Acta Biomater. Acta Materialia Inc.; 2010;6:1749–55.

76. Bohner M, Lemaitre J. Can bioactivity be tested in vitro with SBF solution? Biomaterials. 2009;30:2175–9.

77. Guo K. A Review of Magnesium/Magnesium Alloys Corrosion and its Protection. Recent Patents Corros. Sci. 2010;13–21.

78. Wang Y, Wei M, Gao J, Hu J, Zhang Y. Corrosion process of pure magnesium in simulated body fluid. Mater. Lett. 2008;62:2181–4.

79. Rettig R, Virtanen S. Composition of corrosion layers on a magnesium rare-earth alloy in simulated body fluids. J. Biomed. Mater. Res. A. 2009;88:359–69.

80. Müller L, Müller F a. Preparation of SBF with different HCO3- content and its influence on the composition of biomimetic apatites. Acta Biomater. 2006;2:181–9.

81. Ibasco S, Tamimi F, Meszaros R, Nihouannen D Le, Vengallatore S, Harvey E, et al. Magnesium-sputtered titanium for the formation of bioactive coatings. Acta Biomater. Acta Materialia Inc.; 2009;5:2338–47.

82. Lindström R, Johansson L, Thompson G. Corrosion of magnesium in humid air. Corros. Sci. 2004;46:1141–58.

83. Jönsson M, Persson D, Thierry D. Corrosion product formation during NaCl induced atmospheric corrosion of magnesium alloy AZ91D. Corros. Sci. 2007;49:1540–58.

84. Giester G, Lengauer C, Rieck B. The crystal structure of nesquehonite, MgCO3· 3H2O, from Lavrion, Greece. Mineral. Petrol. 2000;365:153–63.

85. Goh KH, Lim TT, Dong Z. Application of layered double hydroxides for removal of oxyanions: A review. Water Res. 2008. p. 1343–68.

86. Kloprogge JT, Wharton D, Hickey L, Frost RL. Infrared and Raman study of interlayer anions CO32-, NO3-, SO42- and ClO4- in Mg/Al hydrotalcite. Am. Mineral. 2002;87:623–9.

87. Khan AI, O'Hare D. Intercalation chemistry of layered double hydroxides: recent developments and applications. J. Mater. Chem. 2002;12:3191–8.

88. Boclair J, Braterman P. Layered double hydroxide stability. 1. Relative stabilities of layered double hydroxides and their simple counterparts. Chem. Mater. 1999;11:298–302.

89. Boclair JW, Braterman PS, Jiang J, Lou S, Yarberry F. Layered double hydroxide stability. 2. Formation of Cr(III)-containing layered double hydroxides directly from solution. Chem. Mater. 1999;11:303–7.

90. Basile F, Fornasari G, Gazzano M, Vaccari A. Synthesis and thermal evolution of hydrotalcite-type compounds containing noble metals. Appl. Clay Sci. 2000;16:185–200.

91. Fernández M, Ulibarri A, Labajos FM, Rives V. The effect of iron on the crystalline phases formed upon thermal decomposition of Mg-Al-Fe hydrotalcites. J. Mater. Chem. 1998;8:2507–14.

92. Marchi A, Apesteguía C. Impregnation-induced memory effect of thermally activated layered double hydroxides. Appl. Clay Sci. 1998;13:35–48.

93. Miyata S. Physico-Chemical Properties of Synthetic Hydrotalcites in Relation to Composition. Clays Clay Miner. 1980. p. 50–6.

94. Panda HS, Srivastava R, Bahadur D. Stacking of lamellae in Mg/Al hydrotalcites: Effect of metal ion concentrations on morphology. Mater. Res. Bull. 2008;43:1448–55.

95. Brindley G, Kikkawa S. A crystal-chemical study of Mg,Al and Ni,Al hydroxy-perchlorates and hydroxy-carbonates. Am. Mineral. 1979;64:836–43.

96. Vucelic M, Jones W, Moggridge G. Cation ordering in synthetic layered double hydroxides. Clays Clay Miner. 1997;803–13.

97. Sui M, Zhou Y, Sheng L, Duan B. Adsorption of norfloxacin in aqueous solution by Mg-Al layered double hydroxides with variable metal composition and interlayer anions. Chem. Eng. J. 2012;210:451–60.

98. Li B, He J, Evans D, Duan X. Inorganic layered double hydroxides as a drug delivery system—intercalation and in vitro release of fenbufen. Appl. Clay Sci. 2004;27:199–207.

99. Tzou Y-M, Wang S-L, Hsu L-C, Chang R-R, Lin C. Deintercalation of Li/Al LDH and its application to recover adsorbed chromate from used adsorbent. Appl. Clay Sci. 2007;37:107–14.

100. Fogg A, Freij A, Parkinson G. Synthesis and anion exchange chemistry of rhombohedral Li/Al layered double hydroxides. Chem. Mater. 2002;232–4.

101. Parker LM, Milestone NB, Newman RH. The Use of Hydrotalcite as an Anion Absorbent. Ind. Eng. Chem. Res. 1995;34:1196–202.

102. Ulibarri MA, Pavlovic I, Barriga C, Hermosín MC, Cornejo J. Adsorption of anionic species on hydrotalcite-like compounds: Effect of interlayer anion and crystallinity. Appl. Clay Sci. 2001;18:17–27.

103. Theiss FL, Ayoko GA, Frost RL. Removal of boron species by layered double hydroxides: A review. J. Colloid Interface Sci. 2013;402:114–21.

104. Chibwe K, Jones W. Synthesis of Polyoxometalate-Pillared Layered Double Hydroxides via Calcined Precursors Unusual Crystal Growth Morphologies in the Niobium-Selenium System. Chem. Mater. 1989;1:489–90.

105. Dimotakis E, Pinnavaia T. New route to layered double hydroxides intercalated by organic anions: precursors to polyoxometalate-pillared derivatives. Inorg. Chem. 1990;29:2393–4.

106. Zhang M, Reardon EJ. Removal of B, Cr, Mo, and Se from wastewater by incorporation into hydrocalumite and ettringite. Environ. Sci. Technol. 2003;37:2947–52.

107. Carpani I. Study on the intercalation of hexacyanoferrate(II) in a Ni, Al based hydrotalcite. Solid State Ionics. 2004;168:167–75.

108. Carpani I, Berrettoni M, Giorgetti M, Tonelli D. Intercalation of iron(III) hexacyano complex in a Ni,Al hydrotalcite-like compound. J. Phys. Chem. B. 2006;110:7265–9.

109. Rojas R, Bruna F, de Pauli CP, Ángeles Ulibarri M, Giacomelli CE. The effect of interlayer anion on the reactivity of Mg-Al layered double hydroxides: Improving and extending the customization capacity of anionic clays. J. Colloid Interface Sci. 2011;359:136–41.

110. Ren L, He J, Zhang S, Evans DG, Duan X. Immobilization of penicillin G acylase in layered double hydroxides pillared by glutamate ions. J. Mol. Catal. B Enzym. 2002;18:3–11.

111. Frunza MS, Popa MI, Lisa G, Hritcu D, Lion MSI, Marcel Lone Pop A. New Hybrid Compounds Containing Intercalated Ciprofloxacin into Layered Double Hydroxides: Synthesis and Characterization. Rev. Roum. Chim. 2008;53:827–31.

112. Tang P, Feng Y, Li D. Fabrication and properties of acid blue 25 dye-intercalated layered double hydroxides film on an anodic alumina/aluminum substrate. J. Phys. Chem. Solids. Elsevier; 2012;73:1505–9.

113. Wang J, Ren X, Feng X, Liu S, Sun D. Study of assembly of arachidic acid/LDHs hybrid films containing photoactive dyes. J. Colloid Interface Sci. 2008;318:337–47.

114. Musumeci AW, Mortimer GM, Butler MK, Xu ZP, Minchin RF, Martin DJ. Fluorescent layered double hydroxide nanoparticles for biological studies. Appl. Clay Sci. 2010;48:271–9.

115. Elkhattabi EH, Lakraimi M, Badreddine M, Legrouri A, Cherkaoui O, Berraho M. Removal of Remazol Blue 19 from wastewater by zinc–aluminium–chloride-layered double hydroxides. Appl. Water Sci. 2013;3:431–8.

116. Hwang S-H, Han Y-S, Choy J-H. Intercalation of functional organic molecules with pharmaceutical, cosmeceutical and neutraceutical functions into layered double hydroxides and zinc basic salts. Bull. Chem. Soc. 2001;22:1019–22.

117. Baikousi M, Stamatis A, Louloudi M, Karakassides MA. Thiamine pyrophosphate intercalation in layered double hydroxides (LDHs): An active bio-hybrid catalyst for pyruvate decarboxylation. Appl. Clay Sci. 2013;75-76:126–33.

118. Ambrogi V, Fardella G, Grandolini G, Perioli L. Intercalation compounds of hydrotalcite-like anionic clays with antiinflammatory agents--I. Intercalation and in vitro release of ibuprofen. Int. J. Pharm. 2001;220:23–32.

119. Ambrogi V, Fardella G, Grandolini G, Perioli L, Tiralti MC. Intercalation compounds of hydrotalcite-like anionic clays with anti-inflammatory agents, II: Uptake of diclofenac for a controlled release formulation. AAPS PharmSciTech. 2002;3:E26.

120. Frunza M, Lisa G, Popa MI, Miron ND, Nistor DI. Thermogravimetric analysis of layered double hydroxides with chloramphenicol and salicylate in the interlayer space. J. Therm. Anal. Calorim. 2008;93:373–9.

121. Tammaro L, Costantino U, Bolognese A, Sammartino G, Marenzi G, Calignano A, et al. Nanohybrids for controlled antibiotic release in topical applications. Int. J. Antimicrob. Agents. 2007;29:417–23.

122. Ma X, Zheng J, Pang H. Intercalation of Mg–Al layered double hydroxides by l-proline: synthesis and characterization. Res. Chem. Intermed. 2011;38:629–38.

123. Whilton NT, Vickers PJ, Mann S. Bioinorganic clays: synthesis and characterization of amino- and polyamino acid intercalated layered double hydroxides. J. Mater. Chem. 1997. p. 1623–9.

124. Choy J-H, Kwak S-Y, Park J-S, Jeong Y-J, Portier J. Intercalative Nanohybrids of Nucleoside Monophosphates and DNA in Layered Metal Hydroxide. J. Am. Chem. Soc. 1999;121:1399–400.

125. Choy J-H, Kwak S-Y, Park J-S, Jeong Y-J. Cellular uptake behavior of [γ32P] labeled ATP–LDH nanohybrids. J. Mater. Chem. 2001;11:1671–4.

126. Basu D, Das A, Stöckelhuber KW, Wagenknecht U, Heinrich G. Advances in layered double hydroxide (LDH)-based elastomer composites. Prog. Polym. Sci. Elsevier Ltd; 2014;39:594–626.

127. Lv K, Kang H, Zhang H, Yuan S. Molecular simulation studies for intercalation of photoactive dyes into layered double hydroxide. Colloids Surfaces A Physicochem. Eng. Asp. Elsevier B.V.; 2012;402:108–16.

128. Clearfield A, Kieke M, Kwan J, Colon JL, Wang R-C. Intercalation of dodecyl sulfate into layered double hydroxides. J. Incl. Phenom. Mol. Recognit. Chem. 1991;11:361–78.

129. Iyi N, Ebina Y, Sasaki T. Synthesis and characterization of water-swellable LDH (layered double hydroxide) hybrids containing sulfonate-type intercalant. J. Mater. Chem. 2011. p. 8085.

130. Kuang Y, Zhao L, Zhang S, Zhang F, Dong M, Xu S. Morphologies, Preparations and Applications of Layered Double Hydroxide Micro-/Nanostructures. Materials (Basel). 2010;3:5220–35.

131. Lin Q, Sun H, Dong M, Chen D, Wu Q, Chen X. Facile synthesis of pyroaurite-type Co–Fe layered double hydroxides for anionic dye adsorbents. Micro Nano Lett. 2012;7:476.

132. Hu G, O'Hare D. Unique layered double hydroxide morphologies using reverse microemulsion synthesis. J. Am. Chem. Soc. 2005;127:17808–13.

133. Yan Y, Liu Q, Wang J, Wei J, Gao Z, Mann T, et al. Single-step synthesis of layered double hydroxides ultrathin nanosheets. J. Colloid Interface Sci. Elsevier Inc.; 2012;371:15–9.

134. Jiang Z, Li Z, Qin Z, Sun H, Jiao X, Chen D. LDH nanocages synthesized with MOF templates and their high performance as supercapacitors. Nanoscale. 2013;5:11770–5.

135. Shao M, Ning F, Zhao J, Wei M, Evans DG, Duan X. Hierarchical Layered Double Hydroxide Microspheres with Largely Enhanced Performance for Ethanol Electrooxidation. Adv. Funct. Mater. 2013;23:3513–8.

136. Wang Y, Zhang F, Xu S, Wang X, Evans DG, Duan X. Preparation of Layered Double Hydroxide Microspheres by Spray Drying. Ind. Eng. Chem. Res. 2008;47:5746–50.

137. Tokudome Y, Tarutani N, Nakanishi K, Takahashi M. Layered double hydroxide (LDH)-based monolith with interconnected hierarchical channels: enhanced sorption affinity for anionic species. J. Mater. Chem. A. 2013;1:7702.

138. Liu Q, Yu J, Zhang X, Wang J, Li Z, Zhou J, et al. Hierarchically porous MgAl mixed metal oxide synthesized by sudden decomposition of MgAl layered double hydroxide gel. New J. Chem. 2013;37:2128.

139. Olanrewaju J, Newalkar BL, Mancino C, Komarneni S. Simplified synthesis of nitrate form of layered double hydroxide. Mater. Lett. 2000;45:307–10.

140. Costantino U, Marmottini F, Nocchetti M, Vivani R. New Synthetic Routes to Hydrotalcite-Like Compounds – Characterisation and Properties of the Obtained Materials. Eur. J. Inorg. Chem. 1998;1998:1439–46.

141. Ogawa M, Kaiho H. Homogeneous Precipitation of Uniform Hydrotalcite Particles. Langmuir. 2002;18:4240–2.

142. Tsujimura A, Uchida M, Okuwaki A. Synthesis and sulfate ion-exchange properties of a hydrotalcite-like compound intercalated by chloride ions. J. Hazard. Mater. 2007;143:582–6.

143. Meyn M, Beneke K, Lagaly G. Anion-Exchange Reactions of Layered Double Hydroxides. Inorg. Chem. 1990;5201–7.

144. Trikeriotis M, Ghanotakis DF. Intercalation of hydrophilic and hydrophobic antibiotics in layered double hydroxides. Int. J. Pharm. 2007;332:176–84.

145. Chibwe K, Jones W. Intercalation of organic and inorganic anions into layered double hydroxides. J. Chem. Soc. Chem. Commun. 1989;926.

146. Wang Q, O'Hare D. Recent advances in the synthesis and application of layered double hydroxide (LDH) nanosheets. Chem. Rev. 2012;112:4124–55.

147. Hur T-B, Phuoc TX, Chyu MK. Synthesis of Mg-Al and Zn-Al-layered double hydroxide nanocrystals using laser ablation in water. Opt. Lasers Eng. 2009;47:695–700.

148. Zhao Y, Li F, Zhang R, Evans DG, Duan X. Preparation of Layered Double-Hydroxide Nanomaterials with a Uniform Crystallite Size Using a New Method Involving Separate Nucleation and Aging Steps. Chem. Mater. 2002;14:4286–91.

149. Wongariyakawee A, Schäeffel F, Warner JH, O'Hare D. Surfactant directed synthesis of calcium aluminum layered double hydroxides nanoplatelets. J. Mater. Chem. 2012;22:7751.

150. Tyner KM, Roberson MS, Berghorn KA, Li L, Gilmour RF, Batt CA, et al. Intercalation, delivery, and expression of the gene encoding green fluorescence protein utilizing nanobiohybrids. J. Control. Release. 2004;100:399–409.

151. Chen M, Cooper HM, Zhou JZ, Bartlett PF, Xu ZP. Reduction in the size of layered double hydroxide nanoparticles enhances the efficiency of siRNA delivery. J. Colloid Interface Sci. Elsevier Inc.; 2013;390:275–81.

152. Giannini L, Lostritto A, Cipolletti V, Mauro M, Longo P, Guerra G. Layered double hydroxides with low Al content and new intercalate structures. Appl. Clay Sci. 2013;71:27–31.

153. Poeppelmeier K, Hwu S-J. Synthesis of lithium dialuminate by salt imbibition. Inorg. Chem. 1987;5:3297–302.

154. Khusnutdinov VP, Isupov VP. Mechanochemical synthesis of a hydroxycarbonate form of layered magnesium aluminum hydroxides. Inorg. Mater. 2011;44:263–7.

155. Ay AN, Zümreoglu-Karan B, Mafra L. A Simple Mechanochemical Route to Layered Double Hydroxides: Synthesis of Hydrotalcite-Like Mg-Al-NO_3-LDH by Manual Grinding in a Mortar. Zeitschrift für Anorg. und Allg. Chemie. 2009;635:1470–5.

156. Carlino S, Hudson M. Reaction of molten sebacic acid with a layered (Mg/Al) double hydroxide. J. Mater. Chem. 1994;4:99–104.

157. Hudson M, Locke W, Mitchell P, Hu X. Intercalation of cobalt phthalocyanine into the layered host material antimony hydrogen phosphate HSb (PO4)2: In situ synthesis of guest molecules. Solid State Ionics. 1993. p. 131–7.

158. Lin Y-J, Li D-Q, Evans DG, Duan X. Modulating effect of Mg–Al–CO3 layered double hydroxides on the thermal stability of PVC resin. Polym. Degrad. Stab. 2005;88:286–93.

159. Schiller C, Epple M. Carbonated calcium phosphates are suitable pH-stabilising fillers for biodegradable polyesters. Biomaterials. 2003;24:2037–43.

160. Zhi Y, Li Y, Zhang Q, Wang H. ZnO nanoparticles immobilized on flaky layered double hydroxides as photocatalysts with enhanced adsorptivity for removal of acid red G. Langmuir. 2010;26:15546–53.

161. Pradhan B, Srivastava SK. Layered double hydroxide/multiwalled carbon nanotube hybrids as reinforcing filler in silicone rubber. Compos. Part A Appl. Sci. Manuf. Elsevier Ltd; 2014;56:290–9.

162. Wang X, Zhou S, Xing W, Yu B, Feng X, Song L, et al. Self-assembly of Ni–Fe layered double hydroxide/graphene hybrids for reducing fire hazard in epoxy composites. J. Mater. Chem. A. 2013;1:4383.

163. Huang X, Brazel CS. On the importance and mechanisms of burst release in matrix-controlled drug delivery systems. J. Control. release. 2001;73:121–36.

164. Parello ML, Rojas R, Giacomelli CE. Dissolution kinetics and mechanism of Mg-Al layered double hydroxides: a simple approach to describe drug release in acid media. J. Colloid Interface Sci. 2010;351:134–9.

165. Khan AI, Ragavan A, Fong B, Markland C, O'Brien M, Dunbar TG, et al. Recent Developments in the Use of Layered Double Hydroxides as Host Materials for the Storage and Triggered Release of Functional Anions. Ind. Eng. Chem. Rev. 2009;48:10196–205.

166. Bégu S, Aubert-Pouëssel A, Polexe R, Leitmanova E, Lerner DA, Devoisselle J-M, et al. New Layered Double Hydroxides/Phospholipid Bilayer Hybrid Material with Strong Potential for Sustained Drug Delivery System. Chem. Mater. 2009;21:2679–87.

167. Gu Z, Thomas AC, Xu ZP, Campbell JH, Lu GQ (Max). In Vitro Sustained Release of LMWH from MgAl-layered Double Hydroxide Nanohybrids. Chem. Mater. 2008;20:3715–22.

168. Zhang H, Xu ZP, Lu GQ, Smith SC. Computer Modeling Study for Intercalation of Drug Heparin into Layered Double Hydroxide. J. Phys. Chem. C. 2010;114:12618–29.

169. Gu Z, Rolfe BE, Xu ZP, Thomas AC, Campbell JH, Lu GQM. Enhanced effects of low molecular weight heparin intercalated with layered double hydroxide nanoparticles on rat vascular smooth muscle cells. Biomaterials. 2010;31:5455–62.

170. Gu Z, Rolfe BE, Thomas AC, Campbell JH, Lu GQM, Xu ZP. Cellular trafficking of low molecular weight heparin incorporated in layered double hydroxide nanoparticles in rat vascular smooth muscle cells. Biomaterials. 2011;32:7234–40.

171. Del Arco M, Cebadera E, Gutiérrez S, Martín C, Montero MJ, Rives V, et al. Mg,Al layered double hydroxides with intercalated indomethacin: Synthesis, characterization, and pharmacological study. J. Pharm. Sci. 2004;93:1649–58.

172. Silion M, Hritcu D, Jaba IM, Tamba B, Ionescu D, Mungiu OC, et al. In vitro and in vivo behavior of ketoprofen intercalated into layered double hydroxides. J. Mater. Sci. Mater. Med. 2010;21:3009–18.

173. Cao F, Wang Y, Ping Q, Liao Z. Zn-Al-NO(3)-layered double hydroxides with intercalated diclofenac for ocular delivery. Int. J. Pharm. 2011;404:250–6.

174. Li A, Qin L, Wang W, Zhu R, Yu Y, Liu H, et al. The use of layered double hydroxides as DNA vaccine delivery vector for enhancement of anti-melanoma immune response. Biomaterials. 2011;32:469–77.

175. Qin L, Xue M, Wang W, Zhu R, Wang S, Sun J, et al. The in vitro and in vivo anti-tumor effect of layered double hydroxides nanoparticles as delivery for podophyllotoxin. Int. J. Pharm. 2010;388:223–30.

176. Chakraborti M, Jackson J, Plackett D, Gilchrist S, Burt H. The application of layered double hydroxide clay (LDH)-poly (lactide-co-glycolic acid)(PLGA) film composites for the controlled release of antibiotics. J. Mater. Sci. Mater. Med. 2012;23:1705–13.

177. Xu ZP, Jin Y, Liu S, Hao ZP, Lu GQ (Max). Surface charging of layered double hydroxides during dynamic interactions of anions at the interfaces. J. Colloid Interface Sci. 2008;326:522–9.

178. Gordijo CR, Barbosa CAS, Da Costa Ferreira AM, Constantino VRL, de Oliveira Silva D. Immobilization of ibuprofen and copper-ibuprofen drugs on layered double hydroxides. J. Pharm. Sci. 2005;94:1135–48.

179. Zhang H, Pan D, Zou K, He J, Duan X. A novel core-shell structured magnetic organic-inorganic nanohybrid involving drug-intercalated layered double hydroxides coated on a magnesium ferrite core for magnetically controlled drug release. J. Mater. Chem. 2009. p. 3069.

180. Zhang H, Pan D, Duan X. Synthesis, Characterization, and Magnetically Controlled Release Behavior of Novel Core−Shell Structural Magnetic Ibuprofen-Intercalated LDH Nanohybrids. J. Phys. Chem. C. 2009;113:12140–8.

181. Guo X, Zhang F, Evans DG, Duan X. Layered double hydroxide films: synthesis, properties and applications. Chem. Commun. (Camb). 2010;46:5197–210.

182. Yan T, Xu S, Peng Q, Zhao L, Zhao X, Lei X, et al. Self-Healing of Layered Double Hydroxide Film by Dissolution/Recrystallization for Corrosion Protection of Aluminum. J. Electrochem. Soc. 2013;160:C480–C486.

183. Han J, Dou Y, Wei M, Evans DG, Duan X. Antireflection/antifogging coatings based on nanoporous films derived from layered double hydroxide. Chem. Eng. J. 2011;169:371–8.

184. Kong X, Rao X, Han J, Wei M, Duan X. Layer-by-layer assembly of bi-protein/layered double hydroxide ultrathin film and its electrocatalytic behavior for catechol. Biosens. Bioelectron. Elsevier B.V.; 2010;26:549–54.

185. He S, Zhao Y, Wei M, Duan X. Preparation of Oriented Layered Double Hydroxide Film Using Electrophoretic Deposition and Its Application in Water Treatment. Ind. Eng. Chem. Res. 2011;50:2800–6.

186. Lee JH, Jung D-Y. Highly oriented nanoplates of layered double hydroxides as an ultra slow release system. Chem. Commun. (Camb). 2012;48:5641–3.

187. Shao M, Wei M, Evans DG, Duan X. Magnetic-field-assisted assembly of CoFe layered double hydroxide ultrathin films with enhanced electrochemical behavior and magnetic anisotropy. Chem. Commun. (Camb). 2011;47:3171–3.

188. Aradi T, Hornok V, Dékány I. Layered double hydroxides for ultrathin hybrid film preparation using layer-by-layer and spin coating methods. Colloids Surfaces A Physicochem. Eng. Asp. 2008;319:116–21.

189. Berry DJ, Harmsen WS, Cabanela ME, Morrey BF. Twenty-five-Year Survivorship of Two Thousand Consecutive Primary Charnley Total Hip Replacements. J. Bone Joint Surg. Am. 2002;84-A:171–7.

190. Pramanik S, Agarwal A, Rai K. Chronology of total hip joint replacement and materials development. Trends Biomater. Artif. Organs. 2005;19:15–26.

191. Bozic KJ, Kurtz SM, Lau E, Ong K, Vail TP, Berry DJ. The epidemiology of revision total hip arthroplasty in the United States. J. Bone Joint Surg. Am. 2009;91:128–33.

192. Park JH, Lee DY, Oh KT, Lee YK, Kim KM, Kim KN. Bioactivity of calcium phosphate coatings prepared by electrodeposition in a modified simulated body fluid. Mater. Lett. 2006;60:2573–7.

193. Ehlert N, Mueller PP, Stieve M, Lenarz T, Behrens P. Mesoporous silica films as a novel biomaterial: applications in the middle ear. Chem. Soc. Rev. 2013;42:3847–61.

194. Hall-Stoodley L, Hu FZ, Gieseke A, Nistico L, Nguyen D, Hayes J, et al. Direct detection of bacterial biofilms on the middle-ear mucosa of children with chronic otitis media. JAMA. 2006;296:202–11.

195. Lensing R, Bleich A, Smoczek A, Glage S, Ehlert N, Luessenhop T, et al. Efficacy of nanoporous silica coatings on middle ear prostheses as a delivery system for antibiotics: an animal study in rabbits. Acta Biomater. Acta Materialia Inc.; 2013;9:4815–25.

3 Magnesium Degradation under Physiological Conditions

3.1 Preface

This chapter deals in two articles with the corrosion examination of pure magnesium discs (section 3.2) and magnesium alloy ZEK100 plates under physiological conditions (section 3.3). Comprehensive examination, including appropriate testing devices, application of physiological media and identification of corrosion products could contribute to a better understanding of corrosion processes, which exact mechanism has not been entirely revealed yet.

Experimental setups for the corrosion examination of pure magnesium as described in section 3.2 comprised the application of physiological media (HBSS, DMEM and SBF) and cell culture conditions, in particular CO_2 gassing. In order to examine the influence of proteins on the corrosion, foetal bovine serum (FBS) was supplemented in varying amounts to the respective media. Tracking of the corrosion process was performed by the estimation of the weight loss over time, osmolality, pH and by optical evaluation. Crystalline corrosion products formed were identified by XRD measurements. Nesquehonite, $Mg(HCO_3)(OH)\cdot 2H_2O$, was found as the dominant product on all samples that were immersed at least for one day. Brucite, $Mg(OH)_2$, was among the corrosion products on samples that were immersed in lowly buffered HBSS setups. Calcium phosphates were found on a sample that was immersed in SBF for seven days; these were presumably formed due to the high calcium and phosphate content of the SBF. The formation of the magnesium carbonate compound instead of magnesium hydroxide was attributed to the presence of CO_2 gassing, acting as carbonate source.

As described in section 3.3, magnesium alloy ZEK100 plates were exposed to physiological conditions that included HBSS as the medium in flow mode. After the respective examination periods, the plates were characterized via four point bending tests with regard to their mechanical properties and via SEM, EDX and XRD with regard to surface alterations and the formation of corrosion products. Mechanical tests indicated varying bending strengths in the course of the immersion, whereas the bending strength after the longest incubation time was increased in comparison to the samples of the shorter periods. Surface examination revealed considerable contributions of Ca, P and O according to EDX data, indicating the presence of calcium phosphates. However, according to XRD measurements, brucite, $Mg(OH)_2$, was found as the solely crystalline corrosion product, whereas neither magnesium carbonates nor crystalline phosphates were found. However, the presence of magnesium hydroxide as a

corrosion product of magnesium exposed to lowly buffered HBSS is in accordance with the study presented in section 3.2.

In the studies presented in sections 3.2 and 3.3, it was shown that the formation of different corrosion products depends strongly on the corrosion conditions. Magnesium hydroxide was predominantly found when magnesium and its alloy ZEK100 were immersed under lowly buffered, physiological conditions as met in HBSS. The formation of nesquehonite, $Mg(HCO_3)(OH)\cdot 2H_2O$, was favored in carbonate enriched conditions in DMEM and SBF with CO_2 gassing. Hence, the formation of magnesium carbonates should be considered for further investigations of the corrosion behavior and the applications of magnesium as a degradable implant material.

By using soluble magnesium salts as precursors, the formation of different magnesium carbonate compounds under different synthesis conditions has further been examined in the B. Sc. thesis of Dennes Nettelroth: “Darstellung von Magnesiumhydroxycarbonaten mit definierter Morphologie” (“Preparation of Magnesium Hydroxy Carbonates with Defined Morphology”, 2012, Leibniz Universität Hannover), supervised by the author. It was shown that the formation and the morphologies of the magnesium compounds, in particular nesquehonite, $Mg(HCO_3)(OH)\cdot 2H_2O$), and hydromagnesite, $Mg_5(CO_3)_4(OH)_2\cdot 4H_2O$, strongly depend on the synthesis parameters.

Despite the progress achieved by the employment of studies comprising combined methods and sophisticated test devices and analytical methods, results of *in vitro* and corresponding *in vivo* studies still differ considerably. In order to further increase the predictive power of *in vitro* studies, the identification of the corrosion products that form along the reaction pathways is crucial. Also, the use of corrosion media which most closely resemble the *in vivo* conditions is advised. With regard to medical applications of magnesium-based implants, biocompatibility and the corrosion behavior could be investigated in the course of *in vivo* studies with regard to the respective human application. Furthermore, the influence of alloying elements and the efficacy of anticorrosion strategies could be interesting for future examinations.

For the article presented in section 3.2, the author of this thesis and Frank Feyerabend are the first authors, who contributed equally to this study. The manuscript was for the most part drafted by the author of this thesis. All XRD measurements and according data interpretation were performed and contributed accordingly to the publications by him. The immersion experiments, SEM imaging and the examination with regard to corrosion rates, osmolality and pH values were performed and contributed to the manuscript by Frank Feyerabend. Regine Willumeit and Peter Behrens supervised the studies

and revised the manuscript. This study was primarily initiated by Frank Feyerabend and Peter Behrens.

For the article presented in section 3.3, Hazibullah Waizy is the first author, and the author of this thesis is a co-author. All XRD measurements and according data interpretation were performed and contributed to the publication by the author of this thesis. The manuscript was prepared by Hazibullah Waizy, and written by Andreas Weizbauer and Christian Modrejewski. Data analysis was performed by Hazibullah Waizy and Andreas Weizbauer. The *in vitro* corrosion examinations were performed by Christian Modrejewski under the supervision of Hazibullah Waizy. The ZEK100 plates were manufactured and analyzed (SEM and EDX) by Arne Lucas. Berend Denkena, Peter Behrens, Andrea Meyer-Lindenberg and Friedrich-Wilhelm Bach revised the manuscript primarily. The study was initiated by Fritz Thorey, who participated in its design and coordination. Further coordination was contributed by Frank Witte and Henning Windhagen, who also helped to draft the manuscript.

3.2 Degradation Rates and Corrosion Products of Magnesium Exposed to Different Aqueous Media under Physiological Conditions

Marc Kieke*, Frank Feyerabend*, Regine Willumeit, Peter Behrens

*These authors contributed equally to this study.

This section will be submitted as an original research article.

Degradation Rates and Corrosion Products of Magnesium Exposed to Different Aqueous Media under Physiological Conditions

Marc Kieke ▪ Peter Behrens ▪ Frank Feyerabend ▪ Regine Willumeit

Abstract

Since magnesium and many of its alloys are a promising class of degradable implant materials, a thorough understanding of their degradation under physiological conditions is a key challenge in the field of biomaterial science. In order to increase the predictive power of *in vitro* studies, it is necessary to imitate the *in vivo* conditions, track the decomposition process and identify the corrosion products that form during the degradation pathway. In this *in vitro* study, slices of pure magnesium were exposed to Hank's balanced salt solution (HBSS), Dulbecco's modified eagle medium (DMEM) and Simulated body fluid (SBF), respectively, under cell culture conditions, which included CO_2 gassing. The series were repeated with supplements of FBS, added to the respective media. Degradation rates, osmolality and pH were found to vary with the choice of medium and supplementation with proteins. In order to identify the crystalline degradation products, the crusts formed on the specimens were investigated via XRD measurements. Brucite ($Mg(OH)_2$) was found among the corrosion product as anticipated; interestingly, nesquehonite ($MgCO_3 \cdot 3H_2O$ / $Mg(HCO_3)(OH) \cdot 2H_2O$) could be found to be the dominant corrosion product in this study.

Keywords: magnesium, degradation, corrosion, brucite, nesquehonite

M. Kieke and F. Feyerabend contributed equally to this study.

M. Kieke · P. Behrens (✉)

Institute for Inorganic Chemistry, Leibniz University of Hannover,
Callinstr. 9, 30167 Hannover, Germany,
e-mail: Peter.Behrens@acb.uni-hannover.de

F. Feyerabend · R. Willumeit (✉)

Institute for Materials Research, Department for Structure Research on Macromolecules,
Helmholtz-Zentrum Geesthacht,
Max-Planck-Str. 1, 21502 Geesthacht, Germany,
e-mail: Regine.willumeit@hzg.de

1 Introduction

Since many decades magnesium has gained an increasing interest in the field of implant materials [1].Biodegradable cardiovascular magnesium stents were successfully tested for clinical applications [2,3]. Due to its mechanical properties, which are comparable to those of bone, magnesium is also of high interest for orthopedic research [4]. In addition, metallic magnesium and its corrosion product magnesium hydroxide also show osteoconductive properties [5,6].

Since magnesium is highly susceptible to degradation in aqueous environments, efforts have been made both to decelerate as well as to exploit this process. For the application as a part of large, load-bearing prosthesis, an uncontrolled, i.e. too rapid, degradation is obviously a major disadvantage. On the other hand, the osteoconductive properties mentioned can support the incorporation of an implant made of or coated with magnesium or magnesium compounds [7,8].

Thus, the degradation of metallic magnesium is an obstacle as well as a chance in the field of degradable biomaterials. A thorough understanding of the kinetics and mechanisms of this process is therefore crucial in order to better understand the corrosion behavior and in this way increase the predictive power of *in vitro* studies, the results of which have so far often differed considerably from those of *in vivo* studies[4,9]. *In vitro* degradation setups provide many opportunities to follow the course of decomposition online, such as pH and conductivity monitoring [10,11], but the identity of the corrosion products formed from magnesium and the supplements of the media cannot be derived from these parameters alone. Electron-dispersive X-ray spectroscopy (EDS) analysis can be performed discontinuously on the corrosion products to gain information on their composition, but without differentiating between different products with the same elemental formula. Moreover, most instruments only give semi-quantitative data, because they are not calibrated to the respective elements. X-ray diffraction is suitable for the identification of crystalline phases that may have formed and have been deposited during the degradation process either directly or by follow-up reactions.

Magnesium hydroxide is the dominant crystalline corrosion product of magnesium and its alloys upon exposure to aqueous media, as has been shown before by various studies [12]. Since the solubility of the hardly soluble $Mg(OH)_2$ can be increased, for example by the presence of chloride ions [13,14] and by buffering of pH, magnesium hydroxide is not the only product which can be expected. Alternative products such as phosphates and carbonates, respectively, were found in various studies. In an *in vivo* approach, a magnesium containing calcium phosphate ($Mg_xCa_y(PO_4)_z$) was found after the degradation on the surface of a Mg-Mn-Zn alloy [7], while the degradation of a magnesium rare-earth alloy led to the *in vitro* formation of complex products with the general formula $(Mg,Ca)_x(PO_4)_y(CO_3)_z(OH)_i$ [15]. The formation of magnesium carbonates ($MgCO_3$) was reported by various authors, when pure magnesium was exposed to different aqueous media [16,17]. However, many studies did not distinguish between different modifications of the carbonates and phosphates, respectively.

With regard to the issues mentioned, it is of central interest to estimate the degradation rates of magnesium exposed to aqueous media under conditions similar and relevant to *in vivo* conditions. For this purpose, we have studied the degradation of pure magnesium under cell culture conditions in cell free media. As the respective media Hank's Buffered Salt Solution (HBSS), Simulated Body Fluid (SBF) and Dulbecco's Modified Eagle Medium (DMEM) were applied. The cell culture conditions included a CO_2 (5 %) and O_2 (21 %) gassing, as well as a temperature of 37 °C and 95% relative humidity over the entire experiment. In an additional set of experiments, fetal bovine serum (FBS) was added to all the respective media. Degradation rates were determined by measuring the weight loss of the samples. In order to identify the corrosion products, the surfaces of specimens were investigated via SEM and X-ray diffraction (XRD).

2 Materials and Methods

2.1 Magnesium casting

Magnesium ingot (purity 99.95 wt.%) was prepared by permanent mould casting. The material was molten under protective atmosphere (Ar + 2% SF_6) at a temperature of 750 °C. The melt was stirred for 30 min with 200 rpm prior to casting the material into preheated moulds (550 °C) made out of mild steel. To assure cleanliness of the cast ingots, a filter (Foseco SIVEX FC, Foseco GmbH, Borken, Germany) was used. Cylindrical specimens with a diameter of 10 mm and a height of 1.5 mm were cut from the cast blocks via electrical discharge machining. The samples were used without further surface treatment.

2.2 Degradation media

Three different media were used for the degradation tests: (I) Hank's balanced salt solution (HBSS) without Ca and Mg ions (Life Technologies, Darmstadt, Germany) as a low-buffered solution; (II) Dulbecco's modified eagle medium Glutamax-I (Life Technologies, Darmstadt, Germany) as a more complex, highly buffered solution, and (III) simulated body fluid (SBF-JL2, according to [18]). The compositions of these solutions are given in Table 1. For the preparation of the SBF two solutions were prepared. All chemicals were obtained from Merck (Darmstadt, Germany). (I) Solution A: 6.129 g NaCl, 5.89 g $NaHCO_3$ and 0.498 g $Na_2HPO_4 \cdot 2H_2O$ were dissolved in 1 L of double-distilled water. After dissolution, 0.934 mL of 1 M HCl was added. (II) Solution B: 6.129 g NaCl and 0.54 g $CaCl_2$ were dissolved in 1 L double- distilled water and 0.934 mL HCl was added. Both solutions were kept separately in the fridge and mixed (1:1) directly before the experiment. The pH value of the resulting solution was 7.4. In a second set of experiments , 10% or 20% FBS (FBS, PAA Laboratories, Linz, Austria) were added to these media.

Table 1 Composition of the used corrosion media

	HBSS		DMEM		SBF	
ingredient	mg/L	mM	mg/L	mM	mg/L	mM
amino acids			1852	10.29		
vitamins			31.6	0.15		
inorganic salts						
calcium chloride ($CaCl_2 \cdot 2H_2O$)			264	1.80	270	1.84
ferric nitrate ($Fe(NO_3)_3 \cdot 9H_2O$)			0.1	0.000248		
hydrochloric acid (HCl)					934	0.934
magnesium sulfate ($MgSO_4 \cdot 7H_2O$)			200	0.813		
potassium chloride (KCl)	400	5.33	400	5.33		
potassium phosphate monobasic (KH_2PO_4)	60	0.441				
sodium bicarbonate ($NaHCO_3$)	350	4.17	3700	44.05	2945	35.05
sodium chloride (NaCl)	8000	137.93	6400	110.34	6129	104.88
sodium phosphate monobasic ($NaH_2PO_4 \cdot 2H_2O$)			141	0.916		
sodium phosphate dibasic (Na_2HPO_4) anhydrous	48	0.338			249	1.45
other components						
D-glucose (dextrose)	1000	5.56	4500	25.00		
phenol red			15	0.0399		
sodium pyruvate			110	1.000		

2.3 Determination of degradation rate, pH and osmolality

The degradation rate was determined by weight loss. Each sample was weighed (Scaltec SBA52, Scaltec Instruments GmbH, Göttingen, Germany) and sterilized (20 minutes in ultrasonic bath with 70% ethanol) prior to the immersion (n = 3 per solution). After three days of incubation under cell culture conditions the samples were taken from the different corrosion media and dried at 37°C under vacuum overnight. Corrosion residues from the samples were removed by immersion in chromic acid (180 g/L in distilled water, VWR International, Darmstadt, Germany). The immersion was carried out for 2 times 10 minutes, with the samples being turned over in between. Afterwards the samples were rinsed in distilled water and 100% ethanol. After drying, the weight of the samples was measured again and the degradation rate (DR) was calculated according to equation 1 [19].

Eq. 1

$$DR = \frac{8.76 \cdot 10^4 \cdot \Delta W}{A \cdot t \cdot \rho}$$

A = surface area [cm^2], t = time [h], ρ= density (Mg = 1.74) [g/cm^3]), ΔW = mass loss [g].

After the immersion of the specimens the different corrosion media were removed from the wells and used for analysis of the pH value and osmolality. Solutions without samples were incubated in parallel as controls. The pH value was measured by a standard laboratory pH-meter (Sentron SI600, Sentron Europe BV, Roden, Netherlands) with an ISFET electrode. The osmolality of the supernatants was analyzed by a cryoscopic osmometer (Osmomat Auto, Gonotec GmbH, Berlin, Germany). 50 µL of the supernatant were used for the measurement. The device is a freezing point osmometer which determines the osmolality by measuring the freezing point. This decreases by 1.86° C when 1 mole of a nonionic solute is added to one kilogram of solvent [20].

2.4 Identification of corrosion products

2.4.1 Immersion procedure

Magnesium samples were sonificated for 20 min in dry isopropanol, dried and gamma-sterilized at the In core irradiation (ICI) facility of the Geesthacht neutron facility with a total dosage of 29 kGy. All specimens were immersed under sterile conditions in 1 mL of the respective media in agarose-coated 12-well plates (Greiner Bio-One, Frickenhausen, Germany). Then the samples were incubated under cell culture conditions (37°C, 5% CO_2, 21% O_2 and 95% relative humidity) in an incubator (Heraeus BBD 6620, Fisher Scientific, Schwerte, Germany). The immersion time was one, two, three, four and 7 days, respectively. Neither a pH adjustment nor a liquid stream was applied. After the immersion all samples were rinsed with deionized water for 1 min, dried under vacuum and stored at room temperature. Immersion experiments were performed in duplicate.

2.4.2 Characterization

The samples were visualized by scanning electron microscope (SEM; Auriga, Zeiss, Oberkochen, Germany) to visualize the corrosion layers. Images were taken at an accelerating voltage of 20 keV with the secondary electron detector (SE2). In order to identify the crystalline products formed and deposited, X-ray diffraction (XRD) measurements were performed on a Stoe Theta/Theta diffractometer (Stoe, Darmstadt, Germany) in reflection mode using CuKα radiation (λ = 1.54060 Å). The 2Θ range was scanned applying a step size of 0.01° (3.0 s per step). The diffractometer was operated at 40 kV and 30 mA. No further sample preparations were made for the XRD measurements. All samples were placed flatly in a sample holder and adjusted to the X-ray beam.

2.4.3 Statistics

Data are displayed as mean ± SD. Statistical analysis was performed by using the SigmaStat Software (Systat GmbH, Erkrath, Germany; version 11.0). Comparison of corrosion rates was analyzed by applying the one-way analysis of variance (ANOVA) with Holm-Sidak post-hoc test. The significance level was $p<0.05$.

3 Results

3.1 Morphological analysis

All samples showed obvious signs of corrosion on the surface. Exemplary photographs of immersed samples (respective media, and FBS supplemented media) are given in Fig. 1 (HBSS and HBSS+10%FBS), Fig. 2 (DMEM and DMEM+10%FBS) and Fig. 3 (SBF and SBF+10%FBS). In general, the amount of white crust and flakes fallen off the samples, respectively, increased with immersion time; however, the exact time points of the chipping were not determined. According to the appearances, degradation occurred fastest in HBSS. When FBS was supplemented to HBSS and DMEM, degradation seemed to be reduced. In contrast, degradation did apparently not decrease when FBS was supplemented to SBF.

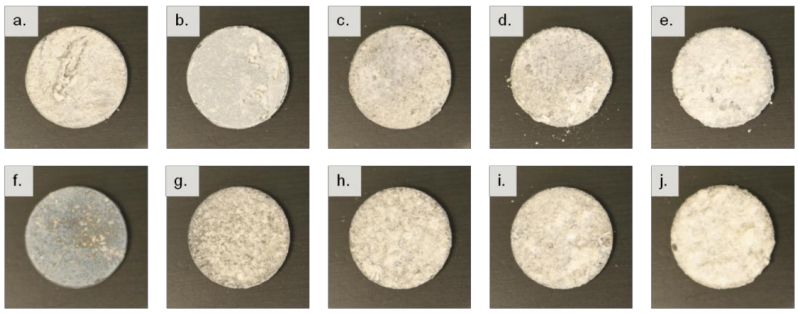

Fig.1 Pictures of the samples immersed in (a. to e.) HBSS and (f. to j.) HBSS+10%FBS. One, two, three, four and 7 days, respectively, from left to right

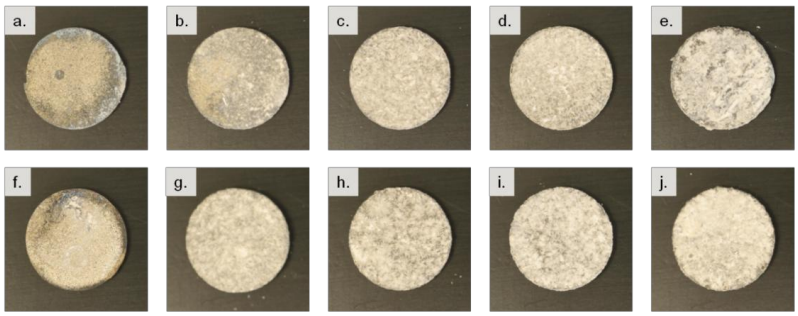

Fig. 2 Pictures of the samples immersed in (a. to e.) DMEM and (f. to j.) DMEM+10%FBS. One, two, three, four and 7 days, respectively, from left to right

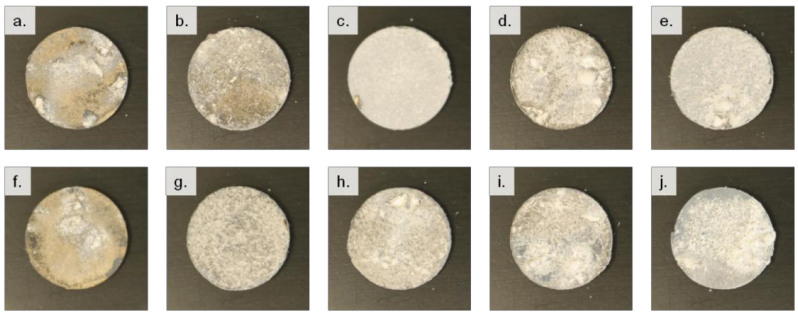

Fig. 3 Pictures of the samples immersed in (a. to e.) SBF and (f. to j.) SBF+10%FBS. One, two, three, four and 7 days, respectively, from left to right

In general, according to the SEM images, two different morphologies could be observed predominantly (Fig. 4). First, intergrown needles, which are a typical morphology for magnesium carbonates such as nesquehonite and secondly, flake-like shaped crystals. However, the morphology of the crystals that form the crusts on the samples does not allow direct conclusions to the identity of the crystalline phases. Comparison of the samples surfaces after immersion in the different media showed differences between the surface morphologies. Samples immersed in HBSS exhibited mostly flake-like crystals, whereas on DMEM-immersed samples mainly interconnected needles were visible. In all cases the corrosion morphology changed with the addition of proteins.

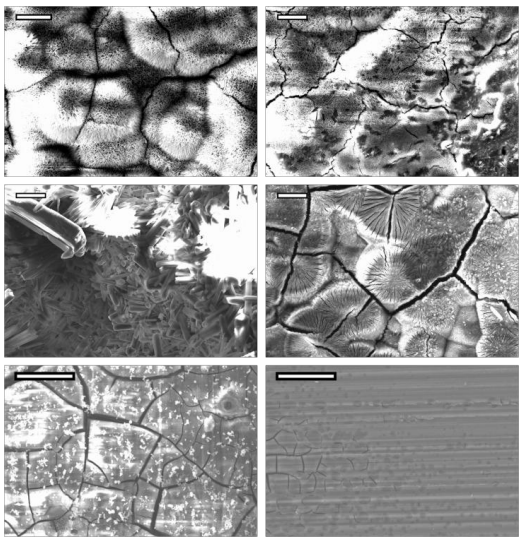

Fig. 4 SEM images of samples immersed for 72 hours in the respective media without (left column) and with FBS supplementation (right column). From top to bottom: SEM images of samples immersed in HBSS, HBSS+10%FBS, DMEM, DMEM+10%FBS, SBF, SBF+10%FBS. Scale bars represent 25 μm

3.2 Degradation rate, pH and osmolality

The degradation rate was highest in HBSS and lowest in SBF. According to the statistical analysis, the HBSS treatment led to significantly higher degradation rates (compared to all other treatments, Fig. 5). Using HBSS the addition of proteins exhibited a significant decrease of degradation rate due to the addition of proteins. This effect was much weaker for DMEM, where only the addition of 20 % led to a significant decrease. Presumably, due to the low amount of samples no significant differences between DMEM and SBF could be observed. The addition of proteins generally resulted in a decrease of the degradation rate, except for SBF, where the higher amount of protein increased the degradation rate again (Fig. 6 left). The measurement of osmolality reproduces this behavior for DMEM and SBF, but shows a different trend for HBSS (Fig. 6 middle), whereas the increase of pH is not correlated to the degradation rate (Fig. 6 right). However, the increase is much lower for DMEM and SBF which have a higher buffering capacity than HBSS.

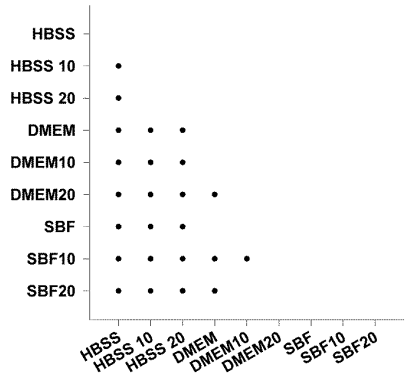

Fig. 5 Multiple comparison graph of significant differences between the corrosion rates in the different solutions (ANOVA, $p<0.05$)

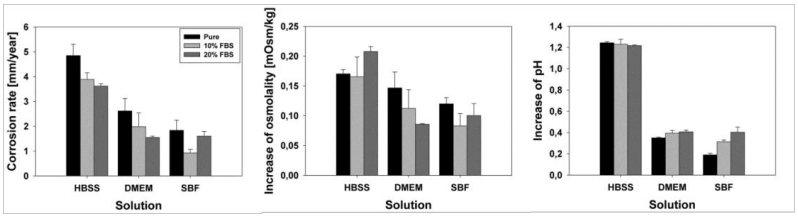

Fig. 6 Degradation rate, osmolality and pH in the different media after 72 h

3.3 Phase identification via XRD

Exemplary XRD patterns of samples immersed in HBSS and HBSS+10%FBS are shown in Fig. 7, patterns of the DMEM series in Fig. 8, and patterns of the SBF series in Fig. 9 It is to be pointed out that a quantitative evaluation of the species is not possible by XRD means in this study. Furthermore, crumbles of different sizes fell off most samples at undetermined time points. Next to texture effects, reflections of products formed appear in many cases vastly undersized due to high relative intensities of reflections associated with other compounds or the magnesium substrates. In particular, reflections that can be assigned to brucite ($Mg(OH)_2$) or to magnesium could in some cases hardly be distinguished from noise.

Magnesium-associated reflections (●, 32.2°, 34.4° and 36.6°) were present in all diffractograms allowing the conclusion that the penetration depth of the X-ray beam was sufficient to examine the crusts in their entire thickness, allthough the relative intensities were remarkably low in the DMEM series. The reflections are marked in the patterns obtained from samples with an immersion time of one day, and selections of reflections of the other products are marked, if appropriate, in the respective patterns. According to our evaluation, brucite ($Mg(OH)_2$) could be found as one of the corrosion products. Corresponding reflections (▲, 18.5° and 38.0°) could be found in the HBSS series. Nesquehonite ($Mg(HCO_3)(OH)\cdot 2H_2O$) characteristic reflections (★, 13.6°, 23.0°, 29.5° and 34.2°) were dominant in our study, and could be found in all diffractograms in both the HBSS series and for all specimens that have been exposed to SBF (+10%FBS) and DMEM (+10%FBS) for longer than one day.

Calcium phosphates were found according to XRD results on a sample immersed in SBF+10%FBS for 7 days (Fig. 8). The reflections (◆) can be assigned to a mixture of $Ca_2P_4O_{12}\cdot 4H_2O$ and $Ca_2P_2O_7\cdot 2H_2O$. However, some reflections, e.g. 10.2° and 11.6° remain unassigned.

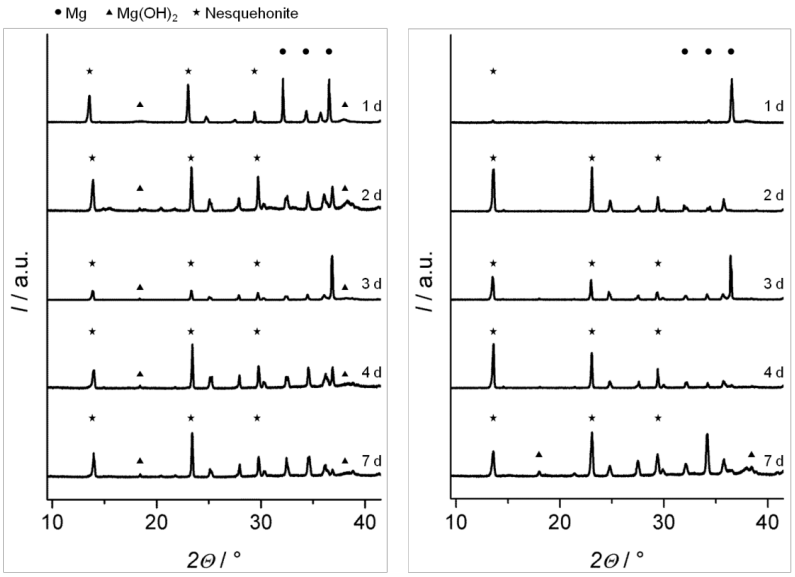

Fig. 7 XRD patterns obtained from samples immersed in (left) HBSS and (right) HBSS+10%FBS. From top to bottom: One, two, three, four and 7 days

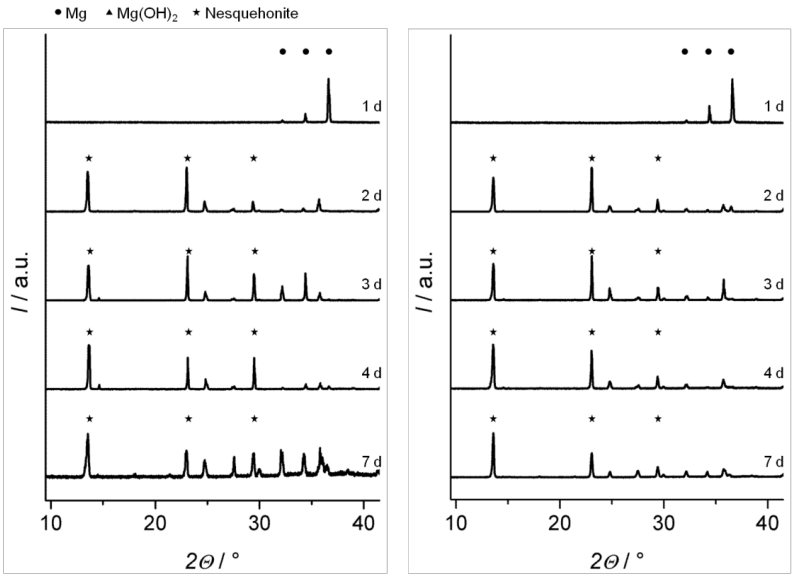

Fig. 8 XRD patterns obtained from samples immersed in (left) DMEM and (right) DMEM+10%FBS. From top to bottom: One, two, three, four and 7 days

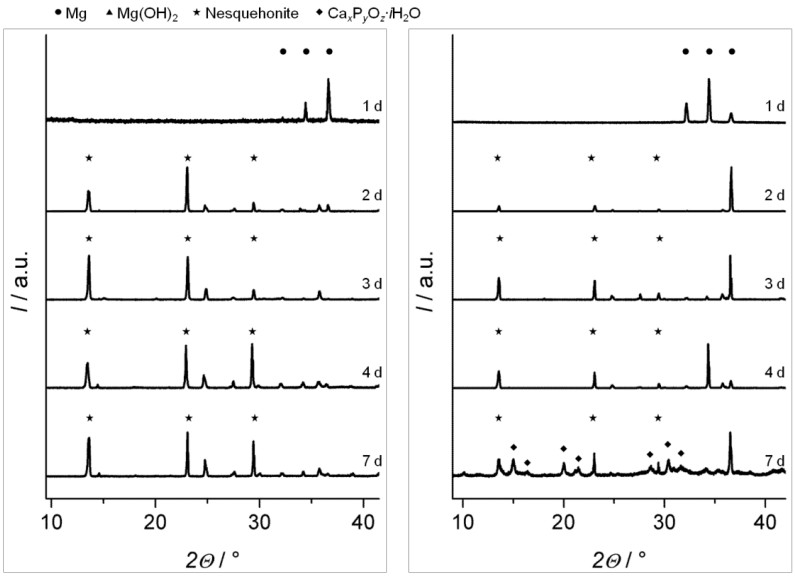

Fig. 9 XRD patterns obtained from samples immersed in (left) SBF and (right) SBF+10%FBS. From top to bottom: One, two, three, four and 7 days

4 Discussion

4.1 Influence of the medium and proteins on the degradation rates and osmolality

In this study, slices of pure magnesium were exposed to different aqueous media. HBSS has been evaluated to be the simplest medium, followed by SBF, while DMEM also includes organic substances [16]. Corrosion rates decreased in the order of HBSS, DMEM, SBF. Since proteins are known to retardate magnesium degradation under certain conditions [17], a reduction of the decomposition rates was expected in this study. The expectation was confirmed for samples immersed in HBSS and DMEM, but not for samples immersed in SBF. As stated above, osmolality examinations reproduced this behavior for DMEM and SBF, but not for HBSS. Presumably due to the high degradation rates in HBSS, which were highest in this study, and due to the high salt content, correlation could not be found.

4.2 Corrosion products

Two magnesium compounds were found to be the dominant corrosion products in this study: $Mg(OH)_2$ and nesquehonite. The latter was found in all media, while $Mg(OH)_2$ was found exclusively in the HBSS studies. Measurements revealed the highest pH when HBSS was used as the medium, hence, the presence of $Mg(OH)_2$ in the crusts is plausible. Unfortunately, the XRD investigations in this study were not suited to be used for quantification.

The formation of different magnesium carbonate compounds might occur if conditions of future immersion setups are altered slightly. Syntheses of different magnesium carbonates described by various authors reveal that the formation of different magnesium carbonate species can occur in similar chemical systems. Nesquehonite could be synthesized by the addition of a $NaCO_3$ solution to a $MgCl_2$ solution at room temperature [21], while the $NaCO_3$–$MgCl_2$ system led to the formation of hydromagnesite ($Mg_5(CO_3)_4(OH)_2 \cdot 4H_2O$) at slightly elevated temperatures [22]. Furthermore, the alteration of nesquehonite to hydromagnesite is reported in the context of dypingite ($Mg_5(CO_3)_4(OH)_2 \cdot 5H_2O$) [23,24], which was found to be a byproduct in the synthesis of magnesite ($MgCO_3$) [25]. Hydromagnesite and magnesite, respectively, were occasionally found to be associated with Holocen dolomite (South Australia) [26]. It is noted that some formulae only differ in one equivalent of crystal water, a difference that in some cases semi-quantitative methods are probably not able to detect reliably, and the formulae of dypingite and giorgiosite are the same ($Mg_5(CO_3)_4(OH)_2 \cdot 5H_2O$).

The calcium phosphates found in the SBF series most likely derived from the supplements of the medium, which contains a supersaturated calcium phosphate system. Reflections of crystalline magnesium phosphates were not detected in this study: either the amount of product was not sufficient to be detected or the magnesium phosphates are amorphous, therefore not detectable by XRD means. However, it cannot be excluded by the means applied, that certain amounts of Ca^{2+} were replaced with Mg^{2+}.

4.3 CO_2 gassing

The formation of $Mg(OH)_2$ as the only crystalline corrosion product has been described by various studies that did not include CO_2 gassing as part of their setup [12]. However, the formation of $Mg(OH)_2$ was not hindered entirely in this study. As described above, a variety of magnesium carbonates compounds can be obtained by altering the degradation setup. The introduction of CO_2 is an additional source of hydrogen carbonates and carbonates.

In this study, the CO_2 gassing is likely to be crucial for the formation of nesquehonite. It could be shown that the formation of magnesium carbonates is of relevance for CO_2 storage using mineral carbonation [27]. Taking also the increase of solubility of $Mg(OH)_2$ due to the presence of chlorides [4] into account, a hypothetical scheme for the formation of nesquehonite and magnesium/calcium phosphates is shown in Fig. 10. This *in vitro* scheme is in accordance earlier findings [28], including the more direct reaction $Mg + CO_2 + O_2 \rightarrow 2MgCO_3$ [10].

Since the degradation of magnesium is a complex process, the formation of nesquehonite or other carbonates might not be describable by a single synthesis route. In future *in vitro* studies the CO_2 pressure of the *in vivo* environment or technical application site should be considered. Since proteins are known to bind CO_2 [29], it is also likely that certain reaction pathways are more affected by the presence of proteins than others.

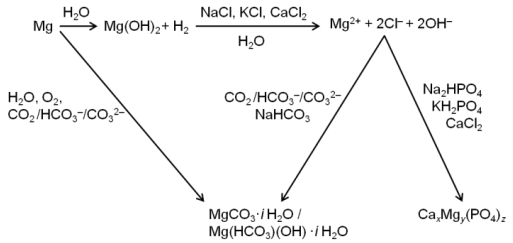

Fig. 10 Possible reaction scheme of magnesium compounds under physiological conditions

5 Conclusion

In this study, the degradation occurred fastest in HBSS, while the supplement with proteins led to a decrease of degradation in case of HBSS and DMEM, but not in case of SBF as the respective medium. As expected, brucite $Mg(OH)_2$ could be found as one of the corrosion products when HBSS was used. Nesquehonite ($Mg(HCO_3)(OH)\cdot 2H_2O$) was found to be the dominant, crystalline corrosion product, formed within short terms in all media.

Since it is likely that the additional carbonate source promoted the formation of the magnesium carbonate, CO_2 pressure ought to be taken into account for the evaluation of further *in vitro* studies. Furthermore, it is likely that different magnesium carbonates might be found if the experimental setups are altered. While crystalline calcium phosphate compounds could be found on one sample of the SBF series, no crystalline magnesium phosphates were found in this study.

6 References

1. Witte F. The history of biodegradable magnesium implants: a review. Acta Biomater. Acta Materialia Inc.; 2010;6:1680–92.

2. Waksman R, Erbel R, Di Mario C, Bartunek J, de Bruyne B, Eberli FR, et al. Early- and long-term intravascular ultrasound and angiographic findings after bioabsorbable magnesium stent implantation in human coronary arteries. JACC. Cardiovasc. Interv. American College of Cardiology Foundation; 2009;2:312–20.

3. Erne P, Schier M, Resink TJ. The road to bioabsorbable stents: reaching clinical reality? Cardiovasc. Intervent. Radiol. 2006;29:11–6.

4. Witte F, Hort N, Vogt C, Cohen S, Kainer KU, Willumeit R, et al. Degradable biomaterials based on magnesium corrosion. Curr. Opin. Solid State Mater. Sci. Elsevier Ltd; 2008;12:63–72.

5. Janning C, Willbold E, Vogt C, Nellesen J, Meyer-Lindenberg A, Windhagen H, et al. Magnesium hydroxide temporarily enhancing osteoblast activity and decreasing the osteoclast number in peri-implant bone remodelling. Acta Biomater. 2010;6:1861–8.

6. Witte F, Kaese V, Haferkamp H, Switzer E, Meyer-Lindenberg A, Wirth CJ, et al. In vivo corrosion of four magnesium alloys and the associated bone response. Biomaterials. 2005;26:3557–63.

7. Xu L, Yu G, Zhang E, Pan F, Yang K. In vivo corrosion behavior of Mg-Mn-Zn alloy for bone implant application. J. Biomed. Mater. Res. A. 2007;83:703–11.

8. Ibasco S, Tamimi F, Meszaros R, Nihouannen D Le, Vengallatore S, Harvey E, et al. Magnesium-sputtered titanium for the formation of bioactive coatings. Acta Biomater. Acta Materialia Inc.; 2009;5:2338–47.

9. Mueller W-D, Lucia Nascimento M, Lorenzo de Mele MF. Critical discussion of the results from different corrosion studies of Mg and Mg alloys for biomaterial applications. Acta Biomater. Acta Materialia Inc.; 2010;6:1749–55.

10. Feyerabend F, Drücker H, Laipple D, Vogt C, Stekker M, Hort N, et al. Ion release from magnesium materials in physiological solutions under different oxygen tensions. J. Mater. Sci. Mater. Med. 2012;23:9–24.

11. Yang L, Hort N, Willumeit R, Feyerabend F. Effects of corrosion environment and proteins on magnesium corrosion. Corros. Eng. Sci. Technol. 2012;47:335–9.

12. Waizy H, Weizbauer A, Modrejewski C, Witte F, Windhagen H, Lucas A, et al. In vitro corrosion of ZEK100 plates in Hank's Balanced Salt Solution. Biomed. Eng. Online. BioMed Central Ltd; 2012;11:12.

13. Wang Y, Wei M, Gao J, Hu J, Zhang Y. Corrosion process of pure magnesium in simulated body fluid. Mater. Lett. 2008;62:2181–4.

14. Fournier V, Marcus P, Olefjord I. Oxidation of magnesium. Surf. Interface Anal. 2002;34:494–7.

15. Rettig R, Virtanen S. Composition of corrosion layers on a magnesium rare-earth alloy in simulated body fluids. J. Biomed. Mater. Res. A. 2009;88:359–69.

16. Tie D, Feyerabend F, Hort N, Willumeit R, Hoeche D. XPS Studies of Magnesium Surfaces after Exposure to Dulbecco's Modified Eagle Medium, Hank's Buffered Salt Solution, and Simulated Body Fluid. Adv. Eng. Mater. 2010;12:B699–B704.

17. Yamamoto A, Hiromoto S. Effect of inorganic salts, amino acids and proteins on the degradation of pure magnesium in vitro. Mater. Sci. Eng. C. Elsevier B.V.; 2009;29:1559–68.

18. Bohner M, Lemaitre J. Can bioactivity be tested in vitro with SBF solution? Biomaterials. 2009;30:2175–9.

19. ASTM International, Standard Guide for Laboratory Immersion Corrosion Testing of Metals. ASTM Stand. NACE / ASTMG31 - 12a. West Conshohocken, PA, USA: ASTM International; 2012.

20. Abele J. The physical background to freezing point osmometry and its medical-biological applications. Am. J. Med. Electron. 1962;2:32–41.

21. Kloprogge J, Martens W. Low temperature synthesis and characterization of nesquehonite. J. Mater. Sci. Lett. 2003;22:825–9.

22. Cheng W, Li Z. Controlled Supersaturation Precipitation of Hydromagnesite for the MgCl2− Na2CO3 System at Elevated Temperatures: Chemical Modeling and Experiment. Ind. Eng. Chem. Res. 2010;5:1964–74.

23. Davies PJ, Bubela B. The Transformation of Nesquehonite into Hydromagnesite. Chem. Geol. 1973;12:289–300.

24. Canterford JH, Tsambourakis G, Lambert B. Some observations on the properties of dypingite , Mg5(CO3)4(OH)2 x 5H20 , and related minerals. Mineral. Mag. 1984;48:437–42.

25. Anjos APA, Sifeddine A, Sanders CJ, Patchineelam SR. Synthesis of magnesite at low temperature. Carbonates and Evaporites. 2011;26:213–5.

26. Warren J. Sedimentology and mineralogy of dolomitic Coorong lakes, South Australia. J. Sediment. Res. 1990;60.

27. Prigiobbe V, Mazzotti M. Precipitation of Mg-carbonates at elevated temperature and partial pressure of CO2. Chem. Eng. J. Elsevier B.V.; 2013;223:755–63.

28. Willumeit R, Fischer J, Feyerabend F, Hort N, Bismayer U, Heidrich S, et al. Chemical surface alteration of biodegradable magnesium exposed to corrosion media. Acta Biomater. Acta Materialia Inc.; 2011;7:2704–15.

29. Cundari TR, Wilson AK, Drummond ML, Gonzalez HE, Jorgensen KR, Payne S, et al. CO2-formatics: how do proteins bind carbon dioxide? J. Chem. Inf. Model. 2009;49:2111–5.

3.3 In vitro corrosion of ZEK100 plates in Hank's Balanced Salt Solution

Hazibullah Waizy, Andreas Weizbauer, Christian Modrejeksi, Frank Witte, Henning Windhagen, Arne Lucas, Marc Kieke, Berend Denkena, Peter Behrens, Andrea Meyer-Lindenberg, Friedrich-Wilhelm Bach, Fritz Thorey

BioMedical Engineering OnLine **2012**;*11*:12

DOI: 10.1186/1475-925X-11-12

The final publication is available at

http://www.biomedical-engineering-online.com/content/11/1/12

Waizy et al. BioMedical Engineering OnLine 2012, 11:12
http://www.biomedical-engineering-online.com/content/11/1/12

BioMedical Engineering OnLine

RESEARCH Open Access

In vitro corrosion of ZEK100 plates in Hank's Balanced Salt Solution

Hazibullah Waizy[1*], Andreas Weizbauer[1], Christian Modrejewski[1], Frank Witte[1], Henning Windhagen[1], Arne Lucas[2], Marc Kieke[3], Berend Denkena[2], Peter Behrens[3], Andrea Meyer-Lindenberg[4,5], Friedrich-Wilhelm Bach[6] and Fritz Thorey[1,7]

* Correspondence: Hazibullah.Waizy@ddh-gruppe.de
[1]Department of Orthopedic Surgery, Hannover Medical School, Anna-von-Borries-Str.1-7, 30625 Hannover, Germany
Full list of author information is available at the end of the article

Abstract

Background: In recent years magnesium alloys have been intensively investigated as potential resorbable materials with appropriate mechanical and corrosion properties. Particularly in orthopedic research magnesium is interesting because of its mechanical properties close to those of natural bone, the prevention of both stress shielding and removal of the implant after surgery.

Methods: ZEK100 plates were examined in this in vitro study with Hank's Balanced Salt Solution under physiological conditions with a constant laminar flow rate. After 14, 28 and 42 days of immersion the ZEK100 plates were mechanically tested via four point bending test. The surfaces of the immersed specimens were characterized by SEM, EDX and XRD.

Results: The four point bending test displayed an increased bending strength after 6 weeks immersion compared to the 2 week group and 4 week group. The characterization of the surface revealed the presence of high amounts of O, P and Ca on the surface and small Mg content. This indicates the precipitation of calcium phosphates with low solubility on the surface of the ZEK100 plates.

Conclusions: The results of the present in vitro study indicate that ZEK100 is a potential candidate for degradable orthopedic implants. Further investigations are needed to examine the degradation behavior.

Keywords: Magnesium alloy, Corrosion, Plates, in vitro study

Background

The first published application of a plate for fracture fixation was 1886 by Carl Hansmann [1]. It was not until the beginning of the 20th century when plates as osteosynthesis systems was spread due to the works of William Arbuthnot Lane and Albin Lambotte. In 1907 Lane, a British surgeon, introduced perforated steel plates for use in internal fixation [2]. Lambotte was one of the first to apply pure magnesium plates in a clinical case to stabilize a fracture in a young man. After implantation he observed extensive subcutaneous gas cavities and local swelling caused by rapid degradation [3].

In recent years, new innovative magnesium alloys are being intensively investigated as potential resorbable materials with appropriate mechanical and corrosion properties. Particularly in orthopedic research magnesium is interesting because of its mechanical properties close to those of natural bone, the prevention of both stress shielding and

removal of the implant after surgery [4]. Orthopedic implants need to provide an initial fixation and a predictable, gradually degradation adapted to the bone healing process.

ZEK100 is a magnesium alloy which contains 1 wt% zinc, 0.1 wt% zirconium and 0.1 wt % rare earth metals [5]. Magnesium and its degradation products are non-toxic and it is an essential co-factor for many enzymes; especially for DNA replication and repair processes [6,7]. Furthermore, magnesium acts as a stabilizer of DNA and chromatin structure. The recommended daily dietary is approximately 300 mg for adults [6]. Zinc as an alloying ingredient contributes to strength due to solid solution strengthening [7]. In addition, zinc is one of the essential micro-nutrients in the human body with an estimated daily requirement of 15 mg. It is essential to structure and function of over 300 enzymatic reactions [8]. The zinc finger motif, which is determined by a single zinc ion in the base, is most frequently occurring in transcription factors [8]. Zirconium is usually used as a grain refinement agent in magnesium alloys without aluminum and thereby contributes to strengthening [7]. In an in vitro study with binary magnesium alloys an addition of Zn or Zr showed good cytocompatibility, improved strength and a reduced corrosion rate [9]. The rare earth metals comprise seventeen elements which can be classified into two groups: elements with high and limited solubility in magnesium [10]. Rare earth (RE) metals improve strength by solid solution strengthening and precipitation strengthening [7]. The in vitro test with Mg-Y indicate no significant cytotoxicity to osteoblasts; furthermore good cytocompatibility was observed with Mg-Zn-Y alloys [9,11]. Several RE containing alloys such as WE43 or LAE443 have been investigated in former studies and reported good biocompatibility in vivo [12-16].

The disadvantage of magnesium alloys is the production of hydrogen gas which accumulates in tissue cavities. The amount of gas production is dependent on the corrosion rate. The accumulation of gas of ZEK100 implants was found in the medullary cavity via μ-computed tomography (μCT) examinations, though it did not became clinically visible [17].

In the present study, ZEK100 plates were examined in an in vitro model with Hank's Balanced Salt Solution under physiological conditions. A constant laminar flow of the corrosion medium was adjusted. The mechanical properties of the plates after corrosion were determined via four-point bending test. The surfaces of the immersed specimens were characterized by SEM, EDX and XRD.

Methods

Material

In this study plates for bone fixation of a biodegradable magnesium alloy were examined. The magnesium alloy ZEK100 contains 1 wt% zinc, 0.1 wt% zirconium and 0.1 wt% rare earth metals [5]. The analyzed chemical composition of the alloy by ICP-OES is given in Table 1. The ZEK100-specimens were cut into plates with dimensions of 50 mm × 8 mm × 1 mm by milling processes. In every plate five screw holes were

Table 1 Nominal and analyzed composition of the ZEK100 alloy

Element	Mg	Zn	Zr	Rare Earth Elements			
				Y	Nd	Ce	La
Analyzed composition	98.53	0.961	0.211	0.146	0.02	0.092	0.042
Nominal composition	98.8	1	0.1	0.1			

drilled and counterbored. These screw holes have an inner diameter of 3 mm on the bone-side and a counterbore diameter of 5 mm (Figure 1).

Microstructural characterization

The corroded plates were analyzed by a scanning electron microscope (SEM) EVO 60 VP by Zeiss. Theses analyses also included an energy dispersive X-ray analysis (EDX) to detect the distribution of elements on the surface of the corroded specimens and on the cross-section area of the plates. Therefore the plates were cut in the section of the middle bore. To achieve an electro conductive surface for the SEM analysis the specimens were also sputtered with gold.

X-ray diffraction (XRD) investigations were performed with a STOE Theta-Theta diffractometer in reflection geometry (wavelength λ = 1.54059 Å). The 2θ range from 2 to 65° was scanned with a step size of 0.01° (3.0 s per step) using monochromatized Cu Kα1 radiation.

Immersion test in a system with a constant flow rate

The immersion test was carried out in Hanks' Balanced Salt Solution (HBSS) to simulate normal ion concentration under physiological tissue conditions. The chemical composition of HBSS is given in Table 2. The HBSS were produced as dry substance with phenol red by Biochrom AG, Berlin. The temperature in the test system was measured by a thermometer (Fisher Scientific, Schwerte, Germany) during corrosion every day and regulated to 37.4°C +/- 0.5°C. Also the pH was controlled every day during

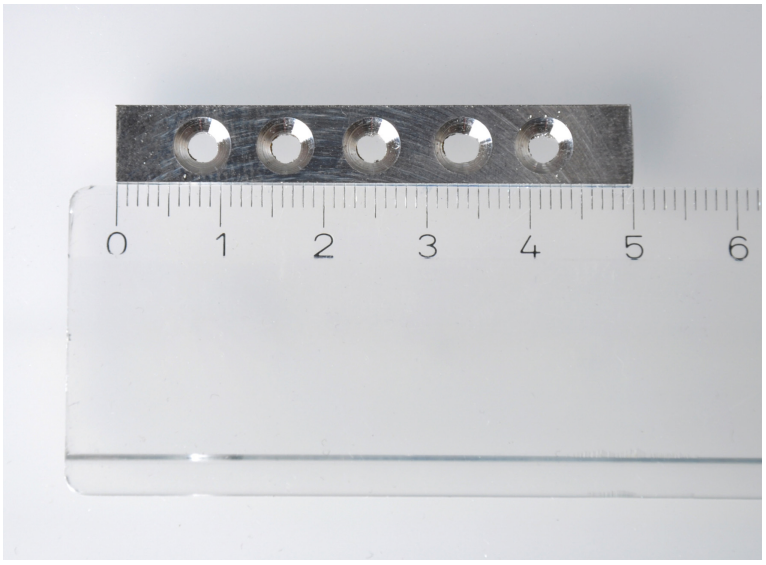

Figure 1 Picture of a non-corroded plate. The plate consists of ZEK100 and has a dimension of 50 mm × 8 mm × 1 mm. In every plate five screw holes were drilled and counterbored with an inner diameter of 3 mm on the bone-side and a counterbore diameter of 5 mm.

Waizy et al. BioMedical Engineering OnLine 2012, 11:12
http://www.biomedical-engineering-online.com/content/11/1/12

Table 2 Chemical composition of Hanks' Balanced Salt Solution

Reagents	Concentration (mg/l)
NaCl	8000
KCl	400
Na_2HPO_4	48
KH_2PO_4	60
$MgSO_4{\cdot}7H_20$	200
$CaCl_2$	140
Glucose	1000
Phenol red	10
$NaHCO_3$	350

corrosion and remained at 7.4. Flow rate was regulated to 2.5 to 3.5 ml/min. After passing the ZEK100 alloys the solution was discarded (Figure 2).

In this study twelve ZEK100 plate demonstrators, divided into 3 groups with 4 demonstrators, were corroded and tested. The demonstrators were fixed into a test frame which allows a laminar flow of the HBSS. The first group was corroded over 14 days, the second group over 28 d and the third group over 42 days.

Mechanical testing

In order to specify the mechanical properties of the specimens, they were tested according to ISO 9585:1990. The four point bending test setup (Figure 3) was designed for tests with an uniaxial material-testing machine (Mini Bionix 858, MTS Systems in Mineapolis, USA). The test system consisted of four rollers with a diameter of 8 mm. The distance between the lower and outer rollers was 32 mm. 10 mm distance was

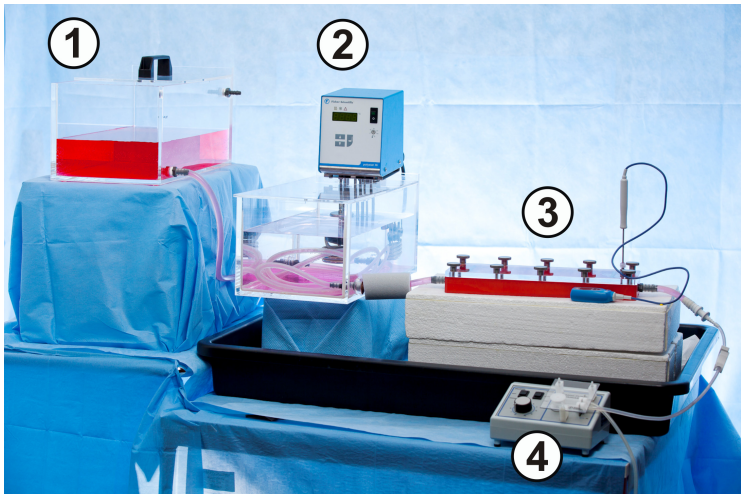

Figure 2 Picture of the in vitro corrosion testing setup. **1**: Glass basin with Hank's Balanced Salt Solution. **2**: The corrosion medium was warmed in a water bath to 37.4 +/- 0.5°C. **3**: HBSS passes the test system with the specimens with a laminar flow rate of 2.5 to 3.5 ml/min Temperature is checked with a thermometer. The system is protected against heat loss with styrofoam. **4**: The flow rate was maintained with a pump. The solution was then discarded in a container.

Waizy et al. BioMedical Engineering OnLine 2012, 11:12
http://www.biomedical-engineering-online.com/content/11/1/12

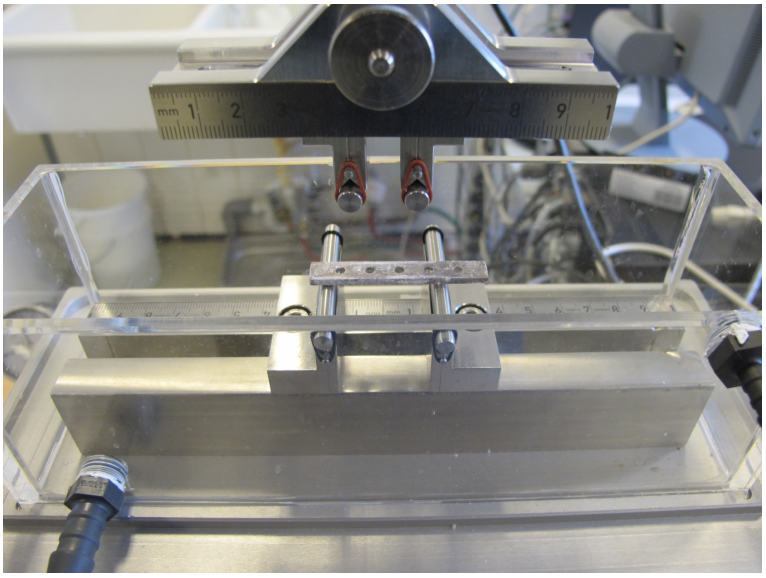

Figure 3 Picture of the mechanical four-point bending test setup. The test system consisted of four rollers with a diameter of 8 mm. The distance between the lower and outer rollers was 32 mm. 10 mm distance was between the upper and inner rollers. The plates were positioned on the lower rollers according to the protocol of ISO 9585:1990.

between the upper and inner rollers. The plates were positioned on the lower rollers according to the protocol of ISO 9585:1990. The distance between the outer and inner rollers was 11 mm and contains a screw hole of the demonstrators. The test rig was produced by the Research Work Shop of the Medical School, Hannover, Germany.

Results

Microstructure and surface composition after immersion

The surface morphology of ZEK100 plates after exposure in Hank's Balanced Salt Solution are shown in the SEM images of Figures 4 and 5. On the corrosion surface cracks were found after all immersion intervals which might be caused by drying. At higher magnifications, some needle-shaped clusters appeared on the surface of the 2 weeks group and the 6 weeks group (Figure 4b, g). A more detailed picture of that structure is given in Figure 4h. In the SEM picture after 4 weeks immersion a peeling of corrosion surface can be observed in high magnification view. Small, agglomerated particles seemed to be formed on the surface (Figure 4e). The pictures of the cross-sections reveal local pits on the surface (Figure 5). More distinct and deep pits were found after 4 and 6 weeks immersion (Figure 5b, c).

EDX analyses were conducted on a small surface area after every corrosion interval to determine the elemental composition (Figure 6). The results revealed the presence of high amounts of the elements O, P and Ca and small amounts of C, Na, Mg, Cl and K (Table 3).

Waizy et al. BioMedical Engineering OnLine 2012, 11:12
http://www.biomedical-engineering-online.com/content/11/1/12

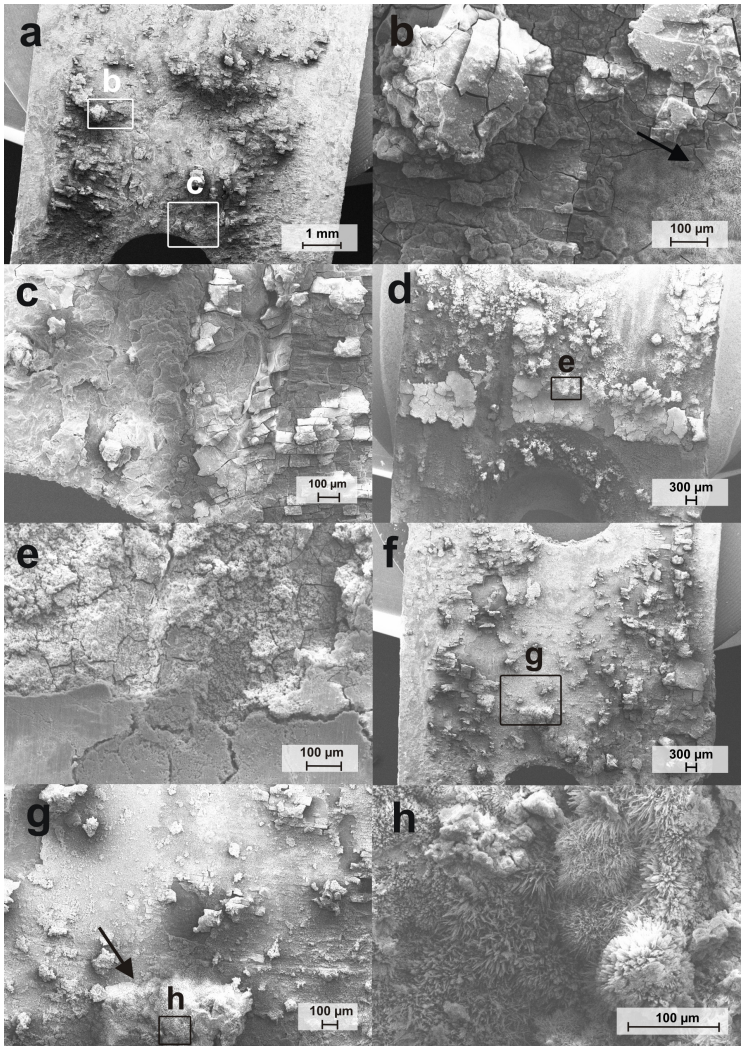

Figure 4 SEM pictures of the surface morphology of ZEK100 plates immersed in Hank's balanced salt solution. a)-c) after 2 weeks, d)-e) after 4 weeks, f)-h) after 6 weeks. The black arrow marks needle-shaped clusters.

X-ray diffraction (XRD) was applied to identify some of the corrosion products on the surface. Figure 7 presents the XRD patterns of the ZEK100 plates after all three different immersion intervals. In all spectra large magnesium and $Mg(OH)_2$ peaks are clearly visible.

Waizy et al. BioMedical Engineering OnLine 2012, 11:12
http://www.biomedical-engineering-online.com/content/11/1/12

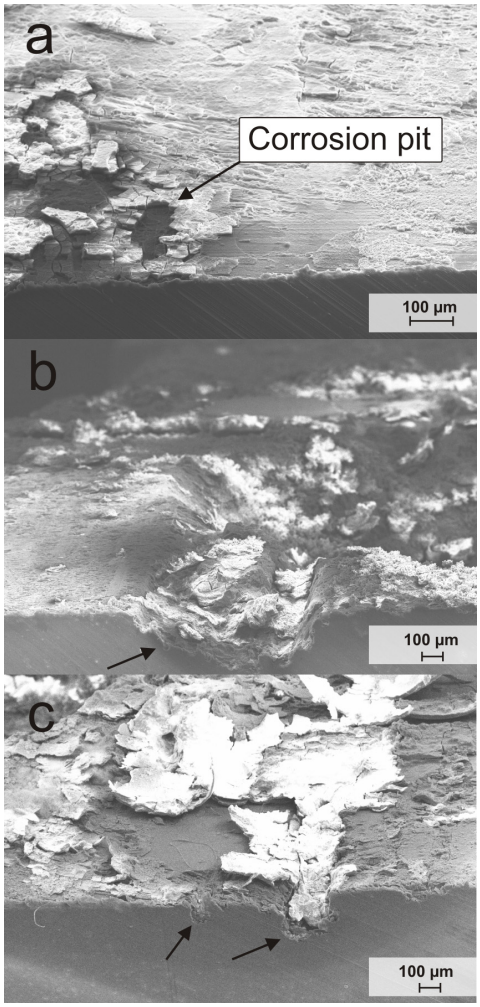

Figure 5 SEM pictures of the cross-section area. a) 2 weeks, b) 4 weeks c) 6 weeks. The corrosion pits are marked by black arrows.

Mechanical characterization of the specimens after immersion

The bending strength was calculated from obtained load-deflection curves. The results are presented in Figure 8. The results of the bending test displayed a decrease of bending strength from immersion week 2 to immersion week 4. The tested plates after 6 weeks corrosion showed an increased bending strength.

Discussion

Fracture healing is a complex pathway with determine steps and the healing quality and speed depends on the size of the fracture gap and the achieved stability. Therefore an adjusted stability is essential for fracture healing. The discrepancy of the Young's

Waizy et al. BioMedical Engineering OnLine 2012, 11:12
http://www.biomedical-engineering-online.com/content/11/1/12

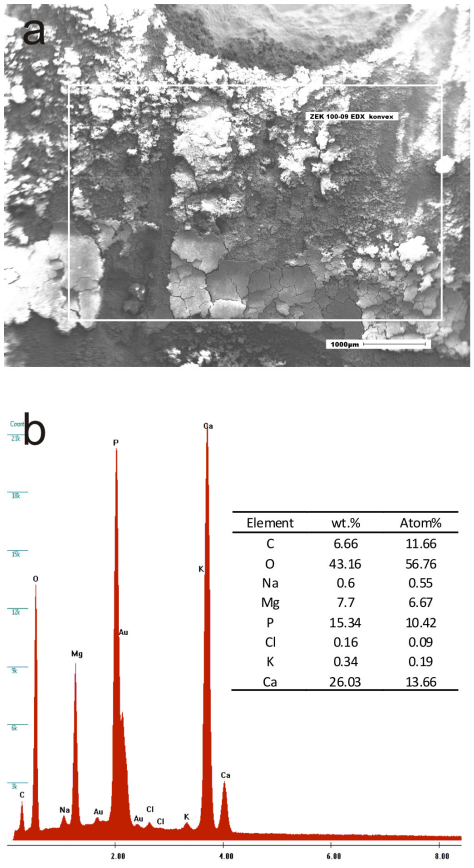

Figure 6 Example of the EDX analysis. The energy dispersive X-ray analysis (EDX) was applied in order to detect the distribution of elements on the surface of the corroded specimens.

Table 3 Results of the EDX analysis of the ZEK100 alloy

Element	2 weeks		4 weeks		6 weeks	
	wt%	at%	wt%	at%	wt%	at%
C	6.21	10.8	6.66	11.66	6.3	11.01
O	43.07	56.24	43.16	56.76	42.3	55.48
Na	0.63	0.57	0.6	0.55	1.94	1.77
Mg	10.88	9.35	7.7	6.67	10.36	8.94
P	16.94	11.43	15.34	10.42	14.99	10.16
Cl	0.08	0.05	0.16	0.09	0.06	0.04
K	0.28	0.15	0.34	0.19	0.6	0.32
Ca	21.92	11.42	26.03	13.66	23.45	12.28

Waizy et al. BioMedical Engineering OnLine 2012, 11:12
http://www.biomedical-engineering-online.com/content/11/1/12

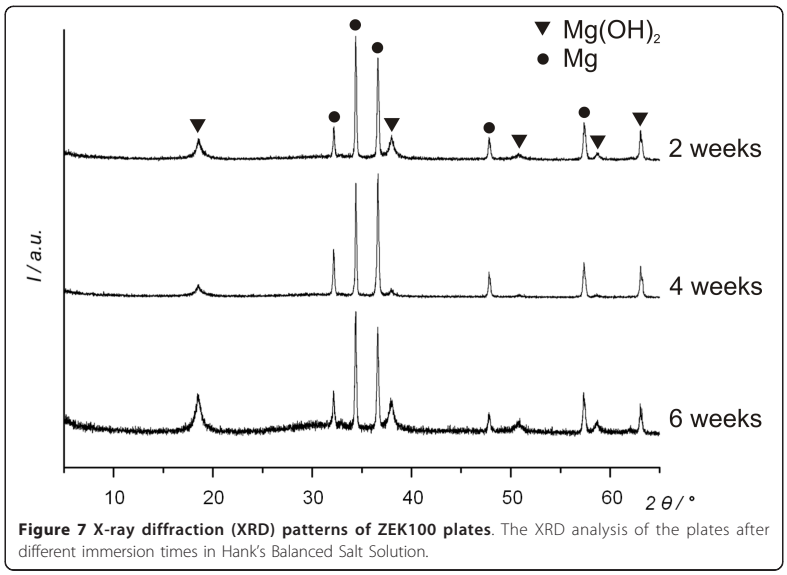

Figure 7 X-ray diffraction (XRD) patterns of ZEK100 plates. The XRD analysis of the plates after different immersion times in Hank's Balanced Salt Solution.

modulus of the conventional implants (stainless steel or titan) in regard to bone promotes the occurrence of stress shielding with negative effects to the bone healing. Degradable implants from magnesium alloys are desirable because of the mentioned promising characteristics of magnesium. Standard tests with those implants according to ASTM protocols are rare.

In the present study, ZEK100 plates were examined in an in vitro model with Hank's Balanced Salt Solution under physiological conditions. The corrosion medium used in

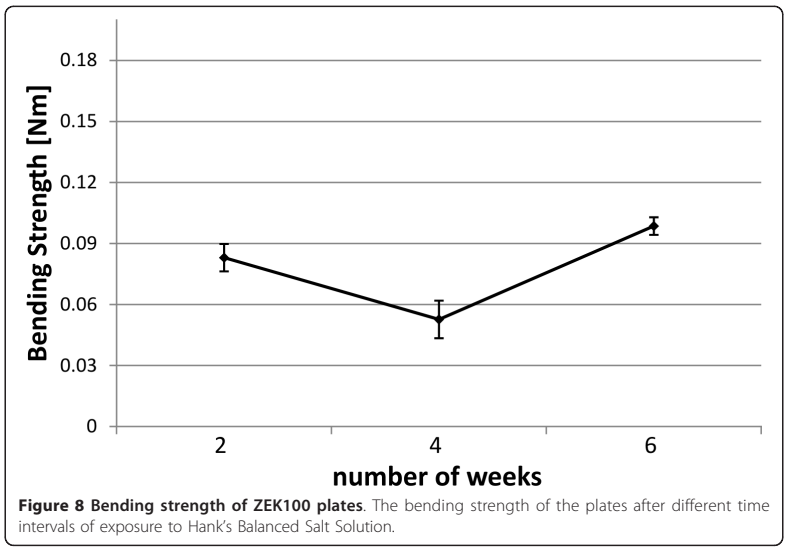

Figure 8 Bending strength of ZEK100 plates. The bending strength of the plates after different time intervals of exposure to Hank's Balanced Salt Solution.

this study is in its ionic content similar to blood plasma with a high chloride concentration. The degradation of magnesium and its alloys are described according to the following reactions [18]:

Anodic reaction: $Mg \rightarrow Mg^{2+} + 2e^-$

Cathodic reaction: $2\ H_2O + 2e^- \rightarrow H_2\uparrow + 2\ OH^-$

$$Mg^{2+} + 2\ OH^- \rightarrow Mg(OH)_2\ (s)$$

It is reported that the protective $Mg(OH)_2$-film is formed rapidly after 2 h immersion [19]. The $Mg(OH)_2$-layer on the surface is dissolved by Cl^- into soluble $MgCl_2$:

$$Mg(OH)_2 \rightarrow MgCl_2 + 2\ OH^-$$

An illustration of the reactions on the surface of the magnesium alloy is given in Figure 9. This diagram is in accordance with previous illustrations in Ref. [20,21] and is intended to demonstrate the corrosion processes on the surface. This dissolution reaction elevates the local hydroxide concentration near the surface. It is reported that in stagnant corrosion systems the degradation of magnesium and its alloys lead to an alkalization of the corrosive medium [22]. As a result of alkalization, a greater tendency for film formation is reported when the local pH value rise above 10.5 [23]. However, this effect might be minor in this study due to the $NaHCO_3$ buffer in the corrosion medium and the flow rate applied in this system. Nevertheless, it is reported that this buffering agent accelerates the dissolution of magnesium because of the consumption of the generated OH^- [24].

The corrosion in our model is most likely more influenced by the velocity. The accelerating corrosive effect of the flow rate obtains to (i) shear forces, (ii) the destruction or prevention of a protective surface layer and (iii) the prevention of micro-alkalization on the surface [7,23]. It is noticeable that a corrosion layer could be identified considering the flow rate adjusted in this immersion model. Wang et al. compared the degradation rate of a dynamic system with a flow rate to static conditions with Hank's Balanced Salt Solution by weight loss method [25]. An accelerated degradation rate was reported in this study under dynamic conditions; though the applied flow rate remains unclear [25].

The EDX analysis of our plates revealed a high amount of the elements Ca, P and O which indicates the precipitation of calcium phosphates with low solubility which was reported in previous studies [15,18,26]. The corrosion medium Hank's Balanced Salt Solution contains a certain amount of Ca^{2+} and PO_4^{3-} (Table 1). The most stable calcium phosphate is hydroxyapatite which forms according to the following reaction:

$$10\ Ca^{2+} + 6\ PO_4^{3-} + 2\ OH^- \rightarrow Ca_{10}(PO_4)_6(OH)_2\ [27].$$

Additional types of calcium phosphates are in order of increasing solubility: $Ca_2(PO_4)_3{\cdot}nH2O$ (TCP), $Ca_8H_2(PO_4)_6{\cdot}5H2O$ (OCP) and $Ca(HPO_4){\cdot}5H_2O$ (DCPD) [27]. Hydroxyapatite is an essential component of the human bone and therefore the biocompatibility of this precipitation layer can be assumed. In addition, it has been shown that hydroxyapatite coated carboxymethyl chitosan (CMCS) enhances the proliferation and differentiation of osteoblasts and stem cells [28]. In a different study $Ca_3Mg_3(PO_4)_4$ was detected on the surface via XRD analysis of a Mg-Mn-Zn alloy immersed in

Waizy et al. BioMedical Engineering OnLine 2012, 11:12
http://www.biomedical-engineering-online.com/content/11/1/12

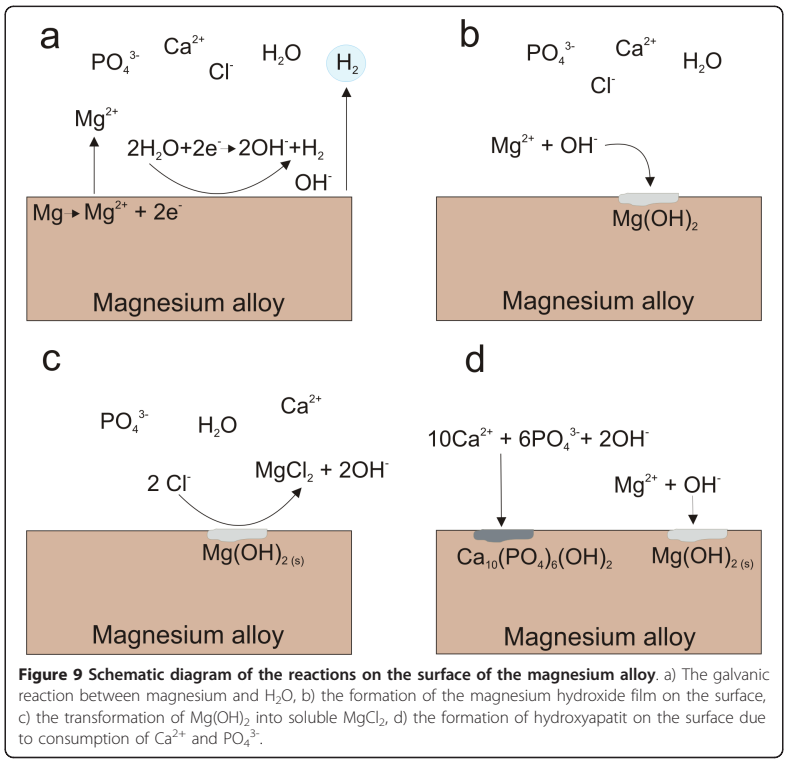

Figure 9 Schematic diagram of the reactions on the surface of the magnesium alloy. a) The galvanic reaction between magnesium and H_2O, b) the formation of the magnesium hydroxide film on the surface, c) the transformation of $Mg(OH)_2$ into soluble $MgCl_2$, d) the formation of hydroxyapatit on the surface due to consumption of Ca^{2+} and PO_4^{3-}.

Hank's solution [18]. The occurrence of this specific precipitation layer in our study is not supported by the low Mg content in our EDX analysis. The precipitation layers protect the magnesium alloy against aggressive ions in the corrosive medium and therefore reduce the corrosion rate [18]. In corrosive media containing HCO_3^-, which is the case in HBSS and blood plasma, the surface layer might consist of amorphous carbonated calcium phosphate with a schematic formula as follows: $(Mg, Ca)_x(PO_4)_y(CO_3)_z(OH)_i$ [29].

An advanced deposition of calcium and phosphate on the surface was determined by EDX analysis in all specimens. These results are comparable with Huan et al., who investigated an Mg-Zn-Zr alloy which is comparable to ZEK100 [30]. In this mentioned study the atomic content of Mg decreased slightly from 7 days immersion to 24 days while the atomic content of P and Ca increased [30]. The growth of the corrosion precipitation layer could not be detected in this study by EDX analysis after the different immersion time intervals. This let us assume that after 2 weeks the composition on the surface is stable which might be explained by an equilibrium between precipitation and erosion.

The effect of corrosion on the bending strength of plates with medical geometry has not been studied previously. In the present work a decreased bending strength of the plates was determined after 4 weeks in Hank's Balanced Salt Solution in comparison to the 2 week and 6 week group. It can be concluded that the change of the bending

strength after 4 week and 6 week immersion might be caused by the embrittlement of the magnesium alloy. As described hydrogen gas evolve as bubbles from the magnesium surface in consequence of dissolution. It is also reported that some hydrogen atoms enter the metal lattice [31,32]. This storage of hydrogen atoms results in hydrogen embrittlement of the magnesium alloy which degree is dependent on the immersion time [31]. It is reported that the cohesive strength of a magnesium alloy (AZ31) is reduced by hydrogen embrittlement [31].

In a previous in vivo study the bending stiffness of ZEK100-implants was determined via 3 point bending test. The maximum force (F_{max}) at the point of breakage of the explanted implants was decreased by 35% after 3 months and 60% after 6 months. These in vivo results differ from the results determined in this study. The geometry of the implant affects the determination of the mechanical properties of the specimen. In the in vivo study by Hühnerschulte et al. pins were used as implant geometry [17]. Further in vivo evaluations with the dimensions examined in this study would be helpful to improve the comparability between the in vivo and in vitro corrosion behavior. Different biomechanical results may be caused by different corrosion rates in vitro and in vivo [33,34]. It is reported that the in vitro corrosion rate is faster than in comparable in vivo studies [33]. Müller et al. reported that the corrosion rate was in vitro 1.7 times greater than in vivo for LAE442 [33]. Faster corrosion rates should be accompanied with an earlier loss of mechanical strength. A rapid decrease of the bending strength was determined from week 2 to week 4 in this in vitro study.

In contrast to this, in vivo μCT scans first demonstrate a decrease of the implant volume until week 4, thereupon an increased volume was determined up to week 8. After week 8 a continuously reduction of the volume was observed [17]. This increase of implant volume could be explained by the corrosion products on the surface which is not differentiated by the contour [17]. We assume that this increase of the volume caused by precipitation in the first weeks of corrosion affects the bending strength of the implants at that time. In our study the precipitation of calcium phosphates on the surface was observed via EDX analysis. This might explain the higher bending strength in week 6.

Primary bone healing is induced by a stiff construct and secondary bone healing by limited passive or active dynamization. However the role of mechanical stability in the fracture healing process is not totally cleared yet. Therefore it is not desirable to produce a total rigid complex. A mechanical stimulus is essential for bone growth and consolidation. It is still controversial which tactic would best improve the duration and strength of the healing fracture. But it is clear that stress shielding occurs as a result of the different Youngs moduls. The mention benefit of magnesium based implants is the low Youngs modul, this could avoid stress shielding.

There is a discrepancy between the maximum strength and the optimum strength. Magnesium plates are able to offer a time depending stability. However, it is important to define the demanded stability of a specific fracture. The needed stability of fracture depends on the bone quality, fracture geometry, localization of the fractured bone and the demand in rehabilitation. Therefore, the first demand should be define. According to the required implant characteristics the test standards should also be adjusted.

Conclusion

In the present work the degradation of ZEK100-plates was investigated. The bending strength increased after 6 weeks immersion compared to the 2 week group and 4 week group. The characterization of the surface revealed the presence of high amounts of O, P and Ca on the surface and small Mg content. This indicates the precipitation of calcium phosphates with low solubility on the surface of the ZEK100 plates. The present in vitro study indicates that ZEK100 is a potential candidate for degradable orthopedic implants. Further investigations are needed to examine the degradation behavior.

Abbreviations

EDX: Energy dispersive X-ray analysis; HBSS: Hank's Balanced Salt Solution; ICP-OES: Inductively coupled plasma optical emission spectrometry; μCT: μ-computed tomography; RE: Rare earth; SEM: Scanning electron microscope; wt%: Weight percent; XRD: X-ray diffraction; ZEK100: Magnesium alloy with 98.8 wt% magnesium 1 wt% zinc, 0.1 wt% zirconium and 0.1 wt% rare earth metals

Acknowledgements

The authors gratefully acknowledge the financial support given by German research society (DFG) within the collaborative research project (SFB 599). We thank Markus Badenhop for excellent technical support. We thank Christopher Müller for the design of Figure 1 and Hendrik Wardenga for creating Figure 2.

Author details

[1]Department of Orthopedic Surgery, Hannover Medical School, Anna-von-Borries-Str.1-7, 30625 Hannover, Germany. [2]Institute of Production Engineering and Machine Tools (IFW), Leibnitz University of Hannover, Lise-Meitner-Str. 1, 30823 Garbsen, Germany. [3]Institute for Inorganic Chemistry, Leibniz University of Hannover, Callinstr. 9, 30167 Hannover, Germany. [4]Small Animal Clinic, School of Veterinary Medicine Hannover, Bischhofsholer Damm 15, 30173 Hannover, Germany. [5]Clinic for Small Animal Surgery and Reproduction, Centre of Clinical Veterinary Medicine, Faculty of Veterinary Medicine Ludwig-Maximilians-Universität München, Veterinärstr. 13, 80539 Munich, Germany. [6]Institute of Materials Science, Leibniz University Hannover, An der Universität 2, 30823 Garbsen, Germany. [7]Center for Hip, Knee and Foot Surgery, ATOS Clinic Heidelberg, Bismarckstr. 9-15, 69115 Heidelberg, Germany.

Authors' contributions

HW supervised the in vitro corrosion examinations, analyzed the data and prepared the manuscript. AW analyzed the data and wrote the manuscript. CM performed the in vitro corrosion examinations and wrote the manuscript. FW and HW participated in the coordination of the corrosion experiments and helped to draft the manuscript. AL manufactured the plates and analyzed them via SEM and EDX. MK did the XRD analysis of the ZEK100 plates. BD, PB, AML and FWB revised the manuscript primarily although all authors made contributions. FT initiated the study, participated in its design and coordination. All authors read and approved the final manuscript.

Competing interests

The authors declare that they have no competing interests.

Received: 9 December 2011 Accepted: 13 March 2012 Published: 13 March 2012

References

1. Bartonicek J: **Early history of operative treatment of fractures.** *Arch Orthop Trauma Surg* 2010, **130**:1385-1396.
2. Brand RA: **Sir William Arbuthnot Lane, 1856-1943.** *Clin Orthop Relat Res* 2009, **467**:1939-1943.
3. Witte F: **The history of biodegradable magnesium implants: a review.** *Acta Biomater* 2010, **6**:1680-1692.
4. Van Der Elst M, Patka P, van der Werken C: **Biodegradable implants in fracture fixation: state of the art.** *Unfallchirurg* 2000, **103**:178-182.
5. Bach F-W, Rodman M, Rossberg A, Behrens B-A, Kurzare G: **Macroscopic damage by the formation of shear bands during rolling and deep drawing of magnesium sheets.** *J Min Met Mat Soc* 2005, **57**:57-61.
6. Hartwig A: **Role of magnesium in genomic stability.** *Mutat Res* 2001, **475**:113-121.
7. Witte F, Hort N, Vogt C, Cohen S, Kainer KU, Willumeit R, *et al*: **Degradable biomaterials based on magnesium corrosion.** *Current Opinion in Solid State and Material Science* 2008, **12**:63-72.
8. Tapiero H, Tew KD: **Trace elements in human physiology and pathology: zinc and metallothioneins.** *Biomed Pharmacother* 2003, **57**:399-411.
9. Gu X, Zheng Y, Cheng Y, Zhong S, Xi T: **In vitro corrosion and biocompatibility of binary magnesium alloys.** *Biomaterials* 2009, **30**:484-498.
10. Feyerabend F, Fischer J, Holtz J, Witte F, Willumeit R, Drucker H, *et al*: **Evaluation of short-term effects of rare earth and other elements used in magnesium alloys on primary cells and cell lines.** *Acta Biomater* 2010, **6**:1834-1842.
11. Hanzi AC, Gerber I, Schinhammer M, Loffler JF, Uggowitzer PJ: **On the in vitro and in vivo degradation performance and biological response of new biodegradable Mg-Y-Zn alloys.** *Acta Biomater* 2010, **6**:1824-1833.
12. Castellani C, Lindtner RA, Hausbrandt P, Tschegg E, Stanzl-Tschegg SE, Zanoni G, *et al*: **Bone-implant interface strength and osseointegration: Biodegradable magnesium alloy versus standard titanium control.** *Acta Biomater* 2011, **7**:432-440.

13. Reifenrath J, Krause A, Bormann D, von Rechenberg B, Windhagen H, Meyer-Lindenberg A: **Profound differences in the in-vivo-degradation and biocompatibility of two very similar rare-earth containing Mg-alloys in a rabbit model.** *Mat -wiss u Werkstofftech* 2010, **41**:1054-1061.
14. Thomann M, Krause C, Bormann D, von der Höh N, Windhagen H, Meyer-Lindenberg A: **Comparision of the resorbable magnesium alloys LAE442 and MgCa0.8 concerning their mechanical properties, their progress of degradation and the bone-implant-contact after 12 months implantation duration in a rabbit model.** *Mat -wiss u Werkstofftech* 2009, **40**:82-87.
15. Witte F, Kaese V, Haferkamp H, Switzer E, Meyer-Lindenberg A, Wirth CJ, *et al*: **In vivo corrosion of four magnesium alloys and the associated bone response.** *Biomaterials* 2005, **26**:3557-3563.
16. Witte F, Abeln I, Switzer E, Kaese V, Meyer-Lindenberg A, Windhagen H: **Evaluation of the skin sensitizing potential of biodegradable magnesium alloys.** *J Biomed Mater Res A* 2008, **86**:1041-1047.
17. Huehnerschulte TA, Angrisani N, Rittershaus D, Bormann D, Windhagen H, Meyer-Lindenberg A: **In vivo corrosion of two novel magnesium alloys ZEK100 and AX30 and their mechanical suitability as biodegradable implants.** *Materials* 2011, **4**:1144-1167.
18. Yang L, Zhang E: **Biocorrosion behavior of magnesium alloy in different simulated fluids for biomedical application.** *Mater Sci Eng C* 2009, **29**:1691-1696.
19. Song Y, Shan D, Chen R, Zhang F, Han E-H: **Biodegradable behaviors of AZ31 magnesium alloy in simulated body fluid.** *Mater Sci Eng C* 2009, **29**:1039-1045.
20. Li Z, Gu X, Lou S, Zheng Y: **The development of binary Mg-Ca alloys for use as biodegradable materials within bone.** *Biomaterials* 2008, **29**:1329-1344.
21. Zhang S, Li J, Song Y, Zhao C, Zhang X, Xie C, *et al*: **In vitro degradation, hemolysis and MC3T3-E1 cell adhesion of biodegradable Mg-Zn alloy.** *Mater Sci Eng C* 2009, **29**:1907-1912.
22. Song G, Song S: **A possible biodegradable magnesium implant material.** *Adv Eng Mater* 2007, **9**:298-302.
23. Song GL, Atrens A: **Corrosion mechanisms of magnesium alloys.** *Adv Eng Mater* 1999, **1**:11-33.
24. Xin Y, Hu T, Chu PK: **In vitro studies of biomedical magnesium alloys in a simulated physiological environment: a review.** *Acta Biomater* 2011, **7**:1452-1459.
25. Wang H, Shi Z: **In vitro biodegradation behavior of magnesium and magnesium alloy.** *J Biomed Mater Res B Appl Biomater* 2011, **98B**:203-209.
26. Zhang S, Zhang X, Zhao C, Li J, Song Y, Xie C, *et al*: **Research on an Mg-Zn alloy as a degradable biomaterial.** *Acta Biomater* 2010, **6**:626-640.
27. Wang HX, Guan SK, Wang X, Ren CX, Wang LG: **In vitro degradation and mechanical integrity of Mg-Zn-Ca alloy coated with Ca-deficient hydroxyapatite by the pulse electrodeposition process.** *Acta Biomater* 2010, **6**:1743-1748.
28. Budiraharjo R, Neoh KG, Kang ET: **Hydroxyapatite-coated carboxymethyl chitosan scaffolds for promoting osteoblast and stem cell differentiation.** *J Colloid Interface Sci* 2011, **366**:224-232.
29. Rettig R, Virtanen S: **Composition of corrosion layers on a magnesium rare-earth alloy in simulated body fluids.** *J Biomed Mater Res A* 2009, **88**:359-369.
30. Huan ZG, Leeflang MA, Zhou J, Fratila-Apachitei LE, Duszczyk J: **In vitro degradation behavior and cytocompatibility of Mg-Zn-Zr alloys.** *J Mater Sci Mater Med* 2010, **21**:2623-2635.
31. Song RG, Blawert C, Dietzel W, Atrens A: **A study on stress corrosion cracking and hydrogen embrittlement of AZ31 magnesium alloy.** *Mater Sci Eng, A* 2005, **399**:308-317.
32. Zainal Abidin NI, Atrens AD, Martin D, Atrens A: **Corrosion of high purity Mg, Mg2Zn0.2Mn, ZE41 and AZ91 in Hank's solution.** *Corros Sci* 2011, **53**:862-872.
33. Mueller W-D, Nascimento ML, de Mele MF: **Critical discussion of the results from different corrosion studies of Mg and Mg alloys for biomaterial applications.** *Acta Biomater* 2010, **6**:1749-1755.
34. Witte F, Fischer J, Nellesen J, Crostack HA, Kaese V, Pisch A, *et al*: **In vitro and in vivo corrosion measurements of magnesium alloys.** *Biomaterials* 2006, **27**:1013-1018.

doi:10.1186/1475-925X-11-12
Cite this article as: Waizy *et al.*: In vitro corrosion of ZEK100 plates in Hank's Balanced Salt Solution. *BioMedical Engineering OnLine* 2012 **11**:12.

4 LDHs as Tunable Implant Materials with Regard to Orthopedic Application

4.1 Preface

This chapter deals in two articles with the *in vitro* stability of Mg-Al-CO_3-LDHs (section 4.2), and the *in vitro* and *in vivo* examination of Mg-Al- and Mg-Fe-LDHs (section 4.3) with regard to their applicability in orthopedics. Both studies were performed in comparison with magnesium hydroxide. Examination of magnesium hydroxide-derived compounds is of interest due to the osteoinductive properties of magnesium hydroxide, which holds the promise for enhanced implant incorporation when employed as a coating on the implants.

The *in vitro* stabilities of $Mg(OH)_2$ and Mg-Al-LDH coatings were investigated by exposing the substances as coatings on titanium alloy discs to aqueous conditions and repeated sampling from the medium (section 4.2). LDHs with varied cation ratios and $Mg(OH)_2$ were coated using a semiautomatic spray-coating chamber, comprising IR heating and a rotating sample desk. This device evolved from simpler spray-coating techniques as applied for the LDH coatings described in section 5.2, which comprised manually operated airbrush equipment. Mg^{2+} concentrations were estimated by ICP-OES measurements of the samples and the general stability of the coatings was complementarily evaluated according to SEM and XRD data collected before and subsequent to the immersion. The release rates and the according general stabilities of the coatings were shown to depend on the composition of the coatings and on the processing parameters, in particular the spray-coating temperature. The results show that magnesium-containing LDHs are versatile Mg^{2+} sources, which is of high interest with regard to osteoinductive coatings in orthopedics.

For the *in vivo* evaluation of Mg-Al- and Mg-Fe-LDHs and $Mg(OH)_2$ with regard to application in orthopedics (section 4.3), cylindrical pellets (3x3 mm) were produced by pressing powders of the substances. The pellets were implanted into femur condyles of New Zealand White rabbits and were examined in the *ex vivo* state by µCT measurements. Whereas the $Mg(OH)_2$ cylinders decreased considerably in volume, the LDH cylinders remained intact. Host response was evaluated according to histological investigations focusing on the implant-bone interface. With regard to cell compatibility, flat pellets of the same substances were tested with NIH3T3 fibroblasts and MG63 osteosarcoma cells under standard cell culture conditions. It was found that cell densities were reduced in comparison to the polystyrene control surfaces; however, cell compatibility was judged as good overall. According to both, cell tests and *in vivo* host response,

the Mg-Al-LDH system emerged as the most promising biomaterial of this study for orthopedic applications.

Furthermore, magnesium hydroxide with increased surface area (BET) was synthesized as a powder and processed to pellets. These were tested *in vitro* and *in vivo* in accordance with the experimental series for the other substances listed above. Due to the resemblance of the results gained from the two magnesium hydroxide related series, the results from the non-commercially available $Mg(OH)_2$ were neglected for the article. Nonetheless, this finding emphasizes the necessity for tunable magnesium hydroxide derivates, like magnesium containing LDHs.

For the studies presented in sections 4.2 and 4.3, differently composed Mg-LDHs were examined in course of *in vitro* and *in vivo* studies. For these, Mg-LDHs were synthesized and processed into pellets, nanosuspensions and coatings. The studies discussed above present in particular the Mg-Al-CO_3-LDH as a versatile, processable and biocompatible LDH system, with high potential for orthopedic application.

With regard to the application as coatings on hip implants, the *in vivo* examination of coated implants and implant materials, respectively, should be in the focus of future investigations. Furthermore, the examination of drug/LDH mixtures or intercalation compounds could allow for the evaluation of the influence of the respective drugs on implant incorporation.

For the article presented in section 4.2 the author of this thesis is the first author and the manuscript was for the most part drafted by him. The syntheses of the raw LDHs and $Mg(OH)_2$, as well as the further treatment in order to obtain nanosuspensions were performed by the author. All XRD measurements and according data interpretation were performed and contributed accordingly to the publications by him. Immersion experiments and ICP-OES measurements in this study were performed by Tim-Joshua Pinkvos in the course of the work for his B. Sc. thesis: “Zum Verhalten von Mg-Al-Carbonat-Hydroxid-Beschichtungen in wässrigen Medien” (“On the behavior of Mg-Al-carbonate-hydroxide coatings in aqueous media”, 2014, Leibniz Universität Hannover), supervised by the author of this thesis. SEM images were collected by Hendrik Fullriede and Gesa Zahn. Philip Dellinger prepared the metal slides, in particular by sandblasting, and spray-coated the samples with the nanosuspensions. Susanne E. Thürer, Alexandra Satalov and Sabine Behrens established ICP-OES measuring routines and performed maintenance of the ICP-OES devices. Peter Behrens coordinated the study together with Kai Möhwald and Andreas Weizbauer and primarily revised the manuscript. The study was initiated by Peter Behrens.

For the article presented in section 4.3 the author of this thesis and Andreas Weizbauer are the first authors, who contributed equally to this study. The manuscript was mostly written by Andreas Weizbauer. The selection of the applied LDH-compositions based on pre-studies and synthesis of the LDH and $Mg(OH)_2$ as well as their characterization, in particular by XRD means, were performed by the author of this thesis. LDH and $Mg(OH)_2$ pellets for the cell tests and for preliminary studies were fabricated by him or under his supervision. The employed pressing tools for the latter pellets were designed by him and the workshop of the Institute for Inorganic Chemistry (Leibniz Universität Hannover). The final pellets for the main *in vivo* study were fabricated by the Department of Inorganic Chemistry, University of Essen. The *in vitro* cell compatibility tests were performed by Muhammad Imran Rahim and the ICP-OES-analysis of the Mg^{2+}-content of the supernatants were performed by the Medical Laboratory of Bremen. The surgeries of the animals were conducted alternately by Thilo Flörkemeier and Stefan Budde with intraoperative assistance by Andreas Weizbauer. Anesthesia, follow-up examination of the animals and euthanasia were done by Julia Diekmann. Sample explantation was conducted by both Julia Diekmann and Andreas Weizbauer. The *ex vivo* µCT investigations were performed under supervision of Gian Luigi Angrisani by Andreas Weizbauer at the Institute of Materials Science, Leibniz Universität Hannover, and histological investigations were performed by Elmar Willbold or under his supervision. Andreas Weizbauer analyzed the data and coordinated the study. Thilo Flörkemeier, Henning Windhagen, Peter Paul Müller, Peter Behrens, Stefan Budde initiated the study and revised the manuscript.

4.2 Different magnesium release rates from magnesium hydroxide and magnesium containing layered double hydroxide coatings

Marc Kieke, Philip Dellinger, Tim-Joshua. Pinkvos, Susanne E. Thürer, Alexandra Satalov, Andreas Weizbauer, Sabine Behrens, Kai Möhwald, Peter Behrens

This section will be submitted as an original research article.

Different magnesium release rates from magnesium hydroxide and magnesium containing layered double hydroxide coatings

Marc Kieke ▪ Philip Dellinger ▪ Tim J. Pinkvos ▪ Susanne E. Thürer ▪ Alexandra Satalov ▪ Andreas Weizbauer ▪ Henning Windhagen ▪ Sabine Behrens ▪ Kai Möhwald ▪ Peter Behrens

Abstract

The limitation of the longevity of artificial joint replacements due to aseptic loosening and bacterial infections is a key challenge in the field of sustainable implants. Implant coatings that can support the prosthesis fixation and that can combat infections by local drug release would be of high interest. For both purposes, controllable degradation of the coatings would enable their adjustment for the respective applications. Layered double hydroxides (LDHs) are a promising class of biomaterials. Their solubility and their degradation rate can be controlled by their exact composition. As both metallic magnesium and magnesium hydroxide have shown osteoproliferative properties (possibly connected to the liberation of Mg^{2+} ions), magnesium-containing LDHs appear as a suitable material for the coating of implants. In this study, the *in vitro* Mg^{2+} release rate of two such LDHs (with a 2:1 ratio and a 4:1 ratio of Mg and Al, respectively) is determined and compared to the behavior of $Mg(OH)_2$. For this purpose, suspensions of the LDHs and of $Mg(OH)_2$ were spray-coated on TiAl6V4 slides and exposed to aqueous conditions at 37°C. Over the examination time of five days samples were taken repeatedly and the Mg^{2+} concentration was determined by inductively coupled plasma optical emission spectroscopy. In addition, the degradation rate of an LDH (with a 2:1 ratio of Mg and Al) coating which was spray-deposited at elevated substrate temperatures was examined. The results showed that degradation rates of the magnesium containing coatings examined were increased by increased spray coating temperature and as expected by increasing the Mg^{2+} contribution to the coating substance.

Key words: magnesium, layered double hydroxides, coating, degradation, nanosuspension

M. Kieke · T. J. Pinkvos· Alexandra Satalov · P. Behrens (✉)

Institute for Inorganic Chemistry, Leibniz University of Hannover,
Callinstr. 9, 30167 Hannover, Germany
e-mail: Peter.Behrens@acb.uni-hannover.de

P. Dellinger · K. Möhwald

Institute of Materials Science, Leibniz Universität Hannover,
Branch Witten, Stockumer Str. 28, 58453 Witten, Germany

S. E. Thürer · S. Behrens

Institute of Materials Science, Leibniz Universität Hannover,
An der Universität 2, 30823 Garbsen, Germany

A. Weizbauer· H. Windhagen

Laboratory for Biomechanics and Biomaterials, Department of Orthopedic Surgery, Hannover Medical School,
Anna-von-Borries-Straße1-7, 30625 Hannover, Germany

CrossBIT, Centre for Biocompatibility and Implant-Immunology,
Department of Orthopedic Surgery, Hannover Medical School,
Feodor-Lynen-Straße 31, 30625 Hannover, Germany

1 Introduction

Total hip arthroplasty (THA) is considered as a successful surgical intervention and it is the most frequently performed artificial joint replacement procedure. It has a survivorship of more than 80% at 20 years after surgery [1]. More than 800,000 THA are performed worldwide every year [2], providing pain relief for many patients. These orthopedic devices restore the loss of function of damaged or degenerated structures caused by osteoarthritis, avascular necrosis, rheumatoid arthritis, femoral neck fracture, tumours, and developmental dysplasia [3]. The reasons for revision of the primary joint replacement are manifold, and include instability/dislocation, mechanical loosening, and infection[4]. Integration into the surrounding bone is a primary aim in order to enhance implant fixation and prevent infection. For this purpose, (parts of) the shafts of commonly used prosthesis are nowadays coated by calcium-containing compounds (hydroxyapatite, brushite).

Magnesium and its alloys have a long-standing history as degradable biomaterials [5]. Amongst various advantages, their osteoinductive properties have gained them increasing interest in the field of degradable implant materials [6]. Implants made from magnesium or its alloys are expected to initially provide a suitable degree of mechanical stability and then to dissolve while the growth of the surrounding bone is enhanced. However, the osteoproliferative properties are not an exclusive feature of metallic magnesium or its alloys. It was shown that magnesium hydroxide, which is a dominant corrosion product of magnesium and its alloys under various aqueous conditions [7], also has osteoproliferative properties [8]. These could, therefore, be ascribed to the release of Mg^{2+} or OH^- ions. By applying coatings of magnesium hydroxide (or a similar material) on orthopedic prostheses, the osteoproliferative effects could be used on permanent implants, too. However, magnesium hydroxide is an individual compound with a fixed stoichiometry and its degradation cannot be regulated, except for small variations relying on the size of small particles.

Layered double hydroxides (LDHs) containing magnesium which have the general formula $[Mg_{1-x}M^{III}_x(OH)_2^{x+}][A^{n-}]_{x/n}\cdot yH_2O$ are a promising class of biomaterials. Their structure can be derived from the layered structure of magnesium hydroxide by substituting a certain amount of Mg^{2+} ions with trivalent cations M^{III} such as Al^{3+} or Fe^{3+} [9]. The surplus positive charge on the layers has to be balanced by intercalated anions A^{n-}, simple ones as Cl^-, NO_3^-, CO_3^{2-} [10], or more complex ones as anions of pharmaceutically relevant compounds, e.g. ibuprofen and indomethacin [11][12], making this class of material attractive for drug delivery applications. Furthermore, drugs can also be simply mixed with LDHs in order to create effective release systems [13]. In a former *in vivo* study, we have shown that a ciprofloxacin/LDH mixture can curb a bacterial infection when applied as a coating on middle ear implants in rabbits [14].

For both purposes, osteoproliferation as well as drug release from drug/LDH mixtures, tunable Mg-LDH degradation rates would be of interest. As mentioned, Mg-LDHs can be formed with a variety of trivalent cations and anions. Different relative stabilities could be observed for Mg-LDHs with different trivalent cations [15] and also with different anions [16]. Furthermore, the variation of the cation ratio $Mg:M^{III}$ between 2:1 and 4:1 has been reported [9]. This variation is in accordance with the general formula and does not fundamentally change the LDH structure. However, measureable variations of the interlayer distances depending on the respective cation ratios have been reported for Mg-Al-LDHs [17] and Mg-Fe-LDHs [18].

In the present study, we have focussed on the Mg-Al-LDH system, which has proven suitable for implant coatings. Stable nanosuspensions can be obtained via different routes [19]. Since these sols feature a homogenous distribution of particles that are considerably smaller than the diameters of nozzles and tubes of coating devices, spray coating proved to be a suitable technique for the coating of implants with simple and complex geometries. TiAl6V4 was chosen as substrate material, since this alloy is commonly used for hip and knee prostheses. Four different types of coatings, three from LDHs and one of magnesium hydroxide, were examined for their degradation behavior with regard to the composition of the respective coatings and the influence of the substrate temperature during the spray coating.

2 Materials and Methods

2.1 Preparation of suspensions containing magnesium compounds

In the present study three different magnesium compounds were investigated: (I) 2:1-Mg-Al-CO_3-LDH ($Mg_{3.6}Al_2(OH)_{11.2}(CO_3)\cdot yH_2O$), (II) 4:1-Mg-Al-$CO_3$-LDH ($Mg_{5.4}Al_2(OH)_{14.8}(CO_3)\cdot yH_2O$), and (III) $Mg(OH)_2$. The layered double hydroxides (I) and (II) were precipitated from water by adding two solutions, one containing $MgCl_2\cdot 6H_2O$ (purum p.a. ≥98.0%, Fluka, Buchs, Switzerland) and the other $AlCl_3\cdot 6H_2O$ (purum p.a. ≥99.0%, Fluka) to a vigorously stirred solution of NaOH (reagent grade, anhydrous, ≥98%, Fluka) and $Na_2CO_3\cdot H_2O$ (≥99.5%, Fluka). For the preparation of $Mg(OH)_2$ (III), a solution of $MgCl_2\cdot 6H_2O$ (purum p.a. ≥98.0%, Fluka) was added to a vigorously stirred solution of NaOH (reagent grade, anhydrous, ≥98%, Fluka). The respective amounts used are listed in Table 1.

Table 1 Chemicals and their respective amounts used for the preparation of the suspensions of magnesium compounds.

		Amount of substance / mmol			
		$MgCl_2 \cdot 6H_2O$	$AlCl_3 \cdot 6H_2O$	NaOH	$Na_2CO_3 \cdot H_2O$
(I)	2:1-Mg-Al-CO_3-LDH	100	50	300	60
(II)	4:1-Mg-Al-CO_3-LDH	100	25	200	30
(III)	$Mg(OH)_2$	50	-	100	-

Subsequently to the precipitation, the mixtures were allowed to stand for one hour and the raw products were centrifuged repeatedly and washed with deionized water. After three washing cycles the wet materials were redispersed in water and exposed to ultrasonication for 30 min. By diluting with deionized water the respective solid content of all suspensions was adjusted to 3.5 $g \cdot L^{-1}$. All steps were performed at room temperature and all chemicals were used as purchased without further purification.

According to ICP-OES (Spectroflame Ciros Vision CCD, Spektro, Kleve, Germany) measurements the Mg:Al ratio of the (I) 2:1-Mg-Al-CO_3-LDH was estimated to be 1.8:1 and the cation ratio of the (III) 4:1-Mg-Al-CO_3-LDH was estimated to be 3.7:1. However, the LDHs were named according to their expected cation ratios.

2.2 Spray Coating

Cylindrical, sandblasted (corundum) TiAl6V4 slides with a diameter of 1 cm and a height of 3 mmwere spray coated with the magnesium containing suspension described above, using a semi-automatic spray coating chamber. Prior to the coating, the samples as well as the sample holder were heated by four IR lamps (each with 150 W) to the desired temperature within five minutes. For each coating cycle three samples were placed on the rotatable table in order to be coated equally. Accordingly, degradation experiments were performed in triplicate. The spraying setup was characterized by a spray angle of 45° and a nozzle-to-sample distance of 10 cm. For each coating cycle an amount of 7 mL of the suspensions (3.5 $g \cdot L^{-1}$) was used. After each coating cycle the spray gun was cleaned. All three suspensions (I)-(III) were sprayed applying a sample temperature of 150°C. The setup was repeated with a substrate temperature of 300°C to investigate the influence of the sample temperature.

In order to determine if the samples were successfully coated with LDH/$Mg(OH)_2$ and if the respective crystal structures were maintained, X-Ray diffraction (XRD) measurements were performed on a Theta/Theta diffractometer from Stoe (Stoe, Darmstadt, Germany) in reflection mode using Cu Kα radiation ($\lambda = 1.54060$ Å). The 2Θ range of 5-50° was scanned applying a step size of 0.01° (2.5 s per step). The diffractometer was operated at 40 kV and 30 mA. All samples were placed flatly in a sample holder and were rotated during the measurement. No further sample preparations were made for the XRD measurements.

For morphological evaluations, SEM images were collected before and after the immersion studies using a JSM-6610LV (Jeol, Eching, Germany), operated with an accelerating voltage of 10 kV using the SEI detector. High-resolution SEM images were collected with a JSM-6700F (Jeol, Eching, Germany), operated with an accelerating voltage of 2.0 kV using the SEI-detector.

2.3 Degradation setup

The coated TiAl6V4 slides were placed into each a reactor of a liquid handling system (LHS) (Liquid Station PS-C520, Duratec Analysentechnik, Hockenheim, Germany) using common cable binders (Conrad Electronic SE, Hirschau, Germany) for fixation. Three slides were immersed simultaneously, each in an individual reactor, containing deionized water (50 mL, 37°C). The sampling process included the extraction of 1 mL from the medium and the restocking with 1 mL deionized water, keeping the total medium volume in the reactors constant. After the extracted samples were transferred to storage vessels, nitric acid (2 N, 400 µL) and deionized water (8.600 mL) were added in order to adjust the samples to the ICP-OES calibration. Sampling and pH monitoring was performed automatically by the LHS after 0 h, 6 h, 12 h, 18 h, 24 h, 36 h, 48 h, 60 h, 72 h, 84 h, 96 h, 108 h and 120 h, totaling in 13 samples for each slide. Over the examination period, the medium was stirred using a magnetic stirring bar (300 rpm). All devices were rinsed with diluted nitric acid and then deionized water before use.

2.4 Mg^{2+} and Al^{3+} concentration measured with ICP-OES

Magnesium concentrations of the samples taken and adjusted by the LHS were estimated using a Spectroflame Ciros Vision CCD (Spektro, Kleve, Germany), operated with Ar 4.6 (Air Liquide, Düsseldorf, Germany) and a plasma power of 1400 W. Calibration for both Mg^{2+} (279.553 nm) and Al^{3+} (167.078 nm) was done according to the following concentrations: 0.005 $mg \cdot L^{-1}$, 0.010 $mg \cdot L^{-1}$, 0.020 $mg \cdot L^{-1}$, 0.050 $mg \cdot L^{-1}$, 0.100 $mg \cdot L^{-1}$, 0.200 $mg \cdot L^{-1}$, 0.500 $mg \cdot L^{-1}$, 1.000 $mg \cdot L^{-1}$ using single-element ICP-standard-solutions by Roth (Carl Roth, Karlsruhe, Germany), diluted with an autodiluter microLAB 600 series (Hamilton Company, Reno, USA). Correlation coefficients were found to be 0.99994-1.

3 Results

3.1 Chemical analysis of the coatings

According to optical evaluation and evaluation of the SEM images Fig. 1 (left), coatings were obtained from all three magnesium sources, sprayed at 150°C and 300°C, respectively. The appearances of the coatings sprayed at 150°C are in accordance with the expectations based on earlier spray coating experiments. Despite the presence of cracks, the coatings seem to cover most of the metal slides and were mechanically stable when handled as needed for the analyses. The samples sprayed at 300°C appear remarkably patchy at micrometer scale. High-resolution SEM images are shown in Fig. 2 and reveal no noticeable difference between the samples at nanometer scale. The chemical stability of the substances at these temperatures was confirmed by XRD measurements of coated samples. As shown in Fig. 3 (left), X-ray diffractograms obtained comprised combined XRD patterns of the respective coating materials and the TiAl6V4 slides. In the case of the spray coating at 300°C the main reflections of the Mg-LDH are broadened, probably due to a deterioration of the 2:1-LDH at 300°C. All X-ray diffractograms also contain reflections that can be attributed to corundum (Al_2O_3) presumably residing from the sandblasting.

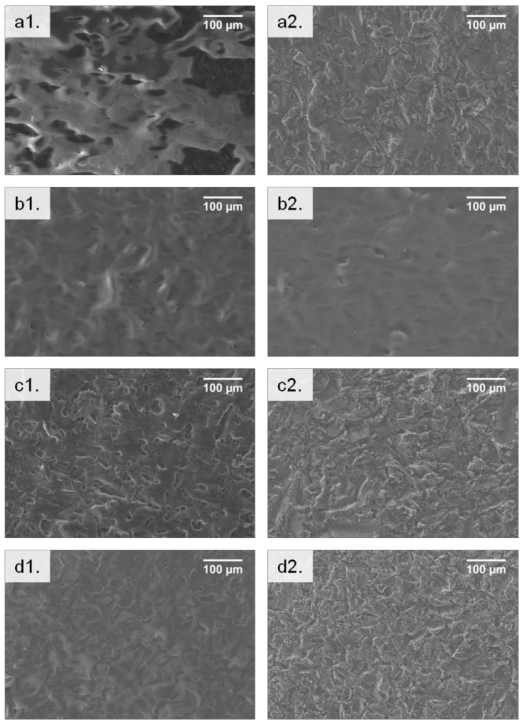

Fig. 1 Exemplary SEM images of coatings (1) before and (2) after immersion; (a) 2:1-LDH sprayed at 300°C, (b) 2:1-LDH sprayed at 150°C, (c) 4:1-LDH sprayed at 150°C and (d) $Mg(OH)_2$ sprayed at 150°C

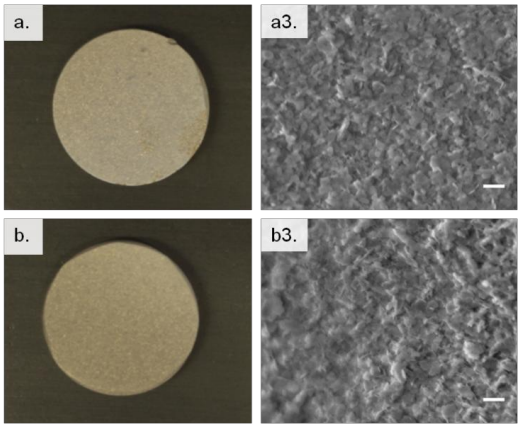

Fig. 2 Photographs and (3) high-resolution SEM images of (a) 2:1-LDH sprayed at 300°C and (b) 2:1-LDH sprayed at 150°C. Scale bars represent 200 nm

3.2 Post-immersion analysis of the coatings

After the immersion studies, SEM images of the dried samples were collected and compared to the images of the un-immersed samples. Fig. 1 (right) shows exemplary SEM images of dried samples from the immersion studies. In the case of the 2:1-LDH coating (150°C) only minor signs of alteration can be seen, while the comparison of the other series, i.e. 4:1-LDH (150°C), $Mg(OH)_2$ (150°C) and 2:1-LDH (300°C) revealed fundamental changes at the samples surfaces. After the degradation studies, the sample surfaces of the latter series resemble uncoated, sandblasted TiAl6V4 substrates.

A selection of XRD patterns of dried samples is shown in Fig. 3 (right). A pronounced decomposition of the coating is expected to result in a fundamental decrease of the relative reflection intensities derived from the respective compounds. In the case of the 2:1-LDH coating (150°C) the relative intensities did not decrease noticeably, which is in accordance with the observations gained from the SEM images. The fading of the coatings in the other series is in agreement with the decrease of their relative intensities in the XRD patterns shown. In the case of the 4:1-LDH and 2:1-LDH (300°C) series, newly formed $Mg(OH)_2$ can be found according to the XRD patterns.

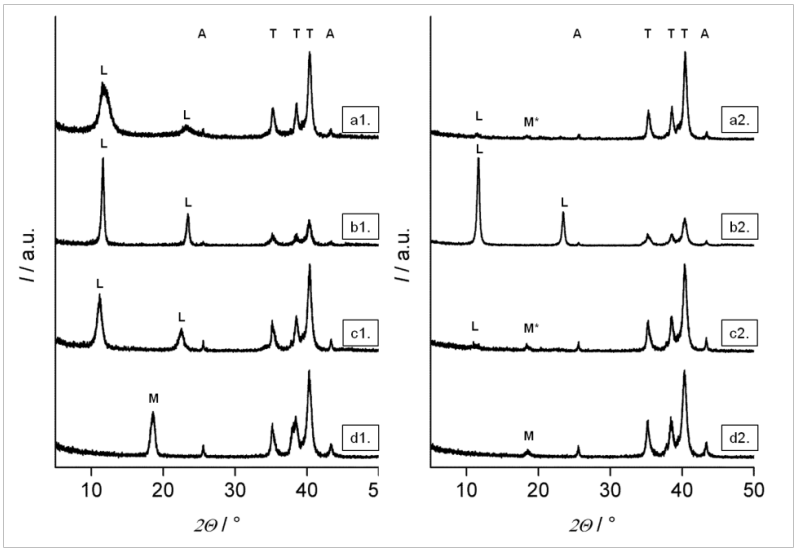

Fig. 3 Exemplary XRD patterns of coatings (1) before and (2) after immersion; (a) 2:1-LDH sprayed at 300°C, (b) 2:1-LDH sprayed at 150°C, (c) 4:1-LDH sprayed at 150°C and (d) $Mg(OH)_2$ sprayed at 150°C. Reflections of different compounds are marked with: L = layered double hydroxide, A = Al_2O_3 (cordundum), T = titanium alloy, M = $Mg(OH)_2$ (brucite), M* = newly formed brucite

3.3 Mg^{2+} release

Mg^{2+} release from the different coatings was determined by ICP-OES. The magnesium concentrations as a function of time are shown in Fig. 4 . In general, burst release behavior was observable for all four release systems. After the initial higher release rates, gradients decreased distinctly. In case of the coatings sprayed at 150°C, the release rates increased with the respective Mg^{2+} contribution to the substance. Accordingly, the degradation rate and final Mg^{2+} concentrations were lowest for the 2:1-LDH (150°C) coating and highest for the $Mg(OH)_2$ coating. The initial release rate of the 2:1-LDH coating sprayed at 300°C resembles the one of the 4:1-LDH (150°C). Remarkably, the release rate for 2-5 days was the highest in the study. The initial and progressed Mg^{2+} release rates, final concentrations and pH values are listed in Table 2.

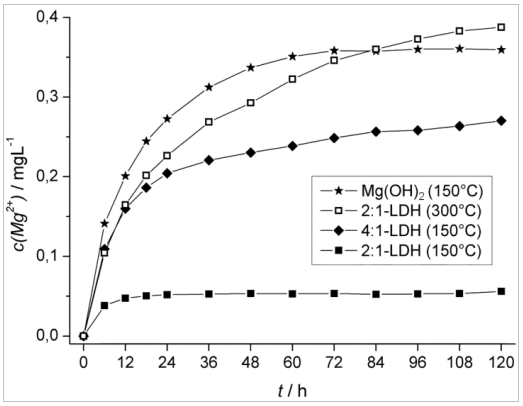

Fig. 4 Mg^{2+} ion release from different coatings as a function of time. Error bars are in the scale of the symbols, hence neglected for clarity

Table 2 Mg^{2+} release rates, final Mg^{2+} concentrations and final pH values

coating substance	spray temperature	Mg^{2+} release rate / $mg \cdot L^{-1} \cdot h^{-1}$		final Mg^{2+} concentration / $mg \cdot L^{-1}$	final pH
		0-12 h	2-5 days		
2:1-LDH	300°C	0.082	0.019	0.388 ± <0.001	8.1
2:1-LDH	150°C	0.024	<0.001	0.056 ± <0.001	6.9
4:1-LDH	150°C	0.080	0.008	0.270 ± 0.001	7.4
$Mg(OH)_2$	150°C	0.101	0.009	0.359 ± 0.002	8.0

3.4 pH and Al^{3+} release

In accordance with the Mg^{2+} release curves, pH increased with a burst-like behavior for all coatings. After 12 h the increase of the pH was attenuated in the case of the 2:1-LDH coatings, and even decreased in the case of the 4:1-LDH (150°C) and $Mg(OH)_2$ (150°C) coatings (Fig. 5). The highest pH was found in the medium of the $Mg(OH)_2$ coating (8.8 ± 0.3, 12 h).

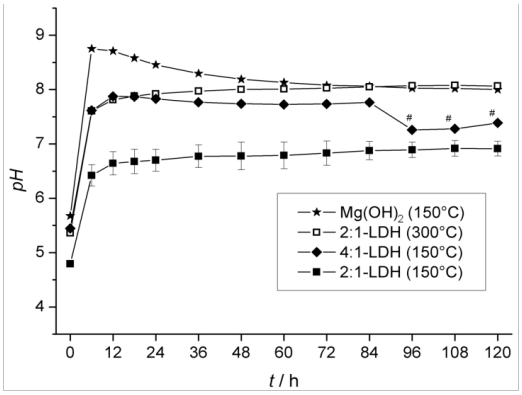

Fig. 5 PH of the medium of different coatings as a function of time. Error bars are exemplarily shown for the 2:1-LDH (150°C) series. Data points marked with # had a three to four-fold error due to unresolved reasons

Besides the Mg^{2+} concentration, also the Al^{3+} concentration was estimated. Al^{3+} concentrations released from the LDH coatings were noticeably lower than expected, presumably due to the low solubility of $Al(OH)_3$ at moderate pH values. Hence, these data were neglected for further considerations. A minor final Al^{3+} concentration around 0.013 $mg\text{-}L^{-1}$ was found in the $Mg(OH)_2$ (150°C) series. Since Al is not present in the coating, at higher pH probably $Al(OH)_4^-$ was formed according to $Al_2O_3/Al(OH)_3 + OH^- \rightarrow Al(OH)_4^-$ on the surfaces of the TiAl6V4 substrate or corundum residing from the sandblasting, respectively.

4 Discussion

4.1 Material stability during spray coating

Long-term stable suspensions were obtained from all four substances, which proved to be stable under the applied spraying conditions. XRD measurements confirm the presence of expected, crystalline substances on the TiAl6V4 substrates. However, crystallinity of the 2:1-LDH sprayed at elevated temperatures seemed somewhat mitigated. According to the morphologic evaluation, dense coatings could be obtained at 150°C substrate temperature, whereas the 2:1-LDH coating obtained at 300°C had a patchy appearance at micrometer scale. Nonetheless, all coatings examined were sufficiently mechanically stable when handled as needed for the analyses.

4.2 Degradation rates depending on the composition (150°C)

For the coatings, sprayed at the same substrate temperature, Mg^{2+} release rates were found to be increased in the following order of substances: 2:1-LDH < 4:1-LDH < $Mg(OH)_2$. The findings are in accordance with the XRD and SEM post-immersion analyses of the coatings.

This sequence is in agreement with the increasing Mg^{2+} contribution to the coating substances, leading to an increased concentration gradient and by this an increased release rate. In case of the Mg-Al-CO_3-LDHs, the decrease of the Al^{3+} content could also lead to a destabilization of the layer structure, which is stabilized by electrostatic interactions. A decrease of the Al^{3+} content decreases the number of carbonate anions in the interlayers, while the layer distances are widely maintained. The sequence of final pH values is in agreement with the Mg^{2+} release sequence. As known, LDH weathering kinetics depend on pH and the strength of the cation binding [20]. However, no signs for crystalline aluminium hydroxides were found in this study.

4.3 Degradation rates depending on the substrate temperature (150°C/300°C)

The 2:1-LDH suspension was spray coated at 150°C and 300°C, respectively. The latter coating showed higher release rates at the beginning and at later time points, higher pH throughout the experiment, and higher final Mg^{2+} concentrations. The initial release rate is close to the one of the 4:1-LDH (150°C) coating, while the final concentration is close to the one of $Mg(OH)_2$. Remarkably, the gradient of the release curve for the period of 2-5 days is twice the gradient of the $Mg(OH)_2$ curve.

According to SEM images no difference at nanometer scale (Fig. 2), but on micrometer scale (Fig. 1) can be observed. Due to the patchy texture of the coating a presumably considerable amount of LDH particles are exposed to the medium, which might have enhanced degradation [20]. Also XRD results (Fig. 3) indicate a change in the properties of the material, which might have caused the increase of the release rates. Structural alterations at elevated temperatures were also reported for hydrotalcite, which can be designated as the prototype compound for Mg-Al-LDHs. While lattice parameters and orientation of CO_3^{2-} ions were maintained in course of dehydration at 150°C, at 250°C a change of lattice parameters and a grafting of CO_3^{2-} ions occured [21]. A change of local coordination of carbonate ions at elevated temperatures, was also reported for dehydrated Mg-Al-CO_3-LDHs [22]. However, the exact causes and mechanisms that led to the increased release rates or the formation of $Mg(OH)_2$ in two series, cannot be derived from the data gained in this study.

4.4 Considerations for further application

Different Mg^{2+} release rates, hence, degradation rates were found for different magnesium hydroxide based coatings. The possibility to take influence on the degradation rates by the choice of the material and the coating parameters could be useful for various release systems such as drug delivery systems. Nonetheless, as known in magnesium chemistry, results from *in vitro* and *in vivo* setups can differ drastically [23].

The spray ciating system can be used for different geometric samples such as cylindrical dental implants as well.

Drug/LDH intercalation compounds have drawn an increasing interest as drug delivery vehicles [24]. It is pointed out that, syntheses and processing of intercalation compounds are demanding processes that have to be adjusted for every drug/LDH system and not all drugs are suitable for the intercalation. If appropriate and compatible with the application, drug molecules could be added to the chosen LDH/$Mg(OH)_2$ suspension in order to suit the prostheses coating with the respective functionalization. Alternatively, drugs and LDH/$Mg(OH)_2$ could be coated in alternating sequences, allowing also for multilayer systems of differently degrading hydroxides. In any case, the drugs have to be stable at elevated temperatures. For some drug/LDH systems the thermal behavior has been reported, showing that LDH can serve as a protection against thermal decomposition [25]. In the case of the drug/LDH intercalation compounds or reactive LDHs such as Cl^-- and NO_3^--LDHs [26][27], also the stability against an anion exchange during the spray coating has to be considered.

5 Conclusion

Water-based suspensions of $Mg(OH)_2$, 2:1-Mg-Al-CO_3-LDH and 4:1-Mg-Al-CO_3-LDH are suitable materials for the spray coating of TiAl6V4 substrates at moderate spraying temperatures. The substances proved chemically inert throughout the spraying process and mechanically stable when handled commonly.

Different degradation behaviors of magnesium hydroxide derived coatings can be realized by increasing the spray coating temperature and as expected by increasing the Mg^{2+} contribution to the coating substance.

For further applications, the availability of a repertoire of differently degrading, magnesium containing coating substances and their combinations, respectively, could be of advantage.

6 Acknowledgement

Our work is funded by the German Research Foundation (DFG) within the Collaborative Research Centre SFB 599 (subprojects D1 and DR1).

7 Reference

1. Berry DJ, Harmsen WS, Cabanela ME, Morrey BF. Twenty-five-Year Survivorship of Two Thousand Consecutive Primary Charnley Total Hip Replacements. J. Bone Joint Surg. Am. 2002;84-A:171–7.

2. Ingham E, Fisher J. The role of macrophages in osteolysis of total joint replacement. Biomaterials. 2005;26:1271–86.

3. Pramanik S, Agarwal A, Rai K. Chronology of total hip joint replacement and materials development. Trends Biomater. Artif. Organs. 2005;19:15–26.

4. Bozic KJ, Kurtz SM, Lau E, Ong K, Vail TP, Berry DJ. The epidemiology of revision total hip arthroplasty in the United States. J. Bone Joint Surg. Am. 2009;91:128–33.

5. Witte F. The history of biodegradable magnesium implants: a review. Acta Biomater. Acta Materialia Inc.; 2010;6:1680–92.

6. Witte F, Kaese V, Haferkamp H, Switzer E, Meyer-Lindenberg A, Wirth CJ, et al. In vivo corrosion of four magnesium alloys and the associated bone response. Biomaterials. 2005;26:3557–63.

7. Waizy H, Weizbauer A, Modrejewski C, Witte F, Windhagen H, Lucas A, et al. In vitro corrosion of ZEK100 plates in Hank's Balanced Salt Solution. Biomed. Eng. Online. BioMed Central Ltd; 2012;11:12.

8. Janning C, Willbold E, Vogt C, Nellesen J, Meyer-Lindenberg A, Windhagen H, et al. Magnesium hydroxide temporarily enhancing osteoblast activity and decreasing the osteoclast number in peri-implant bone remodelling. Acta Biomater. 2010;6:1861–8.

9. Khan AI, O'Hare D. Intercalation chemistry of layered double hydroxides: recent developments and applications. J. Mater. Chem. 2002;12:3191–8.

10. Evans DG, Duan X. Preparation of layered double hydroxides and their applications as additives in polymers, as precursors to magnetic materials and in biology and medicine. Chem. Commun. (Camb). 2006;485–96.

11. Ambrogi V, Fardella G, Grandolini G, Perioli L. Intercalation compounds of hydrotalcite-like anionic clays with antiinflammatory agents--I. Intercalation and in vitro release of ibuprofen. Int. J. Pharm. 2001;220:23–32.

12. Del Arco M, Cebadera E, Gutiérrez S, Martín C, Montero MJ, Rives V, et al. Mg,Al layered double hydroxides with intercalated indomethacin: Synthesis, characterization, and pharmacological study. J. Pharm. Sci. 2004;93:1649–58.

13. Chakraborti M, Jackson J, Plackett D, Gilchrist S, Burt H. The application of layered double hydroxide clay (LDH)-poly (lactide-co-glycolic acid)(PLGA) film composites for the controlled release of antibiotics. J. Mater. Sci. Mater. Med. 2012;23:1705–13.

14. Hesse D, Badar M, Bleich A, Smoczek A, Glage S, Kieke M, et al. Layered double hydroxides as efficient drug delivery system of ciprofloxacin in the middle ear: an animal study in rabbits. J. Mater. Sci. Mater. Med. 2013;24:129–36.

15. Boclair J, Braterman P. Layered double hydroxide stability. 1. Relative stabilities of layered double hydroxides and their simple counterparts. Chem. Mater. 1999;11:298–302.

16. Tsujimura A, Uchida M, Okuwaki A. Synthesis and sulfate ion-exchange properties of a hydrotalcite-like compound intercalated by chloride ions. J. Hazard. Mater. 2007;143:582–6.

17. Panda HS, Srivastava R, Bahadur D. Stacking of lamellae in Mg/Al hydrotalcites: Effect of metal ion concentrations on morphology. Mater. Res. Bull. 2008;43:1448–55.

18. Vucelic M, Jones W, Moggridge G. Cation ordering in synthetic layered double hydroxides. Clays Clay Miner. 1997;803–13.

19. Xu ZP, Stevenson GS, Lu C-Q, Lu GQM, Bartlett PF, Gray PP. Stable suspension of layered double hydroxide nanoparticles in aqueous solution. J. Am. Chem. Soc. 2006;128:36–7.

20. Parello ML, Rojas R, Giacomelli CE. Dissolution kinetics and mechanism of Mg-Al layered double hydroxides: a simple approach to describe drug release in acid media. J. Colloid Interface Sci. 2010;351:134–9.

21. Stanimirova TS, Piperov N, Petrova N, Kirov G. Thermal evolution of Mg-Al-CO3 hydrotalcites. Clay Miner. 2004;39:177–91.

22. Valente JS, Rodriguez-Gattorno G, Valle-Orta M, Torres-Garcia E. Thermal decomposition kinetics of MgAl layered double hydroxides. Mater. Chem. Phys. Elsevier B.V.; 2012;133:621–9.

23. Mueller W-D, Lucia Nascimento M, Lorenzo de Mele MF. Critical discussion of the results from different corrosion studies of Mg and Mg alloys for biomaterial applications. Acta Biomater. Acta Materialia Inc.; 2010;6:1749–55.

24. Rives V, Del Arco M, Martín C. Layered double hydroxides as drug carriers and for controlled release of non-steroidal antiinflammatory drugs (NSAIDs): a review. J. Control. Release. 2013;169:28–39.

25. Frunza MS, Popa MI, Lisa G, Hritcu D, Lion MSI, Marcel Lone Pop A. New Hybrid Compounds Containing Intercalated Ciprofloxacin into Layered Double Hydroxides: Synthesis and Characterization. Rev. Roum. Chim. 2008;53:827–31.

26. Ambrogi V, Fardella G, Grandolini G, Perioli L, Tiralti MC. Intercalation compounds of hydrotalcite-like anionic clays with anti-inflammatory agents, II: Uptake of diclofenac for a controlled release formulation. AAPS PharmSciTech. 2002;3:E26.

27. Olanrewaju J, Newalkar BL, Mancino C, Komarneni S. Simplified synthesis of nitrate form of layered double hydroxide. Mater. Lett. 2000;45:307–10.

4.3 Magnesium-containing layered double hydroxides as orthopaedic implant coating materials–an *in vitro* and *in vivo* study

Andreas Weizbauer*, Marc Kieke*, Muhammad Imran Rahim, Gian Luigi Angrisani, Elmar Willbold, Julia Diekmann, Thilo Flörkemeier, Henning Windhagen, Peter Paul Müller, Peter Behrens, Stefan Budde

*These authors contributed equally to this study.

Journal of Biomedical Materials Research Part B: Applied Biomaterials

J Biomed Mater Res Part B. **2015**;*00B:*000–000

DOI: 10.1002/jbm.b.33422

The final publication is available at

http://onlinelibrary.wiley.com/doi/10.1002/jbm.b.33422/full

Society For Biomaterials

Magnesium-containing layered double hydroxides as orthopaedic implant coating materials—An *in vitro* and *in vivo* study

Andreas Weizbauer,[1,2]* Marc Kieke,[3]* Muhammad Imran Rahim,[4] Gian Luigi Angrisani,[5] Elmar Willbold,[1,2] Julia Diekmann,[1,2] Thilo Flörkemeier,[1] Henning Windhagen,[1] Peter Paul Müller,[4] Peter Behrens,[3] Stefan Budde[1]

[1]Laboratory of Biomechanics and Biomaterials, Department of Orthopaedic Surgery, Hannover Medical School, Anna-von-Borries-Straße1-7, 30625 Hannover, Germany
[2]CrossBIT, Centre for Biocompatibility and Implant-Immunology, Department of Orthopaedic Surgery, Hannover Medical School, Feodor-Lynen-Straße 31, 30625 Hannover, Germany
[3]Institute for Inorganic Chemistry, Leibniz Universität Hannover, Callinstraße 9, 30167 Hannover, Germany
[4]Helmholtz Centre for Infection Research, Inhoffenstraße 7, 38123 Braunschweig, Germany
[5]Institute of Materials Science, Leibniz Universität Hannover, An der Universität 2, 30823 Garbsen, Germany

Received 7 May 2014; revised 16 December 2014; accepted 26 February 2015
Published online 00 Month 2015 in Wiley Online Library (wileyonlinelibrary.com). DOI: 10.1002/jbm.b.33422

Abstract: The total hip arthroplasty is one of the most common artificial joint replacement procedures. Several different surface coatings have been shown to improve implant fixation by facilitating bone ingrowth and consequently enhancing the longevity of uncemented orthopaedic hip prostheses. In the present study, two different layered double hydroxides (LDHs), Mg-Fe- and Mg-Al-LDH, were investigated as potential magnesium (Mg)-containing coating materials for orthopaedic applications in comparison to Mg hydroxide ($Mg(OH)_2$). *In vitro* direct cell compatibility tests were carried out using the murine fibroblast cell line NIH 3T3 and the mouse osteosarcoma cell line MG 63. The host response of bone tissue was evaluated in *in vivo* experiments with nine rabbits. Two cylindrical pellets (3 × 3 mm) were implanted into each femoral condyle of the left hind leg. The samples were analyzed histologically and with μ-computed tomography (μ-CT) 6 weeks after surgery. An *in vitro* cytotoxicity test determined that more cells grew on the LDH pellets than on the $Mg(OH)_2$-pellets. The pH value and the Mg^{2+} content of the cell culture media were increased after incubation of the cells on the degradable samples. The *in vivo* tests demonstrated the formation of fibrous capsules around $Mg(OH)_2$ and Mg-Fe-LDH. In contrast, the host response of the Mg-Al-LDH samples indicated that this Mg-containing biomaterial is a potential candidate for implant coating. © 2015 Wiley Periodicals, Inc. J Biomed Mater Res Part B: Appl Biomater 00B: 000–000, 2015.

Key Words: biomaterial, layered double hydroxides, magnesium hydroxide, surface coating, orthopaedic implants, osteoconductivity

How to cite this article: Weizbauer A, Kieke M, Rahim MI, Angrisani GL, Willbold E, Diekmann J, Flörkemeier T, Windhagen H, Müller PP, Behrens P, Budde S. 2015. Magnesium-containing layered double hydroxides as orthopaedic implant coating materials—An *in vitro* and *in vivo* study. J Biomed Mater Res Part B 2015:00B:000–000.

INTRODUCTION

The usage of orthopaedic devices increased over years with total hip arthroplasty being one of the most common artificial joint replacement procedures.[1] The number of revision hip procedures has also grown and is expected to increase further with greater demand for primary total hip replacement.[1,2] Improving the survivability of permanent, uncemented orthopaedic hip prostheses is an important issue that depends on the stable fixation of the implant by bone ingrowth.

Hip prostheses are made of stainless steel, cobalt alloy, or titanium alloys.[3] Insufficient direct bone adherence to the implant and osteolysis due to released metallic and polymeric particles both may cause premature implant failure.[4] Surface coatings may be a useful approach for enhancing bone ingrowth. Recently, many different osteoconductive coatings have been investigated.[5] Calcium phosphate coatings (e.g., hydroxyapatite [HAp]) have been shown to achieve appropriate bone ongrowth to the implant, which increases biological fixation.[6,7] However, HAp degrades over time due to osteoclastic resorption.[6,8] A recent analysis of the Swedish Hip Arthroplasty Register led to the conclusion that HAp coating does not enhance acetabular cup survival,[9] and concerns about osteolysis induced by HAp wear particles have been raised.[10]

*Both authors contributed equally to this work.
Correspondence to: A. Weizbauer; e-mail: weizbauer.andreas@mh-hannover.de
Contract grant sponsor: German Research Foundation (DFG); contract grant number: SFB 599

A novel approach is the use of degradable magnesium (Mg)-containing compounds as surface coatings. Several different implant materials, for example, ceramic and titanium, have been successfully coated with layered double hydroxide (LDH)-particles.[11,12] The release of Mg^{2+} during the degradation process has been reported to be advantageous for bone tissue.[13] Several *in vitro* studies have reported enhanced osteoblast adhesion with Mg^{2+}-supplemented HAp,[14] Al_2O_3-Mg^{2+},[15] or carbonate apatite-containing Mg^{2+}.[16] In addition, Mg^{2+} ions are reported to have a preferable effect on proliferation and differentiation of human mesenchymal stem cells (hMSCs).[17] Layered double hydroxides (LDHs) are materials comprising positively charged layers with intercalated anions and water molecules. A wide variety of chemical compositions can be produced, with the general composition described by the formula $[M(II)_{1-x}M(III)_x(OH)_2(A^{n-})_{x/n} \cdot yH_2O]$, where M(II) represents Mg^{2+}, calcium (Ca^{2+}), or zinc (Zn^{2+}), and so forth; M(III) indicates aluminium (Al^{3+}), manganese (Mn^{3+}), or iron (Fe^{3+}), and so forth; and A^{n-} represents the interlayer anion.[12,18] These compounds have been investigated as a delivery system for antibiotics[12] and different biomolecules (e.g., DNA, ATP, nucleoside monophosphates),[19] as well as a protective coating material to prevent the corrosion of pure Mg and its alloys.[20,21] Mg-Al-LDH particles exhibited low toxicity in a rat experiment, and few systemic effects are observed at doses below 200 mg kg^{-1}.[22] Furthermore, LDHs are routinely administered orally as an antacid drug.

In the present study, two different Mg-containing LDHs were investigated as potential materials for coating of orthopaedic implants. *In vitro* cytotoxicity tests were performed with mouse fibroblasts (NIH 3T3) and a human osteosarcoma cell line (MG 63). The biological response was also investigated *in vivo* in rabbits and the volume loss was determined using μ-CT.

MATERIAL AND METHODS

Implant materials

We assessed two different LDHs: (i) $[Mg_4Al_2(OH)_{12}](CO_3)\cdot 4H_2O$ with M(III) = Al^{3+}, hereafter referred to as Mg-Al-LDH, and (ii) $[Mg_4Fe_2(OH)_{12}](CO_3)\cdot 3H_2O$ with M(III) = Fe^{3+}, hereafter referred to as Mg-Fe-LDH. The respective LDHs were precipitated in water by adding a solution of (i) $MgCl_2\cdot 6H_2O$ (100 mmol, purum p.a. ≥98.0%, Fluka, Buchs, Switzerland) and $AlCl_3\cdot 6H_2O$ (50 mmol, purum p.a. ≥99.0%, Fluka) or (ii) $MgCl_2\cdot 6H_2O$ (100 mmol, purum p.a. ≥98.0%, Fluka) and $FeCl_3$ (50 mmol, reagent grade, >97%, Fluka) to a vigorously stirred solution of NaOH (300 mmol, reagent grade, anhydrous, ≥98%, Fluka) and $Na_2CO_3\cdot H_2O$ (60 mmol, ≥99.5%, Fluka). The mixtures were allowed to stand for 1 h before the raw products were repeatedly centrifuged and washed with deionized water. After three washing cycles, the LDHs were obtained by centrifugation, and air-dried at 60 °C. $Mg(OH)_2$ powder (purum p.a. 96%) was used as a reference material. All chemicals were used as purchased without further purification.

The identities of the LDHs and the $Mg(OH)_2$ were confirmed by powder X-ray diffraction (p-XRD) measurements performed with a Theta–Theta diffractometer by STOE. The 2Θ range was scanned with a step size of 0.02° (5.0 s per step, 30 mA, 40 kV) using monochromatized Cu Kα1 radiation (wavelength = 1.54059 Å).

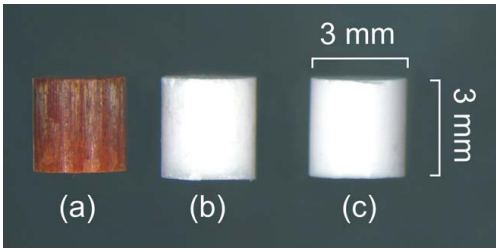

FIGURE 1. Pictures of the cylindrical implants (3 × 3 mm) used in the *in vivo* experiments. Pellets of two different LDHs were investigated: (a) $[Mg_4Fe_2(OH)_{12}](CO_3)\cdot 3H_2O$ (Mg-Fe-LDH), (b) $[Mg_4Al_2(OH)_{12}](CO_3)\cdot 4H_2O$ (Mg-Al-LDH). These samples were compared to pellets made of (c) $Mg(OH)_2$. [Color figure can be viewed in the online issue, which is available at wileyonlinelibrary.com.]

Pellets with a diameter of 13 mm for the *in vitro* cell tests were formed by pressing the respective powders with 5 tons over 5 min. During and prior to processing, all devices and containers were repeatedly rinsed with ethanol. No further sterilization methods were applied.

Cylindrical implants (3 × 3 mm) were formed for the *in vivo* test with a cold isostatic pressure technique (Department of Inorganic Chemistry, University of Essen, Germany) (Figure 1). The samples used for *in vivo* testing were gamma-sterilized with 25–29 kGy cobalt radiation (BBF Sterilisation Service, Kernen-Rommelshausen, Germany).

In vitro cell compatibility tests with NIH 3T3 and MG 63-cells

We tested the cell compatibility of pellets made from Mg-Al-LDH, Mg-Fe-LDH, and $Mg(OH)_2$ using the murine fibroblast cell line NIH 3T3 (ATCC CRL-1685; LGC Standards GmbH, Wesel, Germany), and the mouse osteosarcoma cell line MG 63 (ATCC CRL-1427; LGC Standards GmbH, Wesel, Germany). They were cultured in Dulbecco's modified Eagle's medium (DMEM; Gibco/Life Technologies, Darmstadt, Germany) supplemented with 1% (v/v) glutamine, 1% (v/v) penicillin and streptomycin (100 U mL^{-1} penicillin G and 100 μg mL^{-1} streptomycin) and 10% (v/v) foetal calf serum in a humidified incubator with 5% CO_2 at 37 °C. The cells were detached from the surface of T25 cell culture flasks using trypsin. The cells were washed in DMEM to remove trypsin and resuspended in fresh DMEM. Both cell lines were seeded separately at a density of 1.2 × 10^4 cells mL^{-1} on the pellets as well as on a polystyrene surface (control), which is a widely used, cell culture optimized, standard cell adhesion substrate material.[11,23] Pellets seeded with murine fibroblasts were incubated at 37 °C in a humidified incubator with 5% CO_2 for 48 h, and the mouse osteosarcoma cell line was incubated for 72 h. After the incubation period, media and non-adherent cells were washed off the pellets with 1× phosphate-buffered saline

(PBS). Both cell lines were then stained with the fluorescent cell proliferation dye CFSE (5- and 6-Carboxyfluorescein diacetate succinimidyl ester; eBioscience, San Diego, CA) to observe cell adhesion, spreading, and proliferation on the surface of pellets using an Axio Observer A-1 microscope (Carl Zeiss Microscopy GmbH, Jena, Germany). The images were captured with Axiovision Rel. 4.5 software (Carl Zeiss MicroImaging, Jena, Germany). The samples were tested in triplicate. The data are presented as mean values ± standard deviation. The pH values of the cell culture media were measured with the pellets before seeding the cells and after 48 and 72 h incubation periods for fibroblasts and bone cells, respectively. The content of magnesium was measured using inductively coupled plasma optical emission spectroscopy (ICP-OES, Spectro Arcos, Spectro Analyticals Instruments, Kleve, Germany) at the Medical Laboratory of Bremen.

Animal study

The animal experiment was conducted under an ethics committee approved protocol in accordance with German federal animal welfare legislation (Approval No. 33.9–42502-04-13/1108). Nine female adult rabbits (New Zealand White; Charles River Laboratory, Bad Kissingen, Germany), with a mean body weight of 3.8 ± 0.4 kg and a minimum age of 6 months were used. For each animal, two implants were inserted into the femoral condyles of the left hind leg (one in the medial and one in the lateral condyle).

Surgery was performed under general anaesthesia induced by an intramuscular (i.m.) injection of ketamine (25 mg kg^{-1}; Ketanest, Albrecht, Aulendorf, Germany) and midazolam (5 mg/animal; Dormicum, CuraMED Pharma, Karlsruhe, Germany) and a subcutaneous (s.c.) dose of glycopyrroniumbromid (0.1 mg/animal; Robinul, Riemser Arzneimittel, Greifswald—Insel Riems, Germany). For analgesia, the rabbits were given meloxicam (0.15 mg kg^{-1} peroral (p.o.); Metacam, Boehringer Ingelheim, Ingelheim am Rhein, Germany) 1 day preoperatively, immediately preoperatively, and for the following 2 days. They also received preoperative buprenorphine (0.15 mg/animal, s.c.; Temgesic, Essex Pharma, München, Germany). During endotracheal intubation, each animal received an intravenous injection of propofol (initial 1 mg/kg, Propofol-Lipuro 1%, B. Braun Melsungen, Germany). After endotracheal intubation, anaesthesia was maintained by isoflurane delivered in oxygen (1.5–2.5 vol % isoflurane; Isofluran CP, CP-Pharma, Burgdorf, Germany; oxygen flow: 1.0 L min^{-1}). Ringer's lactate solution was infused (10 mL kg^{-1} h^{-1}) during the entire surgery to ensure proper cardiovascular function.

A median skin incision was performed to access the lateral femoral condyle, the fascia was split, and a 3-mm wide hole was drilled where the cylindrical sample was inserted. Then, the incision was moved to the medial condyle where another implant was set in an analogous manner. After control of bleeding and flushing with 0.9% NaCl, the wound was closed using absorbable suture material (Vicryl5-0; Ethicon, Norderstedt, Germany). For the first 3 days after surgery, antibiotic medication was given (enrofloxacin, 10 mg kg^{-1}, Baytril 2.5%, p.o., once daily, Bayer Animal Health, Leverkusen, Germany).

Six weeks after surgery, all animals were sedated with i.m. ketamine (25 mg kg^{-1}) and midazolam (5 mg/animal) and euthanized by an intravenous overdose of pentobarbital (release ad us. vet.; WDT, Garbsen, Germany). The femoral condyles were explanted and fixed in 3.5% commercial formalin for 1 week.

μ-Computed tomography evaluations

Each sample was scanned with μ-computed tomography (μCT; Micro-CT 80 system, SCANCO MEDICAL, Brüttisellen, Switzerland) before implantation and in the explanted bone. The scan resolution was 36 μm with 55 kV voltage and 72 μA amperage. The integration time was 2 × 500 ms.

The evaluation was performed using the MICRO-CT Evaluation Program V6.0 (SCANCO MEDICAL) by manually contouring the surface of the cylinders. The volume change of each implant was determined.

Histology

Bone samples from each animal were processed for histologic analysis. The explanted bones were fixed in formalin (3.5%), and the samples were dehydrated at room temperature in increasing concentrations of alcohol: 70% ethanol for 2 days, two changes of 96% ethanol for 2 days, and two changes of 2-propanol for 2 days. Samples were degreased in xylene for 2 days and then embedded in methylmethacrylate (Technovit 9100 New®, Heraeus Kulzer, Hanau, Germany) according to the manufacturer's instructions, that is, polymerization under vacuum at −2 to 4 °C in the freezer for 3 days. Then, 40 μm sections of bone were cut perpendicular to the implants with a cutting–grinding technique and then polished (Exakt-Apparatebau, Norderstedt, Germany).[24] The samples were stained with toluidine blue using established protocols.

RESULTS

XRD characterization of the samples

The diffractograms of the two LDHs and $Mg(OH)_2$ are shown in Figure 2. The patterns are as expected for the substances, confirming that they were successfully synthesized.

Cell densities following *in vitro* incubation

We assessed the cytocompatibility of the samples with two different cell lines. Figures 3 and 4 show the cell densities after incubation on different samples. The densities for both cell lines were highest on the control polystyrene surface. The numbers of cells decreased after incubation on the two different LDH pellets. The smallest number of living cells was detected on the $Mg(OH)_2$ samples.

The pH value of DMEM before incubation was 7.95 ± 0.008. After incubation on the control surface, the medium's pH value was decreased (Figure 4). The media of all other tested samples showed a pH increase after incubation. The highest value was observed with $Mg(OH)_2$ pellets (pHs of 8.48 and 8.50, respectively). The Mg^{2+} concentrations in the media after incubation with the tested samples

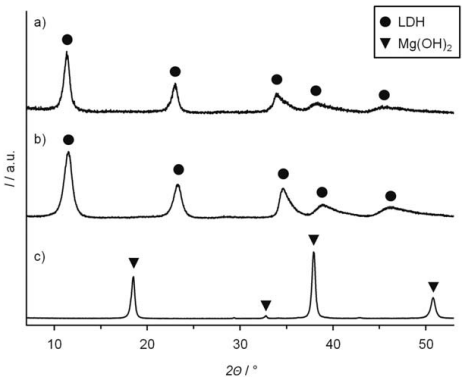

FIGURE 2. Powder XRD patterns of a) Mg-Fe-LDH, b) Mg-Al-LDH, and c) $Mg(OH)_2$. Reflection positions for the LDH and for $Mg(OH)_2$ are indicated.

were higher than for the control surface. The highest value was found in media incubated with $Mg(OH)_2$ samples (Figure 4).

Mg-Al-LDH samples showed an appropriate bone response *in vivo*

Post-operative clinical monitoring of the rabbits revealed solid swellings on both sides of the joint of the left hind for example, which mostly regressed in the 3 weeks after surgery. These swellings were not painful on palpation. Except for one animal, all rabbits moved without lameness. The animal with the persistent moderate lameness was euthanized 1 week after surgery because of a patella luxation.

Microscopic evaluation of the histological samples revealed a thick layer of connective tissue around Mg-Fe-LDH-samples [Figure 5(d)]. Nearly no direct bone–implant contact was observed in the samples. We did not observe alterations of the living bone around the implant site. The bone adjacent to these implants had an abrasive surface due to bone resorption. However, non-calcified bone (ncb) was detected at the implant interface [Figure 5(a)].

The Mg-Al-LDH-samples showed some direct bone–implant contact and a thin seam of connective tissue around the implant. The contours of the implant were well defined.

Similar to the Mg-Fe-LDH-implants, the fibrous capsule was pronounced in bones implanted with $Mg(OH)_2$ samples [Figure 5(c)]. The implant was covered by a layer of corrosion products [Figure 5(f)].

Cylindrical pellet volume loss was determined using μ-CT. The cylindrical implants had an average volume of 21.5 ± 0.8 mm^3 before implantation. After 6 weeks, the volume of the $Mg(OH)_2$ pellets was decreased by 40%, but the volumes of the two tested LDH implants remained nearly unchanged [Figure 6].

DISCUSSION

An ideal orthopaedic implant surface coating should improve bone ingrowth and in this way support implant fixation. In the present study, we evaluated two different Mg-containing LDHs as potential coating materials in comparison to conventional $Mg(OH)_2$. Several different studies have reported an osteoconductive effect of Mg-containing materials.[13–15]

The *in vitro* experiments described here revealed a tendency of decreased cell density with an increase in the pH values of the media to alkaline ranges and higher Mg^{2+} concentrations. The degradation of LDH in cell culture media releases several ions (e.g., Mg^{2+}, Al^{3+}, OH^-, etc), which alters the pH.[19] A direct cytotoxicity test was used in the present study; other optional *in vitro* test methods are indirect cytotoxicity tests, where extracts are evaluated or where there is a barrier between the biomaterial and the cells (i.e., Millipore filter or agar overlay).[25] We assume that direct contact with the surface of the LDH test items most closely simulates *in vivo* conditions. The alkalization of the media might inhibit cell proliferation and viability. Furthermore, Mg^{2+} accumulation in the media might have additional adverse effects on cells. It is reported that the tolerance limit for Mg^{2+} is about 22 m*M* for the MG 63 cell line[26]; it ranges from 20 to 40 m*M* for other cell lines.[26] Furthermore, the accumulation of released ions from the LDH might negatively impact osmolarity. Increasing the osmolarity to >500 mOsm can cause apoptosis[27]; however, some *in vitro* studies have investigated LDHs and reported low cytotoxicity.[19,28–30] Human promyelocytic leukemia cells (HL-60 cells) exposed to various concentrations of $[Mg_2Al(OH)_6]NO_3$ exhibited no cytotoxic effects at concentrations below 1,000 μg mL^{-1}.[28] The same LDH was reported to have no negative effect on the viability of the human tendinous fibroblasts and human osteosarcoma cells (cell line SaOS-2) at the concentration of 5 μg mL^{-1},[29] and 500 μg mL^{-1} was reportedly not toxic for SaOS-2 and MG 63 cells.[31] Conversely, inhibited profileration of human embryonic kidney cells (HEK293T) was reported at a concentration of 0.125 mg mL^{-1}.[30]

In the present study, the MG 63 cells grew similarly on both LDH-pellets; while, the NIH 3T3 cell density was lower on the Mg-Fe-LDH-pellet. These different results might be caused by a deviating tolerance and susceptibility of the cell lines used. Variations in the sensitivities of different cell

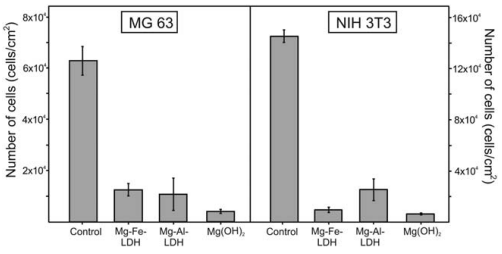

FIGURE 3. Numbers of living cells after incubation on different samples. There were more cells on the LDH pellets than on the degradable $Mg(OH)_2$-pellets. Samples cultured on the polystyrene surface (control) exhibited the highest number of cells.

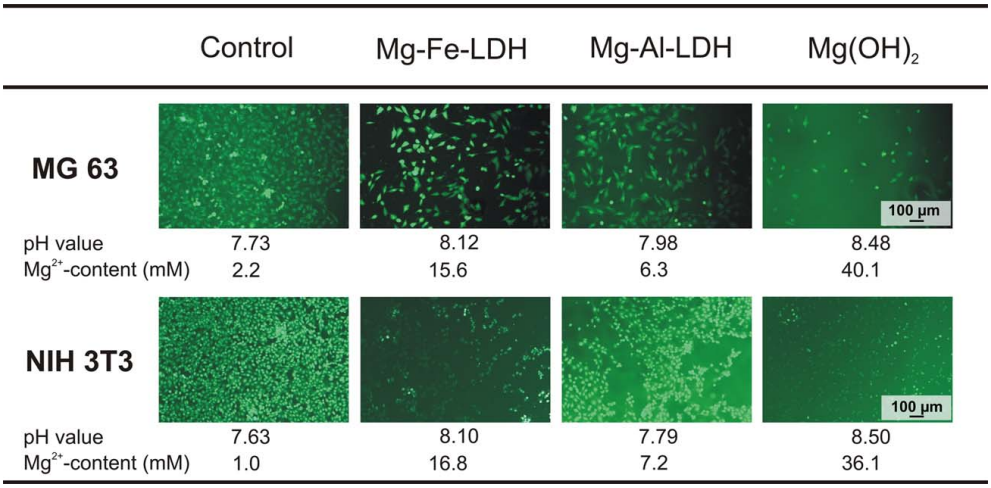

FIGURE 4. Cell densities of the murine fibroblast cell line NIH 3T3 and the mouse osteosarcoma cell line MG 63 after incubation for 48 and 72 h, respectively. The cells were seeded directly onto the pellets. A cell culture-optimized polystyrene surface served as a control. The pH values and the Mg^{2+} contents were determined on the cell culture media at the end of the incubation. [Color figure can be viewed in the online issue, which is available at wileyonlinelibrary.com.]

lines were reported previously in a study investigating the cytotoxicity of rare earth elements.[32] The release of aluminium and iron from the LDH-pellet might have an effect on cells. In a study by Hallab et al. the toxicity of different metals was investigated on MG 63 osteoblasts and iron was rated as one of the most toxic metals.[33] A limitation of this study was that the ion concentrations of Al^{3+} and Fe^{3+} were not quantified in the media of the LDH-samples.

Janning et al. investigated $Mg(OH)_2$ pellets in a rabbit model for up to 6 weeks.[13] Although temporarily enhanced

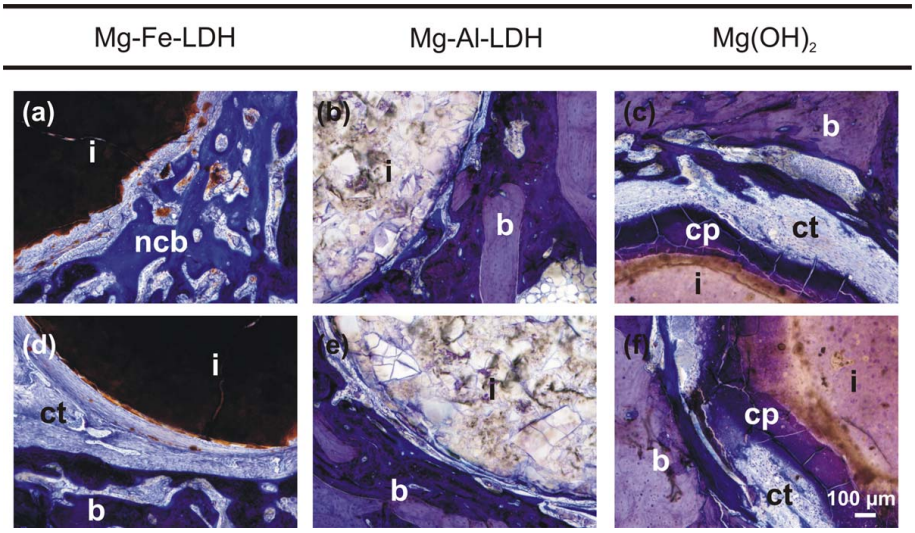

FIGURE 5. Toludine blue-stained histological samples of Mg-Fe-, Mg-Al-LDH, and $Mg(OH)_2$. (a,d) A thick layer of connective tissue was observed around Mg-Fe-LDH samples. (b,e) Sparse direct bone–implant contact was found with Mg-Al-LDH samples. (c,f) Fibrous capsule formation was most pronounced with $Mg(OH)_2$. i, implant; ncb, non-calcified bone; b, bone; ct, connective tissue; cp, corrosion products. [Color figure can be viewed in the online issue, which is available at wileyonlinelibrary.com.]

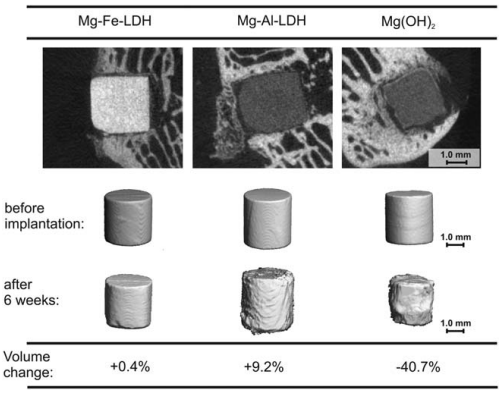

FIGURE 6. μ-CT images taken 6 weeks after cylindrical pellets were implanted in rabbit femoral condyles.

bone growth was reported in the first 4 weeks, the bone volume/tissue volume (BV/TV) as well as the osteoid surface was decreased at 6 weeks.[13] In the present study, we observed pronounced fibrous capsule formation around the magnesium hydroxide implants. *In vivo* the detection of the pH value near degrading $Mg(OH)_2$ samples showed a shift toward alkaline environments immediately after implantation.[34] After 14 days, the pH value shifted toward the acidic range. This was interpreted as the formation of a fibrous capsule due to a foreign body reaction,[34] which is in accordance with the finding in the present study of fibrous capsule formation after $Mg(OH)_2$-implantation. The foreign body reaction is a complex host response to biomaterials that includes the adsorption of different plasma proteins, the adhesion of macrophages, and the formation of foreign-body giant cells.[35] These adherent cells can secrete proteins that facilitate the development of a fibrous capsule and may subsequently lead to implant failure.[35] Our results demonstrated fibrous capsule formation around $Mg(OH)_2$ and Mg-Fe-LDH pellets.

Direct apposition of living bone to the implant without interposing soft tissue layers is advantageous for the long-term function of orthopaedic prostheses.[36] Stainless steel, cobalt alloy, or titanium alloys are the primary biomaterials for modern hip prostheses.[3] The formation of thin soft tissue layers around these metal implant devices has been reported.[36,37] Modification of surface topography (e.g., roughness) and different coatings (e.g., HAp) have been investigated to improve the initial implant ingrowth of uncemented orthopaedic devices.[38] The present study investigated the bone responses to two different degradable LDHs as potential coating materials for orthopaedic devices. Several *in vivo* studies reported appropriate host responses to different LDHs.[22] Rats injected with suspensions of LDH particles showed few effects at doses at or below 200 mg kg^{-1}, but unwanted systemic effects were observed at higher doses (300 mg/kg).[22] The degradation of LDHs *in vivo* and in body fluids may lead to the release of Mg^{2+}, Cl^-, Fe^{3+}, Al^{3+}, CO_3^{2-}, and OH^- ions. Fe^{3+} and its chelated complexes around the implant may be engulfed by macrophages,[39] and these may lead to Fe^{3+}-activated proinflammatory TNF (tumor necrosis factor)-α-releasing macrophages.[40] Elevated levels of pro-inflammatory cytokines can stimulate osteoclastic bone resorption, and Fe^{3+}-loaded macrophages can release toxic radicals (i.e., $OH^{\bullet}$).[40] We therefore assume that locally increased Fe^{3+} concentrations, caused by release from the Mg-Fe-LDH coating materials, might have led to the negative effects observed in our study.

Al^{3+} ions can also have adverse effects on bone formation and may interfere with bone metabolism. Al^{3+} is reported to accumulate in calcified bone, consequently altering mineralization and reducing new bone formation due to a direct effect on osteoblast metabolism.[41] The results of the present study demonstrated that the Mg-Al-LDH material led to an appropriate host response, with no adverse effects on bone remodelling. However, the *in vitro* Mg^{2+}-release portends of lower degradation rates of Mg-Al-LDH than Mg-Fe-LDH; which may result in lower local ion release.

Interestingly, the volumes of the LDH cylinders remained nearly unchanged after 6 weeks of implantation. The volume of the Mg-Al-LDH even appears to have increased which may be due to the intercalation of anionic components of the surrounding body fluids. The low volume change of the Mg-Al-LDH is consistent with the results of a recent animal study in the middle ear of rabbits, where a similar Mg-Al-LDH was applied as a coating on Bioverit® II middle ear prostheses.

The results of this study demonstrate that Mg-Fe-LDH is not suitable or biomedical applications in bone. In contrast, the host response to Mg-Al-LDH indicates that this Mg-containing biomaterial is a potential candidate for implant coating. Further studies are necessary to evaluate the long-term effects of this material.

CONCLUSION

In the present study, we evaluated two different Mg-containing LDHs as potential coating materials and compared them to the simple $Mg(OH)_2$. The *in vitro* cytotoxicity test results revealed that more cells grew on the LDH-samples than on the degradable $Mg(OH)_2$-pellets. The pH and the Mg^{2+} content of the cell culture media were increased after incubation of the cells on the degradable samples. The *in vivo* findings revealed fibrous capsule formation around $Mg(OH)_2$ and Mg-Fe-LDH, with nearly no direct bone–implant contact. In contrast, the host response to the Mg-Al-LDH indicated that this Mg-containing biomaterial is a potential candidate for implant coatings.

REFERENCES

1. Kurtz SM, Ong KL, Schmier J, Zhao K, Mowat F, Lau E. Primary and revision arthroplasty surgery caseloads in the United States from 1990 to 2004. J Arthroplasty 2009;24:195–203.
2. Kurtz S, Ong K, Lau E, Mowat F, Halpern M. Projections of primary and revision hip and knee arthroplasty in the United States from 2005 to 2030. J Bone Joint Surg Am 2007;89:780–785.

3. Hallab N, Merritt K, Jacobs JJ. Metal sensitivity in patients with orthopaedic implants. J Bone Joint Surg Am 2001;83A:428−436.
4. Jiang Y, Jia T, Wooley PH, Yang SY. Current research in the pathogenesis of aseptic implant loosening associated with particulate wear debris. Acta Orthop Belg 2013;79:1−9.
5. Goodman SB, Yao Z, Keeney M, Yang F. The future of biologic coatings for orthopaedic implants. Biomaterials 2013;34:3174−3183.
6. Geesink RG. Osteoconductive coatings for total joint arthroplasty. Clin Orthop Relat Res 2002;395:53−65.
7. Oonishi H, Yamamoto M, Ishimaru H, Tsuji E, Kushitani S, Aono M, Ukon Y. The effect of hydroxyapatite coating on bone growth into porous titanium alloy implants. J Bone Joint Surg Br 1989; 71:213−216.
8. Tonino AJ, Therin M, Doyle C. Hydroxyapatite-coated femoral stems. Histology and histomorphometry around five components retrieved at post mortem. J Bone Joint Surg Br 1999;81:148−154.
9. Lazarinis S, Karrholm J, Hailer NP. Increased risk of revision of acetabular cups coated with hydroxyapatite. Acta Orthop 2010;81: 53−59.
10. Morscher EW, Hefti A, Aebi U. Severe osteolysis after third-body wear due to hydroxyapatite particles from acetabular cup coating. J Bone Joint Surg Br 1998;80:267−272.
11. Badar M, Rahim MI, Kieke M, Ebel T, Rohde M, Hauser H, Behrens P, Mueller PP. Controlled drug release from antibiotic-loaded layered double hydroxide coatings on porous titanium implants in a mouse model. J Biomed Mater Res A 2014. epub ahead of print (DOI: 10.1002/jbm.a.35358)
12. Hesse D, Badar M, Bleich A, Smoczek A, Glage S, Kieke M, Behrens P, Muller PP, Esser KH, Stieve M, Prenzler NK. Layered double hydroxides as efficient drug delivery system of ciprofloxacin in the middle ear: an animal study in rabbits. J Mater Sci Mater Med 2013;24:129−136.
13. Janning C, Willbold E, Vogt C, Nellesen J, Meyer-Lindenberg A, Windhagen H, Thorey F, Witte F. Magnesium hydroxide temporarily enhancing osteoblast activity and decreasing the osteoclast number in peri-implant bone remodelling. Acta Biomater 2010;6: 1861−1868.
14. Webster TJ, Ergun C, Doremus RH, Bizios R. Hydroxylapatite with substituted magnesium, zinc, cadmium, and yttrium. II. Mechanisms of osteoblast adhesion. J Biomed Mater Res 2002;59:312−317.
15. Zreiqat H, Howlett CR, Zannettino A, Evans P, Schulze-Tanzil G, Knabe C, Shakibaei M. Mechanisms of magnesium-stimulated adhesion of osteoblastic cells to commonly used orthopaedic implants. J Biomed Mater Res 2002;62:175−184.
16. Yamasaki Y, Yoshida Y, Okazaki M, Shimazu A, Uchida T, Kubo T, Akagawa Y, Hamada Y, Takahashi J, Matsuura N. Synthesis of functionally graded $MgCO_3$ apatite accelerating osteoblast adhesion. J Biomed Mater Res 2002;62:99−105.
17. Li RW, Kirkland NT, Truong J, Wang J, Smith PN, Birbilis N, Nisbet DR. The influence of biodegradable magnesium alloys on the osteogenic differentiation of human mesenchymal stem cells. J Biomed Mater Res A 2014;102:4346−4357.
18. Khan AI, Lei L, Norquist AJ, O'Hare D. Intercalation and controlled release of pharmaceutically active compounds from a layered double hydroxide. Chem Commun (Camb) 2001;22:2342−2343.
19. Ladewig K, Xu ZP, Lu GQ. Layered double hydroxide nanoparticels in gene and drug delivery. Expert Opin Drug Deliv 2009;6: 907−922.
20. Lin J-K, Uan J-Y, Wu C-P, Huang H-H. Direct growth of oriented Mg-Fe layered double hydroxide (LDH) on pure Mg substrates and in vitro corrosion an cell adhesion testing of LDH-coated Mg samples. J Mater Chem 2011;21:5011−5020.
21. Uan J-Y, Lin J-K, Tung Y-S. Direct growth of oriented Mg-Al layered double hydroxide film on Mg alloy in aquaeous HCO_3/CO_3^{2-} solution. J Mater Chem 2010;20:761−766.
22. Kwak S-Y, Kriven WM, Wallig MA, Choy J-H. Inorganic delivery vector for intravenous injection. Biomaterials 2004;25:5995−6001.
23. Ramires PA, Romito A, Cosentino F, Milella E. The influence of titania/hydroxyapatite composite coatings on in vitro osteoblasts behaviour. Biomaterials 2001;22:1467−1474.
24. Donath K, Breuner G. A method for the study of undecalcified bones and teeth with attached soft tissues. The Sage-Schliff (sawing and grinding) technique. J Oral Pathol 1982;11:318−326.
25. Sjögren G, Sletten G, Dahl JE. Cytotoxicity of dental alloys, metals, and ceramics assessed by millipore filter, agar overlay, and MTT tests. J Prosthet Dent 2000;84:229−236.
26. Yang L, Hort N, Laipple D, Höche D, Huang Y, Kainer kU, Willumeit R, Feyerabend F. Element distribution in the corrosion layer and cytotoxicity of alloy Mg-10Dy during in vitro biodegradation. Acta Biomater 2013;9:8475−8487.
27. Lang F, Foller M, Lang K, Lang P, Ritter M, Vereninov A, Szabo I, Huber SM, Gulbins E. Cell volume regulatory ion channels in cell proliferation and cell death. Methods Enzymol 2007;428: 209−225.
28. Kwak S-Y, Jeong Y-J, Park J-S, Choy J-H. Bio-LDH nanohybrid for gene therapy. Solid State Ionics 2002;151:229−234.
29. Choy JH, Jung JS, Oh JM, Park M, Jeong J, Kang YK, Han OJ. Layered double hydroxide as an efficient drug reservoir for folate derivatives. Biomaterials 2004;25:3059−3064.
30. Ladewig K, Niebert M, Xu ZP, Gray PP, Lu GQ. Efficient siRNA delivery to mammalian cells using layered double hydroxide nanoparticles. Biomaterials 2010;31:1821−1829.
31. Oh JM, Park M, Kim S-T, Jung J-Y, Kang Y-G, Choy J-H. Efficient delivery of anticancer drug MTX and through MTX-LDH nanohybrid system. J Phys Chem Solids 2006;67:1024−1027.
32. Feyerabend F, Fischer J, Holtz J, Witte F, Willumeit R, Drucker H, Vogt C, Hort N. Evaluation of short-term effects of rare earth and other elements used in magnesium alloys on primary cells and cell lines. Acta Biomater 2010;6:1834−1842.
33. Hallab NJ, Vermes C, Messina C, Roebuck KA, Glant TT, Jacobs JJ. Concentration- and composition-dependent effects of metal ions on human MG-63 osteoblasts. J Biomed Mater Res 2002;60: 420−433.
34. Bartsch I, Willbold E, Rosenhahn B, Witte F. Non-invasive pH determination adjacent to degradable biomaterials in vivo. Acta Biomater 2014;10:34−39.
35. Anderson JM, Rodriguez A, Chang DT. Foreign body reaction to biomaterials. Semin Immunol 2008;20:86−100.
36. Albrektsson T, Branemark PI, Hansson HA, Lindstrom J. Osseointegrated titanium implants. Requirements for ensuring a long-lasting, direct bone-to-implant anchorage in man. Acta Orthop Scand 1981;52:155−170.
37. Johansson CB, Albrektsson T, Ericson LE, Thomsen P. A quantitative comparison of the cell response to commercially pure titanium and Ti-6Al-4V implants in the abdominal wall of rats. J Mater Sci Mater Med 1992;3:126−136.
38. Bosco R, Van Den Beucken J, Leeuwenburgh S, Jansen J. Surface engineering for bone implants: A trend from passive to active surfaces. Coatings 2012;2:95−119.
39. Olakanmi O, Stokes JB, Britigan BE. Acquisition of iron bound to low molecular weight chelates by human monocyte-derived macrophages. J Immunol 1994;153:2691−2703.
40. Sindrilaru A, Peters T, Wieschalka S, Baican C, Baican A, Peter H, Hainzl A, Schatz S, Qi Y, Schlecht A, Weiss JM, Wlaschek M, Sunderkötter C, Scharffetter-Kochanek K. An unrestrained proinflammatory M1 macrophage population induced by iron impairs wound healing in humans and mice. J Clin Invest 2011;121:985−997.
41. Cannata Andita JB. Aluminium toxicity: Its relationship with bone and iron metabolism. Nephrol Dial Transpl 1996;11: 69−73.

5 LDHs as Key Components in Drug Release Systems with Regard to Application in the Middle Ear

5.1 Preface

This chapter deals in three articles with the *in vivo* and *in vitro* efficacy of coatings based on mixtures of an antibiotic drug and an LDH. These coatings were prepared with the aim to combat bacterial infections directly from the implant. In the course of the studies, it appeared necessary to study the *in vivo* stability of a pristine LDH coating (section 5.2). The *in vivo* studies were performed in the middle ears of New Zealand White rabbits (sections 5.2 and 5.3) and subcutaneously in Balb/c mice (section 5.4).

The studies were performed considering the background of chronic middle ear diseases that might lead to the loss of the small bones of the ossicular chain, a loss which has to be repaired by placing a total ossicular replacement prosthesis (TORP). The endowment of these with antibacterial functionality is of high interest due to the problem of bacterial infection during and subsequent to the surgery.

Despite numerous studies on biological or medical applications of LDH, *in vivo* assays were reported scarcely and concentrated mostly on the effects of the LDH system on the organism. In the study presented in section 5.2 the degradation behavior and biocompatibility of pure LDH coatings were in the focus of the investigation. For this, middle ear implants suitable for New Zealand White rabbits were coated with a pure Mg-Al-CO_3-LDH and inserted into the middle ears. A direct characterization of the LDH coatings via XRD means was not possible. Hence, the presence of the Mg-Al-LDH coating was indirectly tracked by EDX measurements, in principle based on the detection of the Mg:Al ratios on the surfaces of the implants.

Animal health screening revealed no harmful effects on the animals, implicating an overall good biocompatibility of the pristine LDH coatings under the conditions applied. Hence, Mg-Al-LDHs proved as biocompatible and processable components for drug delivery systems.

In the course of complementary *in vitro* studies, similarly coated middle ear implants were immersed under conditions with resemblance to the *in vivo* conditions in the middle ear, including HBSS as the medium at 38 °C. The general stability of the LDH coatings under these conditions was confirmed by these comparably simple experiments according to EDX data (not shown).

The implants used in this study were endowed with the Mg-Al-CO_3-LDH by spray-coating (using a commercially available simple airbrush equipment),

which allowed the application of a nebulized LDH nanosuspension on heated implants. A direct estimation of the coating thickness, for example by cross section SEM and ellipsometric investigations, proved unsuitable. Hence, flat glass substrates were coated by the same means and coating thickness was estimated by laser scanning microscopy. Prior to this study, dip-coating had been applied as an alternative coating technique, but was turned down due to the small thicknesses achieved.

With regard to the bacterial infections mentioned above, middle ear prostheses suitable for New Zealand White rabbits were endowed with a coating of a ciprofloxacin/LDH mixture (section 5.3). *Pseudomonas aeruginosa* infections were triggered in the middle ears of the rabbits either during or one week subsequent to TORP insertion surgery. Clinical, microbiological and histopathological examination revealed the general efficacy of the functionalized implants against the infections. However, the effects were somewhat mitigated when the infection was triggered with the one week delay, and drug release appeared too fast with regard to general application.

As mentioned above, for direct examination of the coated implants, XRD means proved unsuitable. Hence, similar mixtures were applied to glass substrates and examined, revealing the identity and general stability of the LDH component of the coatings (data not shown).

In the study presented in section 5.2, LDH coatings were shown to be practically biostable over the entire application time. Hence, it is to be expected that the LDH component of the drug delivery system used in the study presented in section 5.3 was stable as well.

Further investigations on the efficacy of LDH-based, antibiotic-loaded coatings on titanium alloy substrates comprised *in vitro* and *in vivo* studies (section 5.4). In the course of the *in vitro* studies, plain and porous titanium alloy discs were coated with differently composed ciprofloxacin/LDH mixtures (via drop coating) and exposed to phosphate buffered saline (PBS). The supernatant was sampled repeatedly and the ciprofloxacin concentration was estimated by UV-Vis spectroscopy. The antibacterial efficacy of the supernatants was shown by the vanishing luminescence of luminescent *P. aeruginosa*. Prolongation of antibiotic release and antibacterial efficacy were found for all ciprofloxacin/LDH mixtures investigated. In the course of the *in vivo* study, coated porous titanium discs were implanted subcutaneously into white mice and infection was triggered seven, 15 and 20 days after implantation, respectively. It could be shown that ciprofloxacin/LDH coatings were able to combat bacterial infections close to the implantation site for over two weeks.

Excellent cell compatibility of the LDH coatings was confirmed by tests with immortalized NIH3T3 fibroblasts, which were directly seeded on the coatings and incubated under standard cell culture conditions. Cells were shown to adhere to the coatings as a confluent cell layer, and antibiotic addition to the LDH coating did not result in impairment. Magnesium hydroxide, however, was shown to not support cell adhesion and cell survival, further emphasizing the promise of LDH-based coatings.

Mg-Al-LDH based coatings proved biocompatible and practically bioinert in the middle ear of rabbits. Cell compatibility of Mg-Al-LDH coatings was shown as well with NIH3T3 fibroblasts. When combined with antibiotics by mixing, these coatings proved active against bacterial infections (*P. aeruginosa*) in *in vitro* and in *in vivo* studies. Intercalation of the drug into LDH interlayers did not appear to be necessary in order to fabricate efficient drug delivery systems.

With regard to alternative application sites and due to the formation of resistances of certain bacteria towards antibiotics, further development and systematic investigation of LDH-based drug release systems is of high interest. In the course of further investigations, variation of antibiotics, mixing ratios, the used LDH system (i.e. cation ratios) and coating techniques could be in the focus.

For the article presented in section 5.2, the author of this thesis and Franziska Duda are the first authors, who contributed equally to this study. The manuscript was for the most part drafted by both the first authors. The syntheses of the raw LDH, as well as the further treatment in order to obtain nanosuspensions were performed by the author. Spray-coating techniques and custom-made SEM/EDX sample holders for this study were developed and applied by him, together with Florian Waltz. Florian Waltz and Maria Schweinefuß collected the SEM images and EDX data, which were interpreted by Franziska Duda and the author of this thesis. Complementary *in vitro* studies, XRD measurements and according data interpretation were performed by the author (data not shown). The surgeries and perioperative treatment of the animals in the course of the animal assays were performed by Franziska Duda and Nils Prenzler. Muhammad Badar aided in the evaluation of alternative coating techniques for the middle ear implants. Peter Paul Müller, Karl-Heinz Esser, Thomas Lenarz, Peter Behrens and Nils Kristian Prenzler initiated the study and revised the manuscript.

For the article presented in section 5.3, Daniela Hesse is the first author, and the author of this thesis is a co-author. All XRD measurements in the course of the study and in the course of complementary studies, and according data interpretation were performed by him (data not shown). The surgeries in the

course of the animal studies were performed by Nils Kristian Prenzler. Daniela Hesse collected the samples, took care of the animals perioperativley and performed statistical analyses. Coating of the middle ear implants was performed by Muhammad Badar. Microbiological investigations were performed by André Bleich, Anna Smoczek and Silke Glage. Peter Behrens, Peter Paul Müller, Karl-Heinz Esser and Martin Stieve initiated the study and revised the manuscript.

For the article presented in section 5.4, Muhammad Badar and Muhammad Imran Rahim are the first authors, who contributed equally to this study. The author of this thesis is a co-author. All XRD measurements and according data interpretation were performed by him and the syntheses of the raw LDH, as well as the further treatment in order to obtain suspensions were performed by the author or under his supervision. The coating of the samples, cell culture tests, the estimation of drug release kinetics, the animal studies and data analysis were performed by Muhammad Badar and Muhammad Imran Rahim. The titanium discs were custom made by Thomas Ebel. Manfred Rohde (SEM imaging), Hansjörg Hauser, Peter Behrens, Peter Paul Müller initiated the study and revised the manuscript.

5.2 Highly biocompatible behavior and slow degradation of a LDH (layered double hydroxide)-coating on implants in the middle ear of rabbits

Franziska Duda*, Marc Kieke*, Florian Waltz, Maria E. Schweinefuß, Muhammad Badar, Peter Paul Müller, Karl-Heinz Esser, Thomas Lenarz, Peter Behrens, Nils Kristian Prenzler

*These authors contributed equally to this study.

J. Mater. Sci. Mater. Med. **2015**;*26*:9

DOI: 10.1007/s10856-014-5334-x

Highly biocompatible behaviour and slow degradation of a LDH (layered double hydroxide)-coating on implants in the middle ear of rabbits

Franziska Duda ▪ Marc Kieke ▪ Florian Waltz ▪ Maria E. Schweinefuß ▪ Muhammad Badar ▪ Peter Paul Müller ▪ Karl-Heinz Esser ▪ Thomas Lenarz ▪ Peter Behrens ▪ Nils Kristian Prenzler

Abstract

Chronic inflammation can irreversibly damage components of the ossicular chain which may lead to sound conduction deafness. The replacement of impaired ossicles with prostheses does not reduce the risk of bacterial infections which may lead to loss of function of the implant and consequently to additional damage of the connected structures such as inner ear, meninges and brain. Therefore, implants that could do both, reconstruct the sound conduction and in addition provide antibacterial protection are of high interest for ear surgery. Layered double hydroxides (LDHs) are promising novel biomaterials that have previously been used as an antibiotic-releasing implant coating to curb bacterial infections in the middle ear. However, animal studies of LDHs are scarce and there exist only few additional data on the biocompatibility and hardly any on the biodegradation of these compounds.

In this study, middle ear prostheses were coated with an LDH compound, using suspensions of nanoparticles of an LDH containing Mg and Al as well as carbonate ions. These coatings were characterized and implanted into the middle ear of healthy rabbits for 10 days. Analysis of the explanted prostheses showed only little signs of degradation. A stable health constitution was observed throughout the whole experiment in every animal.

The results show that LDH-based implant coatings are biocompatible and dissolve only slowly in the middle ear. They, therefore, appear as promising materials for the construction of controlled drug delivery vehicles.

Key words: layered double hydroxides, biocompatibility, biodegradation, Bioverit® II, middle ear implant, coating, local drug delivery, nanosuspension

F. Duda and M. Kieke contributed equally to this study.

F. Duda · T. Lenarz · N. K. Prenzler (✉)

Cluster of Excellence "Hearing4all", ENT Department, Hannover Medical School,
Carl-Neuberg-Str. 1, 30625 Hannover, Germany
e-mail: prenzler.nils@mh-hannover.de

M. Kieke · F. Waltz · M. E. Schweinefuß · P. Behrens (✉)

Cluster of Excellence "Hearing4all", Institute for Inorganic Chemistry, Leibniz University of Hannover,
Callinstr. 9, 30167 Hannover, Germany
e-mail: Peter.Behrens@acb.uni-hannover.de

M. Badar · P. P. Müller

Helmholtz Centre for Infection Research, Inhoffenstr. 7, 38124 Braunschweig, Germany

K.-H. Esser

Institute of Zoology, University of Veterinary Medicine, Foundation, Hannover, Bünteweg 17, 30559 Hannover, Germany

1 Introduction

Chronic otitis media with or without formation of cholesteatoma is often associated with hearing loss due to destruction of the ossicular chain, that is the malleus, incus and stapes [1,2]. To treat this conductive hearing loss it is usually necessary to insert ossicular replacement prostheses [3]. Despite aseptic conditions throughout implantation surgery there is a high risk of re-inflammation and -infection endangering the healing process and the function of the prosthesis [4]. For better control of inflammatory and infectious processes after implantation, a special pharmaceutically active coating of the prosthesis would be useful in order to complement or replace systemic drug applications. This has been shown for the local drug delivery of ciprofloxacin from a nanoporous silica coating on a standard total ossicular chain replacement prosthesis (TORP) [5]. As a material for those implants Bioverit® II has been proven biocompatible in several studies [6]. Bioverit® II is a bioglass-mica composite which is characterized by an easy manufacturing process and high resistance to biodegradation.

A promising class of material that has been employed recently in drug delivery studies are layered double hydroxides (LDHs). LDHs, also known as hydrotalcite-like compounds with the general formula $[M^{II}_{1-x}M^{III}_x(OH)_2^{x+}][A^{n-}]_{x/n} \cdot yH_2O$, are composed of positively and negatively charged layers. M^{II} represents bivalent (e.g. Mg^{2+}, Ca^{2+}, Mn^{2+}, Zn^{2+}) and M^{III} trivalent (e.g. Al^{3+}, Co^{3+}, Cr^{3+}, Fe^{3+}) cations of the main layer [7,8]. The structure of magnesium-containing LDHs (Fig. 1) can be derived from the layered structure of brucite ($Mg(OH)_2$), in which a certain amount of Mg^{2+} ions is replaced with trivalent cations; both types of metal ions are octahedrally coordinated by hydroxide ions (OH^-) in the layers. Resulting surplus positive charges are balanced by anions A^{n-} placed in the interlayer spaces together with water molecules to fill the increased interlayer space [9]. The anions A^{n-} can be simple inorganic ones, as CO_3^{2-} and SO_4^{2-}, but also more complex anionic organic drugs [10–12]. These can then be released, when the LDH is used as a drug delivery system. The release of anions (e.g. drugs) from the LDH interlayer spaces can be achieved by anion exchange of the persisting LDH or by the dissolution of the LDH itself. Under acidic conditions, the dissolution of the LDH is triggered, but LDH will also dissolve slowly under neutral conditions [13].

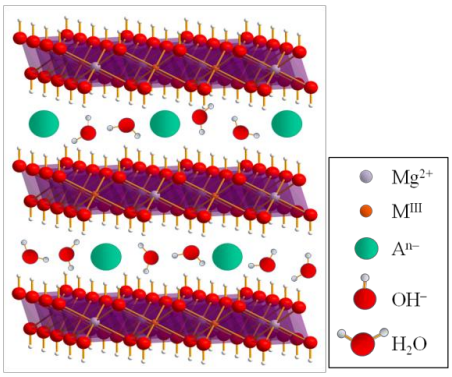

Fig. 1 Schematic structure of layered double hydroxides with positively charged layers and charge-balancing anions and additional water molecules located in the interlayer region (modified from [17])

In former studies several anti-inflammatory or antibacterial agents were applied in combination with LDHs as drug delivery systems. Mostly, only simple release experiments were performed and only few cell culture studies have been published. For example, a decrease in cell proliferation was reported by Dagnon et al. for implant surfaces covered with LDHs loaded with ibuprofen [14]. Strikingly, only very few *in vivo* studies have been reported so far. Silion et al. explored the *in vivo* behaviour of ketoprofen-loaded LDH in mice and found that intercalated ketoprofen has a better gastrointestinal compatibility and a stronger analgetic effect than the plain anti-inflammatory drug [15]. In another mouse study, Li et al. tested the protective potential as well as the therapeutic effects of LDHs as a DNA vaccine delivery vector. The LDH served as a suitable adjuvant to carry the vaccine and could thus inhibit tumour formation and suppress melanoma growth, respectively [16].

In a former study, we have examined the antimicrobial effect of a Mg-Al-SO_4-LDH mixed with ciprofloxacin as a coating on middle ear prostheses for rabbits. The coating used by Hesse et al. showed excellent activity against infection immediately after implantation and persisting attenuated activity when the re-infection was triggered one week after surgery [17]. The *in vivo* studies mentioned above concentrated on the effects of drug loaded LDH coatings on the animals [15–17].

To our knowledge, our present study is the first to examine the degradation behaviour of pure LDH as an implant coating *in vivo*. The aim of this study was to examine the degradation characteristics of LDH under the complex conditions in the middle ear, and by this complement our former investigations. Thorough knowledge on the degradation behaviour of LDH is crucial for further examinations and ultimately for the targeted application of LDHs as key components of controllable drug release systems, in particular for reconstructive middle ear surgery.

2 Materials and methods

2.1 Implants and coating material

Bioverit® II implants were purchased from 3di GmbH (Jena, Germany). The bioceramic implants with an average weight of 8 mg are composed of a 2.1 mm long shaft with a diameter of 0.9 mm attached to a base plate with a diameter of 2.5 mm and a height of 0.5 mm (Fig. 2a.).

For our study we used a water-based suspension of nanocrystals of a Mg-Al-CO_3-LDH with a Mg:Al ratio of 2:1 as the material to prepare the implant coating. In a typical synthesis the raw LDH was precipitated in water by adding a solution of $MgCl_2 \cdot 6H_2O$ (20 mmol, purum p.a. ≥ 98.0 %, Fluka, Buchs, Switzerland) and $AlCl_3 \cdot 6H_2O$ (10 mmol, purum p.a. ≥ 99.0 %, Fluka) to an intensely stirred solution of NaOH (60 mmol, reagent grade, anhydrous, ≥ 98 %, Fluka) and $Na_2CO_3 \cdot H_2O$ (12 mmol, ≥ 99.5 %, Fluka). After the raw product was aged for 15 min, the product was collected by centrifugation, and washed twice with deionized water. The remainder was redispersed in water and exposed to ultrasonication for one hour. The synthesis was performed at ambient conditions and all chemicals were used as purchased without further purification. Information about the crystalline structure of the LDH materials was collected by X-ray diffraction (XRD) with a Theta/Theta diffractometer from Stoe (Darmstadt, Germany).

The coating was performed via a spray-coating technique. For this purpose, the implants were heated to 150 °C and sprayed with the nebulized LDH nanosuspension using a commercially available air brush equipment (Conrad Electronic SE, Hirschau, Germany). Throughout the process the spraying geometry, characterized by an angle of 45 ° and a distance of 30 cm (nozzle to implant), was maintained.

The spraying process and coating thickness were indirectly controlled by energy dispersive X-ray spectroscopy (EDX) to map the initial situation for a comparison with the explanted prostheses. All coated prostheses were characterized individually. The coating process was judged as complete when the EDX spectrum corresponded to the expectation of a high-intensity magnesium peak, a medium-intensity aluminium peak and a low-intensity silicon peak (Fig. 2c.). In all cases the silicon peak from the Bioverit® II could be detected, indicating that the EDX was able to detect signals from both the Bioverit® II substrate and the silicon-free LDH coating, hence, allowing to track even minor degradation.

For this purpose, the implants were rotated by an angle of 90° around their long axis after five sprays had been applied, totalling in 20 sprays for the initial coating. If the EDX spectrum was not satisfactory after 20 sprays, one spray on each side was performed in addition and the EDX measurement was repeated. An average LDH coating thickness on the middle ear implants of approximately 150 nm was estimated according to laser scanning microscopy measurements (*VK-9710*, Keyence, Neu-Isenburg, Germany) of similarly coated flat glass slides.

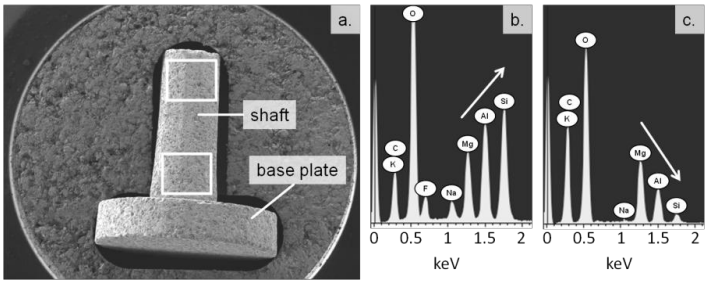

Fig. 2 a. SEM picture of an uncoated Bioverit® II middle ear implant as produced for the study (EDX sites are marked with white rectangles) **b.** EDX spectrum of an uncoated and **c.** LDH coated prostheses (before the insertion into the ear). The white arrows highlight the intensity sequences of the element peaks of Mg, Al and Si for uncoated and LDH coated prostheses

2.2 *In vivo* setup

The *in vivo* study (permitted by the Lower Saxony State Office for Consumer Protection and Food Safety, Dept. of Animal Welfare, *No. 33.9-42502-04-11/0610*, considering the German Animal Welfare legislation) included 30 approximately six-month-old male New Zealand White rabbits (Charles River Laboratories, Sulzfeld, Germany). The animals had an average weight of 3.3 kg and were housed in single cages with an artificial day-night rhythm of 12 hours in the Institute of Laboratory Animal Science and Central Animal Facility of the Hannover Medical School. The rabbits were accordingly divided into three groups ($n = 10$), each with an observation period after surgery of four, 7 and 10 days.

The anaesthetic management and implantation procedure was performed following the same protocol described in the studies by Hesse et al. and Stieve et al. [17,18]. Accordingly, the prostheses were implanted into the right middle ear via a retroauricular access, while the left ear was used as control. The implantation procedure is documented in Fig. 3. After implantation the animals were supplied with an oral dose of 0.15 $mg \cdot kg^{-1}$ meloxicam (Metacam®, Boehringer Ingelheim, Ingelheim am Rhein, Germany) one day pre-surgery and three days post surgery for analgesia. Oral antibiotic prophylaxis of 10 $mg \cdot kg^{-1}$ enrofloxacin (Baytril®, Bayer, Leverkusen, Germany) also began 24 hours before implantation, and was continued for four days post implantation.

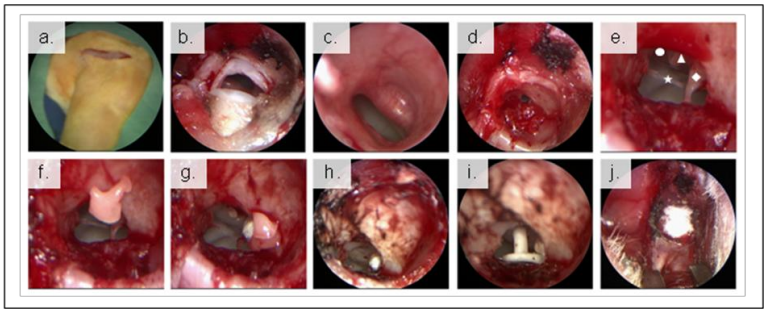

Fig. 3 Sequence of endoscopic images of the implantation procedure with **a.** retroauricular acess **b.** incision of ear canal (*meatus acusticus externus)* **c.** ear canal with *tympanic membrane* **d.** tympanotomy for accessing the middle ear **e.** view on middle ear with ◆ *malleus* ▲ *incus* ● *stapes* and ★ *chorda tymani* **f.** extraction of *incus* **g.** luxation of *malleus* **h.** extraction of *crura stapes* **i.** insertion of middle ear prosthesis between *tympanic membrane* and remaining base of stapes **j.** closure of middle ear

After four, 7 and 10 days, respectively, subjects were sedated and euthanized with regard to animal welfare. Both middle ears were irrigated with 1.5 mL distilled water with a syringe by piercing the tympanic membrane, avoiding damage of the bulla. The rinsing solution was collected immediately and stored in sterile reaction tubes. Afterwards, pH values of the samples were estimated with a calibrated PB-20 Basic pH-Meter (Sartorius, Göttingen, Germany) by directly immersing the electrode into the respective solutions. The *bulla tympanica* was opened to estimate the middle ear microscopically. Finally the prosthesis was explanted and chemically analyzed.

2.3 Clinical evaluation

To examine the health status of the animals, we observed the behaviour, appetite, defecation and urination, body weight and rectal temperature up to four days post implantation. Afterwards, the animals were weighed weekly.

To detect possible systemic inflammation, blood samples were taken before implantation and at the end of the examination periods (per animal 0.5 mL blood in an EDTA micro tube, Sarstedt, Nümbrecht, Germany) and analysed with an animal blood counter (scil Vet ABC™ hematology analyzer, scil animal care company, CSF, Viernheim, Germany).

2.4 Microscopic examination of the middle ear

After ventral opening of the *bulla tympanica* the implant situation in the middle ear was microscopically evaluated using light microscopy (Microscope Zeiss®, Jena, Germany / Camera Lumenera®, Ottawa, Canada),

whereas, the left middle ear served as control. The main focus was on the position and appearance of the prosthesis, the local mucosal reaction, possible inflammation signs e.g. hyper-vascularised mucosa, swelling, aggregation of watery, serous, mucous or bloody fluids.

A JEOL JSM-6700F field-emission scanning electron microscope (Jeol, Eching, Germany) was used for the collection of SEM images of the prostheses. The device was operated with an accelerating voltage of 2.0 kV at a working distance of 8 mm using the LEI-detector. The SEM was equipped with an INCA 300 energy dispersive X-ray (EDX) detector (Oxford Instruments PLC, Abingdon, UK).

2.5 Chemical analyses of the coatings

The main focus was on the tracking of the element ratios, in particular the Mg:Al ratio, at the implant surfaces and the intensities ($I_{element}$) in the respective EDX spectra. To illustrate the course of changes of the coatings, each implant was measured before implantation and subsequently in the post-explanted state. The EDX spectrum of uncoated Bioverit® II is characterized by a low-intensity magnesium peak, a medium-intensity aluminium peak and a high-intensity silicon peak: $I_{Mg}<I_{Al}<I_{Si}$ with a Mg:Al ratio of approximately 0.6. When coated with Mg_4Al_2-LDH, the intensities shifted to the expected, vice versa sequence: $I_{Mg}<I_{Al}<I_{Si} \rightarrow I_{Mg}>I_{Al}>I_{Si}$ (Fig. 2b. and 2c.) with an average Mg:Al ratio of approximately 1.5, close to the ratio of 1.8 of the Mg_4Al_2-LDH in the suspension.

Accordingly, the progress of *in vivo* LDH degradation for each group (four days, 7 days and 10 days) was evaluated at the cation ratio and the intensities of the element peaks in the EDX spectra. Hence, an advanced degradation of the LDH coating is expected to be characterized by an obvious decrease of the Mg:Al ratio and a re-reversion of the peak intensity sequence: $I_{Mg}>I_{Al}>I_{Si} \rightarrow I_{Mg}<I_{Al}<I_{Si}$.

Due to the unique geometry of the implants, customized sample holders were fabricated by drilling the shape of the implants into standard graphite blocks suitable for scanning electron microscopy (SEM). EDX measurements were performed on each of the prostheses, near to and far away from the base plate. As shown in Fig. 2a., the EDX measurements were performed with a 200-fold magnification, totalling in 20 EDX spectra for each group (n = 10, four days, 7 days and 10 days). The JSM-6700F was operated in EDX mode with 10 kV (accelerating voltage) and 10 µA at a range of 0-10 kV with regard to the prostheses elemental composition at the surface, i.e. Mg, Al, Si, O, C, K, F and Na.

3 Results

3.1 Clinical evaluation

All 30 rabbits showed a good general health status throughout the experiment without any inflammation signs of the wound or fever. Food and water intake as well as urination and defecation behaviour were normal. Two animals showed a slight head tilt for not more than three days after implantation, a rare but typical side effect of the implantation as described in earlier studies [17].

All rabbits showed an inconspicuous haematologic status prior to implantation and at the end of the study in agreement with the clinical appearance of the animals.

3.2 pH measurements

After the removal of the implants the pH values were measured in the rinsing solutions taken from the implanted right ears as well as from the left ears (control side). A slightly higher pH could be observed in the implanted ears (7.3 ± 0.3) than in the control side ears (6.7 ± 0.4). No correlation between the pH and the period of application was observed.

3.3 Microscopic examination

The appearance of the examined ears was in agreement with the expectations of an implanted middle ear after respective timepoints. After four days the microscopic view showed a minimal watery-bloody milieu with occasional appearance of a *mucotympanum*. After longer implantation periods, blood clots and mucus were resorbed and smooth mucosa became visible (Fig. 4). No signs of inflammation could be observed by microscopic means.

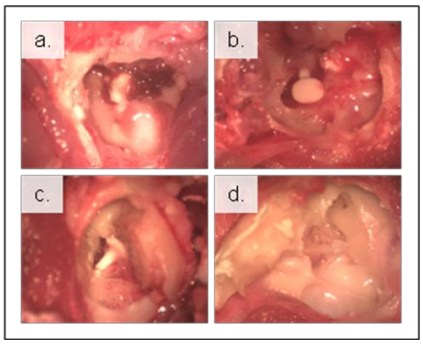

Fig. 4 Representative microscopic views (16x magnification) into the middle ear **a.** Four days post implantation: blood clots surrounding implant **b.** 7 days post implantation: blood resorbed **c.** 10 days post implantation: *mucotympanum* surrounding implant **d.** control side: left middle ear, not implanted

3.4 Chemical analysis of the coatings

The successful synthesis of pure Mg-Al-CO_3-LDH was confirmed by XRD measurements of dried material from the nanosuspension. Unfortunately, a direct detection of LDH on the implant by XRD was not possible due to the geometry and small size of the middle ear implants. Weighing the samples was also not suitable for tracking the coating and was considered to be ineffective once the implants were contaminated with organic material after explantation. In order to prove the general applicability of the LDH nanosuspension for the spray coating process, and to optimize the substrate temperature used in this process (150 °C), flat glass slides were used as test substrates and spray-coated using a process similar to the one applied to the middle ear implants. These samples could be investigated by XRD. Crystalline LDH coatings were observed in all cases.

For each group (four days, 7 days and 10 days) 20 EDX spectra were collected and considered for the evaluation of the LDH degradation. Over the period of 10 days, no remarkable decrease of the magnesium to aluminium ratio determined at the surfaces (Fig. 5) and furthermore no change of the relative intensities of the element peaks in the EDX spectra could be observed. This is a sign that the Mg-Al-CO_3-LDH coatings are practically biostable. As Mg is present with a higher contribution in the LDH coating but occurs with a minor contribution in the Bioverit® II substrate, a degradation of the LDH coating would result in a decrease of the Mg:Al ratio. Also the SEM images did not show any signs for alterations of the surface structure.

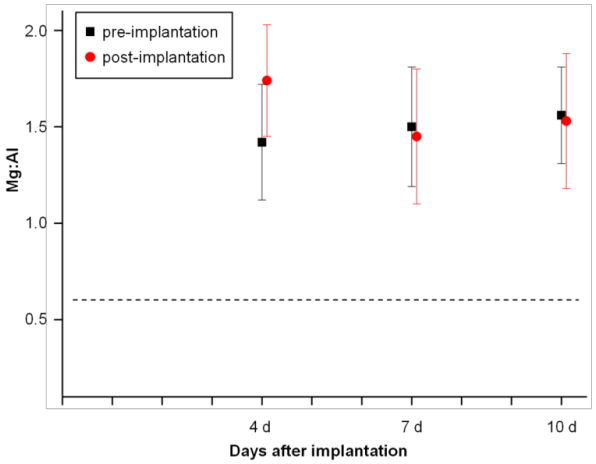

Fig. 5 Mg:Al ratio derived from EDX measurements of pre- and post-implantation samples. The Mg:Al ratio at the surface of uncoated Bioverit® II is highlighted by the dashed line

Whereas the carbon content was low before the implantations, as expected, it was considerably increased after the *in vivo* exposition. Organic debris (blood stains, mucus, and cell detritus) with high carbon content was found adhering to the implants' surfaces in varying amounts and could also be seen by eye. Fig. 6 exemplarily shows photographical and SEM images of two prostheses explanted four days after implantation. An increasing carbon content proportionally decreased the relative contributions of the other elements such as magnesium and aluminium, but did not influence their ratio.

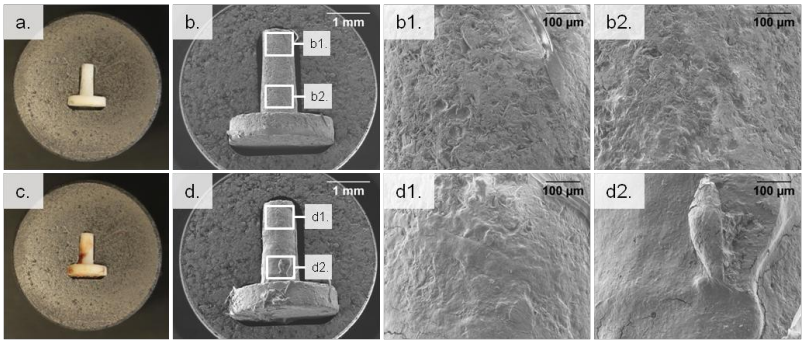

Fig. 6 a. and **c.** Pictures of explanted prostheses, shown here by way of example for prostheses which had remained in the middle ear for four days. **b.** and **d.** SEM images of the samples shown in a. and c., respectively. EDX data were taken at the sites indicated by the white rectangles **b1.**, **b2.**, **d1.** and **d2.** images with higher magnification of the respective sites

4 Discussion

4.1 Animal health screening and microscopic examination

No harmful effect of the LDH coatings could be observed for any of the animals studied. All groups presented normal behaviour and clinical health status. In addition, the microscopic examination of the middle ear showed no pathological findings and no adverse effects of the LDH coating could be detected. This confirms a very good biocompatibility of LDHs as an implant coating material in the middle ear.

4.2 pH measurements

The slight increase of the pH in the operated ears can be assigned to the presence of the layered double hydroxide. Mildly alkaline effects are a consequence of a decomposition of the LDH:

$[Mg_4Al_2(OH)_{12}][CO_3]\cdot yH_2O \rightarrow 4Mg^{2+} + 2Al^{3+} + 12OH^- + CO_3^{2-} + yH_2O$

This reaction probably occurs only to a very small extent which is not detectable in the EDX spectra. Since inflammatory reactions commonly acidify the surrounding tissue, the data shown and the *post mortem* microscopic examinations allow the conclusion that no severe inflammatory reaction was present [19,20].

4.3 *In vivo* stability of LDH coatings

The main result from this study, apart from the conclusion that the LDH has a very good biocompatibility, is the unexpected stability of the LDH coatings. Except for the mildly alkaline effect, no changes could be observed even after 10 days of implantation.

With regard to the estimated coating thickness of 150 nm, suitable implantation periods had to be chosen. Janning et al. examined the dissolution character of magnesium hydroxide ($Mg(OH)_2$), a substance similar to magnesium-containing LDHs, in a peri-implant bone environment and found that the volume of implanted $Mg(OH)_2$ cylinders was reduced by 7 % after two weeks and by 19 % of its initial volume after 6 weeks of implantation [21]. Considering these results, with degradation occurring at the µm scale in the course of several weeks, examination periods of four, 7 and 10 days were chosen with regard to the much thinner coating.

Additionally, many release systems show burst release behaviour [22], making the early stages of possible degradation processes more interesting for this empiric study.

It has to be emphasized that the middle ear illustrates a special environment for implants. For the first days after surgical procedure, the tympanic cavity is liquid-filled, blood and mucus surrounding the implantation site. Throughout the healing, liquids are resorbed, ventilation and pressure equalization of the middle ear are restored and the fluid is replaced by an air-filled environment. Based on our knowledge gained from earlier studies and from human middle ear surgery, our different examination periods seem suitable to include and track the extensive reorganization processes.

It also has to be pointed out that the coated prostheses were implanted under physiological conditions in a healthy middle ear. Commonly, prostheses as therapeutic tools will be implanted into inflamed and infected surroundings, which might influence the degradation process and by this the drug release behavior. Accordingly, examination times have to be adjusted to the indications caused by a corresponding infection model.

4.4 Consequences for LDH-based drug delivery systems

In our former *in vivo* drug delivery study, the delivery system consisted mainly of a physical mixture of ciprofloxacin with a Mg-Al-SO_4-LDH [17]. Considering the results obtained on Mg-Al-CO_3-LDH coatings, we suppose that the LDH component of the ciprofloxacin / Mg-Al-SO_4-LDH mixture used in our earlier investigations did not dissolve entirely. Nonetheless, sufficient amounts of drug could be released to suppress infection. With the findings presented here we expect that the drug had been released independently from the dissolution of the Mg-Al-SO_4-LDH. It is likely that the Mg-Al-SO_4-LDH matrix served mainly as a physico-chemical barrier and as a mild pH-balancing agent. Concerning this matter, the biostability of the Mg-Al-CO_3-LDH shown in this study indicates biodegradation characteristics comparable to an analogous Mg-Al-CO_3-LDH based drug release system. Hence, both LDHs appear promising as key components of drug release systems, in particular in the middle ear. However, drug and indication specific demands, exemplarily desired release rates, have to be considered.

Certainly the preparation of simple physical mixtures is an undemanding process, allowing for the facile and fast preparation of drug delivery systems including easily producible carbonate-LDHs and many other water-stable pharmaceuticals [23]. The LDHs offer a versatile material with regard to their composition and corresponding chemical properties. As mentioned above, the choice of the anion can be altered, as well the cations and their ratio [24,25], while maintaining the general LDH formula $[M^{II}_{1-x}M^{III}_{x}(OH)_2^{x+}][A^{n-}]_{x/n}\cdot yH_2O$.

On the contrary, the preparation of LDH intercalation compounds, where an anionic drug has to be intercalated into the LDH structure in order to form to a true common chemical compound, involves a much larger amount of work effort [26,27]. Synthesis routes with satisfying yields and purities have to be elaborated and adjusted for every individual drug. The release of a drug from a drug-LDH intercalation compound is either accompanied by the decomposition of the LDH coating or occurs via anion exchange. These complex processes can be very different depending on the type of the drug used. When drug / LDH mixtures (in contrast to intercalation compounds) are used, drug release rates can be adjusted by altering the ratio of components and the composition of the LDH. Preferably, the adjustments could be included in the respective coating process. In order to promote the homogeneity of the coatings and to establish a reproducible process eligible for market authorization, automation of the coating techniques, exemplary for our study i.e. controlled spray duration per cycle, humidity and substrate temperature, would be of interest.

5 Conclusion

In the middle ear, Mg-Al-CO_3-LDH can serve as a highly biocompatible and practically biostable (at least for the timeframe of the current investigation of ten days) coating material which can provide mild pH balance and is suitable for the construction of drug release systems, as shown before for Mg-Al-SO_4-LDH [17]. Throughout the examination, the pure LDH coatings on middle ear implants had no harmful effects on the animals' health.

For further drug release applications for which the utilization of sophisticated, pure drug-LDH intercalation compounds has been considered to be necessary, simple mixtures of agents with LDH could prove to be sufficient. This might reduce the effort associated with synthesis and processing of pure intercalation compounds.

Acknowledgement

We acknowledge the financial support of the project by the German Research Foundation (DFG) within the Collaborative Research Centre SFB 599 (subprojects D1 and DR1). This work also profited from collaboration in the Cluster of Excellence "Hearing4all".

References

1. Madana J, Yolmo D, Kalaiarasi R, Gopalakrishnan S, Sujatha S. Microbiological profile with antibiotic sensitivity pattern of cholesteatomatous chronic suppurative otitis media among children. Int. J. Pediatr. Otorhinolaryngol. 2011;75:1104–8.

2. Osma U, Cureoglu S, Hosoglu S. The complications of chronic otitis media: report of 93 cases. J. Laryngol. Otol. 2000;114:97–100.

3. Battaglia A, McGrew BM, Jackson CG. Reconstruction of the entire ossicular conduction mechanism. Laryngoscope. 2003;113:654–8.

4. Hwang J, Chu C, Liu T. Changes in bacteriology of discharging ears. J. Laryngol. Otol. 2002;116:686–9.

5. Lensing R, Bleich A, Smoczek A, Glage S, Ehlert N, Luessenhop T, et al. Efficacy of nanoporous silica coatings on middle ear prostheses as a delivery system for antibiotics: an animal study in rabbits. Acta Biomater. Acta Materialia Inc.; 2013;9:4815–25.

6. Vogt JC, Brandes G, Krüger I, Behrens P, Nolte I, Lenarz T, et al. A comparison of different nanostructured biomaterials in subcutaneous tissue. J. Mater. Sci. Mater. Med. 2008;19:2629–36.

7. Khan AI, O'Hare D. Intercalation chemistry of layered double hydroxides: recent developments and applications. J. Mater. Chem. 2002;12:3191–8.

8. Zhang LH, Li F, Evans DG, Duan X. Cu - Zn - (Mn) - (Fe) - Al Layered Double Hydroxides and Their Mixed Metal Oxides : Physicochemical and Catalytic Properties in Wet Hydrogen Peroxide Oxidation of Phenol. Ind. Eng. Chem. Res. 2010;49:5959–68.

9. Evans DG, Duan X. Preparation of layered double hydroxides and their applications as additives in polymers, as precursors to magnetic materials and in biology and medicine. Chem. Commun. (Camb). 2006;485–96.

10. Khan A, Lei L, Norquist A, O'Hare D. Intercalation and controlled release of pharmaceutically active compounds from a layered double hydroxide. Chem. Commun. 2001;2342–3.

11. Ambrogi V, Fardella G, Grandolini G, Perioli L. Intercalation compounds of hydrotalcite-like anionic clays with antiinflammatory agents--I. Intercalation and in vitro release of ibuprofen. Int. J. Pharm. 2001;220:23–32.

12. Frunza MS, Popa MI, Lisa G, Hritcu D, Lion MSI, Marcel Lone Pop A. New Hybrid Compounds Containing Intercalated Ciprofloxacin into Layered Double Hydroxides: Synthesis and Characterization. Rev. Roum. Chim. 2008;53:827–31.

13. Boclair J, Braterman P. Layered double hydroxide stability. 1. Relative stabilities of layered double hydroxides and their simple counterparts. Chem. Mater. 1999;11:298–302.

14. Dagnon KL, Ambadapadi S, Shaito A, Ogbomo SM, DeLeon V, Golden TD, et al. Poly(L-lactic acid) nanocomposites with layered double hydroxides functionalized with ibuprofen. J. Appl. Polym. Sci. 2009;113:1905–15.

15. Silion M, Hritcu D, Jaba IM, Tamba B, Ionescu D, Mungiu OC, et al. In vitro and in vivo behavior of ketoprofen intercalated into layered double hydroxides. J. Mater. Sci. Mater. Med. 2010;21:3009–18.

16. Li A, Qin L, Wang W, Zhu R, Yu Y, Liu H, et al. The use of layered double hydroxides as DNA vaccine delivery vector for enhancement of anti-melanoma immune response. Biomaterials. 2011;32:469–77.

17. Hesse D, Badar M, Bleich A, Smoczek A, Glage S, Kieke M, et al. Layered double hydroxides as efficient drug delivery system of ciprofloxacin in the middle ear: an animal study in rabbits. J. Mater. Sci. Mater. Med. 2013;24:129–36.

18. Stieve M, Hedrich HJ, Battmer RD, Behrens P, Müller P, Lenarz T. Experimental middle ear surgery in rabbits: a new approach for reconstructing the ossicular chain. Lab. Anim. 2009;43:198–204.

19. Dissemond J, Witthoff M, Brauns TC, Haberer D, Goos M. pH values in chronic wounds. Evaluation during modern wound therapy. Der Hautarzt. 2003;54:959–65.

20. Bartsch I, Willbold E, Rosenhahn B, Witte F. Non-invasive pH-determination adjacent to degradable biomaterials in vivo. Acta Biomater. 2014;10:34–9.

21. Janning C, Willbold E, Vogt C, Nellesen J, Meyer-Lindenberg A, Windhagen H, et al. Magnesium hydroxide temporarily enhancing osteoblast activity and decreasing the osteoclast number in peri-implant bone remodelling. Acta Biomater. 2010;6:1861–8.

22. Huang X, Brazel CS. On the importance and mechanisms of burst release in matrix-controlled drug delivery systems. J. Control. release. 2001;73:121–36.

23. Chakraborti M, Jackson J, Plackett D, Gilchrist S, Burt H. The application of layered double hydroxide clay (LDH)-poly (lactide-co-glycolic acid)(PLGA) film composites for the controlled release of antibiotics. J. Mater. Sci. Mater. Med. 2012;23:1705–13.

24. Panda HS, Srivastava R, Bahadur D. Stacking of lamellae in Mg/Al hydrotalcites: Effect of metal ion concentrations on morphology. Mater. Res. Bull. 2008;43:1448–55.

25. Vucelic M, Jones W, Moggridge G. Cation ordering in synthetic layered double hydroxides. Clays Clay Miner. 1997;803–13.

26. Carlino S, Hudson M. Reaction of molten sebacic acid with a layered (Mg/Al) double hydroxide. J. Mater. Chem. 1994;4:99–104.

27. Del Arco M, Cebadera E, GutiÃ©rrez S, MartÃn C, Montero MJ, Rives V, et al. Mg,Al layered double hydroxides with intercalated indomethacin: Synthesis, characterization, and pharmacological study. J. Pharm. Sci. 2004;93:1649–58.

5.3 Layered double hydroxides as efficient drug delivery system of ciprofloxacin in the middle ear: an animal study in rabbits

Daniela Hesse, Muhammad Badar, André Bleich, Anna Smoczek, Silke Glage, Marc Kieke, Peter Behrens, Peter Paul Müller, Karl-Heinz Esser, Martin Stieve, Nils Kristian Prenzler

J. Mater. Sci. Mater. Med. **2013**;*24*:129-36

DOI: 10.1007/s10856-012-4769-1

The final publication is available at

http://link.springer.com/article/10.1007/s10856-012-4769-1

Layered double hydroxides as efficient drug delivery system of ciprofloxacin in the middle ear: an animal study in rabbits

Daniela Hesse • Muhammad Badar • Andre´ Bleich • Anna Smoczek • Silke Glage • Marc Kieke • Peter Behrens • Peter Paul Mu¨ ller • Karl-Heinz Esser • Martin Stieve • Nils Kristian Prenzler

Abstract
Chronic otitis media is a common disease often accompanied by recurrent bacterial infections. These may lead to the destruction of the middle ear bones such that prostheses have to be implanted to restore sound transmission. Surface coatings with layered double hydroxides (LDHs) are evaluated here as a possibility for drug delivery systems with convenient advantages such as low cytotoxicity and easy synthesis. Male New Zealand White rabbits were implanted with Bioverit® II middle ear prostheses coated with the LDH $Mg_4Al_2(OH)_{12}(SO_4)_2{\cdot}6H_2O$ impregnated with ciprofloxacin. 12 (group 1) were directly infected with *Pseudomonas aeruginosa* and another 12 (group 2) 1 week after the implantation. Clinical outcome, blood counts, histological analyses and microbiological examination showed an excellent antimicrobial activity for group 1, whereas this effect was attenuated in animals where infection was performed 1 week after implantation. This is the first study to demonstrate an efficient drug delivery system with an LDH coating on prostheses in the middle ear.

M. Stieve and N. K. Prenzler contributed equaly to this study.

D. Hesse · M. Stieve · N. K. Prenzler (✉)
ENT Department, Hannover Medical School,
Carl-Neuberg-Str. 1, 30625 Hannover, Germany
e-mail: prenzler.nils@mh-hannover.de

M. Badar · P. P. Müller
Helmholtz Centre for Infection Research, Inhoffenstr. 7,
38124 Braunschweig, Germany

A. Bleich · A. Smoczek · S. Glage
Institute of Laboratory Animal Science and Central Animal
Facility, Medical University of Hannover, Carl-Neuberg-Str. 1,
30625 Hannover, Germany

M. Kieke · P. Behrens
Institute for Inorganic Chemistry, Leibnitz University of
Hannover, Callinstr. 9, 30167 Hannover, Germany

K.-H. Esser
Institute of Zoology, University of Veterinary Medicine
Hannover, Bu¨nteweg 17, 30559 Hannover, Germany

1 Introduction

Chronic otitis media is a common disease in western civilization and is often associated with local complications such as destruction of the ossicular chain, conduction deafness or infectious expansion like in otogenous meningitis or cerebral abscess. The most frequently isolated pathogens are *Staphylococcus aureus*, coagulase-negative *Staphylococcus* and *Pseudomonas aeruginosa*, a gram-negative obligate aerobic rod-shaped germ, which prefers a moist environment [1–3]. Recently, the prevalence of multiresistant *Ps. aeruginosa* stems in chronic otitis media has increased [4]. When the ossicular chain is destroyed, its reconstruction with an allogeneic prosthesis is the only possibility to restore sound transmission. However, recurrence or progression of an inflammation and the development of bacterial biofilms must be avoided. In this context, implants with a drug delivery system with antibiotics are a promising approach to combat peri- and postoperative infection and to support a cellular colonization of the implant. In recent years, the interest in the development of layered double hydroxides (LDHs) as drug delivery systems has strongly increased [5, 6], although only very few in vivo studies have been carried out. LDHs are materials with a layered structure, consisting of positively charged metal hydroxide layers and charge-balancing anions and water molecules located in the interlayer region, as shown in Fig. 1 and described by the general formula $[M^{II}_{1-x}M^{III}(OH)_2]^{x+}[A^{n-}]_{x/n}{\cdot}yH_2O$, where M^{II} and M^{III} represent the metal cations, x stands for the charge per formula unit of the hydroxide layer, A^{n-} means the interlayer anion of charge n, and y is the number of the interlayer water molecules. LDHs are also known as hydrotalcite-like compounds or anionic clays and are for example applied as antacids for the treatment of heart-burn and gastric ulcers. Their flexible composition and the relatively simple synthesis make LDHs interesting materials for a variety of other bioapplications. Their chemistry is furthermore enhanced by the possibilities of the exchange of the interlayer anions and of the intercalation of larger molecules.

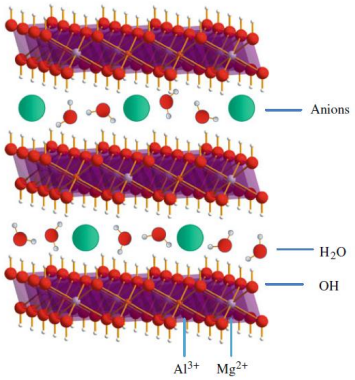

Fig. 1 Schematic stucture of LDHs with positively charged layers and charge-balancing anions and additional water molecules located in the interlayer region

LDH nanoparticles are mainly transported into cells by clathrin-mediated endocytosis [7], which can be different from the cellular uptake mechanism for the pure drugs, as shown in a study about methotrexate-LDHs [8], the first example of an LDH-mediated drug delivery which enabled to overcome drug resistance. Choy et al. examined folic acid derivatives of LDHs and explained the enhanced drug delivery by the increased permeability through the cell membrane and protection of the agent from rapid decomposition [9]. This improved impact was also observed in animal studies. The use of LDHs as DNA vaccine delivery vector in the treatment of melanoma in mice induced an enhanced serum antibody response at a greater extent than naked DNA [10]. Del Arco et al. investigated LDHs with intercalated indomethacin and showed that gastric damage was reduced in comparison to oral intake of indomethacin alone [11]. Another important factor of LDHs is the slowed release and the subsequent extended presence of the drugs. A study in rabbits on LDHs with intercalated diclofenac for ocular delivery revealed a longer detectable time compared with diclofenac only [12]. Moreover, for all therapeutic drug delivery systems a low cytotoxicity is required. Gu et al. [13] examined the effect of heparin intercalated into LDH nanoparticles on vascular smooth muscle cells in rats as an anti-restenotic drug. The cytotoxicity tests showed that LDH itself had a very limited toxicity at concentrations below 50 µg/ml over 6-day incubation.

For the present study, we have investigated the ability of LDH nanoparticles impregnated with the antibiotic ciprofloxacin on Bioverit® II implants to act as a drug delivery system in order to combat an infection with *Ps. aeruginosa* in the middle ear. To our knowledge, this is one of the very few in vivo studies of LDHs and the first report of an application of LDHs in the middle ear. For these in vivo experiments, we chose rabbits as the animal model. This choice was made due to a favourable surgical approach with similar anatomy to the human middle ear [14, 15] and because we have already established an infection model based for the middle ear in this species. Here, we have infected one group of animals during surgery and another group 1 week after

implantation to mimic a recurrent infection and to allow estimation of the duration of the antibacterial efficacy of the ciprofloxacin–LDH system.

2 Materials and methods

2.1 Animals

For this animal study, we used 24 five-month-old healthy male New Zealand White rabbits from Charles River (Sulzfeld, Germany). The rabbits were housed in single cages up to an average weight of 2.4 kg in the Institute for Laboratory Animal Science and Central Animal Facility, Medical University of Hannover, Germany. This study was conducted in accordance with German law for animal protection and with the European Communities Council Directive 86/609/EEC for the protection of animals used for experimental purposes. All experiments were approved by the Local Institutional Animal Care and Research Advisory committee and permitted by the local government (No. 33.9-42502-04-11/0355).

2.2 Implants

The bioceramic Bioverit® II, from 3di GmbH (Jena, Germany), was used as basic implant material for the ossicular reconstruction. The prostheses, with a weight of 8 mg, consisted of a 2.5 mm long cylinder with a diameter of 1 mm and with, at one end, an orthogonal plate 3 mm of diameter. A nanoparticle stock suspension (~ 3.5 g/l) of the LDH with the chemical formula $Mg_4Al_2(OH)_{12}(SO_4)_0{\cdot}6H_2O$ was concentrated by centrifuging the suspension @ 3,000 rpm for 5 min at room temp. Half of the supernatant was removed and the pellet was resuspended in the remaining liquid. This concentrated suspension of LDH was mixed with 1 mg/ml suspension of ciprofloxacin (Fluka Chemie GmbH, Deisenhofen, Germany) in H2O in a 3:1 ratio. Bioverit® II middle ear implants were individually placed in reaction tubes of 0.2 ml volume and 100 µl of the LDH and ciprofloxacin mixture was added to each tube. The tubes were then placed overnight at 37 °C to evaporate the liquid from the tubes. This left the Bioverit implants coated with the mixture of LDH and ciprofloxacin. In vitro experiments on the release kinetics of ciprofloxacin out of the LDH/ciprofloxacin mixture in phosphate buffered saline showed a continuous stable release of the drug for about 2 weeks before the release began to decrease (data not shown, to be published elsewhere).

2.3 Bacteria

The *Ps. aeruginosa* strain "PAO1" was used for this experiment; the sensitivity to ciprofloxacin was confirmed. In previous studies (data not shown) a clinical strain of *Ps. aeruginosa* was tested but found to be too harmful for the rabbits; the PAO1 strain proved to be clinically relevant in this context but did not cause such a high mortality. The bacteria were cultured on blood agar and incubated at 37 °C for 24 h. Afterwards, they were suspended in sterile saline solution and set to an optical density of 0.6 (OD = 0,6) measured at 578 nm, corresponding to a concentration approximately of 106 colony forming units (CFU)/200 µl.

2.4 Middle ear surgery

All rabbits were sedated with an intramuscular injection of 25 mg/kg ketamine (Ketamin Gräub®, Albrecht, Aulendorf, Germany) and 1.25 mg/kg midazolam (Midazolam 5 mg, Cura-Med, Hameln, Germany). Both eyes were given a protective ophthalmic ointment (Bepanthen® Augen- und Nasensalbe, Bayer, Leverkusen, Germany) to prevent desiccation. Subsequently, as subcutaneous injections were given of 0.1 mg/kg of the anticholinergic agent Robinul® (Riemser, Insel Riems, Germany), 0.05 mg/kg of the analgesic buprenorphin (Buprenovet®, Bayer, Leverkusen, Germany) and 4 mg/kg carprofen (Rimadyl®, Pfizer, Karlsruhe, Germany) to inhibit inflammation and pain. Anesthesia was induced with 1 mg/kg of 1% propofol (Propofol-® Lipuro, B. Braun, Melsungen, Germany) intravenously. After endotracheal intubation, narcosis was maintained using a mix of Isofluran® (Baxter, Unterschleißheim, Germany) and oxygen (1.5%/1.5 l/min). During surgery the rabbits were laid in a thoracic-abdominalposition and a heated mat was used to stabilize the bodytemperature. Additionally, 10 ml/kg/h electrolyte solution (Sterofundin HEG-5®, B. Braun, Melsungen, Germany) was used to stabilize the animals' circulatory systems. Breathing, lid reflex, body-temperature and pulse rate were monitored consistently. The prostheses were implanted in the right middle ear cavity. After shaving, disinfection (Braunol®, B. Braun, Melsungen, Germany) and sterile covering of the operational site, a retroauricular incision of 5 cm length was made and the external acoustic meatus was opened between the cartilage- bone junction. Subsequently, a tympanomeatal flap was created to get access to the middle ear. The ossicular chain was removed, partially with the help of a laser microscope (OPMI® Twin ER, Carl Zeiss AG, Oberkochen, Germany), and the prosthesis was placed between the tympanic membrane (with the plate), the remaining malleus and the stapes. Afterwards, the tympanomeatal flap was replaced and a tamponade (Gelita®, B. Braun, Tuttlingen, Germany) was used to support the eardrum. The approach was closed using absorbable surgical suture material (Vicryl®; 4/0, SH-1 plus; Ethicon GmbH, Norderstedt, Germany) and non-absorbable surgical suture material (Supolene®; 4/0; RESORBA Wundversorgung, Nürnberg, Germany) for the skin. Prior to surgery, the animals were split into two groups: one was infected with *Ps. aeruginosa* suspension during the implantation, the other group 1 week after the implantation. Group 1 (n = 12) received 0.2 ml of the bacterial

suspension (106 CFU/200 µl) directly into the middle ear before replacing the tympanomeatal flap. The retarded infection was placed through the tympanic membrane. For this purpose, the animals of group 2 were narcotized with an intramuscular injection of 25 mg/kg ketamine, 1.25 mg/kg midazolam and 0.1 ml medetomidin (Domitor®, Janssen, Neuss, Germany) 1 week after the implantation. Both eyes were given a protective ophthalmic ointment. 0.1 mg/kg of the anticholinergic agent Robinul® and 4 mg/kg carprofen (Rimadyl®, Pfizer, Karlsruhe, Germany) were administered subcutaneously to inhibit inflammation and pain.

2.5 Evaluation of the clinical condition

To evaluate the clinical general condition, we assessed behaviour, feed intake, defecation and urination, body weight and rectal temperature and created a scoring system (Table 1) for the first four parameters. The daily scores of each animal were added to a total clinical score and this was averaged to give the means of the two groups. During the first week after infection rectal temperature was assessed daily. Body weight alterations, compared to the initial weight before infection, was documented for 7 days after infection and additionally prior to euthanasia. The animals received carprofen (Rimadyl®, 4 mg/kg s.c., Pfizer, Berlin, Germany) as an anti-inflammatory and analgesic drug for 2 days after infection and if they showed remaining fever after 2 days, carprofen treatment was continued. Rabbits that did not eat properly were fed a blended special powder for herbivore (Critical Care®, Albrecht, Aulendorf, Germany). Blood samples from the auricular artery were taken daily throughout the first seven days after infection. Samples were put in ethylenediamintetraacetic acid (EDTA) tubes and leukocytes were counted using Vet ABC® Animal Blood Counter (Scil Animal Care Company GmbH, Viernheim, Germany). To evaluate the clinical neurological condition, we additionally noted head tilt, nystagmus, imbalance, circling in cage and rotation around the longitudinal axis with the aid of a scoring system. Score 0 indicates no symptom; a possible score of 5 is obtained if an animal showed all symptoms at the same time.

Table 1 Classification of the total clinical score

Clinical parameters		Score
Behaviour	Lively, attentive, typical movement	0
	Calm, attentive, reduced movement	1
	Apathetic, weak, without movement	2
Feed intake	Normal	0
	Reduced	1
	Non-existent	2
Defecation/urination	Normal	0
	Modified	1
Total clinical score		0-5

2.6 Euthanasia and necropsy

Animals were euthanised three weeks after infection. To this end, they were sedated with an intramuscular injection of 25 mg/kg ketamine (Ketamin Gräub®, Albrecht, Aulendorf, Germany) and 1.25 mg/kg midazolam (Midazolam 5 mg, Cura-Med, Hameln, Germany). Propofol (1%, 1 mg/kg) (Propofol-® Lipuro, Braun, Melsungen, Germany) was administered i.v. to deepen the narcosis before the rabbits were euthanised with 600 mg/kg i.v. pentobarbital (Release®, WDT, Garbsen, Germany). The animals were dissected and organ alterations were documented. Tissue samples of lung, liver, spleen, and kidney and a blood sample were taken for microbiological examination and lung and heart were prepared for histology. Subsequently, the external acoustic meatus was removed and the middle ear was examined and irrigated with 1,000 µl saline solution which was used for further microbiological examination. Afterwards, the bulla was opened from the ventral side and the implant was obtained and rinsed with 100 µl saline solution to determine the growth of *Ps. aeruginosa*. Finally, the skullcap was opened, swab samples of the brain were taken for microbiological examination and the brain was removed and examined histopathologically to detect inflammatory lesions, based on a procedure published by the RITA and NACAD groups [16].

2.7 Microbiological examination

Tissue or swab samples of brain and ear were cultured in Thioglycolat (TG) medium (Thioglycolat Medium U.S.P., Oxoid Deutschland GmbH, Wesel, Germany). Irrigation fluids of implant and middle ear were cultured on standard blood agar (Blood Agar Base No. 2, Oxoid Deutschland GmbH, Wesel, Germany), Gassner agar (Oxoid Deutschland GmbH, Wesel, Germany) and in TG medium. Bacterial growth on blood and Gassner agar

was evaluated for a maximum of 48 h, in the TG medium for 1 week. The evidence for the presence of *Ps. aeruginosa* was ensured by oxidase tests and the API-system (API® 20NE, bioMe´vieux Deutschland GmbH, Nürtingen, Germany). Quantification of *Ps. aeruginosa* from the irrigations of middle ears and implants was achieved by using plating out dilution series and the result is given as CFU/10 µl.

2.8 Statistical methods

GraphPad Prism 5.0 was used for statistical analysis. The parameters of the clinical general examination were analyzed using the unpaired t test. The Fisher's exact test was applied to evaluate the neurological examination, the results of the necropsy and the qualitative microbiological examination. The quantitative microbiological results and the neurological score were analyzed by the Mann– Whitney test. Differences with the value of $P < 0.05$ were considered statistically significant.

3 Results

One animal of each group died in the course of theimplantation due to cardiopulmonary failure. In addition, one animal of group 2 was euthanised preterm on day four after infection due to its poor health condition.

3.1 Clinical examination

Only two rabbits, one of each group, showed behavioural syndromes at the clinical general examination. The animal of group 1 showed reduced food intake and mild diarrhea and decreased defecation throughout the first 4 days. It was also calm but attentive and showed a reduced movement from day one to day four. The rabbit of group 2 showed reduced feed intake on day three and four and a decreased defecation on day four after infection and was also calm, with reduced movement throughout the first 4 days. Both rabbits were allocated to score 3. In total, there was no significant difference between the groups. Furthermore, both above-mentioned animals lost 11% of their initial body weight to day four. In summary, there was only one significant difference for the body weight: animals of group 2 gained more weight than animals of group 1 ($P = 0.04$ Mann–Whitney test, Fig. 2). One rabbit of group 1 showed fever (body temperature > 40 °C) on day one after surgery and the rabbit of group 2, that was euthanised preterm, developed fever on day three and four after infection, despite treatment with carprofen. All in all, there was no significant difference between the groups, Fig. 3. The clinical neurological examination showed that in group 1, one rabbit developed mild imbalance and mild to severe head tilt throughout the whole examination period after infection. It also showed circling in cage for the last 4 days and rotated around its longitudinal axis for the last 3 days. In group 2, vestibular signs were shown by three animals. Two suffered from mild head tilt, one for 2 days after surgery and the second for 2 days after infection. The rabbit, which was euthanised preterm, showed moderate imbalance on day three and a severe imbalance on day four, Fig. 4. Adding and comparing the total neurological score, no significant differences were seen between the groups. Leukocytosis was seen in two rabbits of group 1, and in three animals of group 2, i.e. no significant difference between the groups was found, Fig. 5.

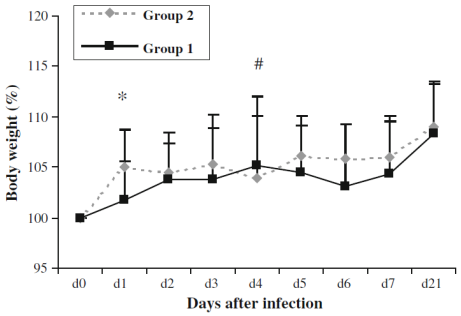

Fig. 2 Relative body weight: means of both groups ($N = 22$). Statistically significant differences ($P < 0.05$) between the groups are marked with *asterisks*. #The preterm death of one rabbit of group 2

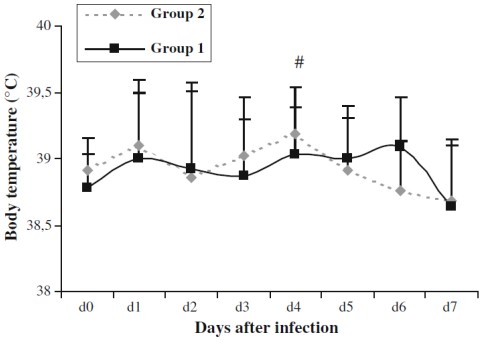

Fig. 3 Body temperature: means of both groups ($N = 22$) in the first 7 days after surgery. #Signifies the preterm death of one rabbit of group 2

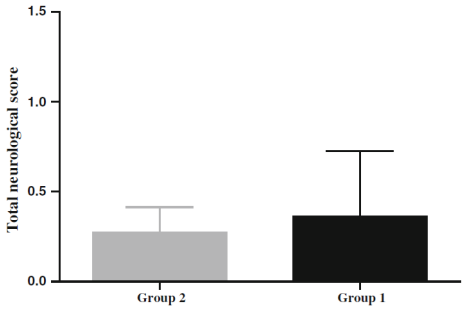

Fig. 4 Total neurological score. Score 0 means no neurological symptoms; score 5 corresponds to the display of five neurological symptoms at the same time as described in the text. This results in the means of both groups ($N = 22$)

3.2 Microbiological examination

The qualitative microbiological examination proved the presence of *Ps. aeruginosa* in two rabbits of group 1: the first rabbit had the germ on blood- and Gassner agar in the implant and middle ear irrigations. For the second animal, the germ was detected on blood- and Gassner agar in the middle ear irrigation. In group 2, *Ps. aeruginosa* was found in five subjects. In the first four animals, *Ps. aeruginosa* was detected on blood- and Gassner agar of the implant and middle ear irrigations. In the fifth, the germ could only be detected in the blood agar of the implant irrigation. The quantitative microbiological examination (CFU) of the implant irrigation showed a much higher value for the animals which were infected 1 week after implantation (P = 0.03), Fig. 6. The CFU titer in the middle ear irrigation was also higher in group 2 but the difference was not statistically significant.

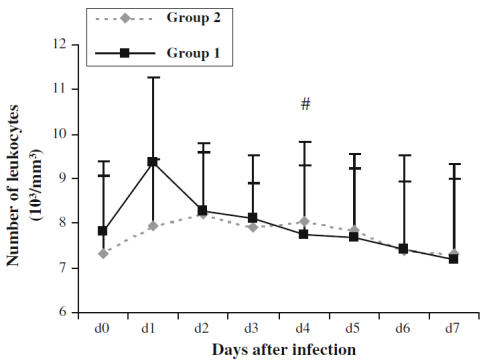

Fig. 5 Number of leukocytes: means of both groups ($N = 22$) in the first 7 days after surgery. #Signifies the preterm death of rabbit of group 2

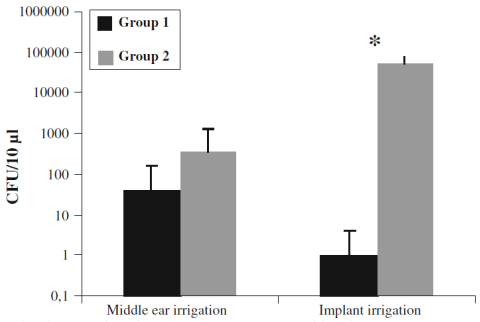

Fig. 6 Quantitative microbiological examination (CFU): means of both groups ($N = 22$). Statistically significant differences ($P < 0.05$) between the groups are marked with *asterisks*

3.3 Histopathological examination

Pulmonary oedema was found in all animals. Only the rabbit of group 2, which was euthanised preterm, had developed a severe meningoencephalitis with an accumulation of neutrophils, Fig. 7. The remaining rabbits of both groups showed no inflammation of the brain.

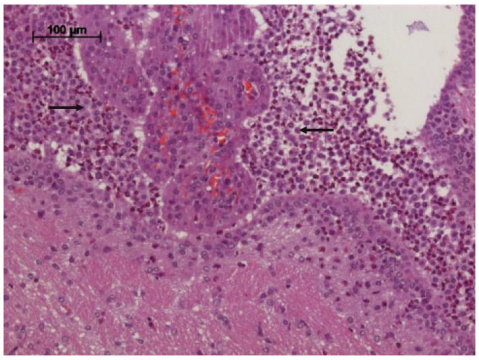

Fig. 7 Histological examination of the rabbit of group 1 which was euthanised preterm: the image shows a severe meningoencephalitis with an accumulation of neutrophils (*arrows*)

4 Discussion

LDH nanoparticles can serve as a local drug delivery system as shown in previous studies of different medical applications. Due to their favourable properties in terms of low cytotoxicity and easy synthesis, they can be a promising agent in the environment of the middle ear. Newly inserted prostheses, especially after various infections, are likely to become covered with bacteria, which prevents proper integration of the prostheses. To test the antimicrobial effect of a formulation comprised of a mixture of an LDH compound and ciprofloxacin as an effective drug against *Ps. aeruginosa* [17, 18], we coated this mixture on Bioverit® II prostheses which show an excellent biocompatibility [19, 20]. In order to mimic a recurrent infection, animals were infected at two different timepoints as explained before. There was no control group due to ethical considerations, as in preliminary studies animals without any antibiotic treatment had a very poor outcome and several of them had to be euthanised preterm (data not shown). Concerning the general condition only minor differences could be observed between the two groups, but it seems that animals that were infected 1 week after implantation had a slightly worse outcome: here, one animal had to be euthanised preterm. The reduced defecation of two animals, one of each group, can be explained by the reduced feed intake, because the stomach of rabbits transports the food only mechanically by permanent feed intake and not actively by muscle contraction. Therefore, they have to eat continuously. Furthermore, the gastrointestinal tract of rabbits is very fragile. Especially, in stress situations associated with surgical operations, gastrointestinal disorders can be observed [21–23]. Some rabbits developed fever and leukocytosis, which is both unusual in rabbits [22, 24, 25]. The most common reason for fever is heat stroke as well as septicaemia and viraemia. Even in the case of an abscess, pyrexia is rare. Also leukocytosis, in the context of an acute infection, occurs rarely in rabbits. For the first days after infection the high leukocyte number could be seen as the result of the immune system to combat the high concentration of bacteria, but also other factors such as pain, anxiety or excitement can play a role [26]. The neurological

examination showed that only one rabbit of group 1 and three rabbits of group 2 suffered from neurological symptoms, including the two animals which showed alterations in the general condition. One rabbit of group 2 showed mild head tilt for only 2 days after surgery without infection. So this observation is not only caused by otitis media or interna, but also by the surgical operation which involved pain and irritation of the vestibular system. Especially, head tilt and nystagmus are signs for a peripheral vestibular disturbance [24, 27]. However, also imbalance, circling and rotation around the longitudinal axis could be a reason for peripheral vestibular lesions. Besides, rolling seems to correlate with head tilt, because rabbits with increased head tilt showed rolling more often, which was recognized likewise in an examination about Encephalitozoonosis in rabbits [28]. The histology of the rabbit of group 2, which was euthanised preterm, revealed a severe meningoencephalitis, which is an indication for the spreading infection of *Ps*. *aeruginosa*. The qualitative microbiological examination showed a clear difference between the two groups. In group 1, *Ps*. *aeruginosa* was proven only in two rabbits in a very low concentration. Although only a few animals showed clinical alterations, the microbiology showed a positive detection for *Ps*. *aeruginosa* in five rabbits of group 2, partially in a very high concentration. However, the quantitative microbiological examination (CFU) showed a statistically significant difference between the groups for the irrigations of the implants ($P = 0.03$ Mann–Whitney test), though there was no significance concerning the irrigations of the middle ear. These results demonstrate the ability of impregnated LDH nanoparticles as a drug delivery system for ciprofloxacin to combat a local bacterial infection in the middle ear of rabbits. In comparison to animals that were implanted without any antibiotic agents (preliminary studies, data not shown), both groups reached excellent results regarding microbiological and clinical outcome. Nevertheless, in case of a recurrent otitis media (group 2) this drug delivery system showed an attenuated efficiency. The reason could be a gradient release of ciprofloxacin accelerated by the bloody and fluid environment in the middle ear after surgery. In this context, further research on the decomposition kinetics of the LDHs in the environment of the middle ear have to be performed in order to establish this drug delivery system as a possible component of middle ear prostheses for a clinical use.

5 Conclusion

This is the first study of LDHs used in the middle ear and one of the few in vivo studies of this material class. It was demonstrated that LDH nanoparticles impregnated with a medical drug can be used as an effective drug delivery system for antibiotics to combat a forced infection of the middle ear of rabbits. However, animals which were concomitantly infected during the implantation of the prostheses showed a better outcome in microbiological examination than subjects which underwent infection 1 week after implantation, so the drug release and the efficiency is proven, but—at least for some application cases—faster than desirable. Further research has to be performed on the decomposition kinetics and the antibiotic release rate in the attempt to establish this new drug delivery system as a therapeutic tool in middle ear surgery.

Acknowledgments

This work was supported by the German Research Foundation (DFG, Collaborative Research Centre SFB 599, work packages D1 and DR1). The authors would like to thank Susanne Häussler from Helmholtz Centre for Infection Research (Braunschweig, Germany) for the kind provision of the *Ps*. *aeruginosa* strain “PAO1”. Moreover, Muhammad Badar was supported by the Higher Education Commission (HEC) and German Academic Exchange Service (DAAD).

References

1. Madana J, Yolmo D, Kalaiarasi R, Gopalakrishnan S, Sujatha S. Microbiological profile with antibiotic sensitivity pattern of cholesteatomatous chronic suppurative otitis media among children. Int J Pediatr Otorhinolaryngol. 2011;75(9):1104–8.
2. Choi HG, Park KH, Park SN, Jun BC, Lee DH, Yeo SW. The appropriate medical management of methicillin-resistant Staphylococcus aureus in chronic suppurative otitis media. Acta Otolaryngol. 2010;130:42–6.
3. Hwang JH, Chu CK, Liu TC. Changes in bacteriology of discharging ears. J Laryngol Otol. 2002;116:686–9.
4. Hirakawa Y, Sasaki H, Kawamoto E, Ishikawa H, Matsumoto T, Aoyama N, Kawasumi K, Amao H. Prevalence and analysis of Pseudomonas aeruginosa in chinchillas. BMC Vet Res. 2010;6:52.
5. Williams GR, O’Hare D. Towards understanding, control and application of layered double hydroxides chemistry. J Mater Chem. 2006;16:3065–74.
6. Del Hoyo C. Layered double hydroxides and human health: an overview. Appl Clay Sci. 2007;36:103–21.
7. Choi S-J, Oh J-M, Choy J-H. Human-related application and nanotoxicology of inorganic particles: complementary aspects. J Mater Chem. 2008;18:615–20.
8. Choi S-J, Choi GE, Oh J-M, Oh Y-J, Park M-C, Choy J-H. Anticancer drug encapsulated in inorganic lattice can overcome drug resistance. J Mater Chem. 2010;20:9463–9.

9. Choy J-H, Jung J-S, Oh J-M, Park M-C, Jeong J, Kang Y-K, Han O-J. Layered double hydroxide as an effective drug reservoir for folate derivatives. Biomaterials. 2004;25:3059–64.
10. Li A, Qin L, Wang W, Zhu R, Yu Y, Liu H, Wang S. The use of layered hydroxides as DNA vaccine delivery vector for enhancement of anti-melanoma immune response. Biomaterials. 2011;32:469–77.
11. Del Arco M, Cebadera E, Gutierrez S, Martin C, Rives V, Rocha J, Sevilla MA. Mg, Al layered double hydroxides with intercalated indomethacin: synthesis, characterization and pharmacological study. J Pharm Sci. 2004;93:1649–58.
12. Cao F, Wang Y, Ping Q, Liao Z. Zn-Al-NO3-layered double hydroxides with intercalated diclofenac for ocular delivery. Int J Pharm. 2011;404:250–6.
13. Gu Z, Rolfe ER, Xu ZP, Thomas AC, Campbell JH, Lu GQM. Enhanced effects of low molecular weight heparin intercalated with layered double hydroxide nanoparticles on rat vascular smooth muscle cells. Biomaterials. 2010;31:5455–62.
14. Stieve M, Hedrich HJ, Battmer RD, Behrens P, Mu¨ller PP, Lenarz T. Experimental middle ear surgery in rabbits: a new approach for reconstructing the ossicular chain. Lab Anim. 2009;43:198–204.
15. Stieve M, Schwab B, Winter M, Lenarz T. Titanium oxide ceramic as an implantation material in otosurgery: animal experimental results and surgical technique. Laryngorhinootologie. 2006;85:635–9.
16. Morawietz G, Ruehl-Fehlert C, Kittel B, Bube A, Keane K, Halm S, Heuser A, Hellmann J. Revised guides for organ sampling and trimming in rats and mice - Part 3. Exp Toxic Pathol. 2004;55:433–49.
17. Stange G. Lokale Therapie von Pseudomonasinfektionen des Ohres. Laryngo-Rhino-Otol. 1989;68:653–6.
18. Drehobl M, Guerrero JL, Lacarte PR, Goldstein G, Mata SF, Luber S. Comparison of efficacy safety of ciprofloxacin otic solution 0.2% versus polymyxin B-neomycin-hydrocortisone in the treatment of acute diffuse otitis externa. Curr Med Res Opin. 2008;24(12):3531–42.
19. Vogt JC, Brandes G, Ehlert N, Behrens P, Nolte I, Mueller PP, Lenarz T, Stieve M. Free Bioverit_ II implants coated with a nanoporous silica layer in a mouse ear model: a histological study. J Biomater Appl. 2009;24:175–91.
20. Vogt JC, Brandes G, Krueger I, Behrens P, Nolte I, Lenarz T, Stieve M. A comparison of different nanostructured biomaterials in subcutaneous tissue. J Mater Sci. 2008;19:2629–36.
21. Koetsche W, Gottschalk C. Krankheiten der Kaninchen und Hasen. 4rd ed. Jena: Gustav Fischer Verlag; 1990. p. 18, 105.
22. Zinke J. Ganzheitliche Behandlung von Kaninchen und Meerschweinchen. Stuttgart: Sonntag Verlag; 2004. p. 4–5.
23. Brooks DL. Nutrition and gastrointestinal physiology. In: Quesenberry K, Carpenter J, editors. Ferrets, rabbits and rodents. 2nd ed. St. Louis: Saunders; 2004. p. 157.
24. Saunders R, Davies R. Notes on rabbit internal medicine. Oxford: Blackwell Publishing; 2005. p. 57.
25. Harcourt-Brown F. Textbook of rabbit medicine. Oxford: Butterworth- Heinemann; 2002. p. 145, 211.
26. Nelson R, Couto C. Innere Medizin der Kleintiere. 2nd ed. Mu¨nchen: Urban & Fischer Verlag; 2010. p. 69, 1281.
27. Keeble E. Nervous and musculoskeletal disorders. In: Meredith A, Flecknell P, editors. Manual of rabbit medicine and surgery. 2nd ed. Quedgeley, Gloucs: BSAVA; 2006. p. 106.
28. Kuenzel F, Joachim A. Encephalitozoonosis in rabbits. Parasitol Res. 2010;106:299–309.

5.4 Controlled drug release from antibiotic-loaded layered double hydroxide coatings on porous titanium implants in a mouse model

Muhammad Badar*, Muhammad Imran Rahim*, Marc Kieke, Thomas Ebel, Manfred Rohde, Hansjörg Hauser, Peter Behrens, Peter P. Müller

*These authors contributed equally to this study.

J Biomed Mater Res Part A. **2014**;*00A:*000–000

DOI: 10.1002/jbm.a.35358

The final publication is available at

http://onlinelibrary.wiley.com/doi/10.1002/jbm.a.35358/full

Society For Biomaterials

Controlled drug release from antibiotic-loaded layered double hydroxide coatings on porous titanium implants in a mouse model

Muhammad Badar,[1,2*] Muhammad Imran Rahim,[1*] Marc Kieke,[3] Thomas Ebel,[4] Manfred Rohde,[1] Hansjörg Hauser,[1] Peter Behrens,[3] Peter P. Mueller[1]

[1]Helmholtz Centre for Infection Research, Inhoffenstrasse 7, 38124 Braunschweig, Germany
[2]Gomal Center of Biochemistry and Biotechnology (GCBB), Gomal University, Dera Ismail Khan, Pakistan
[3]Institute for Inorganic Chemistry, Leibniz University of Hannover, Callinstrasse 9, 30167 Hannover, Germany
[4]Department of Powder Technology, Helmholtz Center Geesthacht, Centre for Materials and Coastal Research, Max-Planck-Strasse 1, 21502 Geesthacht, Germany

Received 5 September 2014; revised 16 October 2014; accepted 21 October 2014
Published online 00 Month 2014 in Wiley Online Library (wileyonlinelibrary.com). DOI: 10.1002/jbm.a.35358

Abstract: As an alternative to degradable organic coatings the possibility of using layered double hydroxides (LDHs) to generate implant coatings for controlled drug delivery was evaluated *in vivo* and *in vitro*. Coatings prepared from LDH suspensions dissolved slowly and appeared compatible with cultured cells. LDH coatings loaded with an antibiotic resulted in antibacterial effects *in vitro*. The LDH coating prolonged the drug release period and improved the proliferation of adherent cells in comparison to pure drug coatings. However, during incubation in physiological solutions the LDH coatings became brittle and pieces occasionally detached from the surface. For stress protection porous titanium implants were investigated as a substrate for the coatings. The pores prevented premature detachment of the coatings. To evaluate the coated porous implants *in vivo* a mouse model was established. To monitor bacterial infection of implants noninvasive *in vivo* imaging was used to monitor luminescently labeled *Pseudomonas aeruginosa*. In this model porous implants with antibiotic-loaded LDH coatings could antagonize bacterial infections for over 1 week. The findings provide evidence that delayed drug delivery from LDH coatings could be feasible in combination with structured implant surfaces. © 2014 Wiley Periodicals, Inc. J Biomed Mater Res Part A: 00A:000–000, 2014.

Key Words: implant infection, local drug delivery, degradable implant coating, bacterial biofilm, layered double hydroxides

How to cite this article: Badar M, Rahim MI, Kieke M, Ebel T, Rohde M, Hauser H, Behrens P, Mueller PP. 2014. Controlled drug release from antibiotic-loaded layered double hydroxide coatings on porous titanium implants in a mouse model. J Biomed Mater Res Part A 2014:00A:000–000.

INTRODUCTION

Various materials, including plain, structured or coated titanium are commonly used as implant materials.[1–3] The ability of pathogenic bacteria to colonize such implants and form biofilms that are resistant to conventional therapies poses a major clinical problem.[4,5] Frequently, the only effective treatment is to first remove the implant and then eradicate the infection.[6,7] Even though device infections may occur even years after implantation, a most risky time period appears to be during the surgery and the subsequent convalescence. After the wound healing is completed implants are protected by a fibrous capsule that is thought to restrict the risk of infection.[8] Due to the limited efficacy of systemic antibiotic treatments various alternative strategies have been devised to prevent bacterial colonization of implants during this critical period.[9] Local drug delivery from degradable implant coatings could be of advantage to temporarily achieve highly efficacious antibiotic concentrations at the site where they are needed while systemic drug levels and side effects could be reduced.[10–13] Polymeric materials can be used as drug carriers but acidic breakdown products have been associated with inflammatory tissue responses.[14–19] Alternatively, inorganic biodegradable coatings could avoid such undesirable byproducts. In this study layered double hydroxides (LDHs) were investigated as a class of inorganic biodegradable materials that have gained considerable interest as potential drug delivery systems.[20] These hydrotalcite-type anionic clays are biocompatible and are certified for human use as antacids.[21] The aim of this study was to demonstrate the feasibility of controlled drug delivery from LDH coatings. Importantly, due to differences between experimental biofilms *in vitro* and *in vivo* a

*These authors contributed equally to this work.
Correspondence to: P. P. Mueller; e-mail: pmu@helmholtz-hzi.de
Contract grant sponsor: Joint stipend of the Higher Education Commission of Pakistan and the German Academic Exchange Service (DAAD), Germany (to MB and MIR)
Contract grant sponsor: German Research Foundation (DFG) within the Collaborative Research Centre (SFB 599, projects D1, D8, and DR1)

mouse model was established to verify *in vitro* observations.[22–24] Antibacterial effects of ciprofloxacin as an efficacious model antibiotic were monitored using a luminescent *Pseudomonas aeruginosa* strain.[25–28] Since LDH coatings appeared fragile on plain surfaces porous titanium discs were used as implants. In this setup, ciprofloxacin-loaded LDH coatings were gradually degraded and biocompatible while showing antibacterial activity.

MATERIALS AND METHODS

Titanium discs

Plain titanium discs were custom made, 7 mm in diameter and 1 mm in height (3di GmbH; Jena, Germany). Porous titanium discs were manufactured from Ti–6Al–4V microbeads grade 23 by metal injection molding of 90% (w/w) beads with a diameter from 125 to 180 μm and 10% Ti–6Al–4V powder with a grain diameter of less than 45 μm. The mixture was sintered at 1100°C for 2 h under high vacuum without further processing. The porous discs were 7 mm in diameter and 2 mm thick and the average weight was 265.5 ± 2.4 mg.

LDH coatings

A suspension of LDH microparticles with the chemical composition $Mg_4Al_2(OH)_{12}(SO_4)_2{\cdot}yH_2O$ (LDH) was prepared as described.[29] Briefly, the Mg–Al–SO_4–LDH was obtained by NaOH-induced coprecipitation from a sterile precursor solution containing $MgSO_4{\cdot}7H_2O$ and $Al_2(SO_4)_3{\cdot}18H_2O$. The precipitate was washed with and then resuspended in sterile distilled water at a concentration of 7 mg/mL. Drug-containing coatings were prepared from a mixture of 5.3 mg/mL LDH suspension with either 2.5, 0.25, or 0.025 mg/mL ciprofloxacin (Fluka Chemie GmbH, Deisenhofen, Germany) as indicated. 1 mL per cm^2 cell growth area of the respective suspension was transferred to 6-well cell culture plates (Nunc, Denmark) for cell compatibility testing or to 48-well plates for coating titanium discs. The suspensions were air dried for 3 days at 37°C. Titanium discs were autoclaved before coating and coating manipulations were done using a sterile laminar flow hood.

X-ray diffraction analysis

X-ray diffraction (XRD) measurements were performed with a STOE Theta/theta Diffractometer (STOE & Cie GmbH, Darmstadt) operated at 40 kV and 30 mA. The samples were scanned in reflection geometry at a step width of 0.02° with 2.0 s counting time per step, employing monochromatized $CuK\alpha_1$ radiation with a wavelength of 1.54060 Å.

Cell culture methods

The biocompatibility of LDH coatings was tested in mammalian cell cultures as described previously.[25] Briefly, immortalized murine NIH3T3 fibroblasts (ATCC CRL-1685) were cultured in Dulbecco's modified Eagle's medium (DMEM; Gibco/BRL, supplemented with 1% (v/v) glutamine, 1% (v/v) penicillin and streptomycin (100 U/mL penicillin G and 100 μg/mL streptomycin), and 10% (v/v) fetal calf serum) at 37°C in a humidified atmosphere with 5% CO_2. Subconfluent cells were detached from tissue culture flasks using trypsin. The cells were washed in DMEM with 10% (v/v) fetal calf serum to inactivate trypsin and then the cells were resuspended in fresh supplemented DMEM medium as above. The cells were seeded at a density of 12,000 cells per cm^2 of a 9.6-cm^2 LDH-coated well of a 6-well plate. The plates were incubated at 37°C in a humidified incubator with 5% CO_2 until the cells reached confluence in untreated control wells. All samples were prepared and evaluated in triplicates. Cell adhesion, spreading and proliferation was observed using Axio Observer A-1 microscope (Zeiss, Germany). The images were recorded by using the Axiovision software, release 4.5 (Carl Zeiss Micro-Imaging, Germany).

Electron microscopy

Porous titanium discs with or without coatings were examined using a Merlin field emission scanning electron microscope (Zeiss, Oberkochen, Germany) using an acceleration voltage of 5 kV with the Everhart-Thornley SE-detector and Inlens SE-detector ratio set to 25:75.

Drug release kinetics

Coated wells with a surface area of 1.9 cm^2 each or coated titanium discs with an exposed surface of 0.38 cm^2 in individual wells of 24-well cell culture plates (Nunclon Delta Surface, Thermo Scientific) were overlaid with 0.25 mL of phosphate-buffered saline (PBS) incubated at 37°C. The plates were incubated at 37°C in a humidified atmosphere with 5% CO_2. Supernatants were collected and replaced daily unless indicated otherwise. The ciprofloxacin concentration in supernatants was determined by measuring the light absorption at a wavelength of 272 nm using a Nanodrop ND-1000 UV-Vis Spectrophotometer (Nanodrop Technologies, Wilmington). An OD_{272} of 0.1 corresponded to 1 μg/mL ciprofloxacin.[30,31]

Luminescent *P. aeruginosa* (PAO1 CTX:lux) were used for monitoring the bacteria.[32,33] The antibacterial activity of ciprofloxacin in supernatants was tested by transferring 50 μL of the supernatants to individual wells of a black 96-well plate (Nunc, Denmark). 50 μL of bacterial cultures in LB medium with an OD_{600} of 0.1 was added to the 50 μL of the supernatants. The bacterial luminescence was determined using an IVIS®−200 *in vivo* imaging system (Xenogen) before and after 4 h incubation at 37°C. The luminescence was recorded with the Living Image software®, version 2.6 (Xenogen) and the average radiation intensity ($p/s/cm^2/r$) determined.[25] Bacterial cultures were prepared in triplicates and the data shown correspond to the mean values and the standard deviation.

Animal handling and *in vivo* imaging

The 10-week-old female Balb/c mice (Harlan-Winkelmann, Borchen, Germany) were kept in cages with individual filtered aeration and fed with a standard diet with water *ad libitum*. Before implantation, the animals were anesthetized by intraperitoneal injection of ketamine (10 mg/kg) and xylazine (4 mg/kg). The implantation site was shaved and sterilized with 70% ethanol in a sterile laminar flow hood.

Porous titanium discs were implanted subcutaneously and the wound closed by simple interrupted wound sutures (Vicryl Ethicon, Johnson and Johnson). The luminescently labeled strain of *P. aeruginosa* (PAO1 CTX::lux) was used to infect implants.[32,33] Bacteria were grown in LB to an optical density (OD_{600}) of 0.5, pelleted by centrifugation and resuspended in PBS to an OD_{600} of 0.1. Mice with implants were anesthetized with ketamine (10 mg/kg) and xylazine (4 mg/kg). Bacterial suspension of 5 μL was injected on top of each implant. Each animal was infected once only at the time point indicated and each implant was infected with a single injection. Subsequently, the bacterial luminescence was monitored at predetermined time points and quantified using an In Vivo Imaging System (IVIS®−200; Xenogen, Alameda, CA). The luminescence intensity was determined using the Living Image software® Version 2.6 (Xenogen). For each type of implant, three samples were used and all animals used in a given experiment were treated in parallel. All animal experiments were done in accordance with the regulations and with the approval from the local authorities Lower Saxony State Office for Consumer Protection and Food Safety (*LAVES*), permission number 33.42502/07–10.5.

RESULTS

Manufacturing of coatings by evaporation of LDH suspensions

To investigate if LDH coatings on plain implant material surfaces were feasible, titanium discs were submerged in aqueous LDH suspensions that were subsequently dried under ambient conditions. For comparison a suspension of pure magnesium hydroxide was used. The resulting LDH coatings appeared homogeneous, smooth and semi-transparent and firmly adhered to the titanium while in comparison pure magnesium hydroxide formed a white opaque layer [Fig. 1(A–C)]. Ciprofloxacin additions to LDH suspensions lead to a concentration-dependent formation of visible precipitates in the resulting coatings [Fig. 1(D–G)]. The performance of LDH coatings was evaluated by incubation in a physiological salt solution for 2 weeks [Fig. 1(H–K)]. LDH coatings dissolved more slowly than the ciprofloxacin and were still visible after the incubation. However, the coatings appeared brittle after the incubation and became fragmented in part. The LDH coatings containing the highest amounts of ciprofloxacin appeared to be dissolved more quickly and fewer remnants could be detected after the incubation [Fig. 1(K)]. Therefore, apart from the brittleness, the lower antibiotic additions to LDH were deemed to be more promising to obtain lowly soluble coatings and to achieve prolonged drug release.

XRD analysis was used to obtain evidence for the presence of LDH structures in the coatings [Fig. 1(L,M)]. In pure ciprofloxacin coatings two minor reflections in the region of 6–7° 2θ were noted without further characterization. The broad diffraction peaks of LDH coatings with or without antibiotic at the 2θ scattering angles of 11 and 22° were typical for Mg–Al LDH films.[34] Therefore the LDH structure was apparently preserved in the coatings.

Compatibility of LDH coatings with cultured cells

Cultured fibroblast cells were used as a representative cell type since *in vivo* fibroblasts can form capsules around implants. Cells seeded on LDH coatings adhered and proliferated to confluency after incubation for 3 days (Fig. 2). In comparison, cells did not form a confluent layer on pure ciprofloxacin coatings [Fig. 2(CFX)]. However, when ciprofloxacin was added to LDH coatings the formation of a confluent cell layer was not impeded [Fig. 2(LDH CFX)]. As expected, magnesium hydroxide did not support cell adhesion or cell survival (data not shown). The quantitative analysis confirmed that cell densities on LDH layers were higher than on pure ciprofloxacin coatings whereas ciprofloxacin additions to LDH did not lead to reduced cell densities. These findings showed that LDH coatings with or without ciprofloxacin additions could be used as a cell adhesion substrate whereas the lower cell density obtained on pure ciprofloxacin was in line with the reported effects of excessively high ciprofloxacin concentrations.[35–37]

Porous carrier improves the stability of LDH coatings

Since exposure to aqueous solutions rendered LDH coatings brittle it appeared essential for the envisioned applications to protect them from mechanical stress. To this end, porous titanium discs were prepared and used as a substrate for coatings. Loose precipitates that accumulated during the coating procedure were pressed into the pores. The amount of LDH on the porous discs was approximately twice of that on the plain discs (Table I). It was attempted to completely fill all pores to achieve a homogenous surface to improve the comparison with the coatings on the flat titanium surfaces. In effect, this resulted in an increased mass of all coatings on porous substrates (Table I, coatings on porous titanium). Minor variations in the coating mass on individual samples may be due to the fact that during the manufacturing process not all of the suspension applied ended up as coating on the titanium samples. With respect to the comparatively smooth coatings on plain surfaces, the coatings on the porous substrates had a rougher surface appearance, with occasional pores or crevices and with platelets in the range from 10 to 200 μm in diameter [Fig. 3(A)]. Antibiotic additions did not lead to noticeable changes in the appearance of the LDH surface whereas in the absence of LDH pure ciprofloxacin suspensions yielded a minor precipitate [Fig. 3(B,C)]. As intended, when incubated in aqueous buffer the LDH layers gradually dissolved without larger chunks breaking loose [Fig. 3(D–K), compare to Fig. 1]. Therefore, LDH coatings were effectively protected by the pores present in the titanium support and appeared more stable during the incubation in aqueous buffer solutions.

Controlled antibiotic release from LDH coatings and from porous carriers

The antibiotic release kinetics from LDH coatings in the presence of a physiological salt solution (PBS) were determined by measuring the UV light absorption. As expected, initial release rates were highest from pure ciprofloxacin coatings and lower when ciprofloxacin was imbedded in

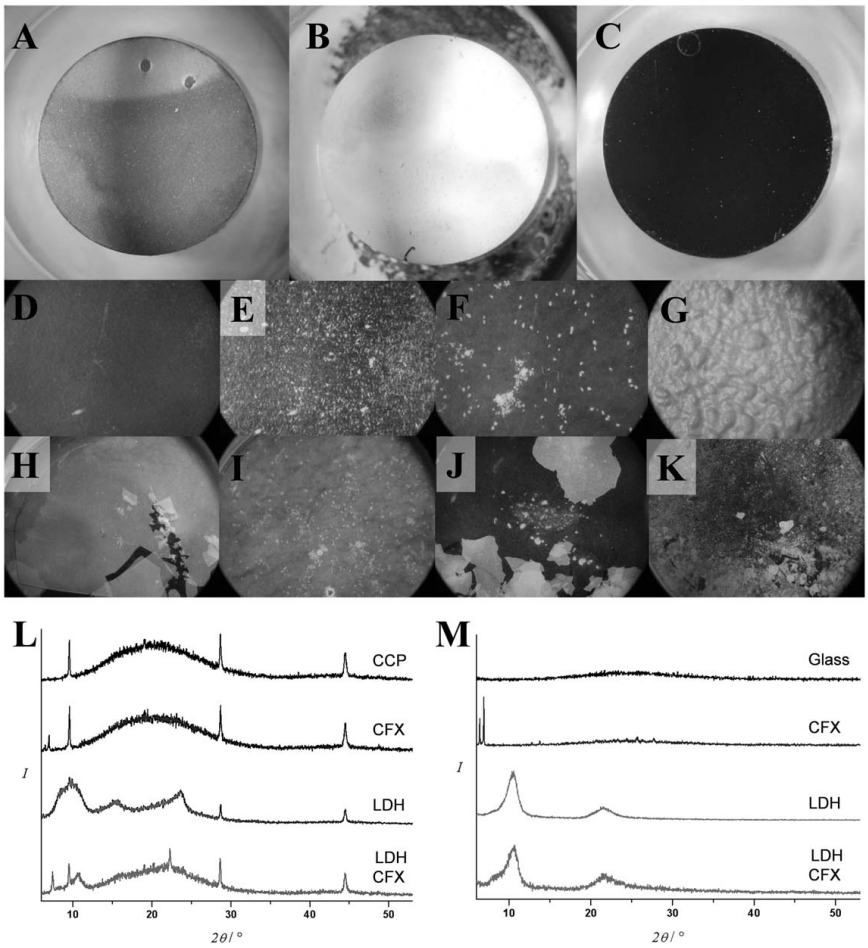

FIGURE 1. Generation of coatings by slow evaporation of LDH suspensions. Titanium discs with a diameter of 7 mm (used here in place of a scale bar) were coated with LDH in individual wells of 24-well tissue culture plates and overlaid with precursor suspensions that were left to dry for 3 days at 37°C at atmospheric pressure. Titanium discs coated with the LDH $Mg_4Al_2(OH)_{12}$ $(SO_4)_2{\cdot}6H_2O$ (A), with magnesium hydroxide (B) or left without coating (C). LDH coatings with increasing ciprofloxacin additions (left to right) in individual wells of 24-well tissue culture plates: LDH (D); LDH with ciprofloxacin at a ratio of 210:1 (w/w; E); LDH:ciprofloxacin 21:1 (w/w) ratio (F) and with a LDH:ciprofloxacin 2.1:1 (w/w) ratio (G). Each illustration of the coatings is shown (D–G), the same type of coating was pictured after incubation in PBS buffer for 14 days under standard cell culture conditions (37°C and a humidified atmosphere with 5% CO_2; H–K, respectively). L: X-ray diffraction (XRD) analysis of cell culture plastic (CCP), ciprofloxacin coatings (CFX), LDH coatings (LDH), and LDH coatings with ciprofloxacin at a ratio of 21:1 (LDH CFX), with all three coatings on cell culture plastic. M: XRD of microscope glass coverslip (Glass), ciprofloxacin coatings (CFX), LDH coatings (LDH), and LDH coatings with ciprofloxacin at a ratio of 21:1 (LDH CFX), all three coatings on glass coverslips. *I*, relative X-ray reflection intensity, 2θ, diffraction angle.

LDH coatings (Fig. 4). In addition, the release from LDH coatings was prolonged, such that after 4 h of incubation the release from the antibiotic supplemented LDH coatings was equal or higher than that from the pure antibiotic coating for all LDH to ciprofloxacin ratios investigated [Fig. 4(A–C)]. The antibiotic release rate from LDH coatings gradually declined over time. Ciprofloxacin could be detected for over 15 days in supernatants from LDH coatings with the highest antibiotic content and for 7 days from the coating with the lowest antibiotic content until the levels reached the detection limit of the instrument. As expected, no antibiotic release could be detected in the supernatants after incubation with plain LDH coatings. The ciprofloxacin release rates from ciprofloxacin-containing LDH coatings or from pure ciprofloxacin coatings, respectively, were mostly proportional to the total amounts of ciprofloxacin deposited. The

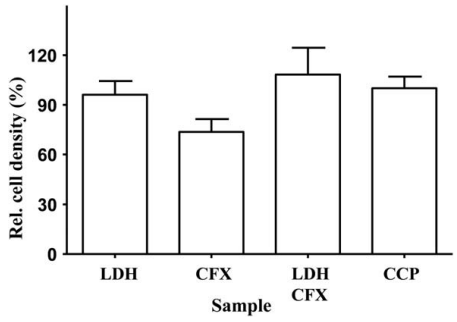

FIGURE 2. LDH coatings are biocompatible in cell culture assays. Polystyrene cell culture plates coated with suspensions of LDH particles or mixtures of LDH and ciprofloxacin were incubated with NIH3T3 murine fibroblasts under standard cell-culture conditions for 3 days when cells on the tissue culture polystyrene substrate reached confluence. The density of adherent and spread out cells was determined by manual counting cells. The bars correspond to the average of three independent material sample assays, each relative to the cell-counts on tissue culture polystyrene (CCP) surfaces that were arbitrarily set to 100%. The error bars correspond to the standard deviation of the three independent assays. The coatings used as cell adhesion substrate were as follows: CCP coated with LDH (LDH); ciprofloxacin (CFX); LDH combined with ciprofloxacin at a 21:1 (w/w) ratio (LDH CFX); CCP without coating (CCP).

TABLE I. Mass of Coatings on Titanium Carriers

Coating Composition	Coating on Plain Ti (mg/cm^2)	Coating on Porous Ti (mg/cm^2)	CFX Content on Porous Ti (mg/cm^2)
LDH + CFX	5.9 ± 0.5	9.4 ± 0.6	0.4 ± 0.03
LDH	4.7 ± 0.3	12 ± 1.2	–
CFX	0.3 ± 0.2	1.2 ± 0.2	1.2 ± 0.2

ciprofloxacin present in the coatings on cell culture wells with the highest quantity of the drug was completely recovered in the first three extractions and undetectable at later time points, amounting to 19 mg ciprofloxacin with the pure ciprofloxacin coating [Fig. 4(A)]. As expected, coatings containing lower amounts of antibiotic yielded proportionally reduced concentrations of ciprofloxacin in the extracts [Fig. 4(B,C)]. The ciprofloxacin release from LDH layers became undetectable before the coating was dissolved. This finding indicated that ciprofloxacin dissolved more rapidly than LDH and without concurrent destruction of the remaining LDH coating. As expected, the release kinetics from plain titanium discs were similar to those from coated cell culture wells [Fig. 4(D) compared to (B)]. Interestingly, the release from the porous surface indicated that even though there was an initial burst release from the pure ciprofloxacin coating, at later time points the release

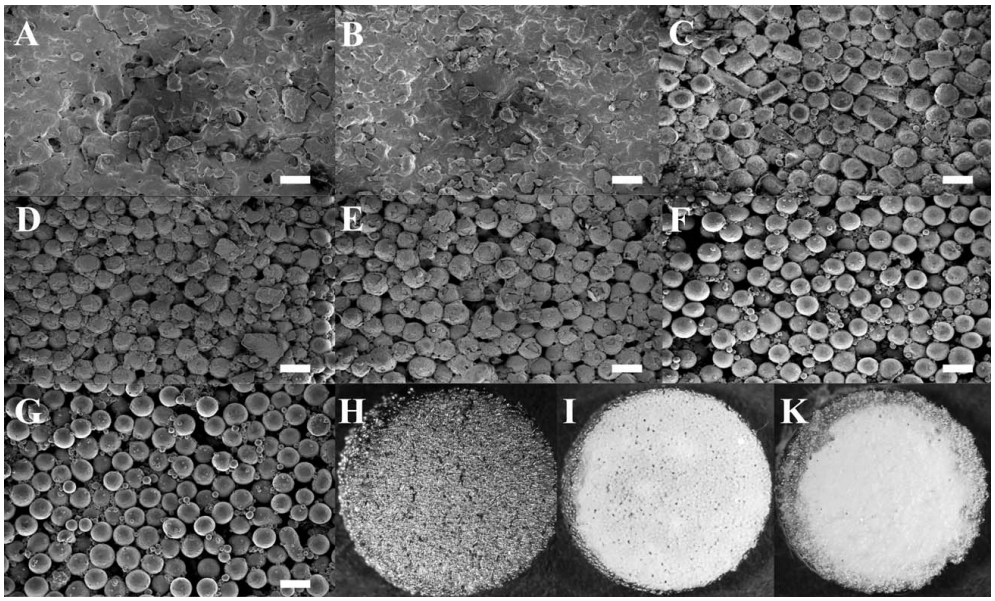

FIGURE 3. Porous titanium substrates can stabilize LDH-ciprofloxacin coatings. Reflection electron microscopy pictures of porous titanium discs coated with LDH (A and D) LDH:ciprofloxacin at a ratio (w/w) of 21:1 (B and E) with pure ciprofloxacin coatings (C and F). The samples were incubated for 15 days in PBS buffer that was replaced daily unless indicated otherwise (see Fig. 4). Pictures were taken before (A–C) or after the incubation (D–F). For comparison, untreated porous titanium discs are shown (G). The scale bar represents 200 μm. Light microscopic pictures of a porous titanium disc before (H) and after coating with LDH and ciprofloxacin (I) and after 2 weeks subcutaneous mouse implant residence time period (K). The diameter of the discs shown corresponds to 7 mm.

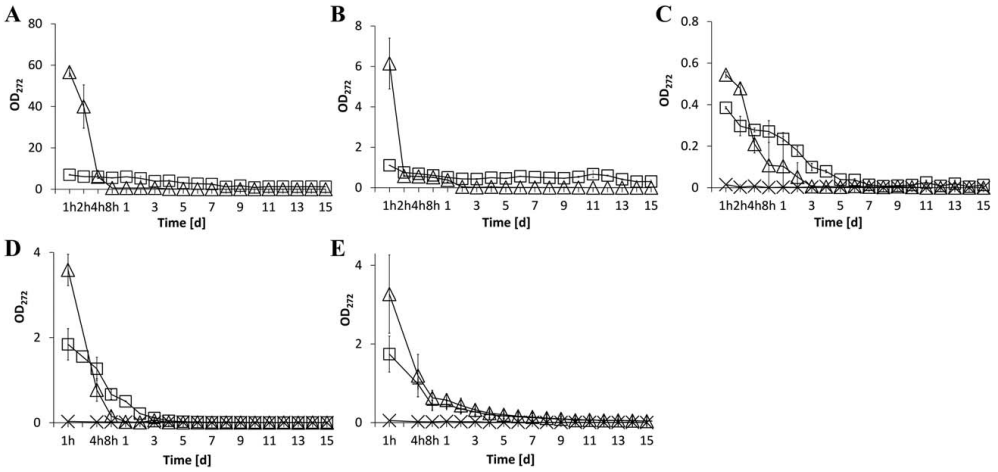

FIGURE 4. Controlled antibiotic release from LDH coatings on plain and porous surfaces. LDH coatings containing ciprofloxacin were prepared on plain and porous surfaces incubated with PBS buffer under standard cell culture conditions. If not indicated otherwise the supernatant was collected daily and replaced with fresh PBS. The ciprofloxacin concentration of each supernatant was determined by measuring the UV light absorption at a wavelength of 270 nm. The mean values of three independent experiments and the standard deviations are indicated in the graph. The following materials were coated: 24-well cell culture wells (A–C), plain titanium discs (D), and porous titanium discs (E). Ciprofloxacin release (squares) were determined from coatings containing the following LDH:ciprofloxacin ratios (w/w): 2.1:1 (A), 21:1 (B, D, and E), and 210:1 (C), respectively. Pure ciprofloxacin coatings (triangles) were deposited at concentrations of 10 mg / cm^2 (A); 1 mg / cm^2 (B, D, and E) and 0.1 mg/cm^2 (C) and pure LDH coatings (x marks in C, D, and E).

appeared to be retarded in comparison to the coated plain surfaces [Fig. 4(E)]. This finding was consistent with the notion that the pure ciprofloxacin exposed on the surface was quickly dissolved but subsequently the remaining ciprofloxacin buried in the pores was released more gradually. Overall, the data indicated that the initial drug release burst could be dampened by the incorporation into LDH and that the release period could be extended by both, the combination with LDH or, somewhat less efficacious, by filling it into pores.

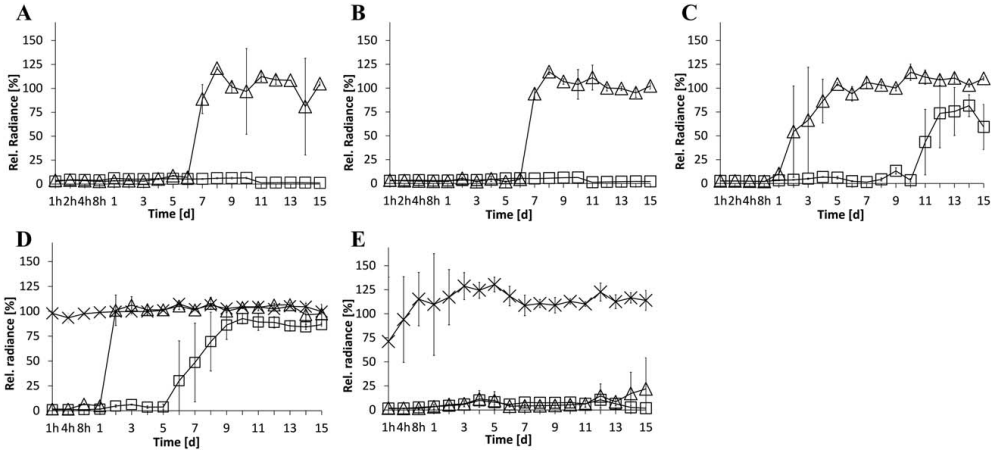

FIGURE 5. Prolonged antibacterial efficacy of antibiotic-loaded LDH coatings on plain and porous substrates. The supernatants from the coated samples described in the legend of Figure 4 were added at a 1:1 (v/v) ratio to cultures of luminescent *P. aeruginosa* and the luminescence was determined. Then the cultures were incubated at 37°C for 6 h followed by a second reading of the luminescence. The data is presented as average luminescence of three independent assays after incubation of the cultures relative to the average luminescence before the incubation. For each data point the luminescence of the corresponding cultures with pure LDH coating extracts (A–C) or the luminescence of cultures with supernatants from uncoated titanium discs (D and E) was arbitrarily set to 100%. The graphic representation, numbering and symbols are as specified in the legend of Figure 4.

Efficacy of antibiotic-loaded LDH coatings

The antibacterial efficacy of ciprofloxacin-loaded LDH coatings against *P. aeruginosa* was examined *in vitro*. When supernatants collected after incubation with antibiotic-loaded LDH coatings were added to bacterial cultures the luminescence was reduced (Fig. 5). Depending on the total amount of ciprofloxacin in the coatings antibacterial effects of pure ciprofloxacin coatings on plain surfaces lasted from 1 to 5 days, whereas the activity of ciprofloxacin-loaded LDH coatings lasted for over 10 days [Fig. 5(A–C)]. The activity of extracts from ciprofloxacin-coated plain titanium discs lasted 1 day and over 5 days from ciprofloxacin-loaded LDH coatings [Fig. 5(D)]. The slightly shorter active time period could be explained by the smaller diameter of the coated titanium discs compared to coated cell culture wells. In comparison, the antibacterial efficacy from porous discs extended for over 15 days for both, pure ciprofloxacin coatings and ciprofloxacin-loaded LDH. These results were consistent with the optical ciprofloxacin determinations and suggested that the ciprofloxacin in the LDH coatings remained active over the entire course of the experiment. This showed that porous titanium substrates could stabilize the coatings and the antibiotic release from LDH coatings was controlled such that bacterial growth could be antagonized for a clinically relevant time period. Overall, it was concluded that from the appearance of the coatings and from the time period during which antibacterial activities could be observed, the LDH:ciprofloxacin ratio (w/w) of 21:1 appeared most promising for the subsequent characterization *in vivo*.

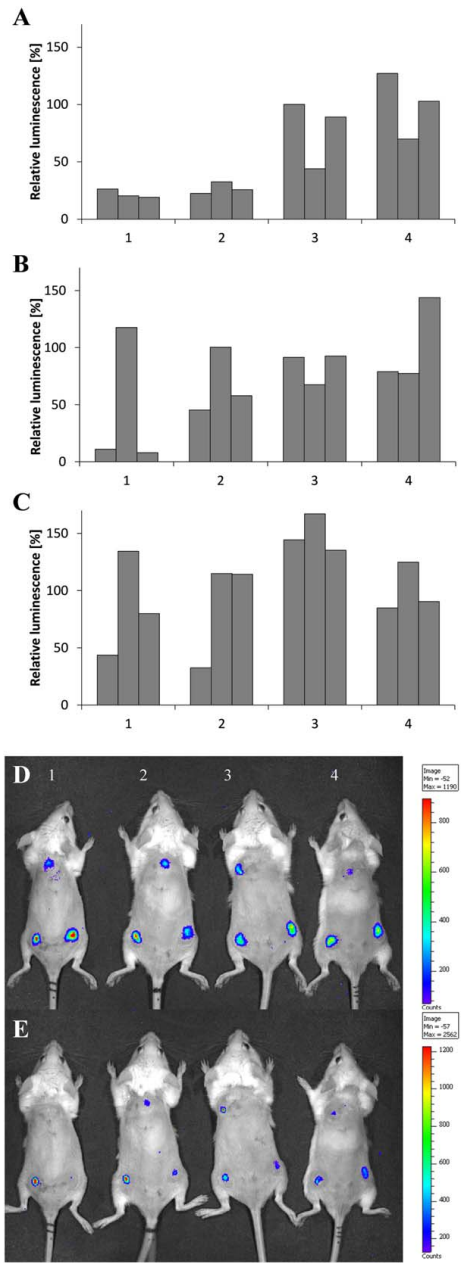

FIGURE 6. Prolonged *in vivo* antibacterial activity of porous implants with antibiotic-loaded LDH coatings. Three porous titanium discs coated with ciprofloxacin and LDH (1); ciprofloxacin (2) or LDH (3); and for comparison, porous titanium discs without coatings (4), respectively, were implanted subcutaneously in Balb/c mice (A–E). After the period indicated the implants were infected by subcutaneous injection of 5 μL of luminescent *P. aeruginosa* bacteria suspension on top of the implanted discs. The antibacterial efficacy of the implants is depicted graphically as the difference between the bacterial luminescence of infected implants determined directly after infection and the luminescence 4 h later. Implants were infected 1 week after implantation (A), 15 days (B), or 20 days after implantation (C), respectively. The average luminescence of the infected bare implants (4) was arbitrarily set to 1. The false color luminescence images of implants infected 15 days after implantation (D) and 4 h after infection (E) are shown. [Color figure can be viewed in the online issue, which is available at wileyonlinelibrary.com.]

***In vivo* antibacterial efficacy of antibiotic-loaded LDH coatings**

To evaluate antibacterial activity of LDH-ciprofloxacin coatings under *in vivo* conditions a mouse model was established. Based on the *in vitro* results, coated porous titanium discs were employed as implants. To allow noninvasive *in vivo* monitoring of the time course of the bacterial infection, the discs were implanted subcutaneously into white mice. Seven days after implantation, luminescent *P. aeruginosa* bacteria were injected on top of the implants and the luminescence was determined (Fig. 6). Both, ciprofloxacin and LDH–ciprofloxacin-coated discs reduced the bacterial luminescence very efficiently [Fig. 6(A1,A2)]. In comparison, in the absence of antibiotic the bacterial luminescence was diminished to a lesser degree [Fig. 6(A3,A4)]. 1 day after

inoculation no luminescence could be detected from any of the infected implants, suggesting that given sufficient time the immune system of the mouse could also control the infection (data not shown). When infected 15 days after implantation, two of the three LDH–ciprofloxacin-coated discs still showed antibacterial effects while pure ciprofloxacin coatings were somewhat less efficacious [Fig. 6(B)]. 20 days after implantation, only one out of three implants showed some activity [Fig. 6(C)]. Tissue responses to pure ciprofloxacin coatings 2 weeks or more after implantation were noted while all LDH coatings appeared well-tolerated [Fig. 6(D,E); data not shown]. This finding was in agreement with previous data indicating cytotoxic effects of excessive ciprofloxacin concentrations.[35–38] Therefore, in this mouse model, LDH–ciprofloxacin-coated porous implants were biocompatible and could curb bacterial infections for over 2 weeks.

DISCUSSION

The structure, biocompatibility, stability and drug delivery potential of LDH coatings prepared from particle suspensions were characterized *in vitro*. When used as implant coatings, the biocompatibility of LDH was confirmed.[29,39,40] Only a brief burst of antibacterial activity at the time of implantation in rabbits in a previous investigation suggested that plain LDH coatings are not suitable for controlled drug delivery.[29] This is in line with the results in this study that indicate that LDH coatings become fragile after exposure to aqueous liquids. Consequently, porous implants improved the stability and a prolonged antibiotic activity was achieved. Several animal models have previously been utilized for noninvasive monitoring of bacterial infections and antibiotic efficacy.[41,42] In this study the inoculated number of bacteria in this infection assay was deliberately high to permit immediate visualization. However, while the efficacious drug release period of 2 weeks appeared clinically useful it could even be underestimated.

CONCLUSION

LDH coatings were generated to demonstrate as a proof of principle that prolonged and efficacious drug delivery from biodegradable inorganic implant coatings could be feasible. Porous implants could protect fragile antibiotic-loaded LDH coatings and prolong the efficacious drug release period in a mouse implant infection model. Therefore, these results may warrant more detailed investigations.

ACKNOWLEDGMENTS

We thank Susanne Häussler for the kind donation of bacterial strains and Stefan Lienenklaus for his introduction to *in vivo* imaging techniques.

REFERENCES

1. Ochsner PE. Osteointegration of orthopaedic devices. Semin Immunopathol 2011;33:245–256.
2. Palmquist A, Omar OM, Esposito M, Lausmaa J, Thomsen P. Titanium oral implants: Surface characteristics, interface biology and clinical outcome. J R Soc Interface 2010;7 Suppl 5:S515–S527.
3. Wongwiwat P, Boonma A, Lee YS, Narayan RJ. Bioceramics in ossicular replacement prostheses: A review. J Long Term Eff Med Implants 2011;21:169–183.
4. Briceno DF, Quinn JP, Villegas MV. Treatment options for multidrug-resistant nonfermenters. Expert Rev Anti Infect Ther 2010;8:303–315.
5. Haussler S. Multicellular signalling and growth of *Pseudomonas aeruginosa*. Int J Med Microbiol 2010;300:544–548.
6. Costerton JW, Montanaro L, Arciola CR. Biofilm in implant infections: Its production and regulation. Int J Artif Organs 2005;28: 1062–1068.
7. Trampuz A, Widmer AF. Infections associated with orthopedic implants. Curr Opin Infect Dis 2006;19:349–356.
8. Busscher HJ, van der Mei HC, Subbiahdoss G, Jutte PC, van den Dungen JJ, Zaat SA, Schultz MJ, Grainger DW. Biomaterial-associated infection: Locating the finish line in the race for the surface. Sci Transl Med 2012;4:153rv10.
9. Salwiczek M, Qu Y, Gardiner J, Strugnell RA, Lithgow T, McLean KM, Thissen H. Emerging rules for effective antimicrobial coatings. Trends Biotechnol 2014;32:82–90.
10. Romanò CL, Toscano M, Romanò D, Drago L. Antibiofilm agents and implant-related infections in orthopaedics: Where are we? J Chemother 2013;25:65–80.
11. Zalavras CG, Patzakis MJ, Holtom P. Local antibiotic therapy in the treatment of open fractures and osteomyelitis. Clin Orthop Relat Res 2004:86–93.
12. Schmidmaier G, Lucke M, Wildemann B, Haas NP, Raschke M. Prophylaxis and treatment of implant-related infections by antibiotic-coated implants: A review. Injury 2006;37 Suppl 2:S105–S112.
13. Hetrick EM, Schoenfisch MH. Reducing implant-related infections: Active release strategies. Chem Soc Rev 2006;35:780–789.
14. Simchi A, Tamjid E, Pishbin F, Boccaccini AR. Recent progress in inorganic and composite coatings with bactericidal capability for orthopaedic applications. Nanomedicine 2011;7:22–39.
15. Hart E, Azzopardi K, Taing H, Graichen F, Jeffery J, Mayadunne R, Wickramaratna M, O'Shea M, Nijagal B, Watkinson R, O'Leary S, Finnin B, Tait R, Robins-Browne R. Efficacy of antimicrobial polymer coatings in an animal model of bacterial infection associated with foreign body implants. J Antimicrob Chemother 2010;65: 974–980.
16. Kluin OS, van der Mei HC, Busscher HJ, Neut D. Biodegradable vs non-biodegradable antibiotic delivery devices in the treatment of osteomyelitis. Expert Opin Drug Deliv 2013;10:341–351.
17. Wohl-Bruhn S, Badar M, Bertz A, Tiersch B, Koetz J, Menzel H, Mueller PP, Bunjes H. Comparison of in vitro and in vivo protein release from hydrogel systems. J Control Release 2012;162:127–133.
18. Kastrati A. Drug for a while, polymer for life: Is it a good solution? Catheter Cardiovasc Interv 2008;71:340–341.
19. Byrne RA, Kastrati A, Tiroch K, Schulz S, Pache J, Pinieck S, Massberg S, Seyfarth M, Laugwitz KL, Birkmeier KA, Schömig A, Mehilli J; ISAR-TEST-2 Investigators. 2-Year clinical and angiographic outcomes from a randomized trial of polymer-free dual drug-eluting stents versus polymer-based cypher and endeavor, drug-eluting stents. J Am Coll Cardiol 2010;55:2536–2543.
20. Cavani F, Trifirò F, Vaccari A. Hydrotalcite-type anionic clays: Preparation, properties and applications. Catal Today 1991;11: 173–1301.
21. Playle AC, Gunning SR, Llewellyn AF. The in vitro antacid and anti pepsin activity of hydrotalcite. Pharm Acta Helv 1974;49:298–302.
22. Chokr A, Leterme D, Watier D, Jabbouri S. Neither the presence of ica locus, nor in vitro-biofilm formation ability is a crucial parameter for some *Staphylococcus epidermidis* strains to maintain an infection in a guinea pig tissue cage model. Microb Pathog 2007;42:94–97.
23. Bjarnsholt T, Alhede M, Alhede M, Eickhardt-Sørensen SR, Moser C, Kühl M, Jensen PØ, Høiby N. The in vivo biofilm. Trends Microbiol 2013;21:466–474.
24. Kadurugamuwa JL, Sin L, Albert E, Yu J, Francis K, DeBoer M, Rubin M, Bellinger-Kawahara C, Parr Jr TR, Jr., Contag PR. Direct

continuous method for monitoring biofilm infection in a mouse model. Infect Immun 2003;71:882–890.
25. Badar M, Hemmen K, Nimtz M, Stieve M, Stiesch M, Lenarz T, Hauser H, Möllmann U, Vogt S, Schnabelrauch M, Mueller PP. Evaluation of madurahydroxylactone as a slow release antibacterial implant coating. Open Biomed Eng J 2010;4:263–270.
26. Ehlert N, Badar M, Christel A, Lohmeier SJ, Luessenhop T, Stieve M, Lenarz T, Mueller PP, Behrens P. Mesoporous silica coatings for controlled release of the antibiotic ciprofloxacin from implants. J Mater Chem 2011;21:752.
27. Koort JK, Makinen TJ, Suokas E, Veiranto M, Jalava J, Knuuti J, Tormala P, Aro HT. Efficacy of ciprofloxacin-releasing bioabsorbable osteoconductive bone defect filler for treatment of experimental osteomyelitis due to *Staphylococcus aureus*. Antimicrob Agents Chemother 2005;49:1502–1508.
28. Sjollema J, Sharma PK, Dijkstra RJ, van Dam GM, van der Mei HC, Engelsman AF, Busscher HJ. The potential for bio-optical imaging of biomaterial-associated infection in vivo. Biomaterials 2010;31:1984–1995.
29. Hesse D, Badar M, Bleich A, Smoczek A, Glage S, Kieke M, Behrens P, Müller PP, Esser KH, Stieve M, Prenzler NK. Layered double hydroxides as efficient drug delivery system of ciprofloxacin in the middle ear: An animal study in rabbits. J Mater Sci Mater Med 2013;24:129–136.
30. Cazedey ECL, Salgado HRN. Spectrophotometric determination of ciprofloxacin hydrochloride in ophthalmic solution. Adv Anal Chem 2012;2:74–79.
31. Nijhu RS, Jhanker YM, Sutradhar KB. Development of an assay method for simultaneous determination of ciprofloxacin and naproxen by uv spectrophotometric method. Stamford J Pharm Sci 2011;4:84–90.
32. Becher A, Schweizer HP. Integration-proficient *Pseudomonas aeruginosa* vectors for isolation of single-copy chromosomal lacZ and lux gene fusions. Biotechniques 2000;29:948–952.
33. Fletcher MP, Diggle SP, Camara M, Williams P. Biosensor-based assays for PQS, HHQ and related 2-alkyl-4-quinolone quorum sensing signal molecules. Nat Protoc 2007;2:1254–1262.
34. Uan J-Y, Lin J-K, Tung Y-S. Direct growth of oriented Mg–Al layered double hydroxide film on Mg alloy in aqueous HCO_3^-/CO_3^{2-} solution. J Mater Chem 2010;20:761–766.
35. Lawrence JW, Claire DC, Weissig V, Rowe TC. Delayed cytotoxicity and cleavage of mitochondrial DNA in ciprofloxacin-treated mammalian cells. Mol Pharmacol 1996;50:1178–1188.
36. Gurbay A, Garrel C, Osman M, Richard MJ, Favier A, Hincal F. Cytotoxicity in ciprofloxacin-treated human fibroblast cells and protection by vitamin E. Hum Exp Toxicol 2002;21:635–641.
37. Miclau T, Edin ML, Lester GE, Lindsey RW, Dahners LE. Effect of ciprofloxacin on the proliferation of osteoblast-like MG-63 human osteosarcoma cells in vitro. J Orthopaedic Res 1998;16:509–512.
38. Gurbay A, Gonthier B, Barret L, Favier A, Hincal F. Cytotoxic effect of ciprofloxacin in primary culture of rat astrocytes and protection by vitamin E. Toxicology 2007;229:54–61.
39. Tyner KM, Roberson MS, Berghorn KA, Li L, Gilmour RF, Jr., Batt CA, Giannelis EP. Intercalation, delivery, and expression of the gene encoding green fluorescence protein utilizing nanobiohybrids. J Control Release 2004;100:399–409.
40. Tyner KM, Schiffman SR, Giannelis EP. Nanobiohybrids as delivery vehicles for camptothecin. J Controlled Release 2004;95:501–514.
41. Barman TK, Rao M, Bhati A, Kishore K, Shukla G, Kumar M, Mathur T, Pandya M, Upadhyay DJ. Non invasive real-time monitoring of bacterial infection & therapeutic effect of anti-microbials in five mouse models. Indian J Med Res 2011;134:688–695.
42. Engelsman AF, van der Mei HC, Francis KP, Busscher HJ, Ploeg RJ, van Dam GM. Real time noninvasive monitoring of contaminating bacteria in a soft tissue implant infection model. J Biomed Mater Res B Appl Biomater 2009;88:123–129.

6 Curriculum Vitae

	Marc Dong Kil Kieke
Date of birth	November the 16th 1985
Place of birth	Daegu City, South Korea
Nationality	German

November 2010 – December 2014	**Dissertation**
	Title: "On the Degradation Behavior of Magnesium, Magnesium Hydroxide Derived Coatings and Magnesium Containing Layered Double Hydroxides with Regard to Medical Applications"
	Institute of Inorganic Chemistry, Leibniz University of Hannover, Prof. Dr. Peter Behrens' group
October 2005 – October 2010	**Study** of Chemistry (Diplom)
	Achieve of Diploma in October 2010
	Diploma thesis: "Doppelhydroxide mit Schichtstruktur: ihr Auflöseverhalten und ihre Eignung als Implantatbeschichtung"
	Institute of Inorganic Chemistry, Leibniz University of Hannover, Prof. Dr. Peter Behrens' group
1998 – 2005	**Gymnasium** Langenhagen
	General qualification for university entrance
1996 – 1998	**Middle school** Godshorn
1992 – 1996	**Elementary school** Engelbostel

7 Supervised Theses, Publications and Conference Contributions

7.1 Supervised Theses

1. Alexandra Satalov; *Synthese von nanoskaligen Mg-Al-Carbonat-Hydroxiden und Charakterisierung ihres Auflöseverhaltens*; B. Sc. Thesis; Sept. **2011**.
2. Dennes Nettelroth; *Darstellung von Magnesiumhydroxycarbonaten mit definierter Morphologie*; B. Sc. Thesis; Sept. **2012**. (In cooperation with Evonik Industries AG)
3. Alexander Mohmeyer; *Morphologiegesteuerte Synthese von Bismut-Verbindungen*; B. Sc. Thesis; Jun. **2013**. (In cooperation with Evonik Industries AG)
4. Tim-Joshua Pinkvos; *Zum Verhalten von Mg-Al-Carbonat-Hydroxid-Beschichtungen in wässrigen Medien*; B. Sc. Thesis; Feb. **2014**.

7.2 Publications

Reviewed

1. Waizy H, Weizbauer A, Modrejewski C, Witte F, Windhagen H, Lucas A, Kieke M, Denkena B, Behrens P, Meyer-Lindenberg A, Bach F-W, Thorey F. In vitro corrosion of ZEK100 plates in Hank's Balanced Salt Solution. Biomed. Eng. Online. BioMed Central Ltd; 2012;11:12.
2. Hesse D, Badar M, Bleich A, Smoczek A, Glage S, Kieke M, Behrens P, Müller PP, Esser K-H, Stieve M, Prenzler NK. Layered double hydroxides as efficient drug delivery system of ciprofloxacin in the middle ear: an animal study in rabbits. J. Mater. Sci. Mater. Med. 2013;24:129–36.
3. Duda F, Kieke M, Waltz F, Schweinefuß ME, Badar M, Müller PP, Esser K-H, Lenarz T, Behrens P, Prenzler NK. Highly biocompatible behaviour and slow degradation of a LDH (layered double hydroxide)-coating on implants in the middle ear of rabbits. J. Mater. Sci. Mater. Med. 2015;26:9. DOI: 10.1007/s10856-014-5334-x
4. Badar M, Rahim MI, Kieke M, Ebel T, Rohde M, Hauser H, Behrens P, Mueller PP. Controlled drug release from antibiotic-loaded layered double hydroxide coatings on porous titanium implants in a mouse model. J Biomed Mater Res Part A. 2014;00A:000–000. DOI: 10.1002/jbm.a.35358
5. Weizbauer A, Kieke M, Rahim MI, Angrisani GL, Willbold E, Diekmann J, Flörkemeier T, Windhagen H, Müller PP, Behrens P, Budde S. Magnesium-containing layered double hydroxides as orthopaedic implant coating

materials-an *in vitro* and *in vivo* study. J Biomed Mater Res Part B. 2015;00B:000-000. DOI: 10.1002/jbm.b.33422

Not reviewed

1. M. Kieke, M. Badar, S. Behrens, F.-W. Bach, P. P. Müller, P. Behrens. Biomaterialien, 2011;12:99.
2. M. Badar, M. Kieke, R. Lensing, H. Hauser, M. Stieve, P. Behrens, P. Müller. Biomaterialien, 2011;12:86.
3. M. D. K. Kieke, A. Weizbauer, S. Budde, T. Flörkemeier, J. Diekmann, M. Badar, M. I. Rahim, P. P. Müller, H. Hauser, H. Windhagen, P. Behrens. Bionanomaterials, 2012;13:105.
4. M. D. K. Kieke, F. Feyerabend, R. Willumeit, P. Behrens, Bionanomaterials, 2012;13:54.
5. M. D. K. Kieke, A. Weizbauer, F. Duda, M. Badar, S. Budde, T. Flörkemeier, J. Diekmann, N. Prenzler, M. I. Rahim, P. P. Müller, H. Hauser, S. Behrens, P. Dellinger, K. Möhwald, T. Lenarz, H. Windhagen, P. Behrens. Biomed Tech, 2013;58 (Suppl. 1).
6. M.I. Rahim, B. Rais, M. Kieke, F. Evertz, A. Weizbauer, H. Windhagen, E. Willbold, M. Kietzmann, B. Glasmacher, M. Stiesch, H. Hauser, P. Behrens, P.P. Mueller. Biomed Tech, 2014;59:15 (s1).
7. M.I. Rahim, F. Evertz, M. Kieke, A. Weizbauer, H. Windhagen, E. Willbold, B. Glasmacher, H. Hauser, P.P. Mueller. Biomed Tech, 2014;59:1156 (s1).

7.3 Conference Contributions

Poster Presentations

XRD-Untersuchungen von unter physiologischen Bedingungen korrodierten Magnesiumplättchen

M. Kieke, P. Behrens, F. Feyerabend, R. Willumeit

Workshop: Neue Horizonte für metallische Biomaterialien, May 2-3, **2011**, Geesthacht, Germany

Layered double hydroxides als degradable Implantatbeschichtung

P. P. Müller, M. Badar, M. Kieke, R. Lensing, H. Hauser, M. Stieve, P. Behrens

Jahrestagung 2011 der Deutschen Gesellschaft für Biomaterialien e.V. (DGBM), November 10-12, **2011**, Gießen, Germany

Evaluating layered double hydroxides as a novel biomaterial

M. Kieke, M. Badar, S. Behrens, Fr.-W. Bach, P. P. Müller, P. Behrens

Jahrestagung 2011 der Deutschen Gesellschaft für Biomaterialien e.V. (DGBM), November 10-12, **2011**, Gießen, Germany

Evaluating layered double hydroxides as novel biodegradable biomaterials

M. Kieke, A. Weizbauer, S. Budde, T. Flörkemeier, J. Diekmann, M. Badar, M. I. Rahim, P. P. Müller, H. Hauser, H. Windhagen, P. Behrens

Jahrestagung 2012 der Deutschen Gesellschaft für Biomaterialien e.V. (DGBM), November 1-3, **2012**, Hamburg, Germany

Layered double hydroxides as a biomaterial

M. Kieke

Colloquium 2012, Collaborative Research Centre SFB 599, November 8-9, **2012**, Hannover, Germany

*Evaluating layered double hydroxides as a novel biomaterial **

M. Kieke, P. Behrens

Summer School 2013 on 'Functional Solids –FERRUM', Zentrum für Festkörperchemie und Neue Materialien (ZFM), July 21-25, **2013**, Goslar, Germany

*This poster was acknowledged with a ZFM Summer School 2013 poster award

In vitro and in vivo evaluation of magnesium-containing layered double hydroxides as implant materials

M. D. K. Kieke, A. Weizbauer, F. Duda, M. I. Rahim, P. Dellinger, S. Budde, T. Flörkemeier, J. Diekmann, N. Prenzler, M. Badar, P. P. Müller, H. Hauser, S. Behrens, K. Möhwald, F.-W. Bach, H. J. Maier, T. Lenarz, H. Windhagen, P. Behrens

48th DGBMT Annual Conference, October 8-10, **2014**, Hannover, Germany

Protective coatings on metallic magnesium to limit hydrogen generation

M. I. Rahim, F. Evertz, M. Kieke, A. Weizbauer, H. Windhagen, E. Willbold, B. Glasmacher, H. Hauser, P. P. Mueller

48th DGBMT Annual Conference, October 8-10, **2014**, Hannover, Germany

Layered Double Hydroxide (LDH) based intrinsic and sustained drug delivery system to combat implant associated infections

M. I. Rahim, M. Badar, M. Kieke, T. Ebel, M. Rohde, H. Hauser, P. Behrens, P. P. Mueller.

Jahrestagung 2014 der Deutschen Gesellschaft für Biomaterialien e.V. (DGBM), November 6-8, **2014**, Dresden, Germany

Oral Presentations

Options and therapeutic strategies in infections of joint prostheses

H. Windhagen, P. Behrens, K. Möhwald, P. P. Müller, A. Weizbauer, S. Budde, M. Kieke, P. Dellinger, M. Badar, S. Behrens, T. Flörkemeier, H. Hauser

Colloquium 2011, Collaborative Research Centre SFB 599, October 14-15, **2011**, Hannover, Germany

Layered double hydroxides as a slow drug release system for medical implants

M. Badar, M. Kieke, N. Ehlert, P. Behrens, P. P. Müller

8. Thüringer Biomaterialkolloquium (8. TBK), September 8, **2011**, Zeulenroda, Germany

XRD studies of corroded magnesium surfaces after incubation under cell culture conditions

M. Kieke, F. Feyerabend, R. Willumeit, P. Behrens

Jahrestagung 2012 der Deutschen Gesellschaft für Biomaterialien e.V. (DGBM), November 1-3, **2012**, Hamburg, Germany

Evaluating a novel class of biomaterials: magnesium-containing layered double hydroxides

M. Kieke, A. Weizbauer, F. Duda, M. Badar, S. Budde, T. Flörkemeier, J. Diekmann, N. K. Prenzler, M. I. Rahim, P. P. Müller, H. Hauser, S. Behrens, P. Dellinger, K. Möhwald, T. Lenarz, H. Windhagen, P. Behrens

Dreiländertagung der Deutschen, Schweizerischen und Österreichischen Gesellschaft für Biomedizinische Technik (BMT), September 19-21, **2013**, Graz, Austria

Cell Culture and animal test models for implant-associated infections
P. P. Müller, M. Badar, M. Kieke, M. I. Rahim, T. Ebel, D. Hesse, A. Bleich, A. Smoczek, S. Glage, K.-H Esser, M. Stieve, H. Hauser, N. K. Prenzler, P. Behrens

International Conference on Biomedical Technology 2013, European Community on Computational Methods in Applied Sciences (ECCOMAS), November 20-22, **2013**, Hannover, Germany

*On the applicability of Magnesium-containing Layered Double Hydroxides as Novel Implant Coating Materials **

M. D. K. Kieke, A. Weizbauer, F. Duda, M. I. Rahim, P. Dellinger, S. Budde, T. Flörkemeier, J. Diekmann, N. Prenzler, M. Badar, P. P. Müller, H. Hauser, S. Behrens, K. Möhwald, F.-W. Bach, H. J. Maier, T. Lenarz, H. Windhagen, P. Behrens

26th European Conference on Biomaterials, The European Society for Biomaterials (ESB), August 31 – September 3, **2014**, Liverpool, UK

Characterization and optimization of antibacterial bacterial implants in vitro and validation in a small animal model

M. I. Rahim, B. Rais, M. Kieke, F. Evertz, A. Weizbauer, H. Windhagen, E. Willbold, S. Schumacher, M. Kietzmann, B. Glasmacher, M. Stiesch, H. Hauser, P. Behrens, P. P. Müller

48th DGBMT Annual Conference, October 8-10, **2014**, Hannover, Germany